THE UNIVERSITY *of* EDINBURGH

Screening for genes involved in cilia formation and function

Emma Andisi Hall

Thesis submitted for the degree of Doctor of Philosophy

The University of Edinburgh

2012

This thesis is composed of original research undertaken by myself, and where the work of others is included their contributions have been duly acknowledged.

Emma Andisi Hall

April 2012

Acknowledgements

Firstly and importantly, thank you to Pleasantine Mill for taking me on as a PhD student, for your endless patience, time and effort in helping me to understand the science and learn the techniques I needed. Especially thanks for knowing what to say when things didn't work out as planned…which is often the case in science! Your love of science and incredible insight into developmental biology inspired me to continue in science. Thank you for investing so much time in me, even when you have new-born or sick children in tow.

Thanks also to Ian Jackson for allowing me to pursue my PhD in his lab, and for your help, advice and encouragement throughout my PhD. You create a relaxed and productive environment to work in and I have thoroughly enjoyed being part of the lab.

Thank you to the rest of the Jackson lab, past and present, in particular; Richard Mort for patience in explaining which statistical test to perform, and then performing them on my data, and for help and advice throughout the project; Peter Budd for help and advice in the lab, especially when cloning, and for continuing the cloning while I've been writing up; Margaret for managing the mouse colonies and doing lots of genotyping PCRs; Shalini for help and advice on the eye phenotype (or lack thereof!) and the rest of the lab for general help and advice. Thanks also to the members (past and present) of C204 office – there has been a lot of comings and goings over the past four years but it has always been a fun and friendly place to work, with plenty of opportunities for distraction!

Thank you to Craig Nichol for helping make figures and print the final copies; Paul Perry, Matthew Pearson and Alan Serrels for help with the microscopes and image analysis, hours in dark rooms staring down microscopes, trying to decide if the green dots overlap with the red ones! Allyson Ross for help with histology and Tracey Davey for endless patience when processing and imaging TEM when I wasn't sure exactly what we were looking for! Lizzie Freyer for help with FACS; Lee Smith and Ian Adams for help analysing the male fertility phenotype. Thanks to Fiona Kilonowski and Joan Slight for expanding and characterising ES cells. Thanks to the Transgenic Unit staff for managing my mouse colony. Special thanks to Carol-Anne and the rest of Andrew Jackson's lab for helpful discussion and lending of many reagents. Thanks to Tamara Caspary for LOTS of antibody, and to Gregory Pazour, Shoji Tajima, Andreas Merdes, Andrew Kodani, Ian Chambers and Paul Lockhart for antibodies and other reagents.

Thanks to friends and former flatmates Judith, Gillian, Aimee, Fiona and Annikki for all your support and, importantly distraction from work! I love you all! You've all made the last four years (and the years before in most cases) lots of fun!

Thanks to my family: Mum, Dad and Tim. Especially to Dad for always making jokes after everything life throws at you. Mum and Tim for support and distraction, thank you for helping Dad when I couldn't be there. And especially thanks for the

endless meals out we have when I'm at home or you visit Edinburgh!! I'm looking forward to spending some more time at home when this thesis is finished.

Last but in no way least, thanks to Jason! Thank you for buying your first home with me…I may not have acted like it but I had loads of fun the week we spent decorating the whole house. It is because of you that I have emerged (almost) sane at the end of this PhD. In particular, thanks for making me cups of tea while I wrote - tea is an important part of the writing process! And for hiding in the garage while I finished the thesis! Thank you for all your support over the past four years and before, I dedicate this thesis to you.

Abstract

Cilia are small microtubule based structures found on the surface of almost all mammalian cells, enclosed in a highly specialised extension of the cell membrane. Components of several key developmental signalling pathways, in particular Hedgehog (Hh) signalling, are enriched in cilia and cells with mutations in cilia structure show aberrant signalling, suggesting cilia act as "antennae" to focus these signalling cascades. A spectrum of human diseases, termed ciliopathies, are caused by problems in cilia formation or cilia function, which display wide ranging phenotypes from embryonic lethality to retinal degeneration, polydactyly to cystic kidneys. Despite recent advances in the understanding of the essential roles cilia play in mammalian development, exactly how these complex structures are put together, how they carry out their diverse functions, and how they are regulated is not well understood. In this thesis, I describe a screen for genes involved in cilia formation and function.

While optimising ciliogenesis and immunofluorescence protocols for the screen, the phenotypes of two ciliary mutant cell lines were analysed. *Wdr35*$^{yet/yet}$ and *Dync2h1*$^{pol/pol}$ mouse lines were identified in an ENU screen for genes involved in early development, and shown to have gross phenotypes similar to other ciliary mutants (Mill *et al.* 2011). Intraflagellar transport (IFT) is the active transport of proteins up and down the ciliary axoneme. Dync2h1 is a retrograde IFT motor component, whereas Wdr35 is part of the retrograde IFT-A complex. In this thesis, the cellular phenotypes of mouse embryonic fibroblasts derived from these mutants are described, showing that despite the fact both genes are thought to be involved in retrograde IFT, they show distinct ciliary phenotypes, suggesting novel roles for Wdr35 in mouse ciliogenesis.

An siRNA screen was carried out in mouse fibroblasts to identify genes involved in (i) **cilia formation**, assayed by immunofluorescence for ciliary markers, and (ii) **cilia function**, assayed by activity of a Hh responsive luciferase transgene as an indirect readout of ciliary function. Although scalable, I initially screened a small test set of thirty-six putative cilia candidates, identified by cross species transcriptomic analysis. We identified several possible hits, many of which were in the ciliome database but also importantly, several genes with no known link to ciliogenesis. Repeats, correlation of phenotype to knockdown efficiencies and localisation studies validated two hits, *Ccdc63* and *Azi1*. *Ccdc63* is a novel coiled-coil gene with no previous link to ciliogenesis; the phenotype for this gene was analysed in real time using fluorescently tagged ciliary markers.

A second hit, *Azi1,* was followed up in more detail. The reduction in ciliogenesis upon *Azi1* knockdown was confirmed with separate siRNAs, and was rescued by overexpressing siRNA insensitive Azi1-GFP, confirming the phenotype is not due to off-target effects of the siRNAs. *Azi1* gene trap mutant mice were generated and confirmed to be null mutations. Surprisingly, the mice survive, showing *Azi1* is not essential for mammalian ciliogenesis. However, mutant males are infertile, with highly reduced sperm count and sperm abnormalities indicative of an arrest at Stage IX of spermiogenesis, when the flagellum, a highly specialised motile cilium, forms. The small number of sperm that do get to the epididymus are immotile. We suggest *Azi1* is essential to in the formation of the sperm flagella and male fertility.

Abbreviations

%	Percent
ºC	Degrees Celsius
β-ME	β-mercaptoethanol
γ-H2AX	Histone H2A (p139)
5HT6	5-hydroxytryptamine receptor 6
aa	Amino acid
AMV	Avian myeloblastosis virus
aPKC	Atypical protein kinase C
Arf4	ADP-ribosylation factor 4.
Arl3/6/13b	Arf-like protein 3/6/13b
ASAP1	Arf/GAP with SH3 domain, ankyrin repeat and PH domain 1
ATCC	American tissue culture collection
Atm	Ataxia telangiectasia mutated homolog
Atr	Ataxia telangiectasia and Rad3 related
AurA	Aurora A kinase
Azi1/Cep131	Induced upon 5-aza-cytidine treatment / Centrosomal protein 131
BBS	Bardet-Biedl syndrome
BCA	Bicinchronic acid
Brca1/2	Breast cancer 1/2
BrdU	Bromodeoxyuridine
BSA	Bovine serum albumin
C57BL/6	C57 Black 6
Ca^{2+}	Calcium
Ccdc63/114/151	Coiled-coil domain containing protein 63/114/151
Cda	Cytidine deaminase
Cdk2	Cyclin dependent kinase 2
cDNA	Complimentary DNA

CEACAM-1	Carcinoembryonic antigen-related cell adhesion molecule-1
CED	Cranioectodermal dysplasia
Cent	Centrosome
Cep110/131/290/151/164	Centrosomal protein 131/290/151/164
Ci	Cubitus interuptis
CLS	Ciliary localisation signal
CMV	Cytomegalovirus
Cng1b	Cyclic nucleotide gated channel 1b
COPI/II	Coat protein I/II
Cos2	Costal 2
Crb3	Crumbs homologue 3
Ctnnb1	Catenin, beta 1
CV	Ciliary vesicle
Daf-19	Abnormal dauer formation gene 19
DAPI	4',6-diamidino-2-phenylindole
Dhh	Desert hedgehog
DIC	Differential interference contrast
DMSO	Dimethyl sulfoxide
DNA	Deoxyribonucleic acid
dNTP	Deoxyribonucleotide triphosphate
DSB	Double strand break
dsRNA	Double stranded RNA
Dvl1	Dishevelled 1
Dyf	Dye filling
Dync2h1	Cytoplasmic dynein 2 heavy chain 1
Dync2li1	Cytoplasmic dynein 2 light chain 1
E	Embryonic day
Ebp4.1l4b	Erythrocyte protein band 4.1-like 4b
ECL	Enhanced chemical luminescence
EDTA	Ethylene diamine tetraacetic acid
eGFP	Enhanced green fluorescent protein

EGTA	Ethylene glycol tetraacetic acid
EM	Electron microscopy
ENU	N-ethyl-N-nitrosourea
ES	Embryonic stem cells
Ery	Erythrocytes
EUCOMM	European Conditional Mouse Mutagenesis Program
Evc2	Ellis van Creveld syndrome protein 2
FABB	Flagellar apparatus-basal body proteome
FACS	Fluorescence-activated cell sorting
Fam92a/b	Family with sequence similarity 92, member a/b
Faps	Flagella associated proteins
FCS	Fetal calf serum
Fgf8	Fibroblast growth factor
FlnA	Filamin A
Foxj1	Forkhead box J 1
FRAP	Fluorescent recovery after photobleaching
Frz	Frizzled
Fu	Fused
Fuz	Fuzzy
g	Gravity
GAP	GTPase accelerating protein
Gapdh	Glyceraldehyde 3-phosphate dehydrogenase
gDNA	Genomic DNA
GDP	Guanosine diphosphate
GEF	Guanine nucleotide exchange factor
GFP	Green fluorescent protein
Gli1/2/3	Glioma-associated oncogene homologue 1/2/3
$Gli3^{A}$	Gli3 activator
$Gli3^{FL}$	Gli3 full length
$Gli3^{R}$	Gli3 repressor
Gmap210	Golgi microtubule associated protein 210

GOI	Gene of interest
GPCR	G-protein coupled receptors
GPI-FP	Glucosylphosphatidylinositol-fluorescent protein
Gt	Gene trap
Gtl3	Gene trap locus protein 3
GTP	Gaunosine triphosphate
h	Hours
H&E	Haemotoxylin and eosin
Hdac6	Histone deacteylase 6
HEF1	Human enhancer of filamentation 1
HEFs	Human embryonic fibroblasts
Hh	Hedgehog
HRP	Horse radish peroxidase
hTERT-RPE	Human telomerase reverse transcriptase immortalised – retinal pigmented epithelial cell line
HTR6	5-hydroxytryptamine (serotonin) receptor 6.
HU	Hydroxyurea
IHC	Immunohistochemistry
Ihh	Indian hedgehog
IF	Immunofluorescence
IFT	Intraflagellar transport
IGMM	Institute of Genetics and Molecular Medicine
IMCD3	Inner medullary collecting duct 3 cell line
IMPACT	Infectious Microbe PCR Amplification Test
Inpp5e	Inositol polyphosphate- 5-phosphatase
Int	Inturned
Inv	Inversin
JATD	Jeune asphyxiating thoracic dystrophy
JBS	Joubert syndrome
Kb	Kilobase
Kif3a/3b/7/13/17	Kinesin family member 3a/3b/7/13/17

LB	Luria-Bertani
LC-MS	Liquid chromatography-mass spectrometry
Lrrc48	Leucine-rich repeat-containing protein 48
M	Molar
MAP	Microtubule associated proteins
Mch1r	Melanin-concentrating hormone receptor 1
MDCK	Manin-Darby canine kidney cell line
MEFs	Mouse embryonic fibroblasts
MeOH	Methanol
MFD	Maximum feret diameter
min	Minutes
miRNA	Micro RNA
MKS	Meckel syndrome
Mllt4	Myeloid/lymphoid or mixed-lineage leukemia translocated to 4 gene / Afadin
MN	Micronucleated
MRC HGU	Medical Research Council, Human Genetics Unit
mRNA	Messenger RNA
ms	Milliseconds
MTOC	Microtubule organising centre
MudPIT	Multi-dimensional protein identification technology
NEAA	Non-essential amino acids
Nek1	NIMA-related kinase 1
Nesprin2	Nuclear envelope spectrin repeat protein 2
NIMA	Never in mitosis protein a
NLS	Nuclear localisation signal
Nme7	Non-metastatic cells protein 7
NPC	Nuclear pore complex
NPHP	Nephronopthisis
Nphp1-12	Nephrocystin 1-12
NPI	Normalised percentage index
nt	Nucleotide

NVP	Nodal vesicle particle
Oda16	Outer dynein arm protein 16
ODF	Outer dense fibres
Ofd1	Oral-facial digital protein 1
Orpk	Oak ridge polycystic kidney mouse
Osm3	Osmotic avoidance protein 3
p	Phospho
P	Days post-partum
Pals	Protein associated with Lin-7 1
Par3/6	Protease activated receptor 3/6
Patj	Pals1-associated tight junction protein
PBS	Phosphate buffered solution
PCD	Primary ciliary dyskinesia
Pcdh15/24	Protocadherin 15/24
PCM	Pericentriolar material
PCMD	Periciliary membrane domain
PCP	Planar cell polarity
PCR	Polymerase chain reaction
PDGF	Platelet derived growth factor
PDXL	Podocalyxin
PE	Pre-extraction
PFA	Paraformaldehyde
pH	Potential hydrogen
PI	Propidium iodide
PKD	Polycystic kidney disease
PKD1/2	Polycystin 1/2
Plk4	Polo-like kinase 4
PM	Plasma membrane
PMSF	Phenylmethanesulfonylfluoride
Pp3r1	Protein phosphatase 3 regulatory subunit 1
Prdm1/2	PR domain containing protein 1/2

PRE	Pericentriolar recycling endosome compartment
Prkra1	Protein kinase, interferon-inducible double stranded RNA dependent activator 1
Ptc	Patched
Ptch1/2	Patched homologue 1/2
PTM	Post-translational modification
PVDF	Polyvinylidene difluoride
qPCR	Quantitative PCR
qRT-PCR	Quantitative reverse transcription PCR
RA	Retinoic acid
Rab	Member of Ras oncogene family
Ras	Rat sarcoma virus oncogene
Ret	Reticulocytes
Rfx	Regulatory factor X
RNA	Ribonucleic acid
RNAi	RNA interference
Rp2	Retinitis pigmentosa protein 2
Rpm	Rotation per minute
RT	Reverse transcriptase
RT-PCR	Reverse transcription-PCR
SAGE	Serial analysis of gene expression
Sdccag8	Serologically defined colon cancer antigen 8
SDS	Sodium dodecyl sulfate
SDS-PAGE	Sodium dodecyl sulfate polyacrylamide gel electrophoresis
sec	Seconds
Shh	Sonic hedgehog
shRNA	Short hairpin RNA
siRNA	Short interfering RNA
Slc46a2	Solute carrier family 46, member 2/Tscot
Smo	Smoothened
SNARE	Soluble NSF Attachment Protein Receptor
Spag1	Sperm associated antigen 1

SRP	Short rib polydactyly
ss	Serum starved
Sstr3	Serotonin receptor 3
SuFu	Suppressor of Fused
TBE	Tris/Borate/EDTA buffer
Tbp	Tata binding protein
TBS	Tris Buffered Solution
TBSt	TBS with 0.05% Tween-20
TBST	TBS with 0.1% Triton X
Tcte3	T-complex-associated testis expressed 3
Tctex1d1/2/4	T-complex-associated testis expressed domain containing protein 1/2/4
Tctn1/2	Tectonic 1/2
TE	Tris-EDTA buffer
Tekt2	Tektin2
TEM	Transmission electron microscopy
Tmem	Trans membrane protein
TPB	Triptose phosphate broth
TPR	Tetratricopeptide repeat
Tram-1a	Translocating-chain-associating membrane protein
TRAPPII	Transport protein particle II
Tscot	Thymic stromal cotransporter / Slc46a2
Ttll	Tyrosine tubulin ligase like
Ttc26/28/30a1/30a2/30b	Tetratricopeptide repeat protein 26/28/30a/30b
TZ	Transition zone
U	Units
UPL	Universal Probe Library
UTR	Untranslated region
UV	Ultraviolet
v/v	Volume to volume
WB	Western blot

Wdr15/35/60/78	WD repeat containing protein 16/35/60/78
w/v	Weight to volume
Zmynd10	Zinc finger, MYND domain containing protein 10

Table of Contents

List of Figures

List of Tables

Chapter One. Introduction.

1.1 Cilia Structure

Cilia are organelles that protrude from the surface of almost all mammalian cells. A central axoneme of nine outer microtubule doublets extends from the basal body at the base of the cilia, and is surrounded by a highly specialised extension of the cell membrane (Figure 1.1). There are two main types of cilia, motile and immotile; in general, motile cilia have an additional central pair of singlet microtubules ((9+2) structure), which is absent from most immotile, or primary cilia (9+0). Flagella and cilia have essentially the same ultrastructure and the terms are often used interchangeably, with flagella usually referring to longer, motile structures such as seen in the mammalian sperm. Cells with motile cilia can have a single cilium, often for propulsion *eg.* sperm, or multiple cilia, which beat in a coordinated fashion to generate fluid flow *eg.* bronchial epithelia. In contrast, primary cilia are found singly, and are present on almost all non-dividing mammalian cells.

Although the structure of mammalian primary cilia was described by detailed electron microscopy (EM) studies in the 1960s (Sorokin, 1962; Sorokin, 1968), for many years the functional role of primary cilia was not fully appreciated and they were widely regarded as vestigial organelles. Recent studies have since highlighted the importance of primary cilia in developmental signalling; in particular their requirement for mammalian development and involvement in a group of human diseases, termed ciliopathies (Hildebrandt et al., 2011). This has led to a resurgence in interest in these fascinating organelles. This central involvement in several signalling pathways, including Hedgehog (Hh) signalling, calcium sensing, platelet derived growth factor (PDGF) and Wnt pathways, has led to the analogy of the cilium as the cell's antenna, in which the cilium detects and integrates extracellular signals and transduces these signals to the cell (Singla and Reiter, 2006).

At the cilium core is a microtubule based axoneme, made up of nine microtubule doublets, with or without a central pair, surrounded by a highly specialised ciliary

membrane (Manton and Clarke, 1952; Manton 1957; Fawcett and Porter 1954). This is templated from the basal body, a microtubule organising centre (MTOC), analogous to the centriole (Sorokin 1962; Sorokin 1968). When a cell enters G_1/G_0, ciliogenesis is initiated and the mother centriole migrates to the cell surface, acquiring several appendages and modifications to become the basal body (Rieder et al., 1979; Tucker et al., 1979). The basal body has a core structure consisting of nine microtubule triplets composed of A, B and C fibres and the microtubules of the ciliary axoneme extend from the A and B fibres, giving rise to the microtubule doublets (Allen, 1969, Sorokin 1962; Sorokin 1968) (Figure 1.1). The basal body acts as an interface between the cilia and the cell body, as well as a docking area for proteins involved in cilia formation and maintenance (Deane et al., 2001). The area bridging the basal body and main axoneme is named the transition zone (Czarnecki and Shah, 2012). Here the triplet microtubules of the basal body "transition" to the doublet microtubules of the axoneme (Andersen, 1972; Gilula and Satir, 1972). This structure is thought to play key roles in regulating what enters and leaves the cilium, allowing it to function as a specialised signalling antenna (Craige et al., 2010; Williams et al., 2011; Garcia-Gonzalez et al. 2011) (See 1.5.2). The formation and maintenance of cilia requires an active process known as intraflagellar transport (IFT), which uses motors to transport proteins into and out of the cilium: a heterotrimeric kinesin 2 motor transports proteins to the tip of cilia (anterograde IFT), whereas a cytoplasmic dynein motor transports proteins back to the base of the cilium (retrograde IFT) (See Figure 1.1 and 1.3.1) (Ishikawa and Marshall, 2011; Kozminski et al., 1995; Kozminski et al., 1993b; Pazour et al., 1999; Rosenbaum and Witman, 2002)

1.1.1 Structure of motile cilia/flagella

As well as the presence of the central pair, motile cilia have other structural additions: dynein arms are present on the outer microtubule doublets of motile cilia and radial spokes project from the outer microtubule doublets towards the central pair (Figure 1.1). These structures are involved in the beating movement of motile cilia or flagella (Lechtreck et al., 2008; Randall et al., 1964; Sapiro et al., 2002), with

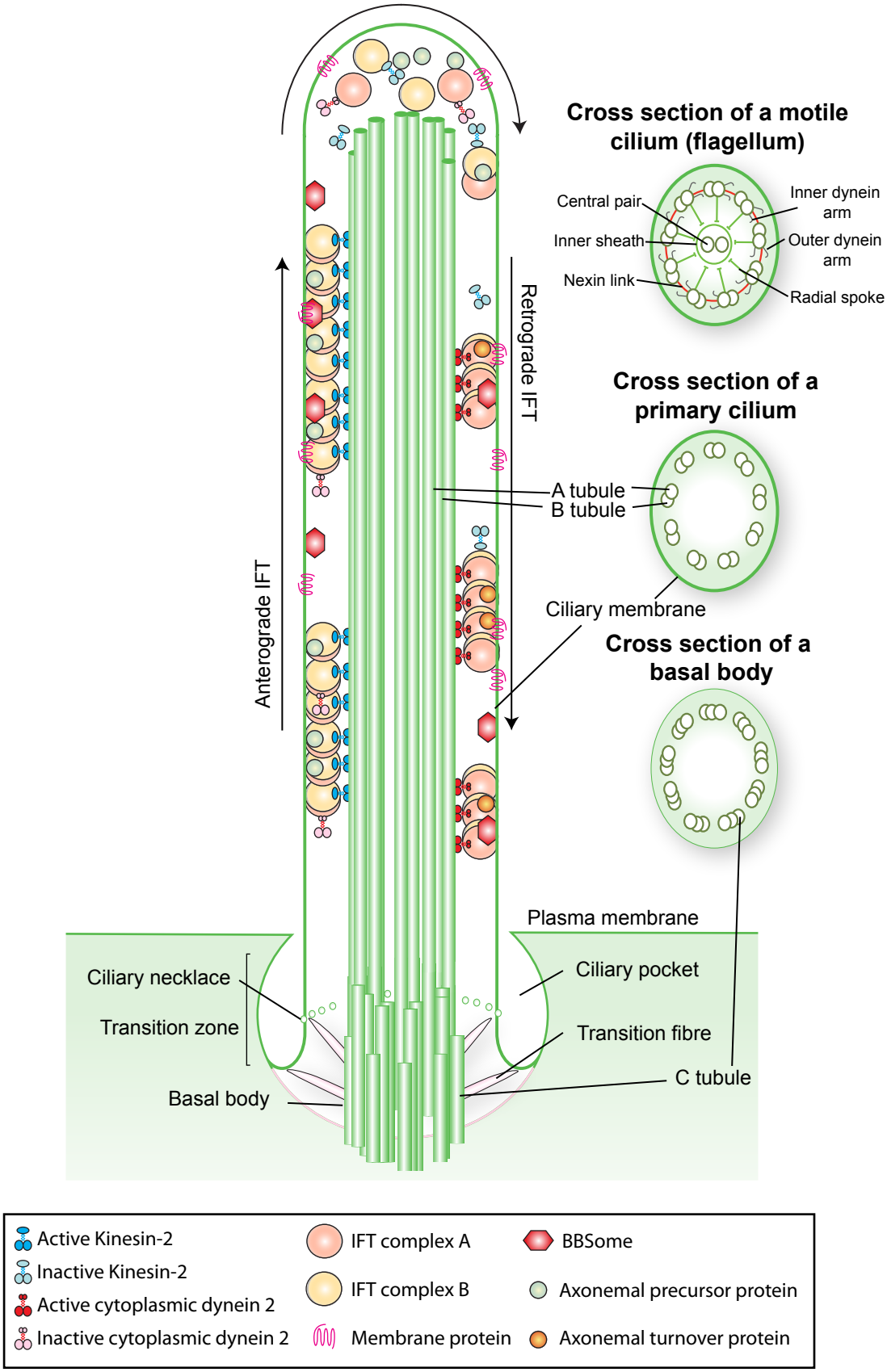

Figure 1.1 Cilia Structure

Figure 1.1 Cilia Structure. Schematic of cilia structure, illustrating the microtubule based axoneme. Cross sections show the 9 microtubule doublets found in both primary and motile cilia. Motile cilia also have an extra central microtubule pair. The basal body is analogous to the centriole and consists of 9 triplet microtubules. The microtubules of each triplet are labelled A, B and C. Triplet C terminates at the transition zone and microtubules A and B continue, nucleating the doublet microtubules of the ciliary axoneme. The cilium is surrounded by a specialised membrane which is distinct from the plasma membrane. Some cilia are found partially within an invagination of the plasma membrane, known as the ciliary pocket. Intraflagellar transport (IFT) is the active process by which proteins enter and leave the cilium. Anterograde IFT (from base to tip) is driven by the heterotrimeric kinesin 2 motor. Retrograde IFT (from tip to base) is driven by a cytoplasmic dynein 2 motor. IFT particles associate with the IFT motors and are involved in cargo attachment and are thought to link the IFT motors to the ciliary membrane. IFT proteins are found in two complexes, IFT-B which bind to the anterograde IFT motor, and IFT-A which bind to the dynein retrograde motor. The anterograde kinesin motor also transports IFT-A proteins and an inactive form of the dynein retrograde motor. Many motors link to form IFT trains: anterograde IFT trains are longer than retrograde trains. At the distal tip, cargo is released and remodelling of trains occurs. The kinesin 2 motor is inactivated and the dynein motor is activated. Retrograde IFT trains form, which are shorter but more abundant than anterograde IFT trains. Retrograde IFT transports IFT-A particles (bound directly), IFT-B particles, inactive kinesin motors and recycled cargo back to the base of the cilium. It is thought the BBSome may act as an adaptor to bind cargo to IFT particles. (Adapted from Ishikawa and Marshall, 2011)

the dynein arms facilitating microtubule sliding and causing the cilia to bend with a characteristic pattern (Silflow and Lefebvre, 2001).

1.2 Evolution of cilia

As cilia/flagella are ancient organelles present in all major eukaryotic groups it is highly likely they were present on the last common ancestor of eukaryotes (Carvalho-Santos et al., 2011; Cavalier-Smith, 2002; Jekely and Arendt, 2006). It is thought the cilium evolved by adaptation of existing structures, involved in microtubule organisation as well as membrane trafficking (Carvalho-Santos et al., 2011; Jekely and Arendt, 2006). Cilia and flagella are known to be involved in motility as well as sensory functions. The nine-fold symmetry of the centriole/basal body and the axoneme is thought to have evolved to optimise cilia motility.

In addition to the molecular motors, many proteins are involved in actively transporting proteins into and out of cilia via IFT, including multimeric complexes of proteins, known as IFT proteins, which bind to these motors and act as scaffolds for cargo binding (Rosenbaum and Witman, 2002). Several of these IFT proteins show homology to components of coat protein I (COPI) and clathrin coated vesicles, which are involved in directed vesicular trafficking (Avidor-Reiss et al., 2004; Jekely and Arendt, 2006). Jekely and Arendt, (2006) proposed therefore that as IFT and cilia co-evolved, perhaps cilium evolution began with ancestral IFT proteins transporting transmembrane proteins to a membrane patch, allowing concentration of signalling receptors and so enhanced sensory functions. This then evolved into the distinct ciliary axoneme and membrane seen today, which is known to concentrate receptor proteins (Nachury et al., 2007; Singla and Reiter, 2006), and this structure subsequently developed motility (Jekely and Arendt, 2006). Although it is likely that the ancestral cilium did have sensory functions, it is not yet clear whether the sensory functions definitely preceded the motility (Carvalho-Santos et al., 2011). IFT proteins can no longer form curved membrane coats or function in vesicle budding, but they can still form flattened coat complexes to transport cargo into and out of the ciliary compartment, thus directly linking the IFT motors moving along the axoneme to the ciliary membrane.

During ciliogenesis, the centriole migrates to the plasma membrane and becomes the basal body, a structure at the base of cilia which templates the axoneme. In animals, the centriole is also involved in cell division as part of the centrosome, by organising microtubules at the spindle poles, as well as nucleation of the ciliary axoneme. All species with centrioles also have cilia, however not all species with centrioles have a centriole-containing centrosome, suggesting the original centriole function would be to nucleate ciliary axonemes. It has been suggested that centrioles are not essential for cell division, and the reason they localise to spindle poles is to enable equal inheritance of the centrioles themselves to daughter cells (Pickett-Heaps, 1974). There are examples of cell division without centrioles. For example it is possible to generate adult flies lacking centrioles, although they are required for the early embryonic divisions (Basto et al., 2006). However, the important role of centrioles in animal cell division suggests they have since acquired functional roles in this

process, such as setting the axis of division and positioning the spindles correctly (Carvalho-Santos et al., 2011; Debec et al., 2010).

The core structural components of cilia and flagella are highly conserved throughout eukaryotes, and so structural studies in model organisms such as *D. melanogaster, C. elegans, T. brucei* and *C. reinhardtii* have been highly informative and relevant to the mammalian system in most cases.

Despite this remarkable conservation of the core microtubule-based ciliary structure throughout eukaryotes, considerable diversity in cilia structure has evolved, both between and within species. Mammalian cilia can be motile or immotile. They can vary in length from ~3-10μm for primary cilia, 50-150μm for sperm flagella to >200μm for olfactory cilia. They can vary in shape, with the connecting cilia of rod and cone photoreceptors showing distinctive variations in shape. Although most mammalian cells are ciliated, other organisms only possess cilia on restricted cell types. For example, *C. elegans* possess only non-motile sensory neural cilia on 60 of their 302 neurons whereas *D. melanogaster* also have sensory neural cilia as well as motile sperm flagella. These sensory neural cilia in *D. melanogaster* and *C. elegans* have evolved elaborate, highly specialised structures, which enhance their ability to perform sensory functions such as proprioception, photoreception, chemosensation and mechanosensation. Unlike in mammals, where lack of cilia is lethal, in *C. elegans* and *D. melanogaster,* cilia are not essential for development (Han et al., 2003; Perkins et al., 1986; Cole et al., 1998); therefore these organisms lend themselves to studies of these structures without the complications of lethality. However, as discussed below, important functional roles of mammalian cilia, such as involvement in developmental signalling pathways are not always conserved to *D. melanogaster* or *C. elegans*, highlighting the importance of cross-species approaches to understanding ciliary biology.

1.3 Building a cilium

1.3.1 Intraflagellar transport

In order to understand cilia function, it is important to understand how cilia are formed and maintained. Cilia elongation from the basal body requires an active process, intraflagellar transport (IFT), which transports proteins into and out of the cilium (Figure 1.1). As no protein synthesis occurs in cilia, IFT transports proteins to the tip of the cilium where cilia elongation occurs, then back down the cilium where the proteins are recycled back into the cilia, degraded or transported elsewhere in the cell (reviewed in (Ishikawa and Marshall, 2011; Rosenbaum and Witman, 2002)). This process was originally identified and studied in *Chlamydomonas reinhardtii,* a single-cell green alga with two flagella which are essential for motility. Particles were observed trafficking up and down the *Chlamydomonas* flagella by differential interference contrast (DIC) microscopy, independently of flagellar beating, in trains moving at 2.0 ±5um/s up the flagella and smaller particles moving at 3.5 ±0.7um/s back down the flagella (Kozminski et al., 1995; Kozminski et al., 1993b). These particles were correlated with raft-like structures observed by transmission electron microscopy connected to both the B tubule of the outer microtubule doublets of the axoneme and the flagellar membrane (Kozminski et al., 1995).

Analysis of the *Chlamydamonas* temperature sensitive *fla-10*^{ts} mutants, which fail to form flagella at the restrictive temperature, identified FLA-10 as being required for anterograde IFT. This gene was subsequently shown to encode the orthologue of mammalian Kif3a, a subunit of the heterotrimeric kinesin-II motor, identifying kinesin-II as the motor which drives anterograde IFT (Cole et al., 1993; Cole et al., 1998; Kozminski et al., 1995; Walther et al., 1994). Retrograde IFT is powered by a specialised cytoplasmic dynein motor; when subunits of this motor dynein 2 (previously cytoplasmic dynein 1b) are mutated, IFT particles build up in the flagella, entering by anterograde IFT but unable to exit without retrograde IFT (Pazour et al., 1999; Pazour et al., 1998; Signor et al., 1999; Wicks et al., 2000). It has since been shown that a second kinesin motor, Osm-3, a homodimeric kinesin

motor is involved in anterograde IFT in *C. elegans*, although it may only have a role in certain specialised cilia. Studies in *C. elegans* suggest it is specifically involved in building the distal tip of the sensory cilia which have a singlet microtubule-based structure. *C. elegans* mutant for subunits of the heterotrimeric kinesin-II motor (*Klp-11* and *Kap-1*) have normal length sensory cilia due to the partially redundant function of Osm3 (Evans et al., 2006; Mukhopadhyay et al., 2007; Pan et al., 2006; Snow et al., 2004).

The motors carry IFT particles, which can be biochemically purified into two complexes, IFT-A and IFT-B. The IFT particles consist of at least 20 proteins, 6 in IFT-A (IFT143, 121, 122, 139, 140 and 144) and 14 in IFT-B (IFT20, 22, 25, 27, 46, 52, 54, 57, 70, 74, 80, 81, 88 and172) (reviewed in (Ishikawa and Marshall, 2011). The dynein motor links directly to IFT complex A, with the Kinesin-II motor binding to IFT B particles (Cole *et al.*1998). The dynein motor is carried to the tip of the cilium by anterograde IFT and conversely, kinesin-II motors are recycled back to the ciliary base by retrograde IFT (Figure 1.5). A recent study using electron tomography on *Chlamydomonas* flagella has identified two distinct classes of IFT trains, one less dense about 700nm long, and one shorter (250nm) and more electron dense (Pigino et al., 2009). Using a *Chlamydomonas fla14* mutants, which have a mutation in LC8, a component of flagellar and cytoplasmic outer dynein arms, and lack retrograde IFT they were able to dissect the nature of these trains. The shorter trains are retrograde IFT trains as they are missing in *fla14* retrograde mutants, whereas the longer trains are anterograde IFT trains, which accumulate in *fla14* mutants. Both these trains have repeating subunits although they differ in size, 40nm in anterograde trains and 16nm in retrograde trains, possibly representing differing IFT cargo (Pigino et al., 2009). Active remodelling of cargo occurs at ciliary tip, where cargo is released from the kinesin motor, and new cargo reattached to dynein motors for transport back to the cell body (Iomini et al., 2001).

Even when the cilium is at full length, the tip of the cilium is incredibly dynamic, with tubulin subunits continually turning over in a process that requires IFT, therefore it is highly likely IFT is primarily involved in the transport of the structural building blocks of the cilium to the tip (Marshall and Rosenbaum, 2001; Song and

Dentler, 2001; Stephens, 1997). Interestingly, disassembly of tubulins at the tip is also an active process which requires kinesin-13 (Blaineau et al., 2007; Dawson et al., 2007; Piao et al., 2009). As well as transporting individual building blocks to the ciliary tip, IFT has also been shown to transport large multiprotein complexes found in motile cilia and flagella, such as dynein arms and radial spokes to the ciliary tip (Hou et al., 2007; Qin et al., 2004). It was shown that partially assembled 12S radial spokes complexes are transported up flagella by anterograde IFT, and then fully assembled 20S radial spoke complexes are recycled back down the flagellum by retrograde IFT, demonstrating both anterograde and retrograde IFT is involved in transport of large multiprotein complexes (Qin et al., 2004). Transporting proteins in complexes reduces the number of modules needed to attach to IFT trains and so reduces the complexity. IFT trains likely use adapter proteins to facilitate binding of cargo, such as Outer dynein arm 16 (Oda16), which links the dynein arms to the IFT machinery (Ahmed et al., 2008; Gao et al., 2010).

As well as proteins involved in ciliary structural maintenance, other proteins such as those involved in signalling and sensory pathways, which are discussed in detail below, are also transported via IFT (Huang et al., 2007; Qin et al., 2005) and many of these may well be cell-type specific cargo. The control of the loading and unloading of cargo onto the IFT motors, both at the base and the tip of the cilium, is not well understood, but will almost certainly play an important role in controlling cilia function.

Many IFT proteins have been shown to be highly conserved and essential for ciliogenesis in several ciliated organisms (Avidor-Reiss et al., 2004) including *C. elegans* (Cole et al., 1998), *D. rerio* (Sun et al., 2004) and *M. musculus* (Huangfu et al., 2003; Pazour et al., 2000). In addition, IFT has been imaged in real time in *C. elegans* (Orozco et al., 1999) and *M. musculus* (Follit et al., 2006; Tran et al., 2008), further demonstrating that it is a conserved process in many diverse organisms. However, cilia/flagella can be formed without IFT, for example the sperm axoneme of *D. melanogaster* and the flagella of *P. falciparum* which are formed in the cytosol, independent of IFT (Avidor-Reiss et al., 2004).

The conservation of the role of Osm-3, the homodimeric kinesin as an accessory anterograde IFT motor, is less clear. Function of heterotrimeric kinesin-II Kif3a/Kif3b/Kap1, the canonical anterograde motor is conserved in all ciliated organisms examined. However, Osm3 function is thought not to be conserved in *Chlamydomonas*, where kinesin-II is thought to be the only anterograde IFT motor (Cole et al., 1998; Fan et al., 2010; Kozminski et al., 1995; Kozminski et al., 1993b). In *C. elegans,* Osm-3 is involved in IFT at the distal-most tips of sensory cilia. In zebrafish, contradictory reports suggest the vertebrate orthologue, *Kif17*, may be involved in formation of some specialised cilia, although the exact role, and in which specialised cilia is unclear (Insinna et al., 2009; Insinna et al., 2008; Zhao et al., 2012). In mammalian cell culture, Kif17 localises to cilia, dependent on a ciliary localisation sequence (CLS) (Dishinger et al., 2010) and it was suggested that Kif17 is required for ciliary targeting of olfactory CNG channels (Jenkins et al., 2006) However, the mouse *Kif17* knockout shows memory defects due to neuronal functions, without mention of a ciliary function (Yin et al., 2011), so the function of Kif17 in vertebrate ciliogenesis is still under investigation.

1.3.2 Formation of specialised cilia

The control of specialised cilia formation is not well understood. Some specialised cilia such as sperm flagella in *D. melanogaster* as well as the flagella of the *P. falciparum* microgamete do not require IFT for formation, and are formed by an alternative cytosolic pathway. However, most specialised cilia do require IFT for their formation, meaning other differences must exist to result in the wide variety of specialised structures which can be formed. These differences could involve modifications to the IFT process, affecting speed, choice of motors used or variation of the cargo loaded onto the motors.

Further upstream, control of the expression of specific genes involved in certain specialised cilia could lead to the diverse structures seen. For example, Foxj1, a transcription factor, has been shown to be a master regulator of the motile ciliogenesic transcription cascade. Foxj1 was shown to be necessary and sufficient

for motile ciliogenesis in zebrafish and *Xenopus* (Stubbs et al., 2008; Yu et al., 2008). *Foxj1* is expressed in tissues with motile cilia (Blatt et al., 1999; Brody et al., 2000; Hackett et al., 1995; Lim et al., 1997), and *Foxj1*$^{-/-}$ mice show left-right asymmetry defects, hydrocephalus and lack motile cilia in the nasal epithelium (Brody et al., 2000; Jacquet et al., 2009). Although multiple basal bodies are formed, these fail to dock at the apical membrane (Huang et al., 2003), suggesting Foxj1 may control genes involved in basal body docking.

Recently, a novel coiled-coil protein Multicilin was shown to shown to be necessary and sufficient to drive the multiciliated differentiation transcriptional programs in *Xenopus* skin and mouse airways, including induction of *FoxJ1* expression (Stubbs et al 2012). In addition to expression of motility related machinery, Multicilin also induced expression of genes necessary for centriole assembly required for massive waves of multiciliation characteristic of cells lining airways, brain ventricles and the female reproductive tract.

Additional layers of developmental complexity may be involved in the formation of specialized cilia. In the case of formation of the mammalian sperm flagella, the players and process of IFT, including its motors, have been implicated in more than one step of mammalian sperm flagella formation. During spermatogenesis, complex morphological changes occur, including loss of cytoplasm, condensation and remodelling of the nucleus and formation of the highly specialised motile flagellum. This involves the formation of a transient microtubule-based structure known as the manchette which is involved in trafficking components to the sperm flagella, known as intramanchette transport as well as shaping the sperm head (Kierszenbaum 2001; Kierszenbaum and Tres 2004). Ift88 has been localised to the manchette and motors similar to those involved in IFT have been implicated in intramanchette transport (Kierszenbaum et al. 2001). *Ift88*^{orpk} mice show male infertility and Kierszenbaum at al. (2001) suggest this is due, at least in part, to defective intramanchette transport leading to impaired flagellar formation.

Certain cilia appear to be more susceptible to perturbations than others, with mutations in many globally expressed and ciliary localised components such as Nphp and BBS proteins lead to restricted defects in specialised cilia such as those present

in the kidney, sperm and photoreceptors, while primary cilia appear unaffected (Fath et al. 2005; Jiang et al. 2008; Mollet et al. 2005; Mykytyn et al. 2004; Nishimura et al. 2004; Won et al. 2011). This could suggest these proteins have roles which can be compensated for in primary cilia, but when forming elaborate specialised cilia, functional compensation for loss of proteins is not so easily achieved. Alternatively, these proteins could have specific non-redundant roles in certain specialised cilia, which may not be required for primary ciliogenesis.

1.3.3 Microtubule Post Translational Modifications

The scaffold of microtubules underlying the basal bodies and axoneme is not static. It is made up of polymerised α and β tubulin subunits, and several tubulin post-translational modifications (PTMs) including acetylation, polyglutamylation, polyglycylation and detyrosination, concentrate at the basal body and axoneme to varying extents (Bre et al., 1994; LeDizet and Piperno, 1991; Verhey and Gaertig, 2007). This enrichment means antibodies to such PTMs are useful as good immunofluorescent markers for cilia studies. These PTMs are associated with older, more stable microtubules, but *in vivo* these PTMs do not increase microtubule stabilisation and so perhaps are marks of microtubules stabilised by another method (Maruta et al., 1986; Webster et al., 1990).

Acetylation was one of the first PTMs identified as enriched at microtubules but it does not seem to be required for ciliogenesis (Gaertig et al., 1995; Kozminski et al., 1993a). Tubulin deacetylase *Hdac6* was shown to be involved in cilia disassembly in mammals but it deacetylates other substrates in addition to tubulin so it is not clear if this disassembly is directly due to tubulin deacetylation (Hubbert et al., 2002; Kovacs et al., 2005; Zhang et al., 2007b).

Polyglutamylation and polyglycylation of tubulin are highly enriched at axonemes, where polyglycylation of tubulin is confined to cilia and flagella in most cell types (Bre et al., 1994). Depletion of *Ttll* (*Tubulin tyrosine ligase-like*) genes, involved in catalysing tubulin glutamylation, can lead to impaired basal body maturation, and injection of anti-glutamylated tubulin antibody into HeLa cells leads to centriole

disassembly suggesting glutamylation may have a role in centriole/basal body assembly (Bobinnec et al., 1998; Wloga et al., 2008). Glutamylation may also have roles in flagella motility (Gagnon et al., 1996; Janke et al., 2005). Glycylation is also thought to have a role in ciliogenesis; morpholinos to *Ttll3*, an enzyme involved in glycylating tubulin, leads to decreased glycylation, and defective motile and primary cilia. Interestingly, decrease in glycylation leads to increase in glutamylation, perhaps as they compete for sites on tubulin, suggesting coordinated roles in cilia assembly and disassembly (Wloga et al., 2009). Consistent with this, morpholinos to *Ttll3*, involved in glycylating tubulin, and *Ttll6*, involved in glutamylating tubulin leads to more severe ciliary phenotypes in zebrafish than the single morphants (Pathak et al., 2011; Pathak et al., 2007). How tubulin PTMs affect ciliogenesis is not yet clear, but they could affect the dynamics of microtubule stability directly, the binding of microtubule associated proteins (MAPs) which may have roles in ciliogenesis, or the binding of microtubule-bound motors, which are involved in building the cilium (Verhey and Gaertig, 2007).

1.4 Cilia Function

Motile cilia have well established roles in mucus clearance in the lungs, as well as roles in cell propulsion demonstrated by the sperm flagella. Specialised primary cilia were also known to have roles in sensing light (in the photoreceptors) and sound (the kinocilium) (Bronshtein and Minor, 1977; Nakamura and Gold 1987; Singla and Reiter, 2006). Recent studies have implicated cilia in a wide range of diverse processes, including kidney development, generation of left-right asymmetry and developmental signalling, with particularly important roles in Hh signalling.

The study of cilia function has been guided by studies of human disease. The role of motile cilia in mammals was elucidated in the 1970s by the study of Kartegener syndrome, a syndrome presenting with pulmonary obstruction, chronic sinus

infection, randomised left-right asymmetry and male infertility. The observation that male infertility was due to immotile sperm flagella which lacked dynein arms lead to the discovery that the pulmonary obstruction and sinus infections were also due to immotile cilia, and the suggestion that left-right determination involved motile cilia (Afzelius, 1976; Camner et al., 1975). The discovery of a link between cilia and polycystic kidney disease (PKD) lead to the suggestion primary cilia play a role in fluid flow detection in the kidneys.

1.4.1 Cilia and fluid flow

Cilia have been shown to play important roles in both generation and detection of fluid flow. Mouse mutants of the anterograde IFT kinesin motor subunits, show defects in cilia formation. As a result of defects in nodal cilia, these mutants display randomised laterality, with 50% showing reversed heart looping (Marszalek et al., 1999; Nonaka et al., 1998; Takeda et al., 1999). The node is a specialised organising centre which forms transiently at the anterior of the primitive streak. Nodal cilia were shown to be motile and their motility sets up a leftward-flow in the node, termed nodal flow, key to left/right determination. This nodal flow was absent in kinesin mutants, which lack nodal cilia. Further supporting this hypothesis, *Inversus viscerum* mice (*Iv*), which have spontaneous mutation in the left-right dynein involved in motility, have grossly normal nodal cilia but these are immotile, so these mice lacked nodal flow and showed randomised symmetry defects (Okada et al., 1999). With the start of flow, there is a reorganisation of the node architecture including the posterior repositioning of cilia on the nodal cell and remodelling of the node pit. A circular clockwise rotation unique to nodal cilia continually refines and reinforces leftward nodal flow (Hirokawa et al., 2009; Okada et al., 2005).

Exactly how this nodal flow is detected and transduced to generate left-right asymmetries is still unclear, although there are two main hypotheses (Figure 1.2). One hypothesis states that a gradient of morphogens is generated by the leftward flow (Tanaka et al., 2005; Fliegauf et al., 2007). Candidate molecules have been

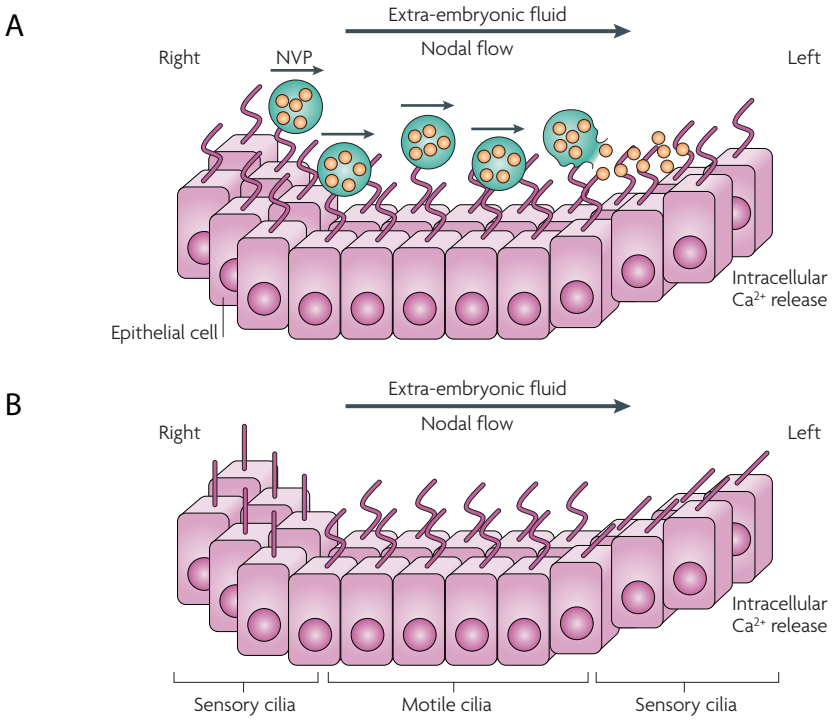

Figure 1.2 Detection of nodal flow. Two models exist for detection of nodal flow. (A) Nodal vesicle particles (NVP) model: NVPs encasing morphogens such as Shh and RA are propelled by the motile cilia of the node towards the left side of the node. The vesicles break open and the morphogens are released and detected, probably by transmembrane receptors on the non-motile cilia at the periphery of the node. (B) Two cilia model: The flow generated by the motile cilia is detected by the passive bending of the non-motile at the left periphery of the node. Both models result in intracellular Ca2+ release and downstream signalling leads to the breaking of symmetry. (Taken from Fliegauf et al., 2007).

suggested, for example Sonic hedgehog (Shh), Retinoic acid (RA) or Fibroblast growth factor 8 (Fgf8). These are packaged into lipid vesicles termed nodal vesicle particles enriched with Shh and RA, which are thought to release their cargo on the left wall of the node (Tanaka et al., 2005). However asymmetric distribution of endogenous morphogens has not been demonstrated in mammals.

The second hypothesis involves immotile cilia present in the periphery of the ventral node, and is known as the two cilia model (as it involves both motile and immotile cilia at the node) (McGrath et al., 2003; Fliegauf et al., 2007) (Figure 1.2). It is suggested that these immotile cilia may detect nodal flow and transduce this flow to the cell, leading to left-right asymmetry. The cation channel PKD2 has been localised to nodal cilia, *Pkd2* knockout mice show randomised left-right asymmetry suggesting it plays a role in left-right asymmetry (Pennekamp et al., 2002). *PKD2* is mutated in polycystic kidney disease (discussed below) and is suggested to have roles in flow sensing involving Ca^{2+} signalling upon ciliary bending (Nauli et al., 2003). Asymmetric calcium signalling is observed at the left margin of the node coincident with leftward flow, therefore it is suggested these immotile primary cilia are involved in mechanically detecting nodal flow (McGrath et al., 2003). However, despite many studies into left-right determination, the exact mechanisms are still unclear (Vandenberg and Levin, 2010).

The first link between polycystic kidney disease (PKD) and cilia was made by Pazour et al., (2000) which showed that the classic mouse mutant, Oak Ridge polycystic kidney (orpk) mouse, was due to a hypomorphic allele of *Tg737/Polaris/Ift88*. When disrupted by targeted knockout, loss of *Ift88* leads to left-right asymmetry due to lack of nodal cilia, along with other developmental defects (Pazour et al., 2000; Murcia et al., 2000). Polycystin 1 and polycystin 2 (PKD1 and PKD2) have since been shown to localise to the primary cilium (Yoder et al., 2002). PKD1 is a large transmembrane protein that interacts with PKD2, a non-selective cation channel and they are thought to form a Ca^{2+} channel which allows Ca^{2+} influx upon bending of the cilium (Gonzalez-Perrett et al., 2001; Qian et al., 1997). Fluid flow over kidney cells leads to calcium influx and this is dependent on cilia, PKD1 and PKD2 (Nauli et al., 2003; Praetorius and Spring, 2001; Praetorius

and Spring, 2003). PKD is not the only link between kidney disease and cilia function, many other human diseases linked to cilia dysfunction, termed ciliopathies, also present with kidney disease. This includes nephronopthisis (NPHP), which is an autosomal recessive cystic kidney disease, associated with other non-renal symptoms, including Senior-Løken syndrome and Joubert syndrome (JBS). NPHP is caused by mutations in one of 12 genes many of which localise to the cilia or basal body (Czarnecki and Shah, 2012; Hildebrandt and Otto, 2005).

How disrupted flow sensation leads to kidney cyst formation is not well understood. Theories include direct control of transcription by translocation of the cytoplasmic tail of PKD1 in the absence of calcium influx to the nucleus, along with STAT6 and P100, which then activate transcription (Chauvet et al., 2004). Alternative theories suggest both canonical and non-canonical Wnt signalling may be involved; this is discussed further in 1.4.2.2.

1.4.2 Developmental signalling

While establishing a role for cilia in establishing left-right asymmetry, observations of phenotypes in mice with ciliary defects such as *Tg737/Polaris/Ift88*, *Kif3a* and *Kif3b* mutants, including mid-gestation lethality and patterning defects which could not be attributed alone to disruption of nodal flow, lead to the theory that primary cilia may have additional roles in developmental signalling (Huangfu et al., 2003; Liu et al., 2005; Marszalek et al., 1999; Murcia et al., 2000; Nonaka et al., 1998).

1.4.2.1 Cilia and Hedgehog signalling

An ENU mouse mutagenesis screen for genes affecting neural tube patterning, a process that requires Shh signalling, identified the mammalian homologues of IFT particles *Ift172* and *Itf88,* where mutants lacked ventral cell types in the developing neural tube (Huangfu et al., 2003). Although it was known from extensive studies in *Chlamydomonas* that IFT is essential for cilia/flagella formation, a role for IFT in mammalian development had been under appreciated (Reviewed in Rosenbaum and Witman, 2002). As these anterograde IFT mutant mice lacked cilia, this suggests

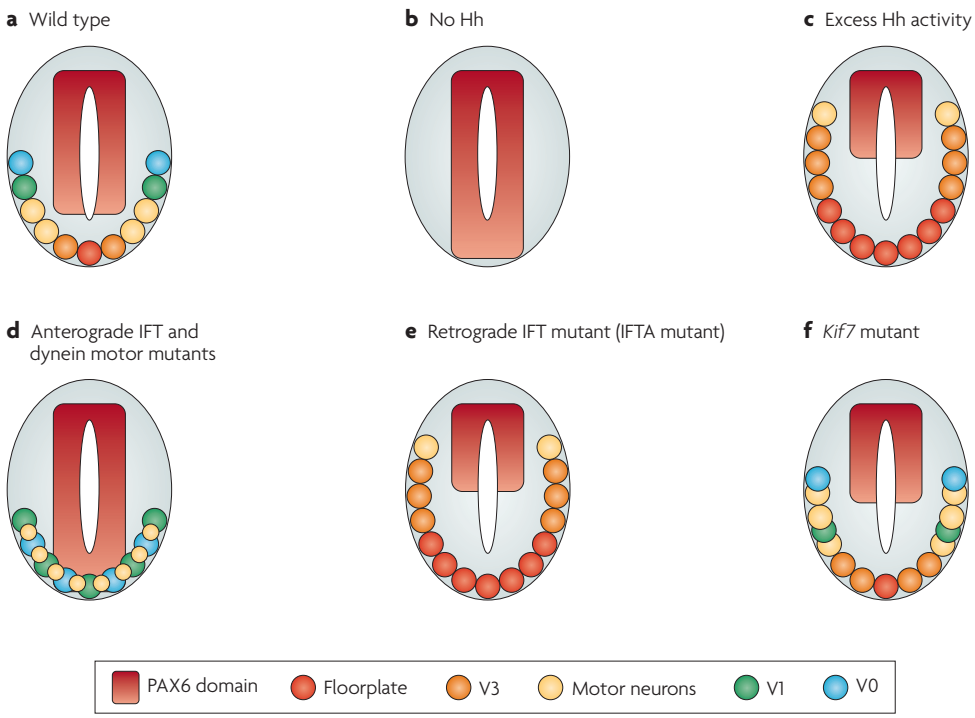

Figure 1.3 Neural tube defects in Hedgehog pathway and cilia mouse mutants. (A) In the wild type ventral neural tube, neural cell types are specified by a gradient of Shh morphogen. (B) In the absence of Shh, where there is too much $Gli3^R$ (eg. *Smo*$^{-/-}$ mice), ventral cell types are absent: the neural tube is completely dorsalised. (C) Excess Shh signalling, where there is excessive and ectopic $Gli3^A$, such as in *Ptch1*$^{-/-}$ embryos, leads to ventralisation of the neural tube. (D) Anterograde IFT mutants such as *Ift172*$^{-/-}$ and *Ift88*$^{-/-}$ mice have a dorsalised neural tube, due to reduced Hh signalling. This is not as severe as in (B) because cilia are involved in both the Gli^A driven response to Shh signalling, and in $Gli3^R$ formation. Mutants in the retrograde IFT dynein motor display a similar phenotype. (E) Some IFT-A mutants (eg. *Ift139*$^{-/-}$) show ventralised neural tube and ectopic digit formation, both phenotypes consistent with elevated Shh signalling. (F) *Kif7* mutants show a slightly ventralised neural tube, with expansions in cell types which require intermediate Shh levels for specification. (Taken from Goetz and Anderson, 2010)

that, in addition to roles in fluid flow generation at the node, cilia are also more broadly required for key developmental signal transduction, including Shh-dependent specification of ventral neural tube and digit identity in the limb buds. Furthermore, mouse mutants in *Kif3a* and *Kif3b*, which are components of the anterograde IFT motor, also showed lack of ventral cell types in the neural tube (Figure 1.3) (Marszalek et al., 1999; Nonaka et al., 1998; Takeda et al., 1999). While most IFT mutants die before digit patterning is complete, loss-of-function alleles of *Ift88*, *Dynch2* and *Ift52* also cause polydactylous limb defects, a phenotype linked to deregulated Hh signalling (Figure 1.3) (Haycraft et al., 2005; Liu et al., 2005; May et al., 2005).

Genetically the Hh signalling cascade had been best defined in *D. melanogaster*. Many of these signalling components are highly conserved. In mammals, there are three diffusible Hh ligands; Sonic hedgehog (Shh), Desert hedgehog (Dhh) and Indian hedgehog (Ihh). These bind to the receptor Patched (Ptch1/Ptch2), which relieves Ptch inhibition of a co-receptor Smoothened (Smo) (Figure 1.4). Through a complex series of events, signalling through Smoothened controls the fate of the bifunctional transcription factors Gli1-3, orthologues of the *D. melanogaster* Cubitus interruptus (Ci) transcription factor, which go on to activate Hh target gene expression, such as *Ptch1* and *Gli1*, in the presence of ligand (reviewed in (Ingham and McMahon, 2001)). In the absence of Hh, the Gli/Ci transcription factors are proteolytically processed to potent repressors of Hh target gene expression; in mammals both Gli3 and to a lesser extent Gli2 are processed from full length to a repressor form (Aza-Blanc et al., 1997; Ohlmeyer and Kalderon, 1998; Sasaki et al., 1997; Sasaki et al., 1999; Wang et al., 2000a). In *Drosophila*, a microtubule-binding protein Costal2 (Cos2) was identified as a central part of the Ci regulatory complex, which acts as a cytoplasmic scaffold, controlling Ci/Gli processing in response to presence or absence of ligand (Robbins et al., 1997; Sisson et al., 1997). What has recently become apparent is that *Drosophila,* which lack primary cilia, have independently developed an alternate microtubule-based strategy to control the Ci/Gli transcription factor fates. In mammals, the ciliary axonemal microtubules, as well as the IFT machinery, have been co-opted for regulating Gli processing events (Figure 1.4).

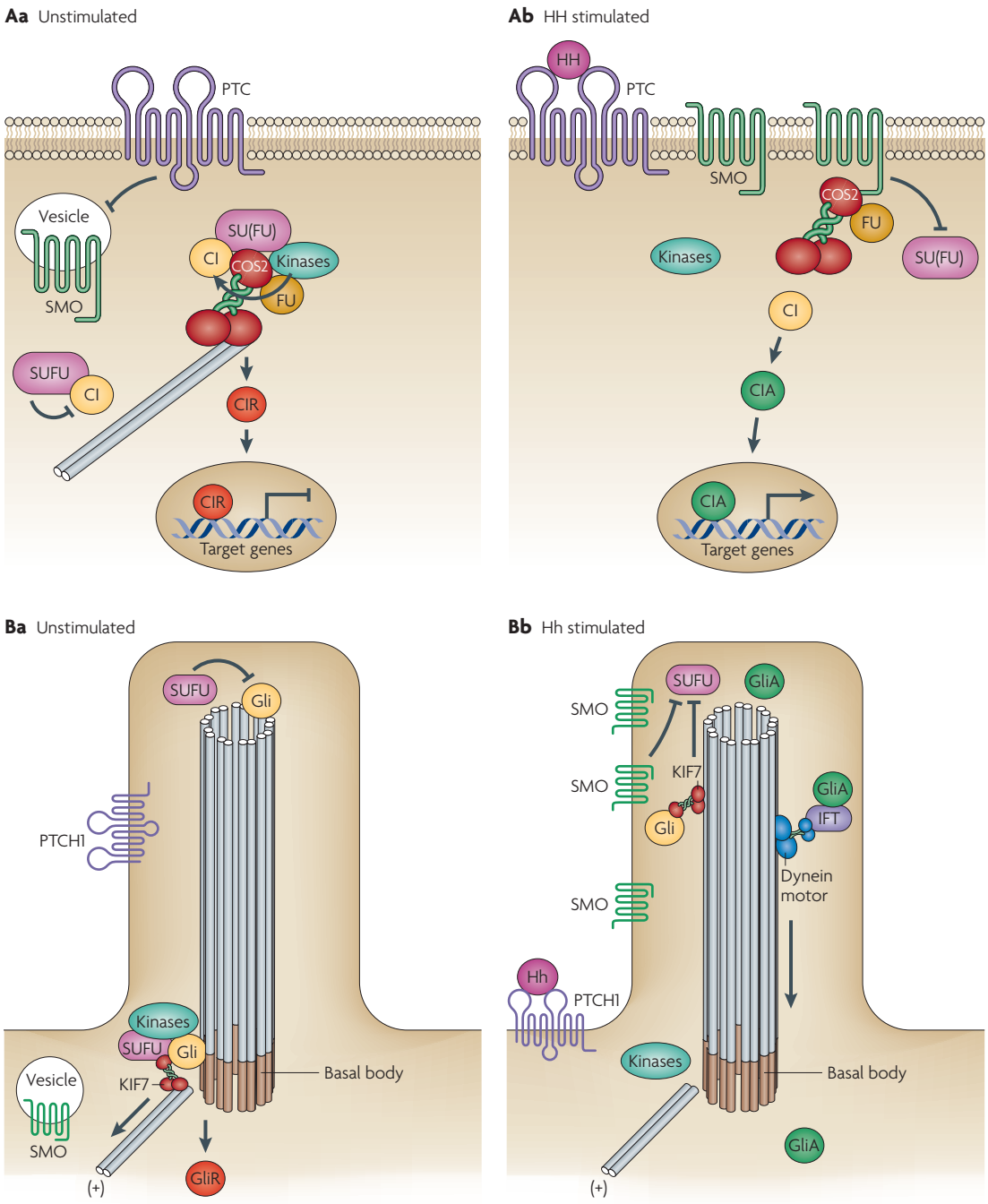

Figure 1.4 Hh signalling in Drosophila and mammals.

Figure 1.4 Hh signalling in *Drosophila* and mammals. (A) In *Drosophila,* the Shh receptor, Ptc localises to the cell membrane. (Aa) In the absence of Hh signalling, Ptc prevents Smo from localising to the cell membrane. A microtubule bound complex including Cos2, SuFu, and the downstream transcription factor Ci, recruits kinases which promote the conversion of Ci to Ci repressor form, Ci^{R}. This leads to the repression of Hh target genes. (Ab) In the presence of Hh, the Hh ligand binds to its receptor Ptc, relieving the inhibition of Smo which translocates to the cell membrane. Fu and Cos2 associate with Smo and so when Smo translocates, so do Fu and Cos2 and so Ci^{A} is released. Ci^{A} translocates to the nucleus where it activates Hh target genes. Ligand binding also leads to the inactivation of Ci^{R}. (B) Cilia are required for mammalian Hh signalling, and many of the pathway components have been found to localise to the cilium. (Ba) In the absence of Hh ligand, Ptc homologue Ptch1 localises to the ciliary membrane and is thought to prevent Smo from translocating here. The Cos2 homologue Kif7 localises to the base of the cilia where it is thought to interact with SuFu, kinases and Gli transcription factors. This Kif7 complex promotes formation of Gli repressors (Gli^{R}), which translocate to the nucleus and repress Hh target genes. Formation of $Gli3^{R}$ is possible without the cilium but happens at much lower levels. Also, in the absence of cilia, $Gli3^{FL}$ does not translocate to the nucleus. (Bb) Upon Hh binding to Ptch1, Ptch1 inhibition of Smo is relieved and Smo translocates to the ciliary membrane. Kif7 enters the cilium and promotes ciliary localisation of Gli2. Gli activators (Gli^{A}) are formed in a process that is not well understood but involves the cilium. Gli^{A} are transported out of the cilium by IFT and then translocate to the nucleus where they activate Hh target genes. (Taken from Goetz and Anderson, 2010).

Mammalian genetic studies have placed IFT proteins downstream of ligand binding and upstream of Gli transcription factors in terms of Hh signalling. In *Ptch1* mutant mice, the Hh pathway is hyperactivated independent of ligand and all cells adopt a ventral fate (Goodrich et al., 1997; Litingtung and Chiang, 2000). In epistasis experiments, *Ptc1;Ift88* and *Ptc1;Ift172* double mutants phenocopy the IFT single mutants, lacking Shh-dependent ventral cell types in the neural tube, therefore placing the anterograde IFT proteins downstream of Ptch1 (Huangfu et al., 2003).

Gli proteins can act as transcriptional activators or repressors, with Gli1 and 2 acting primarily as activators and Gli3 mainly acts as the predominant repressor. Gli3 full length ($Gli3^{FL}$) is cleaved to produce Gli3 repressor ($Gli3^{R}$), and although Gli3 mainly acts as repressor, $Gli3^{FL}$ can also be stabilised and modified by unknown mechanisms to produce an activator of Hh signalling (Sasaki et al., 1999; Wang et al., 2000a). Hh signalling promotes formation of Gli activators and prevents the processing of $Gli3^{FL}$ to $Gli3^{R}$. IFT mutants do not show upregulation of characteristic Gli activator target genes in response to Hh, but also show patterning defects characteristic of defective $Gli3^{R}$ as well as impaired proteolytic processing of Gli3 to its repressor form (Haycraft et al., 2005; Huangfu and Anderson, 2005; Liu et al., 2005; May et al., 2005). Therefore IFT is required for both activation and

repression of Hh signalling by controlling the activity of the Gli transcription factors, meaning cells lacking cilia cannot appropriately respond to Hh signalling. This explains why many IFT mutant mice do not completely phenocopy *Shh* or *Ptch1* mutants, but instead have aspects of Hh loss of function and gain of function mutants, similar to *Gli2:Gli3* double mutants where both activator and repressor functions are impaired (Figure 1.3).

However, cilia are not required for all responses to Hh signalling, but are essential for the ability to detect a gradient of Hh signalling. During development this is key to the correct specification of a variety of cell types in certain tissues, particularly the neural tube and limb bud and helps explain the tissue specificity of the Hh defects observed in ciliary mutants.

Mouse mutants of IFT-B genes or the anterograde motor (Kif3a and Kif3b) lack cilia and show deregulated Hh response. In the neural tube, where Gli activators play an important role in specifying ventral cell types, defects resemble Hh loss of function mutants, whereas in the limb bud, where $Gli3^R$ plays an important role in digit specification, the lack of $Gli3^R$ causes the ciliary mutant phenotype to resemble gain of function Hh mutants with polysyndactyly (Figure 1.3) (Eggenschwiler and Anderson, 2007; Huangfu and Anderson, 2005; Huangfu et al., 2003; May et al., 2005).

Interestingly, the loss of components of the retrograde dynein IFT motor leads to similar dysregulation of Hh signalling to that seen in anterograde IFT mutants (Huangfu and Anderson, 2005; May et al., 2005). However, not all IFT mutants lead to the same developmental phenotype or defects in Hh signalling. In particular, IFT-A proteins, which are involved in retrograde IFT, appear to be negative regulators of Hh signalling. Mutation in IFT-A proteins such as Ift139 and Ift122, leads to shortened, bulging cilia. In contrast to the lack of ventral cell types in the neural tube seen in anterograde IFT and IFT motor mutants, these IFT-A mutants show an expansion of ventral cell types in the neural tube (Figure 1.3) (Qin et al., 2011; Tran et al., 2008). This phenotype distinction had previously been demonstrated in *Chlamydomonas,* where IFT-A and IFT-B mutants show two distinct cilial phenotypes, with IFT-B mutants resembling anterograde motor mutants and, in

general, IFT-A mutants resembling retrograde IFT mutants (Cole et al., 1998; Kozminski et al., 1995; Pazour et al., 2000; Pazour et al., 1998; Piperno et al., 1998). Further functional analysis will resolve whether this reported segregation of Hh regulation and cilia structure holds true for the mammalian system.

It has been suggested that the link between IFT and Hh signalling may not necessarily mean a link between cilia and IFT, as it is known that IFT proteins have non-ciliary roles. However, mouse mutants of other ciliary proteins also show ciliary and Hh signalling defects. For example mice mutant for the small GTPase *Arl13b*, which localises almost exclusively to the ciliary membrane, have shortened cilia with specific structural defects and Hh signalling abnormalities in the neural tube (Caspary et al., 2007). Mutations in basal body proteins, for example, Oral-facial-digital syndrome 1 (Ofd1), also display impaired patterning of the neural tube (Ferrante et al., 2006). This suggests the link is between Hh signalling and cilia, not non-ciliary IFT function.

Remarkably, many key components of the Hh pathway localise to cilia. The localisation of these proteins is dynamic and depends on the activation state of the pathway. In the absence of Hh signalling, Ptch localises to the ciliary base and is inhibits entry of Smo to the cilium, such that Smo is restricted to the plasma membrane and intracellular vesicles (Figure 1.4) (Corbit et al., 2005; Rohatgi et al., 2007). Upon Hh binding to Ptch, Ptch leaves the cilium and Smo accumulates in the ciliary membrane. Hh agonists, as well as activating mutations in Smo cause Smo to localise to the ciliary membrane (Corbit et al., 2005). Smo may localise constitutively to the cilium at low levels as suggested by the fact that Smo accumulates in cilia lacking the retrograde IFT motor (Kim et al., 2009; Ocbina et al., 2009). Smo localisation to cilia alone is not sufficient for pathway activation as it still accumulates in the presence of the Hh antagonist cyclopamine (Wilson et al., 2009).

Gli transcription factors Gli1, 2 and 3 are also localised to the cilium, at the distal tip (Figure 1.4) (Haycraft et al., 2005; Kim et al., 2009; Wen et al., 2010). Gli2 and Gli3

accumulate at the tip in response to Hh activation, and a recent study has shown that Gli2 and Gli3 accumulate within minutes of Hh addition (Wen et al., 2010). They also show that it is $Gli3^{FL}$, not $Gli3^{R}$ which accumulates at the ciliary tip. $Gli3^{FL}$ must be further processed to produce Gli3 activator ($Gli3^{A}$). It is not clear what this processing involves, although it is thought to be cilia dependent (Wen et al., 2010). As $Gli3^{R}$ levels are much reduced in ciliary mutants, cilia are likely to be involved in but not absolutely required for $Gli3^{FL}$ to $Gli3^{R}$ processing (Haycraft et al., 2005; Liu et al., 2005; May et al., 2005).

Suppressor of Fused (SuFu), a negative regulator of mammalian Hh signalling (Cooper et al., 2005) is also found at the cilium (Endoh-Yamagami et al., 2009; Haycraft et al., 2005). However, it seems that the role of SuFu in repressing Hh signalling is cilia independent (Chen et al., 2009; Jia et al., 2009).

The dynamic localisation of Hh pathway components to cilia suggests cilia act as a selective scaffold for concentrating mammalian Hh signal transduction, as well as regulating which components interact by regulating entrance to the cilium in response to signalling. In flies, cilia are dispensable for Hh signalling and most cells lack cilia, except specialised mechano-sensory neurons. It is suggested that the kinesin-like protein Cos2 fulfils the microtubule-based scaffolding role, as it binds to Ci, and is important for formation of Ci repressor in the absence of Hh signalling, and is also required for pathway activation in the presence of Hh by antagonising SuFu (Sisson et al., 1997; Wang et al., 2000b) (Figure 1.4). The closest vertebrate orthologue to Cos2 is thought to be the kinesin Kif7. Residues key for motor activity in the canonical kinesin motor domain of *Cos2* are not conserved, so whether it traffics as a typical kinesin is unclear, however it retains microtubule binding ability and assembles large microtubule bound complexes including Ci (Farzan et al., 2008; Robbins et al., 1997). In contrast, *Kif7* in zebrafish and mouse has maintained what appears to be a functioning motor domain. There are conflicting reports as to whether Kif7 has a central role in vertebrate Hh signalling, but overall it seems the Kif7 is involved in vertebrate Hh signalling in certain cell types (Endoh-Yamagami et al., 2009; Liem et al., 2009; Tay et al., 2005; Varjosalo et al., 2006). Interestingly, Kif7 was found at the base of cilia and moved to cilia tips upon Hh signalling and

this depends on the motor motifs, suggesting it actively traffics along the axoneme in a Hh dependent manner (Endoh-Yamagami et al., 2009). This could suggest the ancestral Cos2/Kif7 orthologue originally acted in cilia to transport Hh components, but as cilia were lost in *Drosophila*, it maintained its microtubule-based scaffolding role in Hh signalling.

The *Fused* (*Fu*) kinase is involved in Hh pathway activation in *Drosophila* (Ingham and McMahon, 2001), and zebrafish, but $Fu^{-/-}$ mice do not show Hh defects suggesting it is not centrally involved in Hh signalling in mammals (Chen et al., 2005; Merchant et al., 2005). $Fu^{-/-}$ mice display hydrocephalus and a recent study has demonstrated that Fu is required for formation of specialised motile cilia in mouse and zebrafish (Wilson et al., 2009). In planaria, *Kif7* and *Fu* are required for motile cilia formation but not Hh signalling (Rink et al., 2009). This suggests that the ancestral role was ciliary for these proteins and that perhaps Hh signalling and cilia were linked in the common ancestor of *Drosophila* and vertebrates (Eggenschwiler and Anderson, 2007).

1.4.2.2 Cilia and Wnt signalling

Although the most well established phenotype of ciliary mutants involves Hh signalling defects in mammals, it has been suggested that cilia could be involved in transduction of other signalling pathways. The role of cilia in Wnt signalling is contentious and conflicting data exists both for and against roles for cilia in Wnt signalling (Wallingford and Mitchell, 2011). One of the first links between cilia and canonical Wnt signalling was suggested by studies of Nphp2/Inversin (Inv). Inv, which localises to cilia, interacts with the Wnt signalling transducer Dvll, a cytoplasmic phosphoprotein which acts directly downstream of the Frizzled (Frz) receptor. Inv is thought to play a role in inhibiting canonical Wnt signalling (Otto et al., 2003; Simons et al., 2005; Watanabe et al., 2003).

Knockdown of genes mutated in the ciliopathy Bardet-Biedl Syndrome (BBS), *Bbs1*, *4* and *6* in mammalian cells and zebrafish lead to increased Wnt signalling (Gerdes et al., 2007). In addition, Corbit et al., (2005) showed that mice mutant for the gene which encodes the anterograde kinesin motor Kif3a show increased Wnt signalling, assayed by *BAT-Gal* staining, a transgenic reporter of canonical Wnt signalling; as

do cells mutant for genes encoding Ift88 or Ofd1, a basal body protein essential for ciliogenesis. Lancaster et al., (2011) further suggest that cilia are involved in dampening Wnt signalling by sequestering β-catenin, a key downstream component, away from the nucleus, thereby inhibiting canonical Wnt signalling. They suggest that lack of cilia releases β-catenin to the nucleus leading to elevated Wnt signalling, whereas a lack of retrograde IFT leads to increased sequestering of β-catenin at the remaining abnormal cilia and decreased Wnt signalling. They also examined Wnt signalling using the *BAT-Gal* reporter in mice with a nonsense mutation early in the *Dync2h1* gene and observed tissue specific effects on ciliogenesis and Wnt signalling. Some tissues, such as limb buds and hair follicles, have shortened cilia which remain and show decreased Wnt signalling, whereas other tissues such as areas of the brain and nasal folds, show an increase in Wnt signalling correlating with a complete loss of cilia. They suggest this is because the shortened cilia that remain sequester more β-catenin due to a lack of retrograde IFT, whereas if the cilium is completely absent, β-catenin is free to enter the nucleus and activate Wnt target genes.

In contrast, Ocbina et al., (2009) found that IFT mutant embryos *Kif3a*, *Ift88*, *Dync2h1* or *Ift172* do not show increased endogenous expression of *Axin2*, a downstream target of canonical Wnt signalling or increased *BAT-Gal* activation. The conflicting data are difficult to reconcile and so conclusions on whether cilia are involved in Wnt signalling are difficult to make, but it is certainly possible that any role for cilia on Wnt signalling may be tissue specific.

Chibby, a basal body protein required for cilia formation in the airways binds β-catenin and negatively regulates canonical Wnt signalling. Tissue specific effects are observed in *Chibby* mutant mice; the airway of *Chibby* mutant mice and *Chibby* mutant MEFs show increased Wnt signalling (Voronina et al., 2009). The fact that ciliary mutant mice do not show any gross phenotypes consistent with abrogated Wnt signalling, supports the theory that any role for cilia in Wnt signalling is likely to be tissue specific (Eggenschwiler and Anderson, 2007).

As mentioned, links have been suggested between Wnt signalling and cystic kidneys seen in human ciliopathies. Such links are complex and conflicting, with mutants of

both negative and positive regulators of Wnt signalling leading to embryonic cystic kidneys (Marose et al., 2008; Pinson et al., 2000; Qian et al., 2005; Saadi-Kheddouci et al., 2001). Mutations in Inv/Nphp2 lead to cystic kidneys (Otto et al., 2003; Phillips et al., 2004; Watanabe et al., 2003). Inv has been shown to interact with Dishevelled (Dvl1), which is involved in transduction of both canonical and non-canonical Wnt signalling, and Inv was proposed to act as a switch between canonical and non-canonical Wnt signalling (Simons et al., 2005). However, no change in canonical Wnt signalling was reported in *Inv* mutant mice (Eggenschwiler and Anderson, 2007). Jouberin, which is mutated in Joubert Syndrome, localises to the cilium and interacts with β-catenin, an integral component of the Wnt signalling pathway. Loss of *Jbn* in mouse leads to kidney cysts and reduced Wnt signalling in adult the kidneys (Lancaster et al., 2009).

Cilia have also been linked to non-canonical Wnt signalling. Planar cell polarity (PCP) is the ability of cells in a sheet to polarise with respect to its plane and in many tissues, this orientation is controlled by the non-canonical Wnt PCP signalling pathway. Disruption of PCP signalling leads to characteristic convergence-extension and neural tube closure defects (Heisenberg et al., 2000; Sokol, 1996). Inv, the ciliary localised protein, may be a switch between canonical and non-canonical Wnt signalling, and reduced *Inv* leads to convergent-extension defects in *Xenopus* (Simons et al., 2005). Morpholinos to *Ofd1* in zebrafish lead to convergence-extension defects (Ferrante et al., 2009). Mice mutant for *Bbs1*, *4* and *6* present with open eyes and disorganised stereocilia, both defects common in PCP mutants (Ross et al., 2005). They also interacted genetically with the PCP gene *Vangl2*. However, *Ift88* mutant zebrafish do not show convergent extension defects and mouse mutants for ciliary genes do not show the specific type of neural tube closure defects associated with PCP signalling defects, once again suggesting any roles for cilia in PCP signalling are not universal (Huang and Schier, 2009; Ocbina et al., 2009).

It has also been suggested that non-canonical Wnt/Planar cell polarity (PCP) signalling could play a role in kidney cyst development, and that misorientated cell division may be involved (Benzing et al., 2007; Saburi et al., 2008). However,

Nishio et al., (2010) showed that kidney cysts can occur before loss of oriented cell division and mice with mutations in *Pkhd1* show misorientated cell division but not kidney cysts, suggesting misorientated cell division is neither necessary nor sufficient for kidney cyst development. Therefore how ciliary defects lead to kidney cysts is not fully understood.

Conversely, it has also been suggested that PCP signalling may regulate ciliogenesis – this is discussed further in 1.6.2.

1.4.2.3 Cilia and PDGF signalling

Although it has been suggested that cilia may play a role in platelet derived growth factor (PDGF) signalling, information on this is still scarce. Fibroblasts which lack cilia have been shown to have impaired PDGF-αα signalling, and Pdgf receptor α (Pdgfr-α) localises to cilia both in fibroblasts and *in vivo* in rat neural stem cells (Danilov et al., 2009; Schneider et al., 2005). Cilia have also been shown to be involved in PDGF dependent migration (Schneider et al., 2010). However, the early lethality of mice that lack cilia precludes *in vivo* analysis of PDGF signalling as lack of *Pdgfr-α* leads to later phenotypes including defects in oligodendrocytes and craniofacial structures (Klinghoffer et al., 2002; Soriano, 1997). Therefore *in vivo* data is lacking and needs to be addressed with conditional ciliary mouse mutants.

1.4.3 Human Ciliopathies

The number of diseases linked to defective cilia formation or function, termed ciliopathies, has grown rapidly in recent years as the role of cilia in wide-ranging systems has been identified (Hildebrandt et al., 2011). These diseases include primary ciliary dyskinesia (PCD), polycystic kidney disease (PKD), nephonophthisis (NPHP), Bardet Biedl Syndrome (BBS), Joubert Syndrome (JBS), Meckel Syndrome (MKS), Senior-Løcken Syndrome and Ellis-Van Creveld Syndrome. PCD results from defects in motile cilia, usually due to disrupted dynein arms, and symptoms include chronic sinus infections, male infertility and, in 50% of cases, *situs inversus*

where PCD presenting with *situs inversus* is termed Kartegener Syndrome. Many of these syndromes are related and phenotypically overlapping. NPHP is characterised by kidney cysts and when it is found in association with retinal degeneration is known as Senior-Løcken syndrome (Czarnecki and Shah, 2012). JBS is slightly more severe, with kidney cysts accompanied by mental retardation, hypoplasia of the cerebellar vermis and retinal coloboma, whereas Meckel Syndrome is the most severe leading to perinatal death with microophthalmia, polycystic kidneys, postaxial polydactyly and situs inversus. BBS is characterised by retinal degeneration, cystic kidneys, cognitive impairment, obesity and polydactyly. Most products of genes mutated in these ciliopathies localise to the cilia or basal body. In the case of BBS, MKS and NPHP at least, multiple causative genes have been shown to encode proteins which act in complexes. For example BBS-1, -2, -4, -5, -7, -8 and -9 form the BBSome, a large multimeric complex which is involved in dynamic transport from the basal body to the ciliary compartment (Fliegauf et al., 2007; Loktev et al., 2008; Nachury et al., 2007) (discussed in 1.5.3.1). In contrast NPHP and MKS proteins form complexes at the transition zone to regulate what enters the cilium (Czarnecki and Shah, 2012) see 1.5.2). It is thought that in these multigene disorders the varying phenotypes can in some cases be attributed to mutations in modifier genes. Alternatively compound heterozygous mutations in different disease causing genes can lead to varying disease phenotypes (Leitch et al., 2008).

Some of these phenotypes can be assigned to roles in Hh signalling such as polydactyly, shortened limbs (found in Elis-van Creveld syndrome) and hypoplasia of the cerebellar vermis (Brancati et al., 2009; Ruiz-Perez et al., 2007; Ruiz i Altaba et al., 2002). Others can be assigned to sensory roles of specialised cilia such as retinal degeneration and anosmia (found in BBS patients) (Kulaga et al., 2004; Mykytyn et al., 2004; Nishimura et al., 2004). Motile ciliary defects can explain lung problems, situs inversus and infertility seen in some syndromes (Mykytyn et al., 2004). However there are many phenotypes in which the exact role of cilia in these processes is unclear. As discussed, the role of cilia in cystic kidneys is yet to be determined (Eggenschwiler and Anderson, 2007). Also the role for cilia in obesity and cognitive impairment in BBS patients is not yet understood, although both are thought to be due to neural functions of cilia (Davenport et al., 2007). However, cilia

are present on differentiating preadipocytes, so cilia may also have non-neural roles in obesity (Marion et al., 2009). These phenotypes suggest there may be novel functions for cilia, and suggests they may play roles in signalling pathways other than Hh, especially in the adult. The ever-increasing numbers of human diseases linked to ciliary function also highlights the importance of understanding these fascinating organelles.

1.5 Cilia as distinct organelles

Although they are not strictly membrane bound, as required by the definition of an organelle, cilia can be functionally considered distinct organelles despite having a membrane which is continuous with the plasma membrane. With the unique make-up of the ciliary membrane, where specific proteins and lipids are highly concentrated and others are excluded, as well as static structures at the base of the cilia which are thought to regulate what enters the cilium, the cilium effectively operates as a separate organelle. As such, processes must exist for delivering specific proteins into the ciliary compartment, as well as for excluding proteins from the cilium; these processes are discussed below (reviewed in Nachury et al., 2010).

1.5.1 A diffusion barrier at the base of the cilium

1.5.1.1 Membrane diffusion barrier

Many signalling receptors and downstream signalling transducers localise to cilia. PKD1 and -2, as well as most components of the Hh signalling cascade, localise specifically to the cilia (Chen et al., 2009; Corbit et al., 2005; Haycraft et al., 2005; Kim et al., 2009; Nauli et al., 2003; Pazour et al., 2002; Rohatgi et al., 2007; Yoder et al., 2002). In the case of Hh signalling, localisation of many of these signalling molecules is dynamic depending on the pathway activation state (Corbit et al., 2005; Rohatgi et al., 2007). The concentration of specific proteins to the ciliary membrane has led to the idea of a diffusion barrier that exists at the base of the cilium (Figure

1.5). However, concentration of such membrane proteins does not prove such a barrier exists – it is possible they could be concentrated here by an active process, such as IFT, followed by slower diffusion back to the plasma membrane leads to build up in the ciliary membrane without a specific diffusion barrier in place.

Suggestion of a diffusion barrier at the base of cilia came from a study in which a fluorescent protein was linked to glucosylphosphatidylinosotisol (GPI-FP), which localised to the apical membrane of Madin-Darby canine kidney (MDCK) cells. The GPI-FP was absent from the ciliary membrane, as well as a circular area with a diameter of 1.2-1.8μm surrounding the cilium, which has a diameter of ~0.3 μm (Vieira et al., 2006). Vieira and colleagues also examined the membrane composition at this periciliary membrane domain (PCMD) and found that lipids were highly compact, and suggested this, combined with a high curvature, could slow diffusion and form a diffusion barrier or diffusion limiter (Figure 1.5) (Breslow and Nachury, 2011; Vieira et al., 2006). It has since been demonstrated that GPI-FP can be found in the cilium; discrepancies are thought to arise between fixed and live samples. This study demonstrated key biophysical properties of the PCMD, though it does not prove a diffusion barrier exists (Meder et al., 2005).

Fluorescence recovery after photobleaching (FRAP) studies have provided more convincing evidence for a diffusion barrier. Fluorescently labelled ciliary proteins move freely within the ciliary membrane, but if the whole cilium is bleached fluorescence does not recover, suggesting proteins do not move freely between the plasma and ciliary membrane compartments (Hu et al., 2010). Interestingly, this study also showed that Septin2 localises to a ring-like structure at the base of the cilium, similar to the PCMD. Septins are GTP-binding proteins with roles in membrane-diffusion barriers such as at the neck of budding yeast during cytokinesis (Saarikangas and Barral, 2011). RNAi knockdown of *Sept2* leads to reduction in cilia number and length, and importantly, increases the mobility of membrane proteins between the ciliary and plasma membrane, suggesting Sept2 functions in setting up the diffusion barrier.

A diffusion barrier may not be the only mechanism regulating entrance of membrane proteins into the ciliary membrane. It is possible proteins are physically tethered to

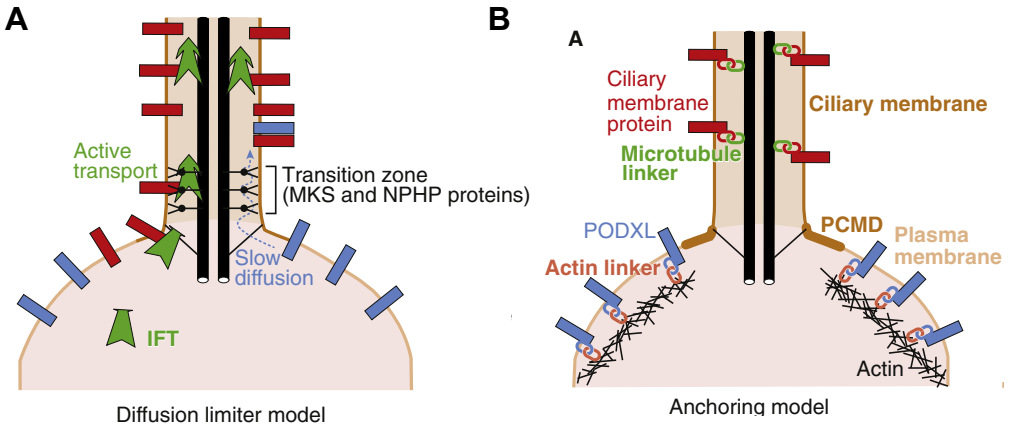

Figure 1.5 Keeping the ciliary membrane distinct from the plasma membrane. Adapted from Breslow and Nachury 2011. (A) In the diffusion limiter model, diffusion of membrane proteins and possibly lipids is slowed at the base of the cilium. There are several theories as to what limits diffusion. The transition zone, which includes proteins mutated in ciliopathies (MKS and NPHP proteins), is thought to play a role in controlling what enters the cilium, as is Septin2 which is found at the base of the cilium and is thought to limit membrane diffusion. It is also possible the curvature of the membrane may contribute to the slowing of diffusion. Rapid translocation of ciliary enriched membrane proteins is thought to occur by IFT. (B) In the anchoring model, proteins are tethered to the plasma membrane via linkers to the actin cytoskeleton, to prevent non ciliary proteins entering the ciliary membrane compartment. In support of this model, proteins, such as PDXL, have been shown to be retained at the plasma membrane via tethers to the actin cytoskeleton. Artificial tethering of ciliary membrane proteins leads to loss of ciliary localisation. Ciliary membrane proteins are thought to enter the cilia by IFT and be tethered to the microtubules via IFT motors. It should be noted that these models are not mutually exclusive and both may be involved in controlling the components of the ciliary membrane.

the plasma membrane to prevent ciliary access (Figure 1.5). Podocalyxin/gp133 (PDXL) localises to the apical membrane of MDCK cells but is excluded from the PCMD at the base of the cilium (Meder et al., 2005). PDXL binds cortical actin via its PDZ domain and mutation of this domain allows PDXL to enter the cilia. In addition, attaching actin tethering domains to ciliary proteins, such as Smo, removes them from the ciliary membrane (Francis et al., 2011). This plasma membrane tethering model and the diffusion barrier model are not mutually exclusive. Indeed it would be difficult to explain the concentration of specific lipids seen in the ciliary membrane by this tethering model (Bielas et al., 2009; Jacoby et al., 2009; Kaneshiro, 1987; Tyler et al., 2009). It is likely a combination of both these models act to keep the ciliary membrane distinct from the plasma membrane (Figure 1.5) (Breslow and Nachury, 2011).

1.5.1.2 Soluble protein diffusion barrier

As membrane proteins do not mix, it is interesting to consider whether soluble proteins face the same barrier to diffusion into the ciliary lumen. In frog photoreceptor cells, 27kDa GFP can equilibrate between the inner (cell body) and outer (analogous to the ciliary lumen) segments of the photoreceptor in the time expected for free diffusion, as can arrestin (41kDa), the rhodopsin desensitizer (Calvert et al., 2010; Calvert et al., 2006; Nair et al., 2005). This has recently been investigated further by a study that demonstrated that in mammalian cell culture 27KDa GFP and 41KDa Protein A can diffuse freely into the cilium, whereas BSA (67KDa) and large dextrans are restricted from entering the cilium (Kee et al., 2012). This indicates a size-dependent exclusion barrier exists at the base of the cilium. This is similar to the nuclear pore complex (NPC), which limits entry of proteins to the nucleus in a similar size-dependent manner. Recent studies suggest a biochemically similar complex may exist at the base of the cilium; several nucleoporins, components of the NPC, localise to the base of the cilium, as well as the nuclear membrane (Kee et al., 2012). It was also shown that Importin β2, a nuclear transport factor localises to cilia and interacts with a specific ciliary localisation sequence (CLS) in Kif17, (homologue of *C. elegans Osm-3*, a homodimeric kinesin motor) and is required for Kif17 entry into cilia (Dishinger et

al., 2010). Also if action of the nucleoporins is blocked, the entry of Kif17 into the cilium is halted. In the nucleus, Ran GTPase is involved in the dissociation of Importins and nuclear localisation signals (NLSs) (Stewart, 2007), and Ran-GTP, the active form of Ran, is found in the cilium (Kee et al., 2012), and its enrichment at cilia is required for ciliary localisation of Kif17 (Dishinger et al., 2010). This is indicative of a functional NPC-like structure at the base of cilia, coined the ciliary pore complex. However, as yet, Kif17 is the only protein shown to be mislocalised when this complex is disrupted, so it will be interesting to see how universal this mechanism of controlling entry to cilia is.

1.5.2 The Transition Zone

The transition zone is an area at the distal basal body, which begins where the three tubules of the basal bodies (triplets: A, B and C), transition to just two (doublets: A and B), and ends in motile cilia where the central microtubule pair begins (Figure 1.6) (Czarnecki and Shah, 2012). The exact structure of the transition zone varies between different species and cilia types, but it is generally comprised of transition fibres, Y shaped links and the ciliary necklace (Czarnecki and Shah, 2012) (Figure 1.6). Transition fibres extend from the C microtubules to the membrane, and despite the name, resemble sheets more than fibres, and are also referred to as alar sheets (Anderson, 1972). The gap between the alar sheets/transition fibres is less than 60nm and, roughly the size expected to prevent trafficking of proteins larger than about 40-50kDa (Nachury et al., 2010), suggesting that the transition zone acts as a ciliary gate regulating what enters and leaves the cilium. The Y shaped links project from the microtubule doublets to the ciliary membrane and it is thought they contact the ciliary necklace structure observed as rows of beads on the membrane by freeze fracture electron microscopy (Gilula and Satir, 1972). As the transition zone has such close contact with the ciliary membrane, it could be involved in gating the ciliary membrane as well as the ciliary lumen. Ift52 has been localised to the transitional fibres, where they touch the ciliary membrane by EM and as many IFT proteins localise to the base of the cilia as well as to the axoneme, this lead to the idea that IFT complexes dock at the transition zone and, possibly in a rate limiting step, acquire cargo before entering the cilium (Deane et al., 2001).

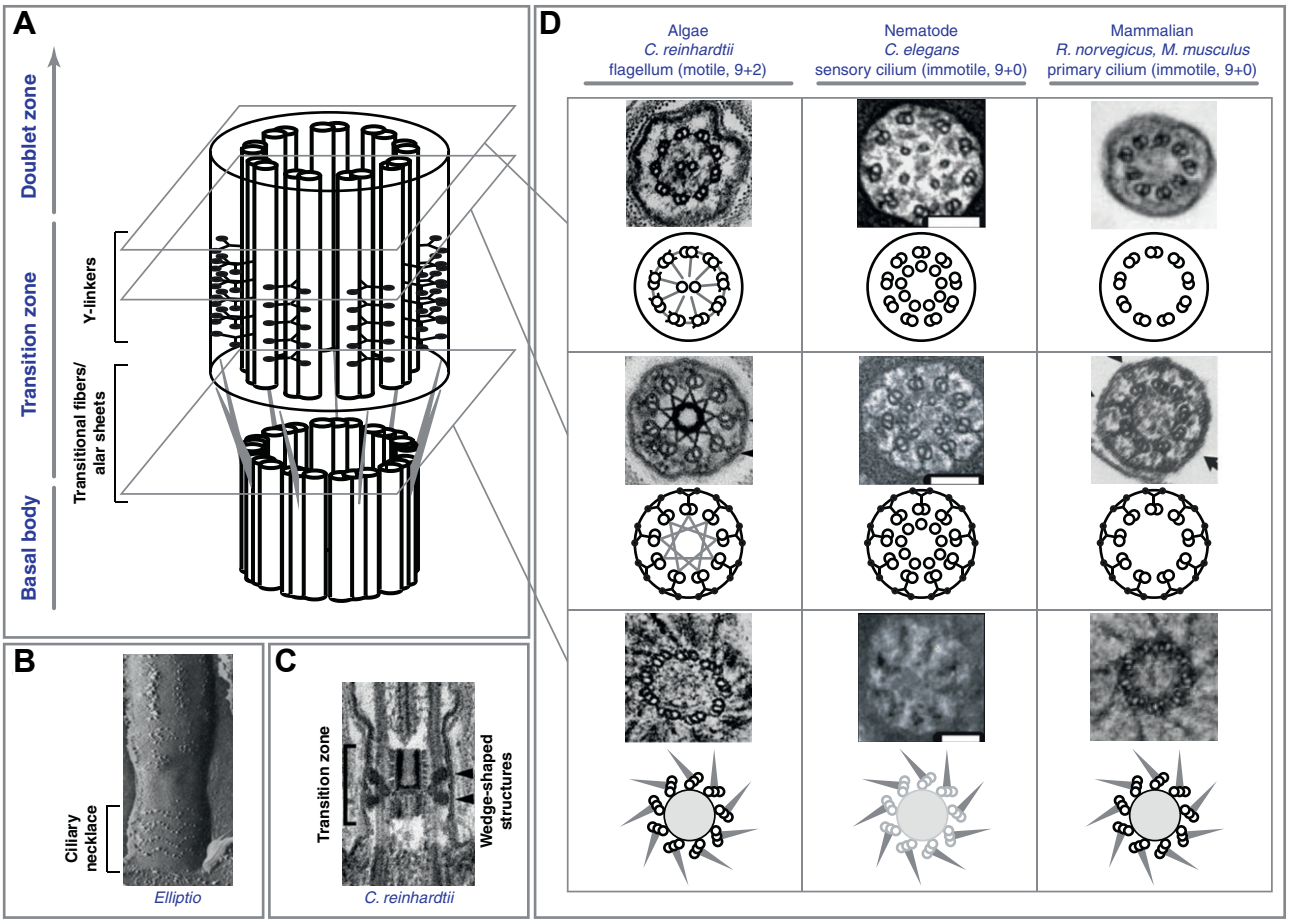

Figure 1.6 The transition zone. The transition zone is a structure just distal to the basal body at the base of the cilium and is thought to regulate what enters and leaves the cilium. (A) A schematic of the transition zone, which extends from where the C microtubules of the basal body triplet microtubules terminate, for roughly 0.5μm into the cilium, although the exact extent of the transition zone varies between species and cell types. At the distal end of the basal body, where the C microtubules terminate, transitional fibres or alar sheets are seen. Y linkers span from the B microtubules to the ciliary membrane throughout the transition zone. (B) Where the Y linkers contact the membrane, a characteristic ciliary necklace structure is observed on the ciliary membrane by freeze fracture electron microscopy. Transmission electron microscopy (TEM) showing a transverse section through a *C. Reinhardtii* transition zone illustrating the electron dense barrel shaped structure and the wedge shaped structures observed in the transition zone of *C. Reinhardtii* flagella. (D) Longitudinal TEM sections through transition zones of different species, along with schematic representations, showing that although highly conserved, differences do exist between the transition zone structures of different species. The transitional fibres or alar sheets mark the beginning of the transition zone and the end of the basal body. They form a structure with a 60nm gap, allowing diffusion of small proteins into the ciliary lumen but restricting diffusion of larger proteins. In C. elegans, triplet microtubules are difficult to resolve, although transition fibres are observed. Transition zones of all cilia show the Y linkers, although they are easier to resolve in some cilia compared to others. *C. Reinhardtii* also show the stellate fibre array connected to the A microtubules, which are not seen in C. elegans or mammalian transition zones. In motile cilia or flagella, the transition zone terminates at the basal plate where the central microtubule doublet appears. *C. elegans* cilia have several singlet mictotubules in the centre of the 9 microtubules doublets. (Taken from Czarnecki and Shah, 2012).

Several proteins have been shown to localise to the transition zone, defined by immunofluorescence as the gap in staining by anti-acetylated alpha tubulin or -polyglutamylated tubulin between the axoneme and the basal body (Lechtreck and Geimer, 2000; Pechart et al., 1999). The absence of such post-translational modifications of the tubulins could reflect masking of the epitopes preventing antibody detection, or could reflect specific biological or structural properties of the tubulin at the transition zone.

Many of the proteins which localise to the transition zone have been implicated in ciliopathies, mainly Nephronophthisis (NPHP), Joubert Syndrome (JBS) and Meckel Syndrome (MKS). Recently, it has been shown that genes mutated in these disorders encode proteins which make up three main complexes at the transition zone, the NPHP-1-4-8 complex (or NPHP complex), NPHP-5-6 complex and the MKS/B9 complex. The latter contains MKS and JBS proteins, including Mks1, Tctn1/Jbts13, Tctn2/Mks8 and B9d1/Mks9, which have been shown to be involved in Hh signalling in mouse (Chih et al., 2012; Czarnecki and Shah, 2012; Garcia-Gonzalo et al., 2011; Sang et al., 2011; Weatherbee et al., 2009).

The MKS/B9 and NPHP complexes have been shown to interact genetically in *C. elagans,* where mutation of components singly have very mild phenotypes, as do double mutants of most of the MKS/B9 complex. In contrast, double mutations of MKS/B9 genes in conjunction with NPHP genes leads to a stronger ciliary phenotype and disruption of the transition zone including loss of the Y linkers. Nphp8/Mks5 is thought to play a role in coordinating these complexes, as it genetically interacts with both complexes to produce a more severe ciliary phenotype and localisation of components of both complexes are mislocalised in *Mks5* mutants (Williams et al., 2011; Williams et al., 2008).

Many of the proteins in the MKS/B9 have membrane targeting domains, including Tctn2/Mks8, Tmem216/Mks2 and Tmem67/Mks3, and components of the complex are found in both membrane and soluble fractions again supporting the close links between the transition zone and the ciliary membrane (Chih et al., 2012). siRNA knockdown or mutations in the mammalian MKS/B9 complex proteins leads to decreased ciliary localisation of ciliary membrane proteins such as Arl13b, ACIII,

Sstr3, Htr6 and Smo, suggesting this complex acts as a gate to control global ciliary entry and exit (Chih et al., 2012; Garcia-Gonzalo et al., 2011). Chih et al., (2012) show that localisation of some members of this complex depend on Sept2, suggesting the septin diffusion barrier acts upstream to organise the B9/MKS complex. Moreover, they show that siRNA knockdown of one component of the B9/MKS complex, *B9d1* leads to increased diffusion between the ciliary and plasma membranes, suggesting it is involved in the diffusion barrier. A mislocalisation of plasma membrane proteins to the ciliary membrane is also seen upon mutation or RNAi of transition zone components, further supporting a role in the diffusion barrier, for example CEACAM-1 and GPI-FP mislocalise to cilia upon siRNA knockdown of the MKS/B9 complex in mammalian cells, as do Rp-2 and Tram-1a upon mutation of several transition zone genes in *C. elegans* (Chih et al., 2012; Williams et al., 2011). Some mouse mutants of MKS/B9 complex genes show tissue specific ciliary defects suggesting the transition zone may have differing roles in certain tissues (Chih et al., 2012; Garcia-Gonzalo et al., 2011; Weatherbee et al., 2009; Williams et al., 2011; Williams et al., 2008).

The NPHP 1,4,8 complex localises to cell-cell contacts as well as to the transition zone, and siRNA knockdown of *Nphp1* and *Nphp4* leads to cell polarisation defects and disrupted tight junction formation (Delous et al., 2009; Sang et al., 2011). The links between cell polarity and ciliogenesis are discussed further in 1.6.2.

The Nphp5-6 complex is considered part of the MKS/B9 complex by some (Garcia-Gonzalo et al., 2011), or as a separate complex by others (Sang et al., 2011). Nphp5/Cep290 mutations in humans can lead to a wide range of ciliopathic phenotypes, from NPHP to MKS (Coppieters et al., 2010). Cep290 has been shown to localise to the Y links in *Chlamydomonas* and mutants lack Y linkers (Craige et al., 2010). However Cep290 is not found in the *C. elegans* genome which retains transition zone Y linkers, suggesting it is not a conserved component of this structure (Czarnecki and Shah, 2012). Mouse *Cep290* mutants show either retinal degeneration alone, or in conjunction with cerebellar defects, but lack kidney cysts or strong developmental phenotypes in contrast to the wide-ranging phenotypes seen in patients with *CEP290* mutations, suggesting either the presence of dominant negative

mutations or modifier alleles in human patients or that the role of Cep290 is not conserved (Chang et al., 2006; Coppieters et al., 2010; Lancaster et al., 2011).

As yet, the ultrastructual localisation of transition zone proteins in mammals is unknown and the ultrastructural consequences to transition zone or cilia integrity in general in the absence of these individual components has yet to be investigated in mammals. It will be interesting to see where these proteins are located with respect to the different ultrastructural components such as the Y linkers and transition fibres and this will help dissect the role of these structures in maintaining ciliary integrity.

1.5.3 Traffic to the cilia

The diffusion barrier and transition zone can explain how entry of proteins to the ciliary membrane or ciliary compartment is controlled once the proteins are in the vicinity of the cilium. However, proteins must first be transported to the cilium, and as with all organelles, this trafficking is a highly controlled process. There are two main models of trafficking to cilia: directed exocytosis to the base of the cilium (this could include membrane or non-membrane proteins) or lateral transport from the plasma membrane (membrane proteins only) (Figure 1.7).

1.5.3.1 Directed exocytosis to the pericilliary membrane domain (PCMD) zone

Evidence for polarised exocytosis towards the base of the cilium came first from studies of trafficking of rhodopsin (Papermaster et al., 1985), in which pulse-chase studies in *Xenopus* photoreceptors showed Rhodopsin localised to the Golgi and to vesicles at the base of the cilium. This polarised trafficking has been shown to involve several proteins involved in vesicular trafficking; one of the first to be identified was Rab8, a small GTPase. Inhibition of Rab8 in frog retinas leads to accumulation of rhodopsin-containing vesicles at the base of the connecting cilium (Moritz et al., 2001). Rab8 localises to the base of cilia and the ciliary membrane at the onset of ciliogenesis, and its levels fall once cilia are extended (Westlake et al., 2011). Active Rab8 is needed for ciliogenesis in cultured mammalian cells, whereas

overexpression of an active form of Rab8 leads to increased ciliary length (Nachury et al., 2007; Yoshimura et al., 2007). However, *Rab8* mutant mice survive to 5 weeks of age, when they die from intestinal problems, suggesting Rab8 is not essential for ciliogenesis (Huangfu et al., 2003; Sato et al., 2007). It is possible other Rab proteins compensate for the lack of Rab8, or that this is not the only mechanism of transport to cilia.

Activation of Rab8 depends on the guanine nucleotide exchange factor (GEF) Rabin8. Knockdown of *Rabin8* leads to reduced ciliary Rab8 and decreased ciliogenesis in hTERT-RPE cells (Nachury et al., 2007). GEF activity of Rabin8 is promoted by Rab11-GTP, the active form of Rab11, which is involved in endosome recycling and localises to the pericentriolar recycling endosome compartment (PRE) (Knodler et al., 2010; Westlake et al., 2011). Expression of dominant negative Rab11 or siRNA to *Rab11* leads to reduced Rab8 and shorter cilia (Knodler et al., 2010). The TRAPPII complex, a tethering complex which mediates COPI vesicle trafficking, is also involved in localisation of Rabin8 to the ciliary base (Westlake et al., 2011). Both Rab11 and TRAPII localise to the PRE, and Smo, a receptor which localises to cilia, is found at the PRE (Kim et al., 2010). ASAP1, a phospholipid-dependent Arf GTPase activating protein (GAP), which is needed for pericentriolar localisation of the PRE, is also required for ciliogenesis, suggesting the centriolar localisation of these vesicles may be important for ciliogenesis (Kim et al., 2010). This study also suggested a role for the actin cytoskeleton in the regulation of the stabilisation of the PRE vesicles, thereby linking the actin cytoskeleton to cilia formation.

What controls the docking of vesicles at the ciliary base? The exocyst, a multisubunit tethering complex involved in vesicular trafficking from a post-Golgi compartment, through the recycling endosome to the basolateral membrane, has also been shown to play a role in trafficking to cilia, and is a candidate for controlling the docking of vesicles at the ciliary base (Kang and Folsch, 2009; Mazelova et al., 2009b; Rogers et al., 2004; Zuo et al., 2009). Components of the exocyst have been shown to localise to the base of the cilium (Rogers et al., 2004) and knockdown of one component, *Sec10* leads to shortened cilia (Zuo et al., 2009). Tethering

complexes, such as the exocyst, are involved in docking of vesicles in coordination with soluble *N*-ethylmaleimide sensitive factor receptors (SNAREs) and Rabs (Brocker et al., 2010). Another subunit of the exocyst, Sec15 interacts with Rab11 and possibly Rabin8, providing a link with Rab8/Rab11 vesicular trafficking and suggesting Rab8/Rab11 and the exocyst may cooperate in the trafficking of proteins to the cilium (Wu et al., 2005; Zhang et al., 2004). SNARE proteins Syntaxin3 and SNAP-25 localise to the base of the connecting cilium and may play a role in trafficking rhodopsin (Mazelova et al., 2009b).

IFT proteins themselves may have a role in trafficking to the cilium and subsequent vesicle fusion at the base of the cilium. Indeed, many IFT proteins have structural homology to components of coat protein-I (COPI) and clathrin coated vesicles, involved in concentrating membrane cargoes and curving membranes, although IFT particles are predicted to form curvature-less coats (Jekely and Arendt, 2006; Rosenbaum and Witman, 2002). Notably, Ift20, part of the IFT-B complex, localises to the trans-Golgi network as well as the cilia and basal body; strong siRNA knockdown of *Ift20* leads to fewer cilia, while partial knockdown leads to a reduction in Pkd2 at the ciliary membrane, suggesting a role for Ift20 in trafficking to cilia (Follit et al., 2006). Electron microscopy has localised Ift20 to the Golgi as well as vesicles near the ciliary base in mouse photoreceptors, and Ift52 is also localised to vesicles at the connecting cilia base (Sedmak and Wolfrum, 2010). Golgin protein Gmap210 tethers Ift20 to the trans-Golgi network, mutant mice show shorter cilia with mislocalised Pkd2, suggesting Gmap210 is not essential for ciliogenesis but is involved in ciliary trafficking (Follit et al., 2008).

Many proteins have implicated in trafficking of proteins to cilia, probably through distinct and overlapping pathways, but what allows these mechanisms select specific cargo for transport into the cilium? Ciliary localisation signals (CLS) have been found on several ciliary proteins, including G protein-coupled receptors (GPCRs) rhodopsin, melanocortin receptor Mch1r, somatostatin receptor Sstr3 and serotonin receptor 5HT6 as well as fibrocystin, cystin, polycystin1 (Pkd1), polycystin-2 (Pkd2) and Kif17 (Berbari et al., 2008a; Dishinger et al., 2010; Follit et al., 2010; Geng et al., 2006; Jin et al., 2010; Tam et al., 2000; Tao et al., 2009; Ward et al., 2011). The

first CLS to be identified was in rhodopsin; mutations in the last five amino acids lead to retinitis pigmentosa and cause mislocalisation of rhodopsin. Fusing the last eight amino acids of rhodopsin to membrane anchored-GFP directs GFP to the ciliary membrane (Deretic et al., 1998; Li et al., 1996; Sung et al., 1994; Tam et al., 2000). VxPx (where x is any amino acid) is likely to be the core CLS of rhodopsin, and is similar to RVxP motifs involved in ciliary localisation of Pkd1, Pkd2 and cyclic nucleotide gated channel, Cng1b (Geng et al., 2006; Jenkins et al., 2006; Ward et al., 2011). A small GTPase, Arf4, binds the VxPx motif of rhodopsin and is essential for its transport from the trans-Golgi network to the connecting cilium in photoreceptors (Deretic et al., 2005; Mazelova et al., 2009a). This is mediated by the small GTPase, Rab11, Arf GAP Asap1 and Rab11 effector Fip3 (Mazelova et al., 2009a). A similar complex has been implicated in the transport of Pkd1 and Pkd2 to cilia (Ward et al., 2011).

Another form of CLS, found on GPCRs Sstr3, Mch1r and 5HT6 is the AQ box found on the third intracellular loop (Berbari et al., 2008a). This motif is recognised by the BBSome and the BBS3 protein Arl6 (Berbari et al., 2008b; Jin et al., 2010). Fourteen genes have been linked to BBS, seven of which (BBS-1, -2, -4, -5, -7, -8 and -9) form a complex known as the BBSome (Fliegauf et al., 2007; Loktev et al., 2008; Nachury et al., 2007). The small GTPase BBS3/Arl6 is not part of the BBSome but both localise to cilia in an interdependent manner and both are essential for ciliary targeting of Sstr3, which is mislocalised in *Bbs2* and *Bbs4* mutant mice (Berbari et al., 2008b). The BBSome forms a coat complex, many of the proteins have structural similarities to classic coatamer coat complexes and is thought to either be involved in vesicle fusion at the ciliary base or lateral transport of proteins from the plasma membrane to the ciliary membrane. This is supported by the fact a CD8α-Sstr3^{i3} fusion (a plasma membrane protein fused to the CLS of Sstr3) localises to cilia, but accumulates in the plasma membrane in the absence of the BBSome or Bbs3/Arl6 (Jin et al., 2010; Nachury et al., 2010). Further evidence for lateral transport from the plasma membrane to cilia is discussed below.

1.5.3.2 Lateral transport from the plasma to the ciliary membrane

An elegant study by Milenkovic et al., (2009) has shown that Smo is primarily transported to cilia by lateral diffusion from the plasma membrane to the ciliary membrane (Figure 1.7). Upon Hh pathway stimulation, Smo localises to the ciliary membrane (Corbit et al., 2005). Pulse-chase experiments, utilising SNAP-tag technology which allows the specific labelling of intracellular versus membrane pools of Smo, show that soon after Hh stimulation (1h), membrane Smo enters the cilium before intracellular Smo replaces it after 4h. This shows Smo enters the cilium by lateral diffusion from the plasma membrane. The fact that CD8α-Sstr3^{i3} fusion protein accumulates at the plasma membrane in the absence of the BBSome suggests that other membrane proteins may be transported in this way and that the BBSome may play a role in helping these proteins to cross the diffusion barrier. Further studies are needed to see how many proteins are transported to the cilia by the lateral transport method, perhaps it is used as a store of protein to allow rapid translocation to the ciliary membrane upon pathway stimulation (Figure 1.7).

1.6 Control of Ciliogenesis

Formation of primary cilia in mammalian cells occurs via two main pathways (Figure 1.8) (Sorokin, 1962; Sorokin, 1968). In the first pathway, observed in epithelial cells, the mother centriole migrates to and docks at the apical plasma membrane, where it acquires appendages such as the basal foot and rootlets stabilising this docking to allow cilium elongation (Figure 1.8). In non-epithelial cells, such as fibroblasts, the mother centriole first fuses with an intracellular vesicle, termed the periciliary vesicle, at the distal end of the centriole. The centriole subsequently elongates and acquires appendages, while further vesicles fuse with the ciliary vesicle, allowing the vesicle to elongate in parallel with axoneme extension. As such, initial steps of ciliogenesis occur within this vesicle in the cell cytosol. The vesicle then fuses with the plasma membrane to release the nascent cilium into the extracellular environment (Figure 1.8). Little is known about the control of this

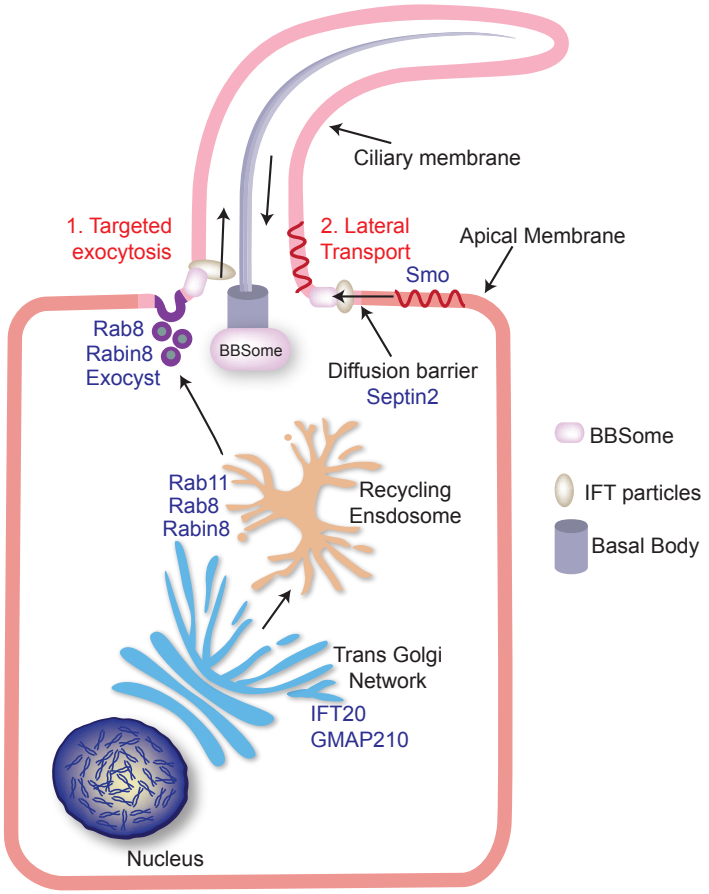

Figure 1.7 Trafficking to the ciliary membrane. Two methods of transporting membrane proteins to the cilium have been proposed. 1. The targeted exocytosis method. Targeted vesicular trafficking delivers ciliary membrane proteins to the ciliary base, within the periciliary membrane domain (PCMD), where IFT proteins and the BBSome are involved in transporting them to the ciliary membrane. The ciliary membrane proteins are transported from the trans Golgi network, where the IFT protein Ift20 localises with its adaptor Gmap210 are thought to be involved in vesicular trafficking. The ciliary membrane proteins then traffic through the pericentrosomal recycling endosome (PRE), which is found in the vicinity of the basal body. Small GTPases Rab11, Rab8 and the GTPase accelerating protein (GAP) Rabin8 are involved in targeted trafficking to the ciliary base, where the tethering complex, the exocyst, is involved in delivery of the ciliary membrane proteins to the PCMD. The BBSome is thought to act as a coat complex to aid entry into the ciliary membrane itself. The PCMD may be maintained by Septin2 which is found at the base of the cilium and controls ciliary/plasma membrane diffusion rates. 2. Lateral transport method. Some ciliary membrane proteins, such as Smo, are found in the plasma membrane and translocate to the ciliary membrane across the diffusion barrier via lateral transport. It is though this method allows rapid accumulation of ciliary membrane proteins in response to a signal, such the presence of Hh ligand. After the initial rapid translocation in response to Hh signalling, it is thought Smo may traffic via the targeted exocytosis method to the ciliary membrane. Adapted from (Kang and Folsch, 2009)

process of ciliary vesicle formation and fusion of secondary vesicles, although it has been suggested that the adaptor protein Hook2 may play a role in attachment of the ciliary vesicle (Baron Gaillard et al., 2011). In some cases, the cilium remains partially intracellular, in a ciliary pocket. It has been suggested this may be similar to the flagellar pocket observed in Trypanosomes (Molla-Herman et al., 2010). The flagellar pocket is the site of all exocytosis and endocytosis in Trypanosomes (Field and Carrington, 2009). Although this is clearly not the case for the ciliary pocket in mammalian cells, a recent study suggested endocytosis, possibly of ciliary membrane proteins, occurs at a higher rate at the ciliary pocket than the rest of the plasma membrane (Molla-Herman et al., 2010). A study in *C. elegans* shows function of endocytosis proteins are critical to regulating ciliary membrane volume (Kaplan et al., 2012).

1.6.1 Centriole/Basal body biogenesis

1.6.1.1 Centriole duplication

As ciliogenesis is closely linked to centriole and basal body formation, control of basal body formation is one of the earliest influences on ciliogenesis. The control of centriole duplication is complex, owing to their roles in cell division and ciliogenesis. I will describe centriole biogenesis briefly, concentrating on the aspects which relate to ciliogenesis, namely the formation of basal bodies. In cycling cells, centrioles duplicate once and only once per cell cycle (Figure 1.9) (Hinchcliffe et al., 1998; Nigg and Stearns, 2011; Tsou and Stearns, 2006). Tight control of centriole duplication must therefore exist. It is thought in most, if not all cells, the presence of an existing centriole represses *de novo* centriole biogenesis and as such, removal of existing centrioles can lead to *de novo* centriole formation (Khodjakov et al., 2002).

Pro-centrioles form orthogonally to the pre-existing centriole and are first visible during the G_1 to S transition (Figure 1.9). This is controlled by the protein kinase Plk4; increased Plk4 leads to extra centrioles, whereas decreased Plk4 levels leads to fewer centrioles (Bettencourt-Dias et al., 2005; Habedanck et al., 2005). The pro-centriole is connected to the mother centriole via the S-M linker, a tight physical

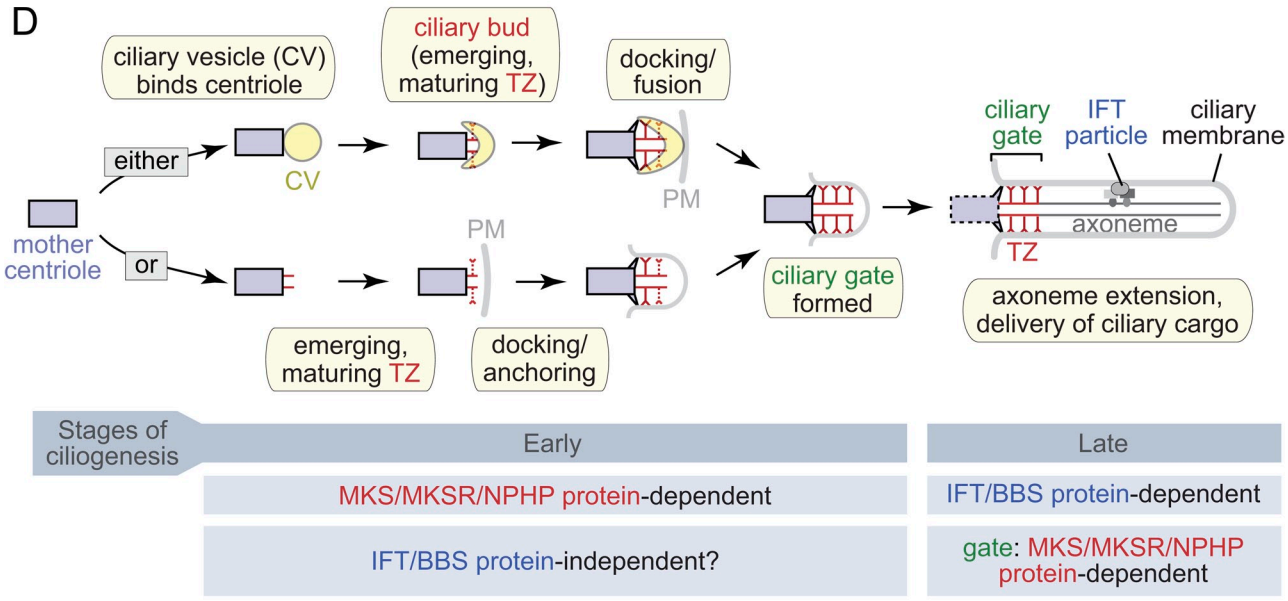

Figure 1.8 Ciliogenesis. The exact steps of early ciliogenesis can depend on cell type. In some mammalian cell types, such as fibroblasts, the mother centriole fuses with a Golgi derived vesicle, termed the ciliary vesicle (CV). The ciliary axoneme begins to elongate from the basal body, encompassed by the CV, which grows as more vesicles fuse to it. The CV then fuses with the plasma membrane (PM) and the cilia elongates by IFT. In other cell types, such as epithelial cells, no ciliary vesicle is involved, and the mother centriole docks straight to the plasma membrane, and the cilia elongates by IFT. It is thought that the early steps of basal body docking and transition zone (TZ) formation may be IFT independent. (Taken from Williams et al., 2011).

association which is thought to prevent formation of more than one daughter centriole at each mother centriole. The pro-centrioles elongate during S and G_2, in a process involving Sas-4 (Cpap/Cenpj), Ofd1, CP110 and Poc5 (Azimzadeh et al., 2012; Kohlmaier et al., 2009; Schmidt et al., 2009; Spektor et al., 2007; Tang et al., 2009; Tsang et al., 2008). CP110 binds the distal end of the centriole forming a cap that limits microtubule elongation to control centriole size (Schmidt et al., 2009). CP110 is also a negative regulator of ciliogenesis, suggesting removal of this cap may be necessary for ciliogenesis (Spektor et al., 2007; Tsang et al., 2008). The S-M linker is thought to prevent centriole overduplication: while centrioles remain "engaged" centriole reduplication is inhibited, and "disengagement" (removal/dismantling of S-M linker) in late M/early G_1 licenses the centrioles for the next round of duplication (Tsou and Stearns, 2006).

Upon dissolution of the S-M linker, or shortly afterward, a second, more loose linkage, termed the G_1-G_0 tether, forms and keeps the centrioles in close proximity, to aid the microtubule nucleating ability of the centrosome. This linkage is lost during G_2 as the centrioles separate to the spindle poles in preparation for cell division. After one and a half cell cycles, a centriole reaches maturity and acquires appendages, both distal, which have roles in basal body formation and ciliogenesis, and subdistal, which have roles in microtubule nucleation. Distal appendages are involved in linking the basal body to the cell membrane and are thought to be the transition fibres/alar sheets of the transition zone (Hoyer-Fender, 2010; Paintrand et al., 1992). Distal appendages contain Cep164, which is required for cilia formation (Graser et al., 2007).

This duplication method leads to inherent asymmetries: the older centriole at G_1 has appendages, while the younger centriole does not. When the cell divides, these asymmetries are inherited with the centrioles; one centriole is newly formed in the previous cell cycle, whereas the other centriole is the older mother centriole. This has functional consequences, as the daughter cell which inherits the older centriole is able to form a primary cilium more quickly, leading to differences in Shh signalling (Anderson and Stearns, 2009). It is also possible that closely associated components of the pericentriolar material (PCM) are asymmetrically inherited.

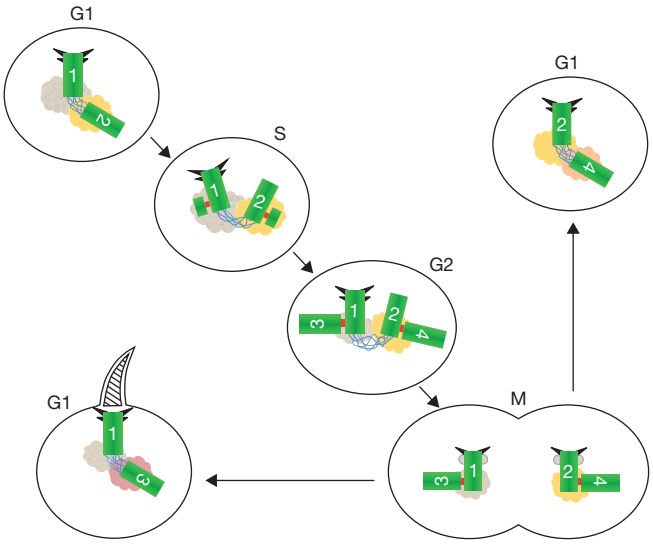

Figure 1.9 Centriole duplication. Centriole 1 is the older of the two centrioles in the upper left cell, and as such has appendages (black triangles). It is tethered to the younger centriole by a G1-G2 tether (blue), although they are disengaged (no S-M linker, red). The grey and yellow clouds represent pericentriolar material (PCM) associated with the older and the younger centriole respectively. Centrioles duplicate in S phase, and daughter pro-centrioles nucleate at right angles from the proximal end of the existing centrioles. Pro-centrioles elongate during G2 and these new centrioles (3 and 4) remain engaged to their respective mother centriole via the S-M linker (red). Centriole 2 acquires appendage proteins during mitosis and full appendages in G1 of the next cell cycle, after division. When the cell divides, one daughter cell receives the older centriole (1) and a newly formed centriole (3), whereas the other cell receives a younger centriole (2) and a newly formed centriole (4). The inherent asymmetries in this replication method can lead to detectable differences in the daughter cells. For example, the daughter cell which inherits the older centriole (1) puts out a cilium more quickly and this can lead to differences in Hh signalling responses. This replication method means it takes one and a half cell cycles for a centriole to fully mature. It is possible that proteins in the PCM may also be inherited asymmetrically. (Taken from Nigg and Stearns, 2011).

The PCM is an amorphous mass of proteins that surrounds the centriole. Together, the centrioles plus the PCM make up the centrosome. Many proteins of the PCM have important roles in control of centriole duplication, as well as in mediating roles of the centrosome, such as the γ-tubulin ring complex (γ-TURC), which is involved in mediating microtubule nucleation and capping (Moritz et al., 2000; Moritz et al., 1995). It has been shown that at least some components of the PCM, including γ-tubulin, remain associated with the centrioles when they become basal bodies and nucleate a cilium (Moser et al., 2010). The composition of the PCM is highly regulated, and this regulation can impact on centrosome function and ciliogenesis (Moser et al., 2010). Recently, it has been suggested that centriolar satellites, electron dense structures observed near centrosomes and basal bodies, may play a role in regulating centrosomal composition (Balczon et al., 1999; Barenz et al., 2011). The localisation of centriolar satellites varies during the cell cycle and they are thought to be involved in transporting proteins to or sequestering proteins from the centrosome (Balczon et al., 1999; Barenz et al., 2011). Centriolar satellites, which are marked by Pcm1, have been shown to actively traffic along microtubules and are thought to have roles in centriole formation and ciliogenesis (Balczon et al., 1999; Barenz et al., 2011; Dammermann and Merdes, 2002; Kim et al., 2004; Kubo et al., 1999).

1.6.1.2 Multiplication of basal bodies in multiciliated cells

Primary cilia form from pre-existing centrioles, generated by the duplication method described above, and can form during G_1/G_0. In contrast, in multi-ciliated epithelia, formation of many basal bodies is required, up to 200-300 per cell in the mammalian trachea. These cells are terminally differentiated and formation of the multiple centrioles is therefore not linked to cell cycle. These centrioles mature to basal bodies as they form and migrate to the cell surface (Dawe et al., 2007).

Two mechanisms have been identified which lead to the formation of these multiple basal bodies: the centriolar pathway and the acentriolar pathway. In the centriolar pathway, multiple centrioles form around an existing centriole (Anderson, 1972; Sorokin, 1968). The acentriolar pathway involves formation of multiple centrioles

around deuterosomes, electron dense structures of two types, hollow or solid, named from their appearance in electron micrographs (Dirksen, 1971; Hagiwara et al., 1992; Sorokin, 1968).

This wave of basal bodies migrate apically, and acquire appendages, including a basal foot which may help stabilise the cilia. Motile cilia have one basal foot which is a conical structure which projects laterally from the basal body in the direction of beating, whereas primary cilia can have up to five (Hoyer-Fender, 2010). In some cases, basal bodies also acquire striated rootlets, which project down from the basal body and contain rootletin (Yang et al., 2002).

The control of basal body migration to the cell membrane is not well understood but it is known that cell polarity is linked to ciliogenesis, and it is likely this is due to basal body migration.

1.6.2 Cell Polarity and ciliogenesis

It is thought the actin cytoskeleton plays a role in basal body orientation. Actin filaments and myosin are associated with centrioles and basal bodies, and inhibition of actin polymerisation can disrupt centriole migration to the cell surface (Boisvieux-Ulrich et al., 1990; Klotz et al., 1986; Lemullois et al., 1987). Talpid3 is a centrosomal protein, which when mutated in chicken cells leads to disrupted actin cytoskeleton and basal bodies which do not dock (Yin et al., 2009). Mks3/Meckelin localises to cilia, but also to actin based projections such as filopodia. It has been shown to interact with actin-binding proteins nesprin2 (nuclear envelope spectrin repeat protein 2) and Filamin A (FlnA), and siRNA knockdown of *Mks3* or *FlnA* leads to similar defects in basal body positioning and ciliogenesis (Adams et al., 2012; Dawe et al., 2009).

The establishment of apicobasal polarity is central to the apical migration of basal bodies and cilia formation in multiciliated epithelial cells. Transmembrane protein Crb3, which has roles in establishing apicobasal polarity and tight junction formation, in complex with Pals1 and Patj, along with the Par3-Par6-aPKC complex, has been shown to localise to the cilia, and knockdown of *Crb3* or blocking aPKC inhibits ciliogenesis (Bossinger and Bachmann, 2004; Fan et al., 2004a).

Interestingly, Nphp1 and Nphp4 have been shown to localise to cell-cell contacts as well as the transition zone, and as mentioned, siRNA knockdown in 3D culture leads to disrupted cell polarity and reduction in ciliogenesis (Delous et al., 2009; Sang et al., 2011). It was also shown that overexpressed Nphp1 and Nphp4 interact with Pals1 and Par6, further supporting a link between cell polarity and ciliogenesis (Delous et al., 2009).

Distinct from and perpendicular to apicobasal polarity, the planar cell polarity pathway (PCP) controls polarisation of a cell within a field of cells, along the plane of the cell sheet, such as an epithelial cell layer. PCP signalling has been implicated in ciliogenesis, possibly by controlling actin dynamics. PCP effectors Inturned (Intu) and Fuzzy (Fuz) were shown to be involved in ciliogenesis in *Xenopus*: morpholinos against *Intu* or *Fuz* lead to decreased ciliogenesis through disruption of the actin cytoskeleton (Park et al., 2006). Dishevelled (Dvl), a core PCP pathway component, was also shown to be involved in actin dynamics, basal body docking and ciliogenesis in *Xenopus* (Park et al., 2008). Disruption of *Dvl* and *Frizzled-2*, another PCP component, in zebrafish leads to reduced cilia numbers and length as well as impaired actin assembly (Oishi et al., 2006). Subsequently, it was found that mutant mice of orthologues of *Int* and *Fuz* also have ciliary defects, displaying embryonic lethality, neural tube closure defects, aberrant Hh signalling and polydactyly. It was shown the spinal cord defects were due to problems with ciliogenesis as $Intu^{-/-}/Ift88^{-/-}$ or $Fuz^{-/-}/Ift88^{-/-}$ double mutants display the same spinal cord phenotype as $Ift88^{-/-}$ single mutants. These epistasis experiments suggest the defects are a result of *Intu* and *Fuz* acting through cilia (Heydeck et al., 2009; Zeng et al., 2010). However there was no mention of actin cytoskeleton abnormalities in the mouse so it is unclear if the ciliogenesis defects involve actin in this case.

1.6.3 Cilia and the cell cycle

Dual roles for centrioles in the cell cycle, at the cycling centrosomes and at non-cycling basal bodies during ciliogenesis, means ciliogenesis is linked tightly to the cell cycle. In most mammalian cells, cilia only form when the cell is in G_1 and are

most abundant in G_0. Cilia are then retracted as the cells enter mitosis (Figure 1.10) (Rieder et al., 1979; Tucker et al., 1979). However the mechanism which controls this cell cycle related assembly and disassembly of cilia is not well understood.

Many proteins which are involved in cell cycle regulation and localise to the centrosome are also required for ciliogenesis (Graser et al., 2007; Mikule et al., 2007). As mentioned earlier, CP110 is localised to the distal end of the centriole and is involved in control of centriole length and is also required for ciliogenesis (Spektor et al., 2007). CP110 is phosphorylated by S phase cyclin dependent kinase 2 (Cdk2) (Chen et al., 2002b), so it is tempting to speculate that cell cycle dependent phosphorylation of CP110 by Cdk2 could cause it to be removed from centrioles to allow ciliogenesis.

What regulation coordinates cilia disassembly with the entry into mitosis? AuroraA kinase (AurA) is a known regulator of mitosis, and AurA along with HEF1 and HDAC6 have been shown to regulate cilia disassembly (Pugacheva and Golemis, 2005; Pugacheva et al., 2007). AurA and HEF1 localise to the centrosome during G_2 and M phase and both are activated at the basal body just prior to cilia disassembly triggered by adding serum to ciliated cells (Pugacheva et al., 2007). Inhibition of AurA leads to a decrease in cilia whereas overexpression leads to an increase. AurA phosphorylates Hdac6, a tubulin deacetylase, leading to decreased tubulin acetylation and decreased cilia stability (Pugacheva et al., 2007). However, it has been shown that microtubule acetylation does not contribute to mitcrotubule stabilisation so the exact mechanism of AurA mediated deciliation is unclear (Maruta et al., 1986). Whatever the mechanism, AurA provides a possible link between cilium disassembly and the cell cycle.

It has also been suggested that cilia may themselves influence the cell cycle. It is clear that in general, cilia are not essential for cell cycle progression as the lack of proteins required for ciliogenesis does not always lead to cell cycle disruption (Graser et al., 2007; Ishikawa et al., 2005). Hints that cilia may play some role in cell cycle control included the observation that lack of IFT27 in *Chlamydomonas* leads to defects in cytokinesis, as well as the expected loss of flagella (Qin et al., 2007). In addition, it was suggested that IFT88 inhibited cell cycle progression in

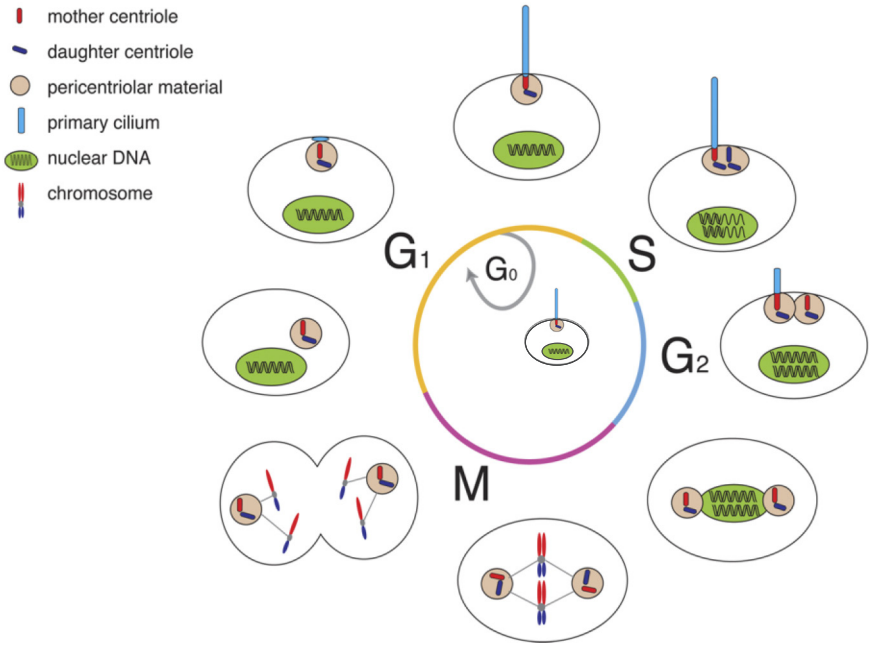

Figure 1.10 Ciliogenesis and the cell cycle. Because of the dual role of the centriole at the basal body during ciliogenesis and at the spindle pole during cell division, ciliogenesis is tightly linked to the cell cycle. During mitosis, centrioles locate to the spindle poles and each daughter cell inherits one centrosome with two centrioles. During G1 the mother centriole migrates to the cell membrane and nucleates a cilium. In terminally differentiated cells, or cells which have arrested cell division and entered G0, the cilium is maintained. In most cells which continue to divide, the centrioles duplicate during S phase and cilia disassembly begins around the end of S phase and beginning of G2, although the exact timing of cilia disassembly can vary between cell types. Cilia disassembly releases the centrioles and allows them to migrate to the spindle poles for the next cell division. (Adapted from Santos and Reiter 2008).

non-ciliated HeLa cells (Robert et al., 2007). A more recent study looked at the role of Ift88 in the cell cycle in several systems and suggested that reduced Ift88 induces mitotic defects, with abnormalities in astral microtubules and spindle pole localisation (Delaval et al., 2011). However, they suggest this is a non-ciliary role of Ift88, where Ift88 is part of a complex including the cytoplasmic dynein-1 motor that is required for astral microtubule formation, necessary to orient the spindle during mitosis (Delaval et al., 2011). Therefore considering the available evidence, it seems unlikely that cilia themselves play a role in cell cycle, although further studies are needed. It is possible that non-ciliary functions of cilia-associated proteins could include roles in cell cycle control, and this must be considered when drawing conclusions about the role of cilia in the cell cycle.

1.7 Defining the ciliome

Cilia are essential for mammalian development, and have been linked to a wide range of human diseases. Therefore, understanding the function of cilia is of utmost importance. As evidenced by the work described so far, although much is known about the formation of cilia and the function of cilia in certain processes, there is clearly much more to learn. The wide range of phenotypes observed in such genetically diverse human ciliopathies hint at as yet unknown functions of cilia. One way to address some of these questions is to perform screens to identify proteins involved in cilia formation and function, including proteomic, transcriptomic, bioinformatic and functional genetic approaches.

Several methods have been used to try to define the ciliome – which includes all the proteins found in the cilium, as well as those involved in the regulation of cilia structure and function. The aim of my thesis was to carry out a functional genetic screen for genes involved in mammalian cilia formation and function (discussed further below). I will discuss key studies which attempt to define the ciliome, with more focus on those completed before I started the screen (2010) to explain where

my work fits into what was known at the time, as well as what has been elucidated since I began.

1.7.1 Proteomic studies

Several proteomic studies have been carried out, isolating cilia or flagella biochemically and analysing the proteins present by mass spectrometry in human and mouse cells, *T. thermophilia*, *C. reinhardtii* and *T. brucei* ((Broadhead et al., 2006; Ishikawa et al., 2012; Liu et al., 2005; Mayer et al., 2008; Ostrowski et al., 2002; Pazour et al., 2005; Smith et al., 2005) reviewed in (Gherman et al., 2006; Inglis et al., 2006)). One of the first studies isolated cilia from human bronchial epithelium using detergent followed by proteolytic digestion with or without gel electrophoresis then liquid-chromatography mass-spectrometry (LC-MS). This did not keep the ciliary membrane and only isolated the axoneme and associated proteins but nevertheless, it identified many structural components such as dyneins and radial spokes (Ostrowski et al., 2002). Pazour et al., (2005) carried out a more careful biochemical purification of *Chlamydomonas* flagella, isolating different fractions including membrane and axoneme, membrane and matrix (proteins not closely associated with either axoneme or membrane *eg.* IFT proteins) or axoneme alone. This is a highly comprehensive list which when combined contains 97 of the 101 *Chlamydomonas* genes known to involved in flagella biology at the time. Transcription analysis of 69 genes showed 60 were upregulated upon flagellar regeneration. They identified many signal transduction proteins, for example receptors, kinases, channels and small GTPases (Pazour et al., 2005). Importantly they also identified many proteins known to be associated with human ciliopathies, including Arl13b, Pkd2, Fibrocystin and Nek1.

One study specifically examined flagellar phosphoproteins in *Chlamydomonas*, identifying 141 phosphopeptides mapping to 32 flagellar proteins, of which 8 were structural, 4 were enzymes and 20 were uncharacterised flagellar associated proteins (Faps) (Boesger et al., 2009). The structural components included inner and outer

dynein arms, radial spokes and IFT43. Many of the phosphorylation sites were dynamic and many proteins have more than one phosphorylation site.

Proteomics have also been carried out on sensory cilia in mammalian olfactory sensory cilia or photoreceptors (Liu et al., 2007; Mayer et al., 2008). Mayer et al., (2008) specifically enriched for membrane proteins in rat olfactory sensory cilia and identified all 25 components of the canonical olfactory signal-transduction cascade. Until recently, the proteome of mammalian primary cilia had not been analysed. This year, Ishikawa et al., (2012) analysed the proteome of cilia isolated by calcium shock from IMCD3 cells, a mouse kidney cell line, using multi-dimensional protein identification technology (MudPIT) followed by protein correlation profiling. As a control, they also performed calcium shock on IMCD3 cells which had been deciliated by nocodazole and cold treatment, and any proteins found by this method were subtracted from the original list, leaving 195 proteins. 75% overlapped with motile or specialised cilia. Interestingly, the 25% identified as putative primary cilia specific proteins included, Evc2, Inpp5e and Inversin, which are known ciliopathy associated proteins (Ishikawa et al., 2012).

Biochemical studies have also been performed on the basal body in *Chlamydomonas* and the centrosome in human cells, and as the centrosome is analogous to the basal body, many of these proteins may have roles in ciliogenesis (Andersen et al., 2003; Graser et al., 2007; Jakobsen et al., 2011; Keller et al., 2005). The human data can be accessed at www.centrosomedb.com.

Problems with proteomic studies include the fact that they rely on biochemical purification techniques, which will never by 100% pure, as well as thresholding problems with sensitivity meaning low abundance proteins will not be detected. For example BBS proteins have not been detected by proteomic methods, perhaps due to problems with isolation or sensitivity. Therefore these lists will contain both false positives and false negatives. Several of these studies have been integrated into a database (www.ciliaproteome.org) including the centrosome/basal body studies. The fairly low level of overlap between these screens could indicate they are not yet saturating, suggesting there may be many more genes involved in cilia formation and function yet to be identified. However it must be considered that the lack of overlap

between studies could be due, at least in part, to differences in organisms and cell types studied.

1.7.2 Transcriptomic studies

Studies have been carried out to identify genes which are upregulated during ciliogenesis. Upon deflagellation, *Chlamydomonas* undergo reflagellation within 90 minutes and this process involves upregulation of many genes (Rosenbaum et al., 1969). (Stolc et al., 2005) carried out a genome-wide microarray analysis of upregulated genes upon *Chlamydomonas* flagellar regeneration. They found 230 upregulated more than 2 fold, of which 85 had previously known links to cilia or basal bodies. This had a reasonably low false positive rate due to high stringency cut-off. One advantage of transcriptomic studies is the identification of proteins involved in cilia that do not necessarily localise to cilia, for example the DNA helicase components *reptin* and *pontin* were upregulated. These have since been shown to be involved in cystic kidneys in zebrafish (Sun et al., 2004).

A second approach to analyse the ciliary trancriptome was to compare ciliated and non-ciliated cells in the same organism. Blacque et al., (2005) used *bbs1-GFP* to label all ciliated neurons in *C. elegans*. Embryos were disrupted, fluorescence-activated cell sorted (FACS) for GFP positive cells and then serial analysis of gene expression (SAGE) was performed. They did the same with pan-neural, intestinal or muscle specific GFP and then looked for genes which were 1.5 fold increased in the ciliated versus non-ciliated cell types. This gave a list of 1,282 genes which included many IFT and BBS genes. This can also be used to identify genes specific to a particular ciliated cell type. For example, Colosimo et al., (2004) looked at the difference in expression profiles between unsorted *C. elegans* cells and two ciliated sensory neurons, AWB olfactory neurons and AFD thermosensory neurons, identifying genes including receptors and kinases. Similarly, in *Drosophila,* Cachero et al., (2011) isolated ciliated chordotonal neuron precursors using *ato-gfp* at different time points during embryogenesis. At time point 3, just as ciliogenesis is about to commence, the gene list is highly enriched for ciliary genes.

An alternate transcriptomic approach was employed by McClintock et al., (2008) who examined databases of microarray expression studies to identify genes expressed in mouse ciliated tissues: olfactory epithelium, testes, trachea, lung and vomeronasal epithelium. They identified 99 genes of which 39 had previous links to cilia. Limitations include the fact these tissues only represent motile and specialised sensory cilia and so primary cilia genes may be missed. This cannot easily be addressed by this method due to the widespread presence of primary cilia in mouse.

Finally, Phirke et al., (2011) examined transcriptional differences between wild type and *daf-19* mutant *C. elegans*. Daf-19/Rfx is a transcription factor, controlling the expression of many ciliary genes, and *daf-19* mutants lack cilia (see 1.7.3.2) (Swoboda et al., 2000). They found 881 genes with greater than 1.5 fold increase or decrease in expression and confirmed ciliary expression for 11 of 14 tested. They characterised phenotypes of mutants of two of these genes which display classic ciliary defects such as dye-filling and osmotic avoidance defects (Dyf and Osm).

The advantage of these approaches mean you can identify genes involved in ciliogenesis that are not localised to cilia and also may have other cellular roles so won't be picked up in comparative genomic screens (see below). However, disadvantages include the high false positive rate, if the stringency of the cut-off is too low, or conversely, false negatives due to genes being expressed at levels below the threshold of detection. In the screens where only specific cell types were used (Cachero et al., 2011; Colosimo et al., 2004), many genes could be over-expressed due to neural specific functions, without a role in cilia. Therefore complementary approaches are needed to confirm ciliary roles.

1.7.3 Bioinformatic approaches

1.7.3.1 Comparative genomics

By subtracting genes conserved in non-ciliated organisms from ciliated organisms, it should be possible to enrich for genes involved in ciliogenesis. Two back-to-back studies carried out this approach to generate lists of putative ciliary genes (Avidor-

Reiss et al., 2004; Li et al., 2004). Li et al., (2004) looked for orthologues between *Chlamydomonas* and human, and then subtracted genes found in the non-ciliated *Arabidopsis* genome. This gave the flagellar apparatus-basal body proteome (FABB) of 688 proteins. This list contained 52/56 known ciliary genes and 4/6 known basal body proteins queried. Interestingly 50% of the 688 proteins had no known link to cilia function or formation. The list contained several human ciliopathy related genes (all of the five BBS genes known at the time, Nphp4 and fibrocystin). The list also showed an enrichment for TPR, WD and IQ calmodulin motifs, characteristic of ciliary genes. They examined the expression of 100 of these genes upon flagellar regeneration and a third were upregulated. One of these was the previously unidentified gene responsible for BBS (*BBS5*), which they showed was mutated in two BBS families. Furthermore, siRNA to 5 of 6 genes not upregulated and so hypothesised to be involved in basal body function gave a flagellar phenotype when knocked down by siRNA.

The second study by Avidor-Reiss et al., (2004) examined nine genomes, six of which were ciliated (*D. melanogaster, H. Sapiens, C. elegans, C. reinhardtii, P. falciparum* and *T. brucei*) and three non-ciliated (*A. thaliana, S cerevisiae* and *D. discoideum*). They used the fact that *P. falciparum* has an unusual method of ciliogenesis, which they term cytosolic, in which it assembles the flagella in the cell cytoplasm and so does not require IFT, to divide the genomes into four groups. It should be noted that *Drosophila* sperm flagella are also formed by the cytosolic method, but the cilia on their sensory neurons are formed by IFT via the "compartmentalised" method. They grouped the genes into four categories: (i) those present in all ciliated organisms, 16 genes, (ii) those present in organisms with motile cilia only (i.e. in all ciliated organisms except *C. elegans,* which lack motile cilia), 18 genes, (iii) those present in organisms with compartmentalised ciliogenesis (i.e. all ciliated organisms except *P. falciparum*), 103 genes, and (iv) those present in organisms with both motile and compartmentalised cilia i.e. "prototypical" cilia, 50 genes. Of these 187 genes, 36 were known ciliary genes and a third have X-boxes in their promoters. Out of 17 genes tested, all localised specifically to the sensory ciliated neurons. They identified several small GTPases, including Arl3, Arl6 and Arl13b, where *ARL6* was subsequently shown to be mutated in BBS.

Again, this method allows identification of genes which do not localise to the cilia and so would be missed by proteomic studies. However, disadvantages include the fact that any genes with both ciliary and non-ciliary roles will be missed. Also technical aspects such as availability and quality of genome sequences and the ability to successfully identify orthologues can limit the power. Despite these caveats, this method seems to have a relatively high true positive hit rate as judged by the follow up studies performed.

1.7.3.2 Promoter motifs

As so many genes are co-ordinately upregulated upon ciliogenesis initiation, there must be transcription factors controlling this process. The two main transcription factors families identified with roles in this process are Regulatory factor X (Rfx) and Foxj1 (Forkhead box J1/Hfh-4) (Thomas et al., 2010). Foxj1 controls expression of genes specific to motile cilia and was shown to be necessary and sufficient for motile ciliogenesis in zebrafish and *Xenopus* (Stubbs et al., 2008; Yu et al., 2008).

Transcriptomic analysis of microdissected forebrains from wild type and *Foxj1*$^{-/-}$ mice showed that Foxj1 controlled the expression of 198 genes, 197 of which were downregulated in *Foxj1*$^{-/-}$ cells. These included cytoskeletal associated motors such as kinesin and dyneins, radial spoke proteins and microtubule associated proteins (Jacquet et al., 2009). In addition, ectopic overexpression of *Foxj1* in *Xenopus* leads to ectopic cilia formation and microarray analysis shows many genes related to motile ciliogenesis are upregulated (Stubbs et al., 2008). Interestingly, Foxj1 is absent from the genomes of cilia model organisms *Drosophila* and *C. elegans.* As *C. elegans* only have non-motile sensory neural cilia, this lack of *Foxj1* is expected. In contrast, *Drosophila* sperm flagellar are motile. However, their formation does not require IFT; they are formed by cytosolic ciliogenesis and so perhaps this explains the lack of requirement for a *Foxj1* orthologue (Mazet et al., 2003).

Rfx is thought to regulate genes required for both motile and non-motile cilia. Therefore Rfx and Foxj1 are thought to have both overlapping and distinct sets of target genes. Swoboda et al., (2000) showed that *C. elegans* Rfx/Daf19 was required

for sensory cilium formation in *C. elegans* and showed that expression of several ciliary genes which have consensus binding sites for Rfx transcription factors, X-boxes, in their promoters were down regulated in *daf-19* mutants. Interestingly, human Rfx3 and at least one of the two *Drosophila* Rfx proteins also control expression of ciliary genes (Bonnafe et al., 2004; Dubruille et al., 2002). This lead to a genome-wide analysis of X-boxes in *C. elegans* (Blacque et al., 2005; Efimenko et al., 2005; Fan et al., 2004b). Fan et al., (2004b) generated a consensus X-box sequence using 14 genes with X-boxes known to be specifically expressed in ciliated cells. They identified Arl6 as a ciliary gene and showed it was mutated in BBS. Efimenko et al., (2005) used a 14bp average X-box sequence to search the *C. elegans* genome. 164 genes were identified with X-boxes within 100bp of the transcription start site. This included a tctex1 domain containing dynein which was shown to undergo IFT when tagged with GFP. Blacque et al., (2005), who performed the SAGE analysis of genes expressed in ciliated versus non ciliated cells in *C. elegans,* also carried out a genome-wide screen for genes containing X-boxes using a Hidden Markov Model trained with 22 X-boxes from known ciliary genes. 14 genes were followed up, ciliary localisation was confirmed and one, dyf-13, was shown to undergo IFT.

Analysis of X-box-containing genes helps identify novel ciliary genes, but it is not an exhaustive list as not all ciliary genes are controlled by Rfx. For example, in worms and flies, Rfx controls many IFT-B and BBS proteins, as well as the retrograde dynein motor, however it does not regulate expression of most IFT-A genes or the anterograde kinesin motor subunits (Efimenko et al., 2005; Thomas et al., 2010). Also the analysis depends on the ability to predict binding sites and so more degenerate binding sites may be missed and if genes are close together or overlapping it may be difficult to assign a predicted binding site to a specific gene.

Many of the above studies have been integrated into a database, www.ciliome.com although it should be noted that this excludes the basal body proteome data and is concentrated on the cilium itself (Inglis et al., 2006).

1.7.4 Functional genetic screens

One of the major drawbacks of the screens mentioned so far is that they fail to give any functional data, they correlate gene expression or protein localisation with cilia, which suggests a role in ciliogenesis or cilia function for that protein but does not indicate what the role could be.

A recent method of large scale functional screening is RNA interference (RNAi) library screening (Mohr et al., 2010). RNAi gene silencing is triggered by short double stranded RNA (dsRNA) molecules, which can be endogenous or exogenously introduced (Carthew and Sontheimer, 2009; Fire et al., 1998; Zamore et al., 2000). Endogenous microRNAs (miRNAs) are expressed as long double stranded pri-miRNAs (Jackson and Linsley, 2010). These are first processed to a 70 nucleotide pre-miRNA by enzymes Drosha and Dgcr8/Pasha (Lee et al. 2002; 2003), then further processed by Dicer to a 22 nucleotide mature miRNA (Grishok et al. 2001; Hutvagner et al. 2001; Lee at al. 2002). One strand (the guide strand) is incorporated into the RNAi-induced silencing complex (RISC), which targets RISC to the 3' untranslated region (UTR) of the target genes. Specificity is determined by a 7-8 nucleotide "seed sequence" which binds the target mRNA, leading to an arrest in translation or mRNA degradation (Jackson and Linsley 2010).

In contrast, short interfering RNAs (siRNAs) are exogenous, and can introduced by an invading virus, or biochemically synthesised and introduced experimentally. These dsRNAs are cleaved by Dicer to 21-22 nucleotide siRNAs (Grishok et al. 2001; Hamilton et al. 1999). As with miRNAs the guide strand binds the RISC complex targeting it to the mRNA leading to cleavage. As opposed to miRNA targeting which depends on the 7-8nt seed sequence present in the 3'UTR of the target mRNA, siRNA-dependent gene silencing is more dependent on the overall 20 nucleotide sequence being complementary to the target mRNA sequence and the target sequence can be anywhere within the mRNA (Jackson and Linsley 2010). Also, although the seed sequence for miRNAs can tolerate 1-2 base pair mismatches,

siRNAs rely on complete complementarity of the seed sequence to the target sequence and any mismatch can greatly reduce the efficiency of silencing.

Importantly, this mechanism allows experimental targeted gene silencing in mammalian cells, by artificially introducing either siRNAs (biochemically synthesised 20-21nt dsRNA molecules transfected into cells using lipid based or electroporation based methods), or shRNAs (these consist of a single RNA molecule which forms a secondary structure loop to make the typical hairpin structure) targeting the gene of choice. The latter are delivered as vector-based plasmids using H1 or U6 RNA pol III promoter, to ensure the shRNA is always expressed, and are usually delivered to cells using viral based methods (Mohr et al., 2010).

Some RNAi screens have been carried out in mammalian cells to identify ciliary genes. A small-scale RNAi screen of 41 centrosomal proteins identified 25 proteins that when knocked down lead to reduced or no cilia formation (Graser et al., 2007). This study showed that Cep290 was involved in cilia formation as suggested by its association with ciliopathies (Baala et al., 2007; Helou et al., 2007; Valente et al., 2006). They further characterised Cep164, and showed it was a distal appendage protein essential for ciliogenesis.

A larger scale RNAi screen against the kinome (all kinases in the murine genome, 812 genes) in mouse S12 cells (C3H fibroblast cell line with a stably integrated Hh responsive luciferase gene) identified 29 genes which when knocked down, abolished Hh response. By further criteria they reduced this to 9 strong candidates. They then discarded two of the genes which they showed when knocked down reduced the percentage of ciliated cells, because they were interested in genes directly involved in Shh signalling (Evangelista et al., 2008). These genes were Nek1, which was already known to function in ciliogenesis (Shalom et al., 2008) and Prkra1, with no previously known role in ciliogenesis.

Kim et al., (2010) performed a siRNA screen of 7,784 therapeutically relevant genes for roles in ciliogenesis. Cilia were marked with Smo-GFP which when overexpressed localises to cilia constitutively in hTERT-RPE cells. As this is not true of endogenous Smo, which shows dynamic localisation in response to Hh

signalling it is possible this could lead to false negatives and positives, however hits were followed up by looking at cilia marked by anti-acetylated α-tubulin, eliminating 4 false positives. They identified 36 positive and 13 negative modulators of ciliogenesis. Although the therapeutically relevant genes are low in ciliome genes, they did identify 12 genes encoding ciliome proteins. They identified several modulators of actin stability and suggested that actin may have a negative role in stabilisation of the recycling endosome at the basal body.

Finally, a high-content siRNA screen to identify functional roles of 40 genes from the ciliome was carried out by Lai et al., (2011) after I began my screen. They selected candidate genes which had at least one hit in a proteomic study (Ostrowski et al., 2002; Pazour et al., 2005) and at least one hit in a genomic comparison study (Avidor-Reiss et al., 2004; Li et al., 2004) and had not been functionally characterised at the time, giving a list of 40 genes to screen. They assayed cilia presence and length in two cell lines (NIH-3T3 and IMCD3-HTR6-GFP) and ciliary transport by looking at HTR6-GFP trafficking and endogenous Gli3 localisation by immunofluorescence. They also assayed cilia function in S12 cells (which have a Gli-luciferase reporter transgene stably integrated) by using Hh signalling as a readout of ciliary function. They categorised hits into six classes: I) defects in ciliation, transport and signalling, II) shortened cilia III) long cilia IV) defects in cilia structure and transport but normal Hh signalling V) defects in transport and signalling but normal structure and VI) defects in Hh signalling alone. All but two genes gave a defect in Hh signalling suggesting it may be the most sensitive readout, although it could reflect non-ciliary modulators of Hh signalling. Interestingly, Arl3 and Nme7 gave defects in transport and since the beginning of their screen, mouse mutants in these genes were shown to have ciliary defects (Schrick et al., 2006; Vogel et al., 2009).

These studies provide functional data for either known or novel ciliary genes. However as with all screens there are disadvantages. One disadvantage is the possibility that siRNAs can also downregulate mRNAs other than the target gene, known as off-target effects. Off-target effects can occur via three main mechanisms: (i) the siRNA can behave in a miRNA-like manner, targeting mRNAs with partial

complementarity to the seed region, for sequence-dependent degradation of non-target mRNAs, (ii) transfection protocols and delivery of siRNAs can cause an inflammatory response, leading to gene expression changes or (iii) siRNAs can saturate the RNAi machinery leading to widespread problems in miRNA processing and subsequent changes in gene expression.

These screens also have a high false-negative rate, probably due to inefficient knockdown of the target gene. To address these problems, screens generally involve 3 or 4 siRNAs targeting each gene, and look for a phenotype in more than one siRNA targeting a specific gene. In addition, follow-up studies must attempt to address the possibility of off-target effects, for example by performing experiments to test whether target mRNA level correlates with phenotype severity, and whether the effect can be rescued by expressing an siRNA-insensitive version of the gene.

Despite these caveats, with appropriate assays, controls and downstream validation techniques RNAi screening is a powerful tool to perform functional genetics in mammalian cells. The lack of overlap between the siRNA screens suggests these screens are far from saturating, either due to technical issues of false-negatives stated above, or lack of overlap between gene lists screened.

Interestingly, McClintock et al. suggested that in 2008, 62% of genes with documented roles in cilia in the literature were not identified in online ciliome databases. Therefore it is likely that many more genes involved in cilia formation and function remain to be identified.

1.8 Thesis aims

To date, screens to define the ciliome have identified over two thousand genes which localise to the cilia or are involved in cilia function (McClintock et al., 2008). However the function of the vast majority of these genes remains unknown, particularly in mammalian systems.

The aim of my thesis was to carry out an RNAi based functional genetic screen in mouse cells to identify genes involved in cilia formation and function. I optimised

two readouts, one for cilia formation and one for cilia function and screened 37 candidate genes. The genes were identified by a developmental expression screen in *Drosophila* as highly expressed in ciliated sensory neurons upon ciliogenesis (Cachero et al., 2011). The list was already highly enriched for ciliary genes, but was further mined by bioinfomatics for highly conserved candidates.

In this thesis I describe optimisation of the screening protocols, which included functionally characterisation of the cellular ciliary phenotype of two novel mouse ciliary mutants, *Wdr35* and *Dync2h1* identified by ENU mutagenesis screen for genes involved in embryonic patterning (Mill et al., 2011) as a test set.

The siRNA screen identified several genes involved in cilia formation and controlling cilia length. Confirmation studies, including biological repeats in two cell lines correlation of mRNA levels to phenotype, and rescue with an siRNA insensitive version of the gene were performed for top hits. Localisation studies and characterisation of the phenotype in real time suggests that one gene, *Ccdc63,* localises to cilia and is involved in cilia formation, possibly due to roles in cilia stability. A second hit, Azi1, is also shown to localise to the base of cilia and siRNA knockdown leads to reduced cilia and cilia length. This reduction in cilia number can be resuced by overexpression of an siRNA resistant GFP tagged Azi1, confirming it is not due to off-target effects of the siRNAs. The role of Azi1 in ciliogenesis *in vivo* is explored further by generation and characterisation of *Azi1* null mice. Surprisingly these mice survive, suggesting Azi1 is not essential for ciliogenesis. These mice display male infertility, with reduced sperm count due to arrest in spermiogenesis at Stage IX, just as the flagella is forming. This suggests Azi1 may have a role in formation of sperm flagella, a specialised motile ciliary structure.

Chapter 2 Materials and Methods

2.1 Microbiology Methods

2.1.1 Growth of bacterial strains

Bacterial strains transformed with the relevant plasmid (Table 2.1) were grown at 37ºC overnight either on L-agar plates (10g/L NaCl, 10g/L Bacto-tryptone, 5g/L Yeast extract, 15g/L Difco Agar) inverted, or in Luria-Bertani (LB) medium (10g/L NaCl, 10g/L Bacto-tryptone, 5g/L Yeast extract), shaking at 200rpm. The appropriate antibiotic was added (Ampicillin at 50µg/L, Kanamycin at 50µg/L).

2.1.2 Transformation of Bacterial strains

1ng of plasmid or 1-4µL of ligation was added to 50µL of chemically competent DH5-α *E. coli* (Invitrogen) and incubated on ice for 30 minutes (min). Cells were then heat shocked at 42ºC for 30 seconds (secs) and placed on ice for 2 min to recover. 950µL of warm LB was added and cells were placed at 37ºC shaking for one hour (h). 20-100µL of transformed cells was placed onto L-agar plated containing the relevant antibiotic. Plates were incubated inverted overnight at 37ºC.

2.2 DNA methods

2.2.1 Purification of DNA from *E coli* cells

A single bacterial colony was picked from an agar plate and used to inoculate 5mL of LB medium plus the relevant antibiotic. For mini-preparation of DNA, this was grown overnight shaking at 37ºC and DNA was isolated using Invitrogen Purelink HiPure Plasmid Miniprep Kit according to manufacturer's instructions. For maxi-preparation of DNA, 5mL cultures were grown at 37ºC for 8h and used to inoculate 100mL of LB broth with the relevant antibiotic, and cultures were grown overnight

Table 2.1 Plasmids used in this thesis

Plasmid	Description	Source
pCMV-Tbp	*Tbp* cDNA under the CMV promoter	Gift from Dr Tilo Kunath, University of Edinburgh
pCMV-Ptc1-GFP	*Ptc1* cDNA with a fluorescent GFP tag expressed under the CMV promoter	Gift from Prof Chi-Chung Hui, University of Toronto
pCAG-eGFP-hyg	Fluorescent protein *eGFP* expressed under the CAG promoter, with a *hph* gene to allow selection for expression with hygromycin in mammalian cells	Gift from Prof. Ian Chambers, University of Edinburgh
pCAG-eGFP-pur	Fluorescent protein *eGFP* expressed under the CAG promoter, with a *pac* gene to allow selection for expression with puromycin	Gift from Prof. Ian Chambers, University of Edinburgh
pAzi1-GFP	*Azi1* cDNA with a fluorescent GFP C terminal tag expressed under the CMV promoter	Created by Peter Budd, MRC HGU, University of Edinburgh
pmKate2-Arl13b	*Arl13b* cDNA with a fluorescent mKate2 C terminal tag expressed under the CMV promoter, with a *neo* gene for selection with G418	Created by Emma Hall
pCentrin2-eGFP	*Centrin2* cDNA with a fluorescent enhanced GFP (eGFP) C terminal tag expressed under the CMV promoter	Created by Emma Hall

`

at 37ºC, shaking. For storage, glycerol stocks were prepared: 500µL of transformed *E. coli* was mixed with 500µl of 50% glycerol and stored in 2 ml Cryo-screw capped tubes (Greiner) at -80°C. From the rest of the culture, DNA was isolated using Invitrogen Purelink HiPure Plasmid Maxiprep Kit according to manufacturer's

instructions. All plasmids were verified by sequencing across the insert and into the plasmid at either side of the insert (see 2.2.10).

2.2.2 Phenol/Chloroform extraction of nucleic acids

An equal volume of 25:24:1 phenol:chloroform:isoamyl alcohol (50% buffered phenol, 48% chloroform (v/v), 2% 3- methyl-1-butanol (v/v) pH >7.8) (Sigma) was added to the DNA preparation and vortexed, then centrifuged at 10,000g for 10 min. The top layer was placed into a clean tube. An equal volume of chloroform was added, and the sample was centrifuged at 10,000g for 10 min. DNA was isolated form the top aqueous layer by ethanol precipitation.

2.2.3 Ethanol precipitation of nucleic acids

0.1 volumes of 3M sodium acetate pH 5.2 and 2 volumes of 100% ice-cold ethanol were added to the DNA sample, mixed and incubated at -20ºC for at least 1h. Samples were centrifuged at 10,000g at 4ºC for 15 min. Pellets were washed with 70% ethanol. Pellets were then air dried and resuspended in Tris-EDTA (TE) (10 mM Tris-Cl, pH 7.5. 1 mM EDTA) buffer.

2.2.4 Agarose gel electrophoresis

DNA samples were analysed by agarose gel electrophoresis with agarose gels ranging from 1-2% agarose/TBE (w/v). Gels were prepared by dissolving agarose (Hi-Pure Low EEO agarose, Biogene) in TBE buffer (89mM Tris base, 89mM boric acid and 20mM EDTA) by microwave. Ethidium bromide was added at 0.5 μg/ml to cooled gel. 6X loading buffer (20% Ficcoll Type 400 w/v 100mM EDTA 0.4% Orange G in H_2O) was added to all samples before loading. Markers containing DNA fragments of known sizes were also loaded for size reference: 1kb DNA Ladder (Invitrogen) or 100bp DNA Ladder (Promega). 80-150V was applied and the gels were visualised with a UV transilluminator (BioDoc-It System, UVP).

2.2.5 Gel purification

The desired DNA fragment was excised from the gel using a clean razor blade and purified using the PureLink Quick Gel Extraction kit (Invitrogen) according to the manufacturer's instructions.

Table 2.2 Primers used in this thesis

Gene/ region to be amplified	Assay/Use	Primer	Sequence	Probe (for qPCR)
Ptc1	qPCR	F	CCAAAAGAAGAAGGCGCTAA	110
		R	GCACAAATGTTCCAACTTCCA	
Tbp	qPCR and RT-PCR	F	GGGGAGCTGTGATGTGAAGT	97
		R	CCAGGAAATAATTCTGGCTCA	
Wdr35	qPCR	F	CCAGTGATCAAAATGGGCTTA	89
		R	CGATTGTTGATCATCTCCTCAT	
Dync2h1	qPCR	F	GGTGGGACCAGAAGGATGT	89
		R	CGGAGCTGAGAGAAGGCATA	
Gapdh	qPCR	F	GGGTTCCTATAAATACGGACTGC	52
		R	CCATTTTGTCTACGGGACGA	
Kif3a	qPCR	F	TGTGTATAACTTAACTGCAAGAC CAA	97
`		R	TTGCCTGTCCCAGTCTGTC	
Ift88	qPCR	F	CAGCAAGCAGTGAGAACCAG	29
		R	GCTGTGCTTGGTATTTTAGCAG	
Sdccag8	qPCR	F	CAGGAGTGCCTGCGAGTC	76
		R	TGCTGAATGCTATCTTTTTCCA	
Bbs5	qPCR	F	CAAAGTCTATTCTGCCAGTCCA	3
		R	TTTGTTCAACAGTCAGAGCTTCA	
Tscot	qPCR	F	GGTCAGCCATGTCCAAACTC	98
		R	ATGTCACCACCCCAGTCAG	
Mllt4	qPCR	F	GAGGCCTGATGGTCAAGG	1
		R	TCCTCCCAATTCAAAGGTTG	
Epb4.1l4b	qPCR	F	CCAGCCTCAGTACCATCCTG	20
		R	TTGTTTGCAGATGGAATGGTT	
Spag1	qPCR	F	CAAGGCTCATCTGTCTAAAATTG A	62
	qPCR	R	GCAAGAAAACTCTTTTCCTTCTC A	
`*Ccdc63*	qPCR	F	GACCGCTCTGAATTTGAGGA	4

Gene/ region to be amplified	Assay/Use	Primer	Sequence	Probe (for qPCR)
`*Ccdc63*	qPCR	R	TCCCAAGCTTCTTGGATTTG	
Prdm1	qPCR	F	GGCTCCACTACCCTTATCCTG	100
		R	TTTGGGTTGCTTTCCGTTT	
Prdm2	qPCR	F	AGGCACTTTGTCTGCTCCTT	85
		R	AGACTGCTGGTCCCTTTGG	
Ttc28	qPCR	F	GTCTAGGAAATGGGCACAGG	40
		R	CCTCTTCTCGAAGCACACG	
Ttc30a2	qPCR	F	TCAACATGGGTTGTCTGCTC	27
		R	GCAAAGCCGCAAAGAATTT	
Arl13b	cloning	F	CGGCACAAGCTTATGTTCAGTCT GATGGCCAACTG	
		R	GCCGTCGGATCCCCTGAGATCG TGTCCTGAGCATC	
Centrin2	cloning	F	AAGAATTCGCCGCCATGGCCTCT AATTTTAAGAA	
		R	TTGTCGACTGATAGAGGCTGGTC TTTTTCA	
Azi1 intron 2 (spans gene trap)	Genotyping	F	GAGGAACCTGGGTGAGACCT	
		R	GCAGCAGATCTTTGGTCCAC	
Gene trap vector	Genotyping	F	GGTCCCGAAAACCAAAGAAG	
		R	AGTATCGGCCTCAGGAAGATCG	
Azi1 exon 2 - 3	RT-PCR	F	ACTCCTGAAGGCAGTCCAGA	
		R	CGTCCATGACTGGTTGACCT	
Azi1 exon 2 – gene trap	RT-PCR	F	ACTCCTGAAGGCAGTCCAGA	
		R	AGTATCGGCCTCAGGAAGATCG	
Azi1 exon 10 - 11	RT-PCR	F	GAACACAGACGGCCTAAGGA	
		R	TGGCTTGTCCTCTGGAGACT	
Azi1 exon 12 - 13	RT-PCR	F	CTGGACTGACGAGGAAGAGG	
		R	CGCTCCTGTCCTGACTTCTC	
Azi1 exon 20 - 21	RT-PCR	F	CAGAGTTGGAGGAGCTGAGG	

Gene/ region to be amplified	Assay/Use	Primer	Sequence	Probe (for qPCR)
Azi1 exon 20 - 21	RT-PCR	R	CTTCCTCCTTCTTGGCACAG	
Azi1 exon 22 - 24	RT-PCR	F	AGCAGGTGGAGCTAGACGAG	
		R	CAAGGGCGATGTCACTTAGA	

2.2.6 Polymerase Chain Reaction

Specific DNA regions were amplified by polymerase chain reaction (PCR). Primers were designed using Primer3 program (available at (http://frodo.wi.mit.edu/cgibin/primer3/primer3_www.cgi), except for primers used for qRT-PCR (see 2.3.6). Primers for RT-PCR were, when possible, designed to span introns, to allow genomic DNA contamination to be distinguished from cDNA. Primer sequences are given in Table 2.2. For standard PCR, Bioexact Taq polymerase (Bioline) was used.

When a high level of accuracy was required (*eg.* for cloning) Phusion Hotstart II (Finnzymes) polymerase was used. PCRs typically contained 0.5U polymerase, 0.2mM dNTPs (Invitrogen), 0.5µM each primer, 1X of the relevant buffer (supplied by the manufacturers for the specific polymerase), 2.5mM magnesium chloride ($MgCl_2$), 1-100ng of template DNA and H_2O up to desired reaction volume. A typical PCR reaction is shown:

	Denaturation	94˚C	2 min
25-35x	Denaturation	94˚C	15 sec
	Annealing	45-65˚C	30 sec
	Extension	72˚C	45 sec per kb
	Extension	72˚C	10 min

*Annealing temperature is based on the melting temperature of primer set used in each PCR.

For genotyping of *Azi1*$^{Gt/Gt}$ mice, primers detailed in Table 2.2, and depicted in Figure 6.3, were used to amplify DNA isolated as described in 2.6.2 and run on the following programme:

	Denaturation	94˚C	2 min
35x	Denaturation	94˚C	15 sec
	Annealing	60˚C	30 sec
	Extension	72˚C	1 min
	Extension	72˚C	10 min

Product was run on a gel (2.2.4) and expected sizes are wild type: 613bp, mutant: 324bp.

2.2.7 Purification of PCR products

PCR products were purified using Invitrogen PCR Cleanup kit according to manufacturer's instructions.

2.2.8 Restriction enzyme digestion

DNA was digested with restriction endonucleases in the buffer supplied and recommended by the manufacturer's (New England Biosystems or Roche). 2-5µg of plasmid/PCR product, 20U of the restriction enzyme and 1X buffer was incubated at 37˚C for at least 2h.

2.2.9 Ligation

100-200ng plasmid DNA plus 2-3X this molar amount of insert DNA, 1U of T4 DNA ligase (Roche), and 1X ligation buffer (Roche) were incubated at 4˚C overnight. 1µl of ligation was used to transform *E coli* (See 2.1.2).

2.2.10 DNA sequencing

Dye terminator sequencing reactions (Applied Biosystems) were performed and processed by the Institute of Genetics and Molecular Medicine (IGMM) sequencing service on a 3130/3730 genetic analyser (Applied Biosystems). The DNA sequencing data was analysed using Sequencher 4.10.1 (Gene Codes Corp.).

2.3 RNA methods

2.3.1 RNA isolation from cells

RNA was isolated from a confluent well of a 6 well plate using the RNeasy Mini Plus or Micro Kit (Qiagen). Wells were rinsed in PBS and 350µl of buffer RLT (Qiagen) was added to lyse the cells. Cells were homogenised through a Qiashredder column (Qiagen) according to manufacturer's instructions. If using the Mini Plus kit, DNA was eliminated by passing the lysate through a gDNA Eliminator Minispin Column (Qiagen). If using the Mini or Micro Kit, on-column DNase digestion was performed according to manufacturer's instructions. RNA was eluted using 30µl or 12µl elution buffer (for Mini or Micro Kit respectively), which was passed through the column twice to increase yield. RNA was stored at -80˚C.

2.3.2 RNA isolation from tissues

RNA was isolated from fresh tissue, or tissue stored in RNAlater (Qiagen) at -80˚C, using RNeasy Mini Plus Kit (Qiagen). Tissue was homogenised with a handheld Pellet Pestle Cordless Motor (Kontes) and then passed through a Qiashredder column (Qiagen). RNA was then isolated as described for cells (2.3.1) according to the manufacturer's instructions.

2.3.3 RNA/DNA quantification

RNA/DNA concentration and purity was analysed by measuring the optical density using a Nanodrop 1000 UV-Vis Spectrophotometer (Thermo Scientific) according to manufacturer's instructions.

2.3.4 cDNA synthesis

cDNA synthesis was carried out using the First Strand cDNA synthesis kit for RT-PCR (AMV Roche). 1µg of RNA was used, along with 20U AMV reverse transcriptase, 1µM dNTPs, 1X AMV reverse transcriptase buffer (Roche), 5mM $MgCl_2$ and 50µg/mL OligodTs. This was incubated at room temperature for 10 min, 42˚C for 60 min, 75˚C for 10 min and stored at -20˚C. Controls lacking reverse transcriptase (minus RT) were performed alongside each set of reactions.

2.3.5 RT-PCR

To detect presence/absence of transcripts, PCR using cDNA as a template (reverse transcription-PCR or RT-PCR) was carried out as described in 2.2.6. cDNA isolated according to 2.3.2 was diluted 1:5 in ddH_2O and 1µl was included in a 20µl PCR reaction. 10µl of the reaction was run on an agarose gel and imaged as described in 2.2.4. Minus RT controls were also used as a template to control for DNA contamination. In addition, intron spanning primers allowed genomic DNA contamination to be distinguished from cDNA due to the difference in product sizes and/or inefficient amplification of large gDNA products.

2.3.6 Quantitative RT-PCR

qRT-PCR was carried out on the Roche LightCycler-480 using the Roche Universal Probe Library (UPL) system. This system uses gene specific probe-primer combinations, identified using the online design tool: https://www.roche-applied-science.com/sis/rtpcr/upl/index.jsp. cDNA isolated according to 2.3.4 was diluted 1:5 and 1µl was used in a 10µl reaction, plus 1X Probemaster LC480 (Roche), 0.5µM of each primer, 0.1µM of the UPL Probe (Roche) and H_2O to 10µl. Reactions were carried out in technical triplicates on 384 well plates. If available, a plasmid encoding the target gene, was used to generate a standard curve of known concentration, if not, cDNA was diluted to generate a standard curve of unknown concentration. All reactions were carried out using the following program:

	Denaturation	95˚C	10 min
45X	Denaturing	95˚C	10 secs
	Annealing/Extension	60˚C	30 secs
	Extension	40˚C	30 secs

Crossing point times were identified, analysed and displayed relative to the control gene (*Tbp* and/or *Gapdh*) using the Roche LC480 software. Primer and probe combinations are displayed in Table 2.2.

2.4 Protein methods

2.4.1 Protein isolation from cells

Protein was isolated from a confluent well of a 6 well plate. Cell media was aspirated, cells rinsed in PBS, and 100µL of 1X Cell Lysis Buffer (Cell Signaling Technology) plus 1mM PMSF (phenylmethanesulfonylfluoride, Thermo Scientific) and protease inhibitor tablet (1 tablet per 10mL, Roche) was added and cells were incubated on ice for 10 min. Cell scrapers were used to remove cells from the well. Lysates were sonicated for 3 X 30 sec blasts (Bioruptor, Diagenode) centrifuged at 14,000g at 4˚C for 15 min. The supernatant was transferred to a clean tube and stored at -80˚C.

2.4.2 Protein isolation from tissue

100mg of freshly dissected, or snap frozen tissue, was homogenised in 1mL of 1X cell lysis buffer (Cell Signaling Technology) plus 1mM PMSF (Thermo Scientific) and Complete protease inhibitor cocktail tablet (1 tablet per 10mL, Roche), using a handheld Pellet Pestle Cordless Motor (Kontes). This was then sonicated and centrifuged as described above (2.4.1).

2.4.3 Determining protein concentration

Protein concentration was determined using the Pierce Bicinchroninic Acid (BCA) Protein Assay Kit, according to the manufacturer's instruction. Briefly, 10µl of sample was mixed with 180µl working reagent (50 parts Reagent A to one part Reagant B - Pierce) and incubated at 37˚C for 1h, then at room temperature for 10 min. Absorbance at 562nm was measured using the Thermo Multiskan Spectrum platereader and compared to a standard curve made using bovine serum albumin (BSA) provided in the kit (Pierce) to work out the protein concentration.

2.4.4. Concentrating of protein samples

In order to aid detection of proteins of a particular molecular weight, total protein lysates were concentrated by spinning through Amicon Ultra-0.5mL 30kDa

Table 2.3 Antibodies used in this thesis

Antibody	Source	Species	Dilution (application)	Fixation method (if for IF)
I and S Afadin	Abcam ab11338	Rabbit	1:500 (IF)	PFA
Arl13b	Kind gift from Dr Tamara Caspary (Emory University, Atlanta)	Rabbit	1:1500 (IF) 1:2000 (WB)	PFA
Azi1 (Aoto)	Kind gift from Prof S Tajima (Osaka University)	Rabbit	1:1500 (IF)	PE + MeOH
Azi1 (Abcam)	Abcam ab110018	Rabbit	1:100 (IF)	PE + MeOH
Azi1 (SF91)	Kind gift from Prof Jeremy Reiter (Univeristy of California, San Francisco)	Guinea Pig	1:500 (IF) 1:500 (WB)	PE + MeOH
BrdU	Abcam (ab6326)	Rat	1:75 (FACS)	
Cleaved Caspase-3 (Asp175)	Cell Signaling Technologies (9661)	Rabbit	1:250 (IHC)	
CD71/ Transferrin Receptor	Lifespan Biosciences	Rat (FITC conjugated)	1:100 (FACS)	
Dync2h1	Kind gift from Prof. Lavallee, Columbia University	Rabbit	1:1000 (IF)	PFA
Gli3 (6f5)	Genentech	Rabbit	1:500 (WB)	
γ-H2AX	Abcam (Ab11174)	Rabbit	1:500 (IHC)	
Ift81	Santa Cruz Biotechnology (sc-107629)	Goat	1:2000 (WB)	
Ift88	Proteintech Group (13967-1-AP)	Rabbit	1:80 (IF) 1:1000 (WB)	PFA
Mks1 (Bbs13)	Proteintech Group (16206-1-AP)	Rabbit	1:100 (IF)	PE + MeOH
Nphp1 640	Kind gift from Prof. Gregory Pazour (University of Massachussetts)	Rabbit	1:1000 (IF)	PE + MeOH

Antibody	Source	Species	Dilution (application)	Fixation method (if for IF)
Pcm1	Prof. Andreas Merdes (CNRS, Toulouse)	Rabbit	1:1000 (IF)	PE + MeOH
Rab8	Sigma-Aldrich (R5530)	Rabbit	1:200 (IF)	PFA
Sdccag8	Proteintech Group (13471-1-AP)	Rabbit	1:100 (IF)	MeOH
α - Tubulin	Abcam (ab4074)	Rabbit	1µg/mL (WB)	
Acetylated α - Tubulin	Sigma-Aldrich (6 11B-1)	Mouse	1:2000 (IF)	PFA/MeOH
γ-Tubulin	Abcam (ab11317)	Rabbit	1:500 (IF)	PFA/MeOH
γ-Tubulin (GTU-88)	Sigma-Aldrich	Rabbit	1:500 (IF)	PFA/MeOH
Poly-Glutamylated Tubulin (GT335)	Enzo Life Sciences	Mouse	1:2000 (IF)	PFA/MeOH

PFA: Paraformaldehyde, MeOH: Methanol, PE: Pre extraction, IF: Immunofluorescence, WB: Western Blot, IHC: Immunohistochemistry

centrifugal filters (Millipore) according to manufacturer's instructions: this removed proteins below 30kDa in size and concentrated the remaining protein.

2.4.5 Resolution of proteins by SDS-PAGE

Protein samples were separated according to molecular weight by SDS-PAGE using Precast Invitrogen NuPage Novex (Invitrogen) gels using the XCell Surelock Mini system (Invitrogen). Equal concentration of protein for each sample, plus 1X sample reducing agent (Invitrogen) and 1X sample loading buffer (Invitrogen) were heated to 72˚C for 10 min then loaded onto a 3-8% Tris-Acetate Nupage gel (Invitrogen) along with Novex Sharp Protein Standard for size comparison. The gel was submerged in 1X Tris Acetate Running Buffer (Invitrogen) plus 1X antioxidant (Invitrogen) and run at 150V for 70 min.

Table 2.4 Secondary Antibodies used in this thesis

Antibody	Source	Species	Dilution (application)
ECL Anti-rabbit IgG, HRP linked	GE Healthcare	Donkey	1:7500 (WB)
ECL Anti-mouse IgG, HRP linked	GE Healthcare	Donkey	1:7500 (WB)
Anti-guinea pig IgG, HRP linked	Invitrogen	Rabbit	1:5000 (WB)
Anti-rabbit IgG, Alexafluor 488 linked	Invitrogen	Donkey	1:500 (IF)
Anti-rabbit IgG, Alexafluor 594 linked	Invitrogen	Donkey	1:500 (IF)
Anti-rabbit IgG, Alexafluor 647 linked	Invitrogen	Donkey	1:500 (IF)
Anti-mouse IgG, Alexafluor 488 linked	Invitrogen	Donkey	1:500 (IF)
Anti-mouse IgG, Alexafluor 594 linked	Invitrogen	Donkey	1:500 (IF)
Anti-mouse IgG, Alexafluor 647 linked	Invitrogen	Donkey	1:500 (IF)
Anti-goat IgG, Alexafluor 488 linked	Invitrogen	Donkey	1:500 (IF)
Anti-rat IgG, Alexafluor 488 linked	Invitrogen	Donkey	1:200 (FACS)
Anti-guinea pig IgG, Alexafluor 488 linked	Invitrogen	Goat	1:500 (IF)
Anti-guinea pig IgG, Alexafluor 488 linked	Invitrogen	Goat	1:500 (IF)

2.4.6 Western blotting

After SDS-PAGE, the stacking gel was removed, and protein samples were transferred onto PVDF membrane (Hybond P, GE Healthcare) using the Invitrogen XCell Surelock Mini system. The membrane was placed briefly (30 secs) in methanol then pre-soaked, along with sponges and Whatman filter paper in 1X transfer buffer (Invitrogen) and 10% methanol. The gel was sandwiched alongside the membrane between Whatman paper, sponges and electrodes according to manufacturer's instructions and transferred at 30V for 70 min. Membranes were washed in TBSt (0.05% Tween-20 in TBS), and then placed in blocking solution (5% Marvel (w/v) (Premier foods) in TBSt) for 1h at room temperature. Primary antibodies were diluted in blocking solution (see Table 2.3) and membranes were incubated in primary antibody mix overnight at 4˚C rocking. Membranes were washed in TBSt 3 times for 10 min and then incubated with the relevant HRP-

conjugated secondary (see Table 2.4). Membranes were washed 3 times for 10 min in TBSt and signal was detected using Amersham Enhanced Chemical Luminescence (ECL) detection kit (GE Healthcare). Membranes were incubated in 1:1 mixtures of Solutions A and B (GE Healthcare) for 30 seconds, blotted to remove excess liquid and exposed to photographic film (Kodak Biomax XAR Film). Film was developed using a Konika SRX-101A Developer. Between antibodies, membranes were stripped with stripping buffer (Invitrogen) for 10-20 min, then washed and blocked in 5% milk before reprobing with a new antibody. For long-term storage, membranes were dried and stored in sealed plastic at room temperature.

2.4.6.1 Densitometry

Films were scanned and images imported into ImageJ. Quantification of protein levels was performed by densitrometry in ImageJ. Levels of individual proteins were normalised to the alpha tubulin loading control.

2.5 Cell Culture

2.5.1 General cell culture

Table 2.5 documents all cell lines used, the media used for maintaining each culture and the media used to freeze each culture. Cells were grown using standard tissue culture techniques in a laminar flow hood to ensure sterility. Cells were maintained at 37˚C + 5% CO_2, and MEFs and HEFs were also cultured in hypoxic conditions of low 3% O_2. In general, cells were passaged every 2-3 days, except E14 ES cells were passaged at least every other day. Primary MEF and HEF cells were only passaged when >80% confluent. To passage, media was aspirated, cells were washed in PBS, 1:1 Trypsin/versene was added to cells and they were incubated for 3-5 minutes at 37˚C. Trypsin was inactivated with media with fetal calf serum (FCS). Cells were spun at 3000rpm for 3 minutes and reseeded at desired density. All cells were kept at low passage number, below passage 15.

Table 2.5 Cell lines used in this thesis

Cell Type	Description	Culture medium*	Freezing medium	Source	Species
E14 ES cells	Embryonic stem cells	GMEM + 1% NEAA, 1mM Sodium Pyruvate, 3.5µL β-ME, 2mM glutamine, 0.1% LIF	28% Ham's F10 media, 40% TPB, 12% DMSO	Gift from Dr Julia Dorin, MRC HGU, Edinburgh	Mouse
HEFs	Human Embryonic Fibroblasts	DMEM or if slow growing: Amniomax plus Amniomax supplements	28% Ham's F10 media, 40% TPB, 12% DMSO	Gift from Dr Paul Lockhart (MCRI, Victoria) Obtained with required consent	Human
HeLa	Human fibroblast cervical cancer cell line	DMEM	28% Ham's F10 media, 40% TPB, 12% DMSO	Gift from Prof Andrew Jackson	Human
hTERT-RPE	Immortalised retinal pigmented epithelial cells	DMEM:F12.+ 2mM L-Glutamine and 0.348% sodium bicarbonate	DMEM + 20% FCS 10% DMSO	ATCC	Human
IMCD3	Inner medullary collecting duct cells	DMEM:F12	DMEM:F12 + 10% FCS 5% DMSO	ATCC	Mouse
MDCK	Madin Darby ciliated kidney cells	DMEM	DMEM + 10% FCS 5% DMSO	ATCC	Canine
NIH/3T3	Immortalised mouse embryonic fibroblast	DMEM	DMEM + 10% FCS 5% DMSO	ATCC	Mouse
3T3-Arl13bmK2	NIH/3T3 stably expressing *CMV-Arl13b-mKate2*	DMEM + 500µg/mL G418	DMEM + 10% FCS 10% DMSO	Generated by Emma Hall	Mouse
ShhLIGHT-II	NIH/3T3 stably expressing *Gli-Firefly Luciferase* and *CMV-Renilla Luciferase*	DMEM + 400µg/mL G418 150µg/mL Zeocin and1.5g/L sodium bicarbonate	DMEM + 10% FCS 5% DMSO	ATCC	Mouse

*All culture medium contains 10% Fetal Calf Serum and 1% Penicillin/Streptomycin. Cell culture medium was from Gibco (Invitrogen). NEAA: Non-essential amino acids (Sigma-Aldrich), β-ME: β-mercaptoethanol (Sigma-Aldrich), TPB: triptose phosphate broth, DMSO: dimethyl sulfoxide, ATCC: American type culture collection.

2.5.2 Freezing cells

Cells were trypsinised and spun as in 2.5.1, then resuspended in freezing medium (See Table 2.5) at 2-5x10^6 cells/mL. Cells were frozen slowly to -80˚C in polystyrene and then stored long-term in liquid nitrogen.

2.5.3 Thawing cells

Cells are rapidly thawed from liquid nitrogen to 37˚C, spun to remove dimethyl sulfoxide (DMSO), resuspended in medium and plated at 1-2x10^6 cells/cm^2.

2.5.4 Mouse Embryonic Fibroblast (MEF) derivation

E11.5 or E13.5 mouse embryos were dissected out of the uterus and from the decidua into cold sterile PBS on ice. Heads and abdominal cavities were removed and tails were kept for genotyping (2.6.2). Embryos were placed in 3mL 1:1 trypsin:versene, minced and incubated at room temperature for 1h. Cells were dissociated by pipetting, then trypsin was inactivated using media + 10% FCS and cells were centrifuged at 3000rpm for 3 min and plated into 25cm^2 flasks and cultured overnight. After 24h large necrotic lumps of tissue were removed and the media was replaced. When cells reached confluency they were passaged 1:3.

2.5.5 Ciliogenesis

To induce ciliogenesis cells (except E14 ES cells) were plated at high density (1x10^5 cells/cm^2) without serum for 48h (note cell densities were different if cells were first transfected, as cell density affects transfection efficiencies – see 2.5.5 or 2.5.6). For E14 ES cells, cells were plated on coverslips coated with matrigel (BD biosciences) and poly-D-lysine (BD bioscience) at a density of 1x10^5 cells/cm^2 with serum. After 24h, 0.5mM mimosine (Calbiochem) was added for 6h to arrest cell cycle.

2.5.6 siRNA transfection

Many different siRNA transfection protocols were tried. siRNA sequences are given in Appendix 1. Optimisation included varying cell density (1-5x10^4 cells/cm^2), varying siRNA manufacturer (Ambion Silencer or Silencer Select, Dharmacon OnTarget Plus), varying siRNA concentration (from 20-40nM), varying transfection

reagent (Lipofectamine RNAimax (Invitrogen), Dharmafect 1 (Dharmacon)), varying amount of transfection reagent added (0.5-3µL/24 well) and varying the timing of serum starvation and analysis after transfection. The final screen protocol is shown in Figure 4.9.

For the screen, a custom Dharmacon OnTarget Plus siRNA library of siRNAs (Appendix 1) was transfected into ShhLIGHT-II or IMCD3 cells, four individual siRNAs to each gene plus a pool of the four. For a 24 well plate, 100µL of optimem was placed into each well, plus 25nM siRNA or 6.25nM each of all four for the pool, and 2µl of Dharmafect 1, mixed and left for 20 minutes at room temperature. $4x10^4$ cells were added, in 400µL media without antibiotics. After 24h, media was changed to serum free media. If required (for the luciferase assay), after a further 12h, 5µM Hh agonist purmorphamine (Calbiochem) or the equivalent concentration of DMSO was added to the cells in plastic 24 well plates. After a further 18h, cells were fixed or lysed. For a 6 well plate, everything was scaled up by a factor of 5. For the live imaging of 3T3-Arl13b-mK2 cells, siRNAs were transfected as described above, media was changed to DMEM without phenol red and without serum (Invitrogen) after 24h and live imaging began 12h later.

2.5.7 DNA transfection

MEFs were transfected with DNA using the Invitrogen Neon transfection system according to manufacturer's instructions. Briefly, $5x10^4$ cells were resuspended in 12µl Solution R (Invitrogen) and mixed with 0.5µg of each plasmid (total 1µg DNA). 5mL of Solution E was added to the Neon Chamber Tube. Cells were taken up in 10µL Neon Tip and microporated at 1350V, 1 pulse for 30ms. 3 transfection reactions were plated into each well of a glass-bottomed 24 well plate (Iwaki) in prewarmed medium without antibiotics. After 24h, cells were serum starved, and imaging began after 24h serum starvation. Live imaging was then performed (see 2.9.2)

ShhLIGHT-II and NIH-3T3s were transfected with Lipofectamine2000 (Invitrogen) according to manufacturer's instructions. Briefly $1x10^6$ cells were plated in T25s the without antibiotics. After 24h 625µL of Optimem (Invitrogen) was mixed with 25µL

of Lipofectamine2000 (Invitrogen). After 5 min at room temperature, this was mixed with 625µL of Optimem plus 5µg of DNA. This was incubated at room temperature for a further 20 min and then added to the cells. These were used to generate stable lines.

2.5.8 siRNA/DNA cotransfection

For DNA/siRNA cotransfections, $4x10^4$ cells were plated onto a glass bottomed 24 well plate (Iwaki), in media without antibiotics. After 24h, 3µL Dharmafect Duo (Dharmacon) was diluted in 50µL Optimem (Invitrogen). After 5 min, 50pmol of siRNA was mixed with 0.5µg DNA in 50µL of Optimem (Invitrogen) and this was added to the Dharmafect Duo dilution and incubated at room temperature for 20 min. This transfection mixture was added to the cells. After 24h cells were placed in medium without serum. After 24h cells were fixed and processed for immunofluorescence (see 2.5.13). For protein or RNA extraction, reactions were scaled up by a factor of 5, plated in a 6 well plate, and cells were processed for RNA (see 2.4.1) or protein (see 2.3.1).

2.5.9 Generation of stable cell lines

Kill curves were performed to determine the relevant dose: a range of drug concentration was applied to non-transfected cells and the lowest concentration which gave complete cell death after 4 days was used (Puromycin: 0.75µg/mL, Hygromycin: 1.75mg/mL, G418: 1mg/mL).

ShhLIGHT-II cells were transfected with *pCAG-eGFP-Pur* or *pCAG-eGFP-Hyg*, NIH-3T3 cells were transfected with *pArl13bmKate2* as described in 2.5.7. After 48h, these were split 1:50 or 1:250 to 10cm plates and the relevant antibiotic selection was applied. After 10-14 days, when single colonies remained in transfected plates but all cells were dead in the control non-transfected plates, colonies were trypsinised and replated. Colonies were picked singly for ShhLIGHT-II cells to generate clonal populations, whereas the NIH3T3 clones were combined to give a non-clonal population. As 3T3-Arl13b-mK2 lines had variable expression levels (probably due to the non-clonal nature) medium expressing cells were fluorescent activated cell sorted (FACS) several times to select for cells with medium

Arl13b-mKate2 expression levels. Cells were propagated in medium plus antibiotics to maintain selection.

2.5.10 Hh pathway manipulation in MEFs

MEFs were plated at $1x10^6$ cells/well of 6 well plate without serum for 48h. Purmorphamine (Calbiochem 5μM unless otherwise stated) or the equivalent concentration of DMSO was added 18h before processing or 1μM cyclopamine-KAAD (Calbiochem) was added 4h before processing for RNA or protein.

2.5.11 Luciferase Assay

Either ShhLIGHT-II cells were treated as described in 2.5.6 (if siRNA transfection was involved) or ShhLIGHT-II cells were plated at $1x10^5$ cells/well of a 24 well plate, after 24h cells were serum starved for 48h and after a further 12h purmorphamine (Calbiochem, 5μM unless otherwise stated) or DMSO was added for 18h. Luciferase assays were performed using the Dual-Luciferase Reporter Assay System (Promega) according to manufacturer's instructions with some modifications. Cells were washed in PBS then lysed with 100μL 1X Passive Lysis Buffer (Promega), 15 min shaking at room temperature. Lysate could be stored at -20˚C or luciferase activity could be read immediately. 5μL of lysate was put in triplicate into a 96 well flat bottomed plate and luciferase activity was read using a FLUOstar Omega plate reader (BMG labtech). 12.5μL of Luciferase Activating Reagent-II (Promega) was injected into each well and then luminescence was measured. 12.5μL of Stop and Glo reagent (Promega) was then injected, which quenches the Firefly luciferase and activates the *Renilla* luciferase, and luminescence was measured. Luciferase activity is plotted relative to *Renilla* luciferase to control for cell numbers and transcription levels.

2.5.12 G_1/S cell arrest using thymidine block

To synchronise HeLa cells in G_1/S border, a double thymidine block was performed. HeLa cells which were plated on acid treated coverslips (2.5.12) at 30-40% confluency were treated with 2mM thymidine for 19h. The cells were washed 3 times in PBS then incubated in fresh media for 9h. 2mM thymidine was then added for 15h. Cells were then washed 3 times in PBS, and released from the thymidine

block by plating in fresh media. Cells were fixed (see 2.5.12) at 0, 2, 4, 6, 8 and 10h after release from the second thymidine block. Cells progress through the cell cycle: G_1/S (0-2h), S (4h) and G_2/M (6-10h).

2.5.13 Immunocytochemistry

Cells were plated on acid treated coverslips or glass plates (Iwaki or PAA). To acid treat coverslips, they were heated to 50-60˚C in 1M hydrochloric acid for 4h, then cooled and rinsed repeatedly in sterile H_2O then 70% ethanol several times.

The cells were fixed in fresh 4% paraformaldehyde (PFA)/PBS for 10 min at room temperature or for 10 min with ice cold methanol on ice (see table 2.3 for antibody specific fixation methods). Some antibodies required a pre-extraction step (Table 2.3), in which case cells were treated with 0.1M PIPES pH 6.8, 2mM ethylene glycol tetraacetic acid (EGTA) and 1mM magnesium sulphate ($MgSO_4$) for 30s on ice, then methanol fixed as above. Coverslips were then washed in TBST (TBS + 0.1% Triton-X), then blocked with 10% donkey serum in TBST and incubated on cells for 1h at room temperature or at 4˚C overnight. Primary antibodies were diluted (Table 2.4) in 1% donkey serum in TBST plus 1mM sodium azide (NaN_3) overnight at 4˚C. Alternatively, if necessary, to enhance GFP signal, GFP Booster (Chromotek), was diluted 1in200 in 1% donkey serum in TBST plus any antibodies for costaining and incubated for 1h at room temperature. Cells were washed 4 X 5 min then 4 X 10 min in TBST. Secondary antibodies were diluted 1:500 in TBST plus 1% donkey serum and added to cells for 1h at room temperature (Table 2.4). Cells were washed 4 X 5 min then 4 X 10 min in TBST. 2µg/mL 4',6-diamidino-2-phenylindole (DAPI) in TBST was added to cells and incubated for 5 min at room temperature, then washed in TBST. Coverslips were mounted on slides with ProLong Gold (Invitrogen), or if cells were in plates, ProLong Gold was added then a coverslip placed on top. Plates/slides were stored in the dark at 4˚C overnight or longer before imaging.

2.6 Mouse Methods

2.6.1 Generation of *Azi1*$^{Gt/Gt}$ mice

Azi1$^{/ Gt(CCOG35)Wtsi}$ embryonic stem cells, which have a gene trap inserted into intron 2 of *Azi1,* were ordered from the Mutant Mouse Regional Resource Centre. Cells were expanded by Joan Slight and Fiona Kilanoswki, who also performed karyotype analysis on the cells. The insertion site was confirmed and mapped to within intron 2 of *Azi1*. The cells were sent for IMPACT testing and determined to be pathogen free. The ES cells (which were derived from 129^{ola}) were injected in C57Bl/6 blastocysts and implanted into a recipient C57Bl/6 female. Male chimeras were identified by coat colour, backcrossed to C57Bl/6 females and germline transmission was assessed by coat colour.

2.6.2 Genotyping

DNA was isolated from ear clips performed by Margaret Keighren (taken from mice P12 or older) or embryo tail tip by one of two methods:

For one, 250µL of quick lysis buffer (100mM Tris pH8.0, 5mM EDTA, 200mM NaCl and 0.2% SDS) and 200µg/mL proteinase K was added and incubated overnight at 60˚C. Samples were spun at 10,000g for 5 min. Supernatant was transferred to a new tube with an equal volume of isopropanol, vortexed and then incubated at room temperature for 30 min. This was spun down for 15 minutes at 10,000g, washed with 70% ethanol, dried and resuspended in 100µL TE.

Alternately, DNA isolation by alkaline lysis method and genotyping was carried out by Margaret Keighren, in which case ear clips were incubated in 25mM sodium hydroxide (NaOH) with 0.2mM EDTA at 95˚C for 20 min, then equal volume of 40mM Tris-HCl is added.

In both cases, 1µL of the DNA solution was added to a genotyping PCR reaction and PCR was performed as in 2.2.6 using primers indicated in Table 2.2.

2.6.3 Bleeding

Mice were tail tipped and blood was collected using a microhematocrit capillary tube with heparin coating (Globe scientific). 50-100µL of blood was collected into 500µL heparin (500U/mL in PBS, Sigma). 180µL of blood was then forcefully pipetted into 2mL of super-chilled methanol and stored at -80˚C until FACs analysis (see 2.8).

2.6.4 Sperm isolation

Testes, cauda and caput epididymi were dissected into 500µL M2 media (Invitrogen), minced and left for 30 min to allow sperm to enter solution. For images of unfixed sperm, sperm from the cauda epididymus was placed on a glass slide, covered with a coverslip and imaged.

For live imaging, movies were made of sperm swimming through M2 media or 1% methyl cellulose (Sigma) in M2 media (Invitrogen), in capillary tubes, with a rectangular cross section and internal dimension of 50µm x 1000µm (Vitrotubes Mountain Leaks, New Jersey). Capillary tubes were filled by dipping into methyl cellulose (for wild type sperm), or M2 media (for mutant sperm) and sealed with Cristaseal sealant (Hawskley) at one end. The other end was dipped into the suspension of mouse sperm for 5 min; wild type sperm was diluted 1:5 in M2 media, whereas mutant sperm was not diluted. The capillary was sealed with cristaseal and imaged as in 2.9.1.4.

Sperm counts were performed on sperm from the cauda epididymus, diluted in H_2O using a haemocytometer, only counting intact sperm (with both head and tail).

For fixed samples, testes were placed through a 100µm nylon mesh (BD Biosciences). Sperm from the caput epididymus and testes were then placed on a 20-40% Percoll gradient (GE Healthcare) and spun at 3,000g for 10 minutes. The sperm, at the bottom of the gradient, were resuspended in 2mL PBS, and spun at 300g for 10 min, then resuspended in 200µL PBS. This was spread on Poly-D-lysine slides (BD Biosciences), allowed to dry for 10 min, then post-fixed in fresh 4% PFA/PBS for 10 min. Cauda sperm was not purified through Percoll, but was placed straight on Poly-D-Lysine slides and fixed for 10 min with 4% PFA. Slides were washed twice in PBS, and then sperm were permeablised with 0.4% Triton-X in PBS

for 10 minutes. Slides were washed 3 X 10 min PBS. Slides were blocked with 10% donkey serum in PBS for 1h at room temperature. Primary antibodies were diluted in PBS (see Table 2.3) and incubated overnight at 4˚C. Slides were washed 3 X 10 min in PBST (PBS + 0.1% Triton X) then secondary antibodies (Table 2.4) were diluted 1:500 in PBST + 1% donkey serum were added and incubated for 1h at room temperature. Slides were washed 3 X 10 min PBST, 2µg/mL DAPI was added for 5 min, slides were washed in TBST and mounted using ProLong Gold (Invitrogen).

2.7 Histology

2.7.1 Histological studies of mutant mice

Eyes were fixed in Davidson's fixative (Sigma) at 4˚C overnight. Kidneys were cut in half and fixed in fresh 4% PFA/PBS at 4˚C overnight. Testes were fixed in Bouin's fixative (Sigma) for 20 min, then cut in half and fixed in Bouin's overnight at 4˚C.

2.7.2 LacZ expression studies

Organs and embryos were dissected and briefly fixed in 4% PFA/PBS for 30-45 min at 4˚C: testes, brains and kidneys were cut in half beforehand, and eyes were slit behind the lens to aid penetration of fixative and stain. They were then washed PBS for 10 min then 3 X 20 min in detergent wash (0.1M phosphate buffer pH7.3 plus 2mM $MgCl_2$, 0.2% sodium deoxycholate, 0.02% NP40). Samples were stained in detergent wash plus 0.085% NaCl, 5mM K_4Fe, 5mM K_3Fe and 300µg/mL X-Gal overnight at 37˚C with continuous rotation in foil wrapped tubes. Samples were washed 3 X 20 min in detergent wash and then post-fixed in fresh 4% PFA/PBS at 4˚C. Samples were imaged with a Nikon-macroscope and then processed for wax sectioning.

2.7.3 Paraffin wax sectioning and counterstains

Samples were dehydrated by sequential 15 min washes in 30%, 50%, 70%, 85%, 95% and 100% ethanol, 50:50 100% ethanol: xylene, followed by 1 X 30 min wash in xylene, then 2 X 30 min in xylene at 50˚C. Samples were then incubated for 30

min in 50:50 xylene: molten paraffin, 2 X 30 min in molten paraffin, then embedded in paraffin in cassettes. Wax blocks were cut to 7-12μm sections using a manual microtome, briefly floated out in a warm water bath and mounted on Superfrost slides (ThermoScientific) which were dried at room temperature and incubated at 50˚C overnight.

For histology, slides were dewaxed through 3 X 5 min xylene and 3 X 5 min 100% ethanol, followed by 3 min washes in 90%, 70%, 50% and 30% ethanol and then rinsed in dH_2O. Slides were then counterstained with haematoxylin and eosin (H&E) or nuclear fast red, dehydrated through alcohols and xylene and mounted with DPX Mountant (Sigma).

2.7.4 Immunohistochemistry

Wax sections on slides were rehydrated through xylene and alcohols stages to water as for sectioning (2.7.3). Antigen retrieval was performed by bringing slides to a near boil in 10mM citrate, 0.1% Tween-20 pH 6.0 for 15min in the microwave. Slides were cooled, then washed in PBS and then blocked in 10% donkey serum in PBS for 60 min at room temperature in a humidified chamber. Slides were incubated in primary antibodies diluted in TBST (TBS plus 0.1% Triton X) overnight at 4˚C (Table 2.3). Slides were then washed in PBS, and secondary antibodies (Table 2.4) were added and incubated for 1h at room temperature. Slides were washed in PBS, 2μg/mL DAPI was added for 5 min, and slides were mounted in ProLong gold.

2.8 Flow cytometry

2.8.1 Cell Cycle Analysis

MEFs were seeded at 1 x 10^6 cells into a T75 flask. After 24h, the cells were pulsed with 10μM BrdU (Sigma) for 30 min. Cells were trypsinised and pelleted at 1200rpm for 3 min, then fixed in ice cold 70% ethanol added drop wise. Cells were fixed overnight at -20˚C. Cells were pelleted at 2,500rpm for 4 min then resuspended in 1mg/mL pepsin in 30mM HCl and incubated at 37˚C for 30 min. Cells were pelleted at 4000rpm for 4 min between each step that follows. Cells were washed twice with PBS/1mM EDTA, then blocked in 2% bovine serum albumin

(BSA) in PBST (PBS plus 0.1% Triton-X). Cells were pelleted then resuspended in 2% BSA in PBST plus anti-BrdU antibody diluted 1:75 and incubated at room temperature for 30 min. Cells were then incubated in donkey anti-rat AlexaFluor 488 secondary antibody (Invitrogen) diluted 1 in 200 in PBST with 2% BSA, for 30 min at room temperature. Cells were washed with PBS/1mM EDTA and resuspended in 0.1mg/mL RNaseA and 50µg/mL propidium iodide (PI) in PBS/0.1mM EDTA. Cells were incubated in the dark for 1h at 4˚C. Flow cytometry was performed on a FACScalibur (BD Biosciences) by Elizabeth Freyer, MRC HGU. Data was analysed using FlowJo software (v7.6.1, Tree Star).

2.8.2 Micronuclei

Blood was collected from *Azi1*$^{+/+}$, *Azi1*$^{+/Gt}$ *or Azi1*$^{Gt/Gt}$, *Mcph1*$^{+/+}$, *Mcph1*$^{+/-}$ or *Mcph1*$^{-/-}$ mice of at least 3 months of age as described in 2.6.3 (*Mcph1* mice were kindly provided by Dr Rachel Rigby and Dr Andrew Jackson). 12mL saline (0.9% sodium chloride, 5.3mM sodium bicarbonate) was added to the blood samples, mixed and then pelleted at 600g for 5 min. Saline was removed, and 10µL of the remaining pelleted blood was added to 1mg/mL RNAseA and 1 in 100 anti-CD71 (Lifespan Biosciences) diluted in saline. Triplicate samples were performed from each mouse. Cells were incubated on ice for 30 min then at room temperature for 30 min. 500µL of 1.25µg/mL PI was then added and flow cytometry was performed on a FACScalibur (BD Biosciences) by Elizabeth Freyer, MRC HGU. Data was analysed using FlowJo software (v7.6.1, Tree Star) as described by (Reinholdt et al., 2004).

2.9 Microscopy

2.9.1 Light microscopy

2.9.1.1 Fluorescence microscopy

Images were captured with a Coolsnap HQ CCD camera (Photometrics Ltd, Tucson, AZ) using a Zeiss Axioplan II fluorescence microscope with 63X or 100X Plan-neofluar objectives, a 100W Hg source (Carl Zeiss, Welwyn Garden City, UK) and

Chroma #83000 triple band pass filter set and Chroma #83700 emission filters (Chroma Technology Corp., Rockingham, VT). The single excitation and emission filters are installed in motorised filter wheels (Prior Scientific Instruments, Cambridge, UK). Image capture and analysis were performed using in-house scripts written for IPLab Spectrum (Scanalytics Corp, Fairfax, VA).

Analysis of intensity was performed in IPLab using in-house scripts. For analysis of Azi1 intensity, the region surrounding the centrosome/basal body was identified using intensity thresholds, then the sum intensity of anti-Azi1 staining within this area was measured. Whether or not a cell had a cilium was decided manually, and then the average Azi1 intensity at >100 basal bodies was compared to > 100 centrosomes (in non-ciliated cells).

For analysis of γH2AX signals, cells were identified by DAPI staining, and the sum intensity of anti-γH2AX staining was calculated within an area defined by, but slightly larger than, the nuclear area. The sum intensity was calculated for >100 cells for each genotype and drug treatment.

2.9.1.2 Brightfield microscopy

Brightfield images were captured with a Coolsnap HQ CCD camera (Photometrics Ltd, Tucson, AZ) Zeiss Axioplan II fluorescence microscope with Plan-neofluar objectives (Carl Zeiss, Welwyn Garden City, UK). Colour additive filters (Andover Corporation, Salem, NH) installed in a motorised emission filter wheel (Prior Scientific Instruments, Cambridge, UK) were used sequentially to collect red, green and blue images that were then superimposed to form a colour image. Image capture and analysis were performed using in-house scripts written for IPLab Spectrum (Scanalytics Corp, Fairfax, VA).

2.9.1.3 Macroscopic imaging

Macroscopic images were taken with a Qimaging Micropublisher 5 cooled colour camera (Qimaging, Burnaby, BC) on a Nikon AZ100 macroscope with 0.5X, 1X, 2X, 4X and 5X objectives and an Intensilight 130W Hg light source. Image capture and image analysis were performed using IPLab Spectrum (Scanalytics Corp, Fairfax, VA).

2.9.1.4 Live imaging sperm

The sperm containing capillaries (as described in 2.6.4) were placed on a microscope at 37ºC and a rapid time lapse sequence of images was captured 10mm from the end of the tube. A Qimaging Retiga camera running at 30 frames per second (bin 2x2 half frame) captured image sequences with a 5x objective at zoom 5 on a Nikon AZ100 macroscope. Movies are shown in real time. Still figures show all time points superimposed into one image to depict the movement, or lack thereof, during the movie.

2.9.1.5 Screening

Images were captured using the Olympus Scan^R, using an Olympus Plan Fluor 40X dry objective. The Scan^R was programmed to image 16 frames per well, using autofocus in the DAPI channel to focus the image. Images were simultaneously acquired, using Olympus Scan^R Acquisition software, and analysed using the Olympus Scan^R Analysis software. Background signal was removed using RollingBall method in the analysis software and cells, centrosomes and cilia were identified using intensity and size exclusions. Cilium length was measured using the maximum feret diameter method. Numerical data were exported into Microsoft Excel and/or R for further analysis (see 2.9.1).

2.9.2 Confocal

Confocal images were captured with a Nikon A1R confocal microscope, comprising a Nikon Eclipse TiE inverted microscope and four laser modules: 405 (laser diode), 457, 488, 514 (multiline Argon) 561 (diode-pumped solid-state) and 638nm (laser diode).

For live imaging, environmental control of the cultured cells was maintained during imaging with a large Solent Scientific incubation chamber incorporating temperature and humidified CO_2 control (Solent Scientific Ltd., Segensworth, UK). Images were taken every 30 minutes for 18-24h. Focus was maintained using the Perfect Focus System.

2.9.3 Transmission Electron Microscopy

Samples were dissected into PBS. Samples were fixed in 2% PFA, 2.5% gluteraldehyde in 0.2M Sodium Cacodylate Buffer pH7.4 + 0.04% $CaCl_2$. After 30 min at room temperatures, samples were cut into 1mm cubes and fixed overnight or longer at 4˚C. Samples were then sent to Newcastle Medical School, where they were processed further, cut into semithin and ultrathin sections and imaged by transmission electron microscopy by Tracey Davey, Newcastle Medical School, Newcastle University.

2.10 Statistical analyses

Throughout this thesis $p < 0.05$ is considered significant, unless otherwise stated. Except for the screen, statistics were carried out in Excel and the test used is specified in the text.

2.10.1 Screen Statistics

Statistical analyses were carried out in R by Richard Mort (MRC HGU), except for hypergeometric tests which were carried using an online calculator: http://stattrek.com/online-calculator/hypergeometric.aspx

2.10.1.1 Cilia numbers

As described in Chapter Five, two methods were used to identify siRNAs which lead to a change in cilia number. For one method, NPI was calculated

$$NPI = \frac{\%\ neg - \%\ goi}{\%\ neg - \%\ pos}$$

% neg = average % of ciliated cells in Neg and *GFP*

% pos = average % of ciliated cells in *Ift88* #3 and #4

% goi = % of cilia in gene of interest siRNA

An siRNA was called as a hit if it was more than two standard deviations from the mean of the genes not involved (*Gapdh, Smo* and *CycB2*).

For the second method, Fisher's Exact test was calculated, with Bonferroni correction using the average number of cells with or without cilia in the negative (neg) and *GFP* siRNA treated wells in that plate to calculate the expected results.

An siRNA was considered a hit if $p < 0.01$. To determine if, over all the plates, the positive control *Ift88* siRNAs significantly reduced cilia number, Wilcoxon rank sum test was performed.

2.10.1.2 Cilia length

For each well the length of cilia was measured by maximum feret diameter. A Kruskall Wallis test was performed on each plate. A significant result was obtained ($P < 0.05$) for all plates, therefore a Wilcoxon rank sum test was performed with Bonferroni correction. Results are shown in Table 5.1 and 5.6 highlighting significant increases and decreases in length, compared to one or both negative control siRNAs on the plate. Wilcoxon test was used to determine if *Ift88* siRNA significantly reduced cilia length across all plates.

2.10.1.3 Centrosome number

The number of cells with >2 γ-tubulin foci, taken to mean >2 centrosomes, was calculated for each well. Fisher's Exact test was calculated, with Bonferroni correction, using the average number of cells with >2 centrosomes in the negative (neg) and *GFP* siRNA treated wells in that plate to calculate the expected results. An siRNA which gave a $p < 0.01$ was considered a hit.

2.11 Online database analyses

2.11.1 Expression database

Analysis of gene expression using online databases was performed by accessing EMBL EBI Gene Expression Atlas at http://www.ebi.ac.uk/gxa/gene/ and the Unigene EST database http://www.ncbi.nlm.nih.gov/UniGene/ESTProfileViewer.cgi

2.11.2 Ciliome databases

Analsysis owhether a protein had previously been found to be part of the ciliome was performed searching two ciliome databases: www.ciliome.org and www.ciliaproteome.org.

2.11.3 Protein domain predictions

Coiled coiled domains were predicted using N-coils and the t-SNARE domain was predicted by the SUPERFAMILY database.

Chapter 3. Characterisation of the ciliary phenotype Wdr35 and Dync2h1 mutant mouse embryonic fibroblasts (MEFs).

Before embarking on a cell-based genetic screen for genes involved in cilia formation and function, I characterised the cellular phenotypes of two ciliary mutants, to determine the roles Wdr35 and Dync2h1 play in ciliary formation, which also allowed me to optimise protocols and familiarise myself with mutant ciliary phenotypes.

An ENU screen for genes involved in embryonic patterning identified two mouse mutants, *yeti* and *polyphemus* with distinct and overlapping phenotypes, including randomised laterality, craniofacial defects and polysyndactyly (Mill et al.) and unpublished). These were found to have point mutations in *Wdr35* and *Dync2h1* respectively, both of which encode proteins that are thought to be involved in retrograde IFT; Dync2h1 is a component of the retrograde IFT motor (Criswell et al., 1996; Huangfu and Anderson, 2005; Porter et al., 1999; Signor et al., 1999) and Wdr35 interacts with IFT-A components (Blacque et al., 2006; Mill et al.; Mukhopadhyay et al.). Both *polyphemus* and *yeti* mutants (termed $Dync2h1^{pol/pol}$ and $Wdr35^{yet/yet}$ respectively for this thesis) die before E12.5 and display hedgehog signalling defects, characteristic of other ciliary mutants ((Mill et al., 2011) and unpublished work). $Wdr35^{yet/yet}$ have a G>A mutation in the splice acceptor of exon 22 of *Wdr35*. These mutants are null for *Wdr35* as judged by lack of mRNA and protein, as well as the fact $Wdr35^{yet/yet}$ mutants phenocopy mutants with a "targeted trap" *tm2a* allele of *Wdr35* (Mill *et al* 2011). $Dync2h1^{pol/pol}$ have a premature stop codon in *Dync2h1* and are probably null for *Dync2h1* as no protein is detectable (data not shown), and because it phenocopies two previously published alleles (Huangfu and Anderson, 2005; May et al., 2005; Ocbina et al., 2011).

3.1 *Wdr35*$^{yet/yet}$ and *Dync2h1*$^{pol/pol}$ MEFs have no/severely reduced numbers of cilia

In order to study the cellular phenotype of the *Wdr35*$^{yet/yet}$ and *Dync2h1*$^{pol/pol}$ mutants, mouse embryonic fibroblasts (MEFs) were derived from E11.5 embryos. In order to induce ciliogenesis in cell culture, cells are generally serum staved for 24-72h. This arrests cells in G_1/G_0, thereby promoting ciliogenesis, which occurs when cells are quiescent. After 48 hours serum starvation, just over 20% of wild type MEFs had a cilium clearly marked by anti-acetylated α-tubulin, which marks the axoneme, and anti-γ-tubulin, which marks the basal body (Figure 3.1A and D). *Wdr35*$^{yet/yet}$ cells completely lack cilia (Figure 3.1B and D) (Mill et al. 2011), while *Dync2h1*$^{pol/pol}$ show severely reduced numbers of cilia; less than 2% of cells have a cilium marked with anti-acetylated α-tubulin ($p<0.001$ Chi squared, Figure 3.1C and D). The few remaining cilia in the *Dync2h1*$^{pol/pol}$ MEFs are slightly shorter than the wild type cilia (although the numbers of cilia present are too low for this to be statistically significant. Figure 3.1E). In both mutant cell lines, increased levels of cortical microtubule arrays stained by anti-acetylated α-tubulin were observed.

3.2 *Dync2h1*$^{pol/pol}$ and *Wdr35*$^{yet/yet}$ MEFs show distinct ciliary phenotypes

To further characterise the ciliary phenotypes of these mutant cell lines, localisation of Ift88, a member of the anterograde IFT-B complex, and Arl13b, a ciliary membrane protein, was examined (Caspary et al., 2007; Murcia et al., 2000; Pazour et al., 2000). In wild type cells, anti-Ift88 shows punctuate staining along the axoneme (Figure 3.2A). *Dync2h1*$^{pol/pol}$ MEFs show large bulbous accumulations of Ift88 in the shortened cilia remnants present in these cells (Figure 3.2C). This is likely due to accumulations of IFT particles due to lack of retrograde IFT, as

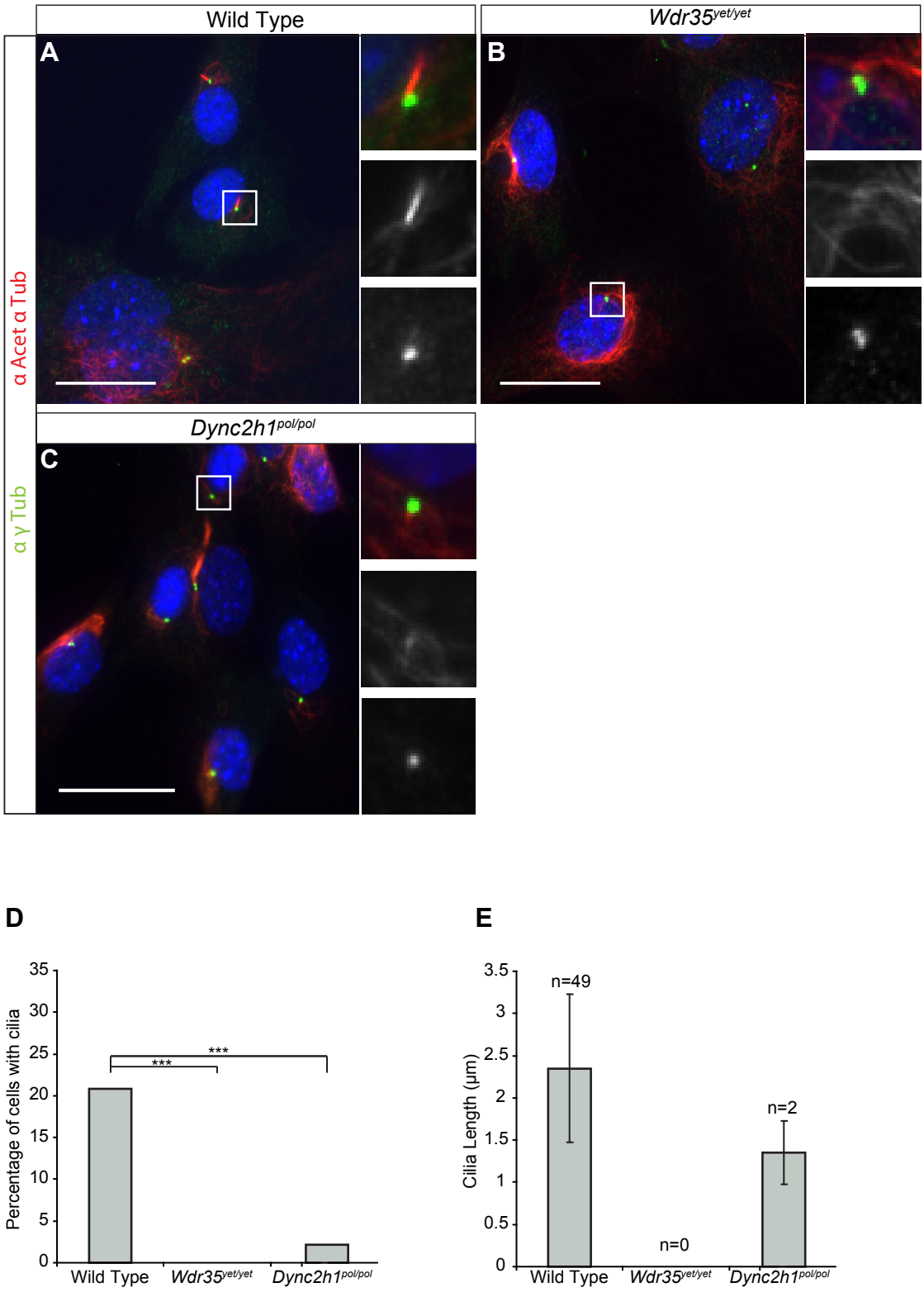

Figure 3.1 *Wdr35*$^{yet/yet}$ MEFs lack cilia and *Dync2h1*$^{pol/pol}$ MEFs have severely reduced numbers of cilia.

Figure 3.1 *Wdr35*$^{yet/yet}$ MEFs lack cilia and *Dync2h1*$^{pol/pol}$ MEFs have severely reduced numbers of cilia. (A - C) MEFs were serum starved and stained with α-Acetylated α-tubulin to mark the cilia axoneme and α-γ-tubulin to mark the basal body. Scale bars show 50μm. Three-fold magnifications of regions of interest (highlighted by white squares) are shown to the right with individual channels, α-Acetylated α-tubulin at the top and γ-tubulin at the bottom. (D) The number of α-Acetylated α-tubulin positive cilia was counted, at least 100 cells were counted from biological duplicates. *Wdr35*$^{yet/yet}$ MEFs have no cilia (B and D) and *Dync2h1*$^{pol/pol}$ MEFs have significantly fewer cilia (*** p<0.001 Chi squared). (E) Lengths of cilia in wild type and those cilia that remained in the *Dync2h1*$^{pol/pol}$ MEFs were measured. The remaining cilia in *Dync2h1*$^{pol/pol}$ MEFs were shorter, although the small number of cilia means this is not statistically significant. n = number of cilia measured.

Dync2h1 is a component of the cytoplasmic dynein 2 motor complex required for returning cargo from the cilia tip. Similar phenotypes of accumulated IFT particles are observed in *C. elegans* and *Chlamydamonas* mutants of *Dync2h1* orthologues (DHC2/CHE3) and have been previously reported for mouse alleles of the same gene (Huangfu and Anderson, 2005; May et al., 2005; Ocbina et al., 2011; Pazour et al., 2000; Porter et al., 1999; Signor et al., 1999). To determine whether other ciliary components were also accumulating in these mutant cilia, localisation of Arl13b, a small GTPase which localises specifically to cilia membranes and is required for correct ciliary architecture, was examined (Caspary et al., 2007; Sun et al., 2004). *Dync2h1* mutant cells also show large accumulations Arl13b (Figure 3.2F compared to D), suggesting it is not just anterograde IFT particles that are entering and accumulating in the cilium; ciliary membrane particles/IFT cargo is also actively entering the cilia and is unable to exit due to the lack of retrograde IFT. As expected, although Dync2h1 was detected as punctuate staining along the axoneme of the wild type cilia, no Dync2h1 staining was detected in the *Dync2h1*$^{pol/pol}$ MEFs further supporting the theory these cells are null for *Dync2h1* (Figure 2.2G and I).

In contrast, despite the fact Wdr35 interacts with the retrograde IFT-A complex, *Wdr35*$^{yet/yet}$ cells do not show such accumulations of Ift88 or Arl13b (Figure 3.2B and E). Ift88 was detected at the centrosome/basal body as shown by punctuate anti-acetylated α-tubulin staining (Figure 3.2B), as was Dync2h1 (Figure 3.2G), suggesting the IFT machinery is correctly loaded at the basal body, but it does not enter the cilium and accumulate as seen in *Dync2h1* mutant cells. In contrast,

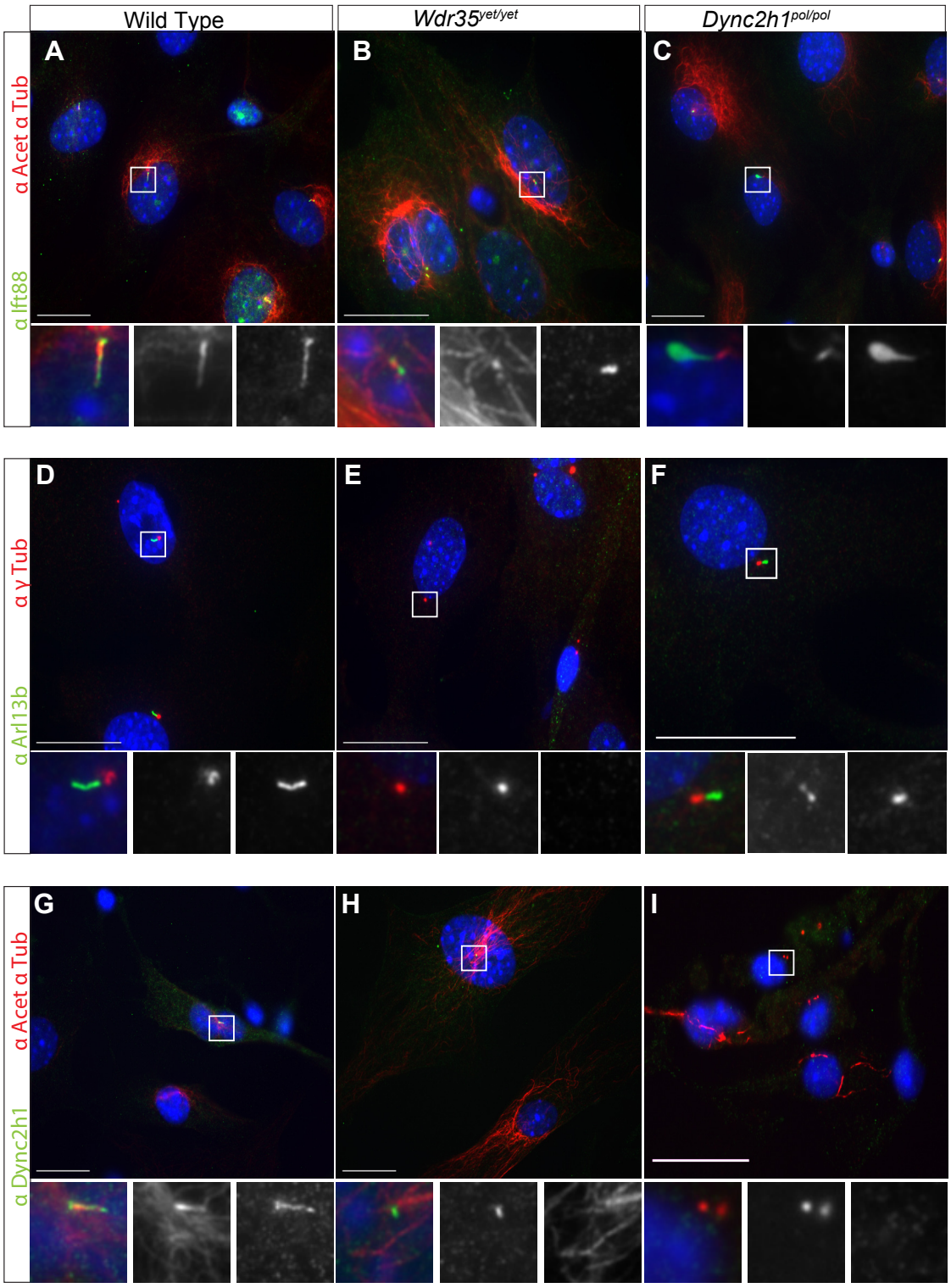

Figure 3.2 *Wdr35*$^{yet/yet}$ and *Dync2h1*$^{pol/pol}$ MEFs show distinct ciliary phenotypes.

Figure 3.2 *Wdr35*$^{yet/yet}$ and *Dync2h1*$^{pol/pol}$ MEFs show distinct ciliary phenotypes. MEFs were serum starved to induce ciliogenesis. (A, B and C) α-Ift88 shows punctate staining along the axoneme (marked by α-Acetylated α-tubulin) in wild type (A), it accumulated in bulges in *Dync2h1*$^{pol/pol}$ cilia (C), and is only present as dots at the basal bodies in *Wdr35*$^{yet/yet}$ MEFs (B). (D, E and F) Arl13b marks the ciliary membrane in wild type cells (costained with α-γ-tubulin which marks the basal body) (D). Arl13b accumulates in *Dync2h1*$^{pol/pol}$ cilia (F), but is absent from *Wdr35*$^{yet/yet}$ basal bodies (E). (G, H and I) α-Dync2h1 shows punctate staining along the axoneme in wild type (G), no staining is seen in *Dync2h1*$^{pol/pol}$ MEFs as expected (I). Dync2h1 localises to basal bodies in *Wdr35*$^{yet/yet}$ MEFs (H). Scale bars represent 50μm. Below each panel is an five-fold magnification of a region of interest (highlighted by a white square) with the red channel in the centre and the green channel on the right.

Arl13b was not found at the basal body in *Wdr35*$^{yet/yet}$ MEFs (Figure 3.2E), suggesting the distinct ciliary membrane compartment usually found around the cilium is not formed in these mutants. Total levels of Ift88 and Arl13b were unchanged in these cells (Figure 3.4B), suggesting the proteins are expressed normally but are mislocalised within the cell in the absence of Wdr35. It is interesting that these genes (*Wdr35* and *Dync2h1*), both components of the retrograde IFT machinery, which show such similar phenotypes when mutated in *C elegans* (Blacque et al., 2006; Signor et al., 1999), should show such distinct ciliary phenotypes in mouse, and perhaps suggests a novel trafficking role outwith retrograde IFT for Wdr35 in mammalian ciliogenesis.

3.3 Human fibroblasts mutant for *WDR35* also lack cilia

Human mutations in *WDR35* can lead to short rib polydactyly (SRP) (Kannu et al., 2007; Mill et al., 2011). SRPs are a group of autosomal recessive, heterogeneous, lethal skeletal dysplasias, characterised by polydactyly and short ribs and limbs, which can also present with other abnormalities including polycystic kidney disease and laterality defects (Baker and Beales 2009). I characterised fibroblast lines from two siblings with SRP, which have a homozygous 2847bp deletion spanning Exon 5 of *WDR35* (termed *WDR35*$^{\Delta 5/\Delta 5}$ 1 and 2) and a third line from an SRP patient with

compound heterozygous mutation, nonsense mutation (c.1633C>T [p.Arg545X]), and a missense mutation affecting a highly conserved tryptophan residue (c.781T>C [p.Trp261Arg]) on the second allele (termed *WDR35*$^{R545X/W261R}$) (obtained by collaborators with informed consent). These fibroblasts are null for *WDR35* as judged by loss of protein expression as well as phenotypic similarities between the human syndrome and mouse null mutant, i.e. polydactyly and absent/shortened ribs (Mill et al., 2011). Staining with Arl13b showed a complete lack of cilia in both *WDR35*$^{\Delta 5/\Delta 5}$ patient cell lines, with no Arl13b localising to the basal body marked by γ-tubulin (Figure 3.3A-C), similar to the phenotype seen in mouse mutant fibroblasts (Figure 3.2 D and F). *WDR35*$^{R545X/W261R}$ fibroblasts were stained with anti-acetylated α-tubulin, which confirmed they also lack cilia. As in the mouse cells, there was an accumulation of cortical acetylated α-tubulin arrays. In all cell lines the basal body, marked by γ-tubulin was normal. These data suggest that Wdr35 is essential for ciliogenesis in human and mouse.

3.4 *Wdr35*$^{yet/yet}$ and *Dync2h1*$^{pol/pol}$ MEFs show aberrant Hedgehog (Hh) signalling

Cilia are essential for Hh signalling in mammals (Huangfu and Anderson, 2005; Huangfu et al., 2003) , acting as a signalling hub, with many Hh signalling components localising to the cilium (Chen et al., 2009; Corbit et al., 2005; Haycraft et al., 2005; Rohatgi et al., 2007; Wen et al., 2010). In order to characterise Hh signalling in the *Wdr35*$^{yet/yet}$ and *Dync2h1*$^{pol/pol}$ MEFs, I treated them with increasing concentration of the small molecule Hh agonist purmorphamine (Sinha and Chen, 2006; Wu et al., 2002). Hh signalling is a fairly complex process, spatially regulated by mammalian cilia and ultimately mediated by the bifunctional Gli transcription factors (summarised in 1.3.2.1). In the absence of Hh ligand, Ptch1 represses signalling through its co-receptor Smo, leading to proteolytic cleavage of Gli3^{FL} to its potent repressor form Gli3^{R}. When Hh ligand binds to Ptch, this releases inhibition on Smo leading to stabilisation of Gli3^{FL}, which in turn activates Hh target

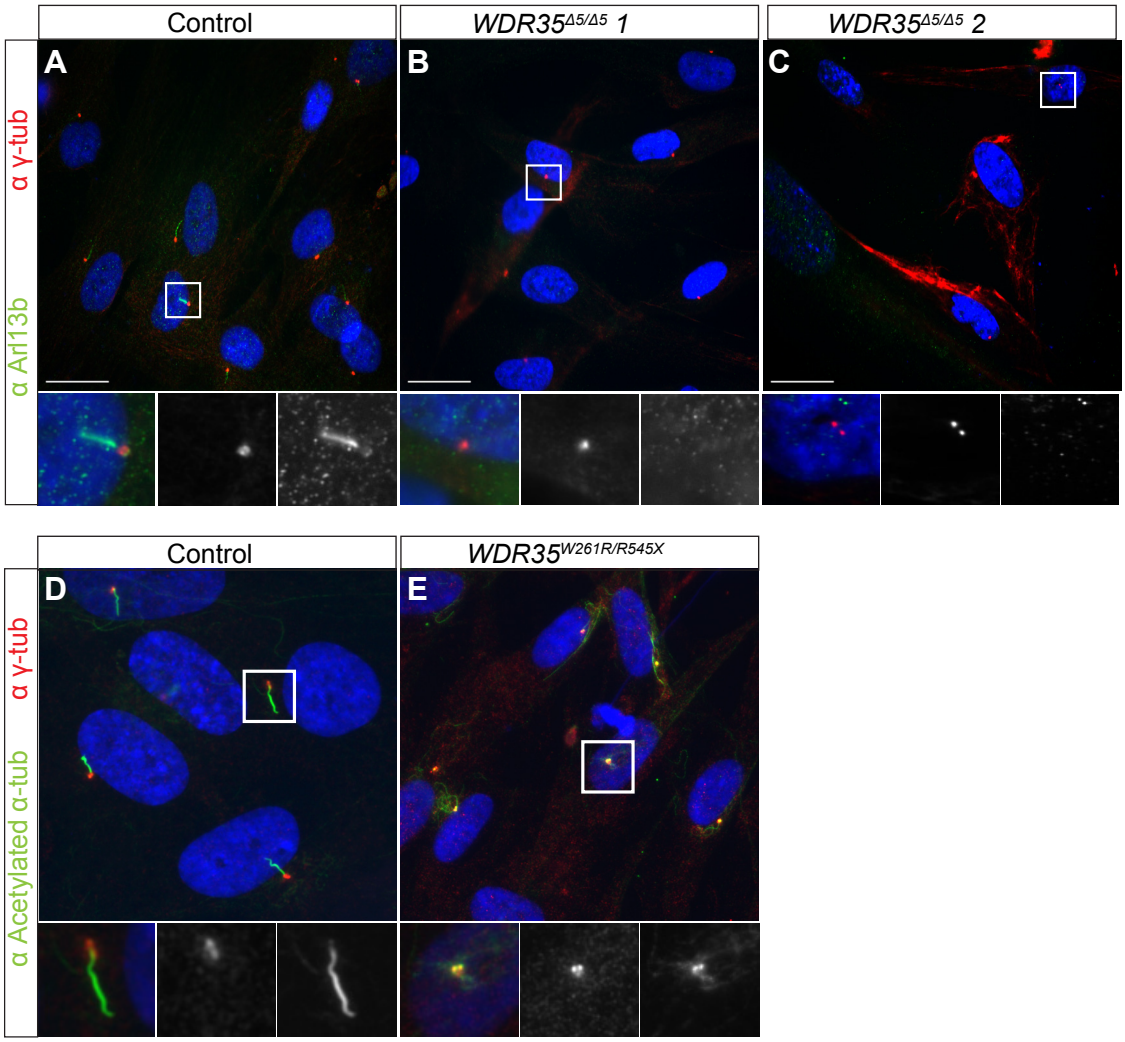

Figure 3.3 *WDR35* mutant human fibroblasts lack cilia (A) In control fibroblast lines, almost every cell has a cilia that is positive for Arl13b. (B and C) Two SRP patient cell lines that lack Exon 5 of *Wdr35* lack cilia, as demonstrated by the lack of Arl13b staining. (D) A second control line stained with α-Acetylated α-tubulin to mark the ciliary axoneme - again almost every cell has a cilia. (E) A third SRP patient cell line *WDR35*$^{W261R/R545X}$ also lacks cilia as shown by α-Acetylated α-tubulin staining. Scale bars represent 50μm, two-fold maginifcation of regions of interest (highlighted by white squares) are shown below each panel, red channel in the centre, green channel on the right.

genes (Ingham and McMahon, 2001). *Ptch1* itself is one such target gene creating a negative feedback loop. Purmorphamine is a Smo agonist and its addition leads to activation of downstream Hh target genes, such as *Ptch1* (Sinha and Chen, 2006). As expected, addition of increasing concentrations of purmorphamine leads to increasing *Ptch1* mRNA levels by qPCR (Figure 3.4A). There is some variation between MEF lines, so each mutant is compared to a wild type littermate. Both $Wdr35^{yet/yet}$ and $Dync2h1^{pol/pol}$ MEFs show impaired Hh signalling, with *Wdr35* mutant cells showing no increase in *Ptch1* mRNA, and *Dync2h1* null cells showing a no response to lower concentrations and a greatly attenuated response to higher concentrations. Interestingly, there may be a slight increase in basal *Ptch1* mRNA levels in the *Wdr35* mutant cells, which may reflect impaired processing of $Gli3^{FL}$ to $Gli3^{R}$, discussed below, although it is not statistically significant.

To further analyse Hh signalling in the *Wdr35* mutant cells, I examined the levels and processing of the downstream transcription factor Gli3 in protein extracts from cells serum starved and treated with either DMSO, purmorphamine or cyclopamine-KAAD, an antagonist of Hh signalling (Chen et al., 2002a). Gli3 can be both an activator or repressor of Hh target genes; when Hh signalling is activated, full length Gli3 ($Gli3^{FL}$ 190kDa) is converted to its active form by an unknown process which is thought to require the cilium, whereas in the absence of Hh activation, Gli3 is cleaved to form a short repressive form ($Gli3^{R}$ 93kDa) (Huangfu and Anderson, 2005; Sasaki et al., 1999; Wang et al., 2000a; Wen et al., 2010). In the *Wdr35* mutant cells, basal levels of both $Gli3^{FL}$ and $Gli3^{R}$ are reduced (Figure 3.4B and C), with a greater reduction in $Gli3^{R}$ meaning there is an increase in the $Gli3^{FL:R}$ ratio (Figure 3.4D). This may lead to a slight increase in basal Hh pathway activation levels seen in Figure 3.4A. Upon the addition of the Hh agonist purmorphamine, wild type cells show a dramatic decrease in Gli3R levels, almost no $Gli3^{R}$ remains, leading to an increase in the $Gli3^{FL:R}$ ratio, whereas in the *Wdr35* mutant cells do not respond to purmorphamine, showing little change in the levels of Gli3R, which were already reduced in the basal state (Figure 3.4B-D). I also added cyclopamine, a Hh antagonist, to the cells, however in repeated attempts, wild type cells do not show an increase in $Gli3^{R}$ levels or a decrease in $Gli3^{FL}$ suggesting this drug treatment may not have worked (Figure 3.4B-D) (Chen *et al* 2002).

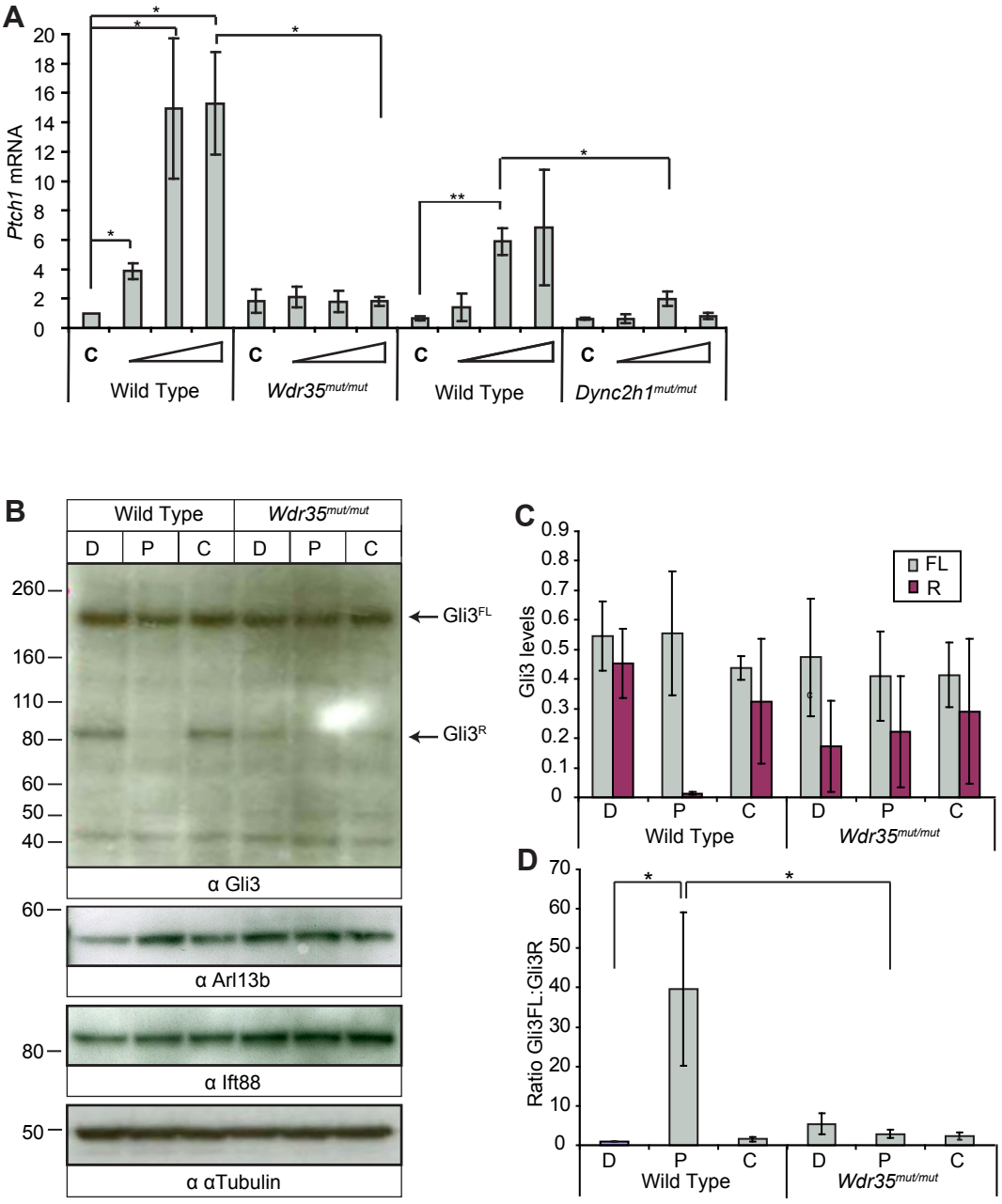

Figure 3.4 *Wdr35*$^{mut/mut}$ and *Dync2h1*$^{mut/mut}$ MEFs show aberrant Hedgehog signalling.

Figure 3.4 *Wdr35*$^{mut/mut}$ and *Dync2h1*$^{mut/mut}$ MEFs show aberrant Hedgehog signalling. (A) qPCR for *Ptch1* relative to *Tbp* in MEFs serum starved and treated with increasing concentrations of Purmorphamine for 30h shows *Wdr35*$^{mut/mut}$ and *Dync2h1*$^{mut/mut}$ do not respond to the drug. Each mutant line is compared to a wild type littermate. Error bars show standard deviation from three technical triplicates and two biological duplicates. (B) Protein lysates from MEFs treated with DMSO (D), Purmorphamine (P) or cyclopamine (C) probed with antibodies to Gli3, Arl13b, Ift88 and α Tubulin, showing *Wdr35*$^{mut/mut}$ MEFs have reduced amounts of Gli3^{R} with no drug treatment, and they do not respond to purmorphamine. Cyclopamine treatment appears to have failed as it has no effect on wild type Gli3 processing. Levels of Arl13b and Ift88 are unchanged in these mutant cells. (C) Quantification of Gli3 full length (FL) and repressor (R) levels. (D) Ratio of Gli3$^{FL:R}$. The average of biological duplicates is plotted in (C) and (D), Error bars show standard deviation. * $p<0.05$ students t-test.

3.5 Discussion

3.5.1 *Wdr35* and *Dync2h1* mutant MEFs have distinct ciliary phenotypes

In this chapter, I analysed the cellular phenotypes of *Wdr35* and *Dync2h1* mutant MEFs, derived from mice generated in an ENU mutagenesis screen with characteristic phenotypes of deregulated Hh signalling (Mill et al., 2011). Interestingly, both these mutants affected cilia structure and signalling processes dependent on cilia. Mutant MEFs had no or greatly reduced numbers of cilia detected by anti-acetylated α-tubulin, which detects stabilised microtubules at the axoneme where staining is brightest, but also marks cortical arrays of stabilised microtubules (MTs) associated with the Golgi and centrosome; this is a dynamic process and these arrays build up at the onset of ciliogenesis (Poole et al., 2001). Both cell lines had increased levels of stabilised cortical acetylated α-tubulin arrays (Figure 3.1). This may suggest that α-tubulin is being successfully acetylated in these mutants, but the lack of a ciliary axoneme means this acetylated α-tubulin is building up in cortical arrays, and is perhaps reflects a stall in the ciliogenesis process.

Dync2h1 is a component of the MT-based motor driving retrograde IFT, while Wdr35 interacts with retrograde IFT-A complex proteins (Mukhopadhyay et al., 2010), *C. elegans* mutants of orthologues of both these genes show similar retrograde IFT phenotypes, with shortened bulging cilia and accumulations of IFT

particles (Blacque et al., 2006; Signor et al., 1999). However, in mouse cells, the ciliary phenotypes of these mutants differ. *Dync2h1* mutant cells show the classic retrograde phenotype, with striking accumulation of IFT-B machinery as shown by Ift88, as well as the ciliary membrane protein Arl13b, (Figure 3.2 and 3.5). Surprisingly, *Wdr35* mutant cells do not show such accumulations, a small amount of Ift88 and Dync2h1 is seen at the basal body, suggesting the IFT complexes and motors may be correctly localising to the base of the cilium but not extending the axoneme (Figure 3.2 and 3.5). Importantly, Arl13b is not seen at or near the basal body, although total levels remain unchanged (Figure 3.4B) suggesting the distinct membrane compartment that surrounds the cilium is not formed in these mutants. Such differences in the ciliary phenotypes suggests novel roles for Wdr35 in mammalian ciliogenesis, in addition to its role in retrograde IFT. Supporting this theory, $Wdr35^{yet/yet}$:$Dync2h1^{pol/pol}$ double mutants do not show accumulation of ciliary membrane proteins characteristic of $Dync2h1^{pol/pol}$ cilia, suggesting Wdr35 function is required for initial compartmentalization or cargo selection necessary for cilia extension from the transition zone (Mill, unpublished data). Alternately, it has been suggested that IFT-A proteins have roles in anterograde as well as retrograde IFT; this has been suggested in *Chlamydamonas* for IFT-A complex: partial loss of IFT-A function leads to shortened bulging flagella, but complete loss of function leads to a loss of flagella (Iomini et al., 2009; Piperno et al., 1998). In mouse it has also been suggested that the IFT-A protein Ift122, which is required for retrograde IFT, may have additional roles in anterograde trafficking; Ocbina *et al.*(2011) show *Ift122* mutation partially rescues $Dync2h1^{lln/lln}$ ciliary structural and signalling defects. It is important to note that, in contrast to $Wdr35^{yet/yet}$ cilia, $Ift122^{sobp/sobp}$ mutant cilia have Arl13b correctly localised (Qin et al., 2011), which suggests a specific role for Wdr35 in trafficking of Arl13b to the cilia.

Further studies to dissect Wdr35 function, including biochemical studies to find protein interactors involved in membrane trafficking, and further genetic studies such as $Dync2h1^{pol/pol}$;$Wdr35^{yet/yet}$ double mutants, may shed light onto the role(s) of Wdr35 in mammalian cilia. It is also important to note that the studies presented in this chapter examine phenotypes after 48h of serum starvation, and so represent a snapshot of a late stage phenotype. Studies using live imaging of fluorescently

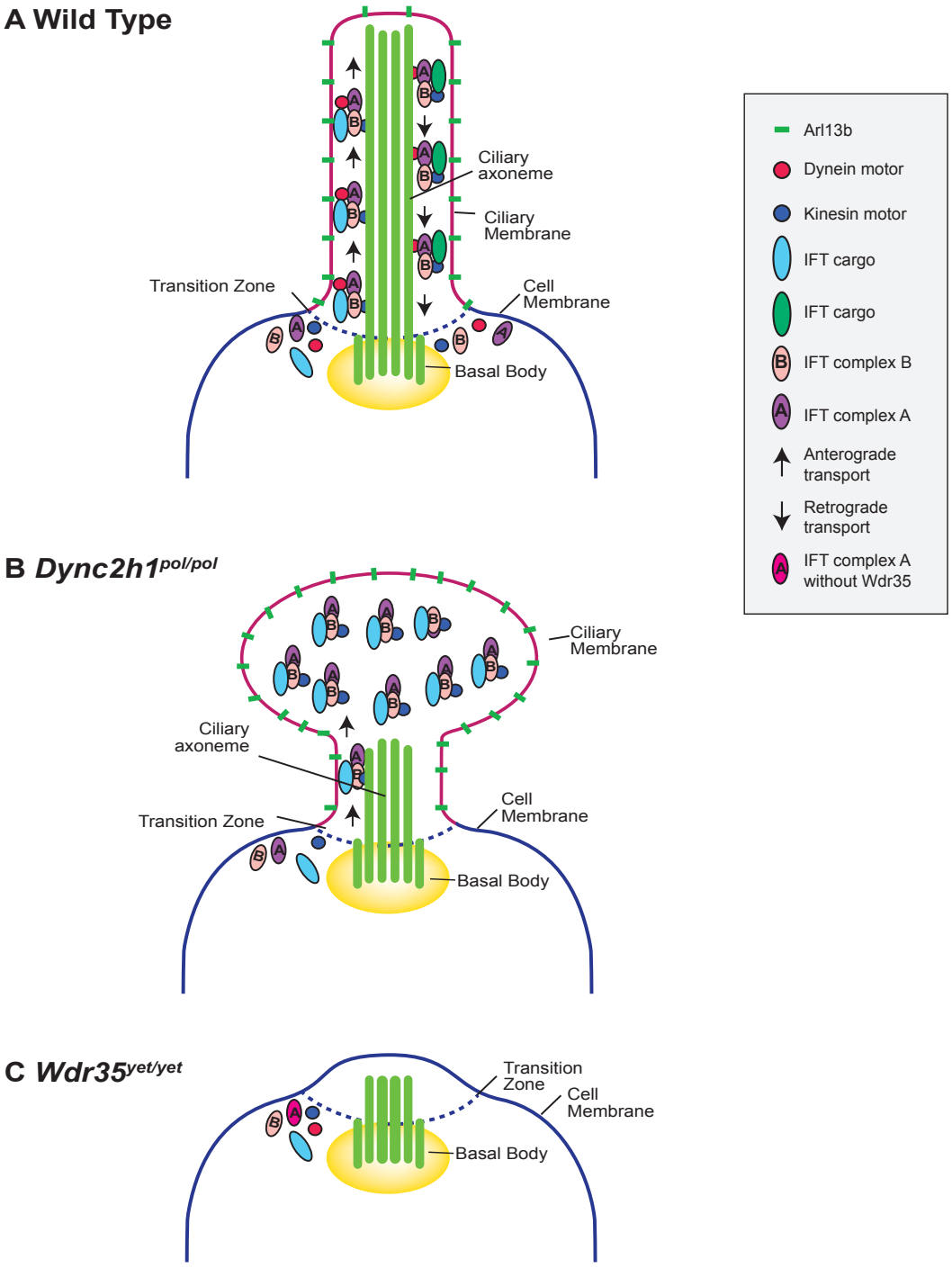

Figure 3.5 Model of the distinct ciliary phenotypes seen in *Dync2h1* and *Wdr35* mutant MEFs.

Figure 3.5 Model of the distinct ciliary phenotypes seen in *Dync2h1* and *Wdr35* mutant MEFs. (A) In wild type cilia, an active process of Intraflagellar Transport (IFT) transports proteins to (anterograde) and from (retrograde) the ciliary tip. IFT proteins and cargo dock at or near the basal body to be loaded onto the IFT motors, which also dock at the basal body. A heterotrimeric kinesin-II motor powers antergrade IFT, and a dynein 2 motor powers retrograde IFT. A distinct ciliary mebrane compartment surrounds the cilium (shown in pink). (B) *Dync2h1*$^{pol/pol}$ MEFs lack the retrograde dynein motor. Anterograde IFT transports proteins into the cilium but the lack of retrograde IFT mean they build up in shortened, bulging cilia. The ciliary membrane protein Arl13b also accumulates. (C) *Wdr35*$^{yet/yet}$ MEFs lack the IFT-A protein Wdr35. IFT-A proteins are though to have a role in anterograde IFT, but the lack of ciliary structures in these MEFs suggest Wdr35 may also have a role in anterograde IFT. Although IFT-B proteins and the Dynein 2 motor localise to the basal body suggesting they are docked ready for IFT, Arl13b is absent from the basal body, suggesting the distinct ciliary membrane domain does not form and indicating a role for Wdr35 in the trafficking of this protein to the cilium.

tagged ciliary proteins to analyse the dynamics of ciliogenesis, including extension and maintenance of cilia, in these mutant cells are on-going.

3.5.2 WDR35 is required for human ciliogenesis

WDR35 has been shown to be mutated in at least two ciliopathies, Short Rib Polydactyly (SRP) and Cranioectodermal dysplasia (CED / Sensenbrenner Syndrome) (Gilissen et al., 2010; Mill et al., 2011). SRP is a lethal skeletal dysplasia, with shortened long bones and ribs, which can present with polydactyly and other ciliopathic phenotypes such as polycystic kidney disease. CED is considered a milder syndrome with skeletal abnormalities, as well as craniosynostosis, nephronophthisis and retinal and brain abnormalities. Interestingly, *DYNC2H1* has also been shown to be mutated in SRP type III, and the related disorder Jeune asphyxiating thoracic dystrophy (JATD) (Dagoneau et al., 2009; Merrill et al., 2009). In this chapter, I show that three human fibroblast cell lines from SRP patients, two siblings with deletions of exon 5 of *WDR35* (*WDR35*$^{\Delta 5/\Delta 5}$) and a third patient with compound heterozygous mutations in *WDR35* (*WDR35*$^{R545X/W261R}$) lack cilia. In *WDR35*$^{\Delta 5/\Delta 5}$ cells Arl13b staining, which clearly marks the ciliary membrane in control human fibroblasts, is absent from *WDR35*$^{\Delta 5/\Delta 5}$ cilia and basal bodies (Figure 3.3). Anti-acetylated α-tubulin staining confirmed the lack of cilia in *WDR35*$^{R545X/W261R}$ cells and there were increased cortical arrays, as seen in the MEFs. It has also been shown the *WDR35*$^{\Delta 5/\Delta 5}$ cells lacked cilia using Ift88, and that Ift88 is found at the basal body

(Mill et al., 2011). Therefore the phenotype of the human *WDR35*$^{\Delta 5/\Delta 5}$ fibroblasts closely resembles that of the mouse *Wdr35*$^{yet/yet}$ fibroblasts, suggesting the role for Wdr35 in Arl13b trafficking to the cilium is conserved.

3.5.3 *Wdr35* and *Dync2h1* mutant MEFs show aberrant Hh signalling

Cilia are required for mammalian Hedgehog (Hh) signalling, and many patterning phenotypes observed in the *Wdr35* and *Dync2h1* mutant mice are due to misregulation of Hh signalling (Mill et al., 2011). Here I show that neither *Wdr35* mutant nor *Dync2h1* mutant MEFs are able to properly activate the Hh target gene *Ptch1* in response to the Hh agonist purmorphamine (Figure 3.4A). *Wdr35* null MEFs have are also unable to efficiently generate Gli3^{R}, and unlike wild type cells, levels do not reduce in response to purmorphamine (Figure 3.4B, C and D). A similar inability to fully process Gli3^{FL} to Gli3^{R} was observed in *Dync2h1*$^{lln/lln}$ mutant embryos (Huangfu and Anderson, 2005). Cilia are required for both activation and repression activities of the Hh pathway, however the exact Hh signalling defects and resulting phenotypes observed differ between IFT mutants, suggesting specific and subtle differences between the functions of these proteins (Caspary et al., 2007; Huangfu and Anderson, 2005; Huangfu et al., 2003; Liu et al., 2005; May et al., 2005; Ocbina et al., 2011; Qin et al., 2011). Although *Wdr35* mutant cells have Gli3^{FL} present, Gli3^{FL} must be further processed by an unknown mechanism, which probably requires the cilium, to become Gli3 activator (Gli3^{A}) (Wen et al., 2010). As these cells lack cilia, the Gli3^{FL} is not processed to Gli3^{A} and so downstream target genes, such as *Ptch1* are not activated (Fig 3.4A). Gli3^{R} is reduced but not completely absent which suggests some processing can occur in the absence of cilia, and this is similar to other cilia mutants (Haycraft et al., 2005; Liu et al., 2005; May et al., 2005). The decrease in Gli3^{R} could lead to slight elevations in basal levels of target gene expression, hinted at in the qPCR for *Ptch1* in these mutant cells, although this is not statistically significant (Figure 3.4A).

In conclusion, I analysed the cellular phenotypes of *Wdr35* and *Dync2h1* mutants and have shown that *Dync2h1* MEFs have reduced numbers of cilia, and those that remain are shortened and filled with accumulations of IFT and ciliary membrane proteins. In contrast, *Wdr35* mutant MEFs and human fibroblasts completely lack cilia and show no IFT accumulations, suggesting a role for Wdr35 in anterograde IFT. Finally, both *Wdr35* and *Dync2h1* mutant cells show aberrant Hh signalling. Importantly, $Wdr35^{yet/yet}$ MEFs have a novel defect in targeting of the ciliary membrane protein Arl13b to the cilium.

The differences observed between individual ciliary mutants highlights the variation in ciliary phenotypes that can occur. This is important to bear in mind when designing a screen for cilia formation and function, which will be described in the next two chapters of this thesis. Whichever readout for cilia formation or function is chosen, it is unlikely to detect every mutant ciliary phenotype, and this must be considered in the analysis of data and in any conclusions drawn.

Chapter Four. Designing a screen for genes involved in mammalian cilia formation and function

The main aim of my PhD was to design and perform a cell-based screen for genes involved in cilia formation and function. Previously in the lab, an ENU mutagenesis screen for genes required for embryonic patterning during early development had identified genes involved in ciliogenesis (Mill et al., 2011), highlighting the functional importance of cilia as signalling antennae. While this strategy is a powerful way to identify novel genes involved in cilia biology, the requisite mapping to determine the causative genes underlying the phenotype is time consuming and labour intensive. Therefore we sought to develop a reverse genetics screen in cells to quickly identify and characterise candidate ciliary genes. Before I began the screen, several screens to identify ciliary genes had been carried out, including proteomic, genome comparison and transcriptomic studies (See Chapter 1.6 and (Avidor-Reiss et al., 2004; Blacque et al., 2005; Efimenko et al., 2005; Inglis et al., 2006; Li et al., 2004; Ostrowski et al., 2010; Pazour et al., 2005; Smith et al., 2005; Stolc et al., 2005)). One RNAi screen had been published, in which they screened the kinome for Hh signalling modulators, and pulled out two ciliary genes (Evangelista et al., 2008). A second smaller scale RNAi study screened 41 centrosomal proteins for those involved in ciliogenesis by immunofluorescence readout (Graser et al., 2007). However these screens were far from saturating, and the chances of discovering more genes involved in the process of ciliogenesis using this method was high. I set out to design and perform an RNAi screen to identify genes involved in cilia formation and function. In this chapter the design and optimisation of the screening protocol is described.

4.1 Optimisation of ciliogenesis and transfection protocols

For a screening protocol to be effective it must be as robust and reproducible as possible to reduce background noise and increase sensitivity for calling hits, therefore I attempted to optimise each step in the screening protocol. An overview of the initial screen design is shown in Figure 4.1, where I would knockdown a large number of genes by RNAi in mammalian cells and assess for phenotypes affecting cilia formation and function. The optimisation and refinement of the screen design is described in this chapter.

4.1.1 Choosing a cell type

First, protocols to induce ciliogenesis were optimised in several different mouse and human cell lines, including the immortalized human retinal pigmented epithelial cell line hTERT-RPE-1, canine kidney cell line MDCK, mouse kidney cell line IMCD3, mouse fibroblast cell line NIH-3T3, mouse ES cells and primary mouse embryonic fibroblasts (MEFs). In general, these protocols involved plating cells at high density and removing serum in order to arrest cells in G_1/G_0, when ciliogenesis usually occurs. We decided to carry out the screen in a mouse cell line as many reagents for follow up and confirmation assays are available in mouse, including ultimately generation of mutant lines to examine the role of proteins *in vivo.* This ruled out MDCK (canine) and hTERT-RPE (human) cells. Although MEFs are primary cell lines which undergo ciliogenesis (Figure 3.1A) and are more reflective of the *in vivo* situation than immortalized cell lines, they undergo senescence after 6-9 passages and are difficult to transfect. The murine cell lines IMCD3, NIH-3T3, and ShhLIGHT-II cells (which are NIH-3T3 cells stably transfected with the Hedgehog (Hh) reporter *Gli-Luciferase* and *CMV-Renilla* (Taipale et al., 2000)) all reproducibly put out cilia after 48h serum starvation, whereas ciliogenesis protocols in ES cells

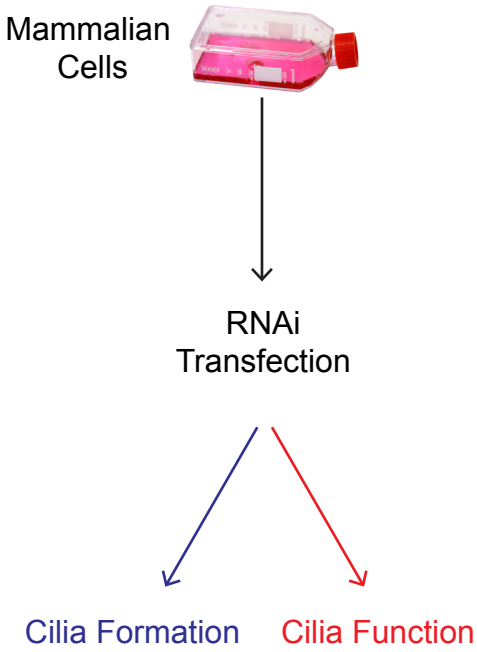

Figure 4.1 Simple overview of screeening strategy. The aim of the screen was to knockdown a large number of genes mammalian cells, then screen for cilia formation and cilia function.

were less reliable. We decided to carry out the screen in ShhLIGHT-II cells as this allowed us to have two readouts; an immunofluorescence based-readout for cilia formation, by staining and counting the cilia, and a second readout of cilia function, analysing Hh target gene activation as an indirect readout of cilia function using the *Gli-luciferase* transgene in these cells.

4.1.2 The screen readouts

4.1.2.1 Readout one: immunofluorescence based assay for cilia formation

Readout one assayed cilia formation by fixing cells, performing immunofluorescence staining for cilia, then analysing parameters such as numbers and length of cilia in a high-throughput and unbiased manner using the Olympus Scan^R. This involved schooling the microscope software to enable it to identify cell nuclei and structures such as cilia and basal bodies in an unbiased way. Several antibodies to ciliary markers including Acetylated α-tubulin, Arl13b and Ift88 were tested (Figure 4.2 A, B and C). Anti-Ift88 gave fairly high background staining, and anti-acetylated α-tubulin stained non-ciliary structures such as stabilised cortical tubulin arrays, therefore automated software had difficulties identifying cilia with these antibodies (Figure 4.2A and C). In contrast, anti-Arl13b, a robust ciliary membrane marker, marked the cilia specifically with little non-ciliary or background staining, and high signal to noise ratio (Figure 4.2B (Caspary et al., 2007)), allowing automated identification of the cilia. Therefore this was used as a marker for cilia identification in the screen. The cells were also costained with DAPI to identify the number of cells in the field as well as an antibody to the centrosome/basal body marker γ-tubulin, which allowed us to monitor centrosome/basal body number. The Olympus Scan^R microscope and analysis software, which is designed for high-throughput screening, was used to automatically image the plates, identify and count the cells, cilia and basal bodies, as well as measure the degree of cell cycle arrest induced by serum starvation using DAPI intensity. It was also able to measure cilia length. The software saves all images and links data points to corresponding images to allow manual quality control. Cilia identification

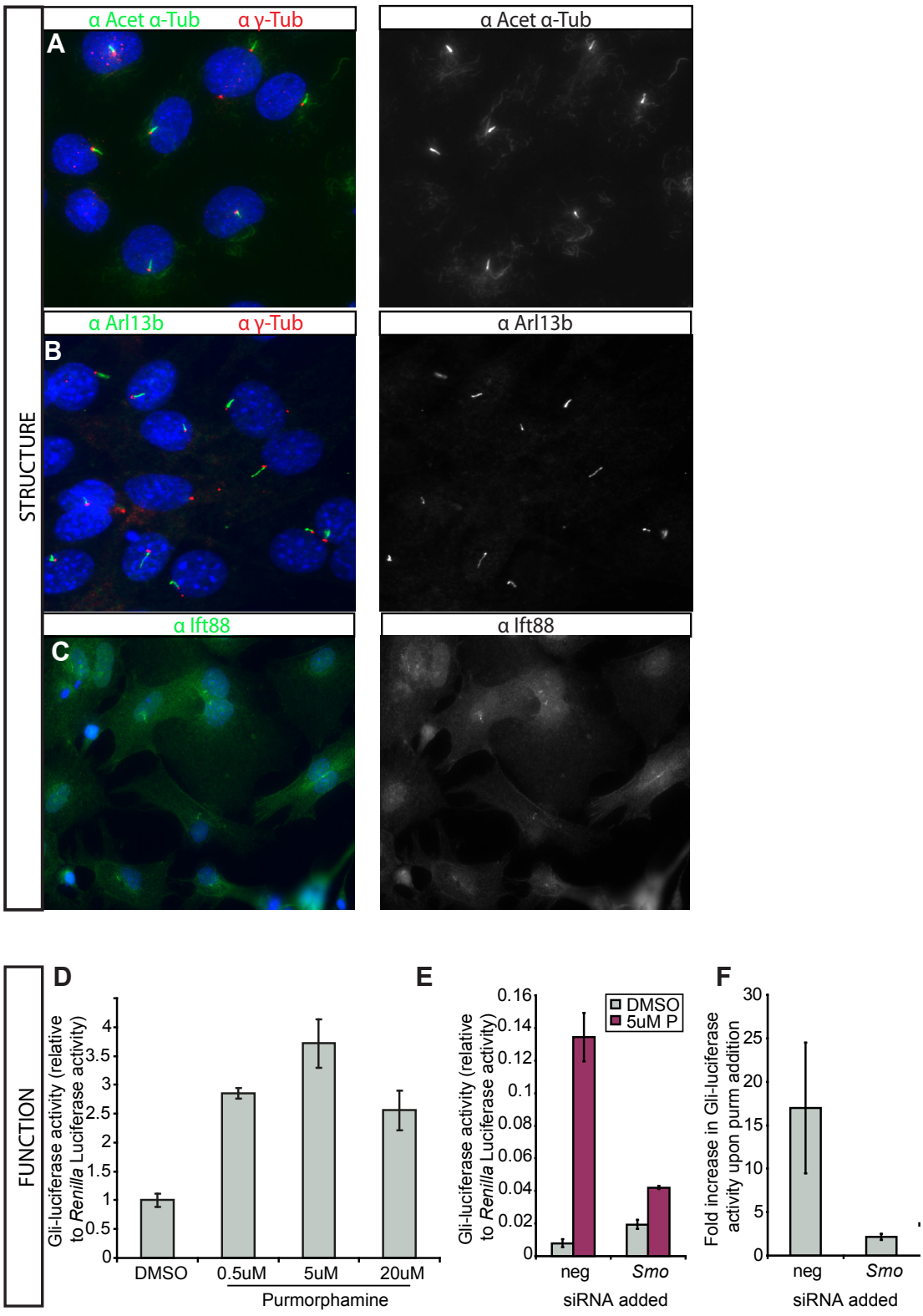
STRUCTURE
α Acet α-Tub
α γ-Tub
A
α Acet α-Tub
α Arl13b
α γ-Tub
B
α Arl13b
α Ift88
C
α Ift88
FUNCTION
D
Gli-luciferase activity (relative to Renilla Luciferase activity)
DMSO
0.5uM
5uM
20uM
Purmorphamine
E
Gli-luciferase activity (relative to Renilla Luciferase activity)
DMSO
5uM P
neg
Smo
siRNA added
F
Fold increase in Gli-luciferase activity upon purm addition
neg
Smo
siRNA added

Figure 4.2 Optimising screen readouts. Optimisation of cilia structure readout: (A, B and C) Ciliogenesis was optimised in several cell lines, and immunofluorescence for several ciliary markers was performed. Shown is ShhLIGHT-II cells (A), hTERT-RPE cells (B) and MEFs (C), stained with α γ-tubulin (A and B) to mark the centrosomes and either α Acetylated α-tubulin (A), α-Arl13b (B) or α-Ift88 to mark the cilia. α-Acetylated α-tubulin also stains stabilised microtubule arrays in the cell cortex and α-Ift88 shows some background cytoplasmic staining, whereas α Arl13b stains cilia specifically with high signal-to-noise ratio, so this was chosen as the marker to screen for cilia formation. Optimisation of cilia function readout. (D, E and F) Addition of purmorphamine (P) to ShhLIGHT-II cells gives a dose dependent increase in Gli-luciferase activity (D). Addition of Smoothened (Smo) siRNA attenuates this response (E and F). Shown is the average of technical triplicates +/- standard deviation.

using the Scan^{R} analysis software was accurate when compared to counting by eye (data not shown).

4.1.2.2 Readout two: a Hh agonist dependent assay of cilia function

The second readout utilised the stably integrated transgene of a series of multimerised Gli-binding sites driving luciferase to allow analysis of Hh signalling, as an indirect measure of cilia function. The luciferase assay lends itself to high-throughput analysis, with ease of sample processing and plate based luminescence readers meaning it is much more efficient than measuring endogenous Hh target gene levels. ShhLIGHT-II cells serum starved for 48h to induce ciliogenesis and treated with purmorphamine (a small molecule Hh agonist) for 30h show a dose-dependent increase in *Gli-luciferase* activity relative to *CMV-Renilla luciferase* activity, compared to cells treated with DMSO (Figure 4.2D). After trying several concentrations of purmorphamine, 5μM was used for screening as it gave the most robust response in these cells (Figure 4.2D). siRNA to *Smoothened,* the Hh co-receptor attenuates this induction, showing I can detect a dynamic range of responses (Figure 4.2 D and E). As cilia are required for Hh signalling, this response should be a sensitive measure of cilia function; it has been shown that siRNA knockdown of several ciliary genes leads to impaired processing of Gli3^{R}, stabilisation of Gli3^{FL}, and impaired response to Hh signalling ((Wen et al., 2010) See Figure 4.5A and B and 4.3.1.2 below). That this method can detect ciliary genes was demonstrated in a study by Evangelista et al., (2008): they used a similar luciferase based readout to screen for Hh pathway components and identified two genes which attenuated Hh signalling, by affecting cilia function. A study published after this screen was started

Lai et al., (2011), in which a similar screening protocol was used to screen a different set of candidate ciliary genes also utilised a luciferase based readout of Hh signalling as readout of cilia function. This method gave the most hits, when compared to cilia number, cilia length and cilia trafficking readouts, and suggests this readout is a very sensitive method of measuring cilia function.

This readout will also identify direct Hh pathway modulators that may not have a role in cilia function or structure, so any hits identified by this method will require further investigation as to whether they affect cilia function, or Hh signalling directly.

4.1.3 Transfection optimisation

In mammalian systems, two main methods of RNAi screening can be used, either short interfering RNAs (siRNAs) or short hairpin RNAs (shRNAs). siRNAs are short 20-21nt double stranded RNA molecules generally transiently transfected using lipid-based or electroporation methods. shRNAs also form short 20-21nt double stranded RNA molecules, which consists of a single RNA molecule which forms a secondary structure loop to make a typical hairpin structure. These are vector-based plasmids using H1 or U6 RNA pol III promoter to ensure the shRNA is always expressed. They can be introduced to mammalian cells either by transient transfection of the shRNA expressing plasmid, or more commonly using lentiviral methods of infection to ensure integration (Carthew and Sontheimer, 2009; Fire et al., 1998; Mohr et al., 2010; Zamore et al., 2000). Although shRNAs offer a longer window of prolonged knockdown, we decided to use siRNAs for screening for several reasons; (i) they are well characterised, many large scale siRNA screens have been carried out (Mohr et al., 2010), (ii) they are relatively easy to transfect into cells under standard culture conditions, (iii) they are relatively cheap compared to other methods such as shRNA libraries.

Therefore siRNA transfection in ShhLIGHT-II cells was optimised. siRNAs to *Wdr35* and/or *Dync2h1* were tested as positive control genes affecting ciliogenesis for the screen, as I had previously characterised the mutant MEF phenotypes and shown that *Wdr35* mutant cells lack cilia, whereas *Dync2h1* mutant cilia are

shortened and bulging (Chapter 3). Additional parameters were optimized including several transfection protocols, varying siRNA concentration, amount and type of lipid-based transfection reagent, the source of siRNAs, as well as the timing of transfection and serum starvation. However, I did not see effective and reproducible knockdown of either *Wdr35* or *Dync2h1* (Figure 4.3A - D). Knockdown efficiency was assessed by qPCR of the target gene relative to the control gene *Tbp*, and is displayed relative to untransfected control (Unt). A negative scrambled control siRNA was also used (neg). Three different siRNAs targeting either *Wdr35* or *Dync2h1* were analysed. Occasionally *Wdr35* mRNA levels reduced to 30% of control levels by qPCR and this correlated with a roughly two-fold decrease in ciliogenesis, as shown in Figure 4.3 A and B, however this was not highly reproducible and so not suitable as a robust positive control for screening. No decrease in cilia numbers was seen upon *Dync2h1* siRNA addition. These experiments were performed using Arl13b to mark cilia, which shows accumulations in the shortened cilia of *Dync2h1* mutant MEFs (Figure 3.2F), and it is possible that this type of ciliary phenotype could be missed by automated cilia counting which gives a yes/no answer. However I did not see a reduction in length or change in intensity or morphology of Arl13b-positive cilia in the *Dync2h1* siRNA treated cells when checked by eye. I also stained with acetylated α-tubulin, a post-translational modification of stabilized microtubules enriched in control cilia but which is not present in *Dync2h1* mutant cilia (Figure 3.1). I similarly saw no reduction in cilia numbers counted by eye upon *Dync2h1* siRNA addition. These observations are supported by the fact I did not get good knockdown of *Dync2h1* at the mRNA or protein level (Figure 4.3 C and D and data not shown).

4.1.3.1 *Ift88* siRNA knockdown gives a robust, reliable and highly significant reduction in cilia numbers

Due to the lack of a reproducible phenotype upon *Wdr35* and *Dync2h1* knockdown, siRNAs targeting two further genes were tested as positive controls for the screen; (i) *Kif3a,* a component of the anterograde IFT motor and (ii) *Ift88*, an anterograde IFT core protein, both of which are essential for cilia formation (Marszalek et al., 1999; Pazour et al., 2000), and for which siRNA knockdown has been published to give a

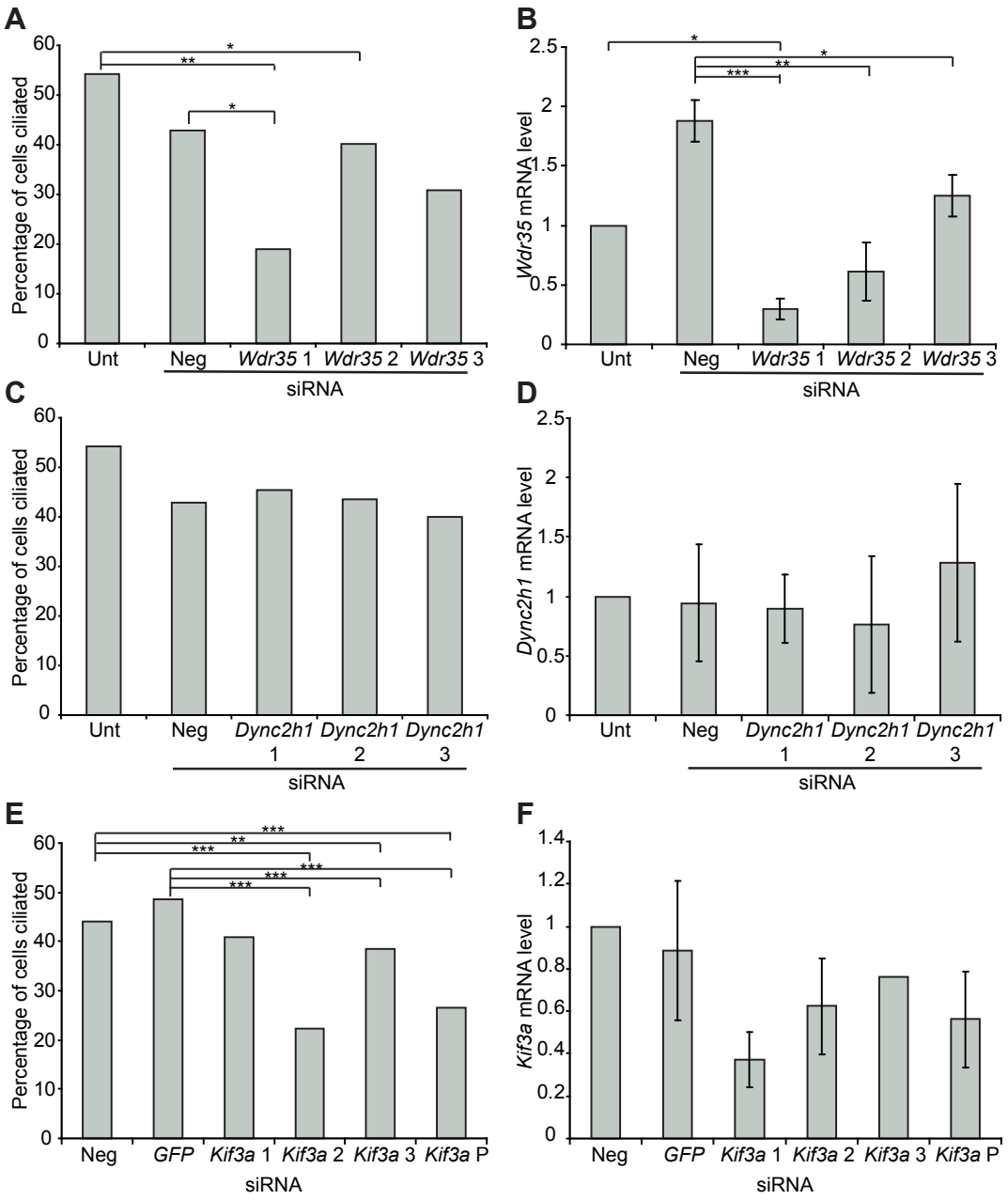

Figure 4.3 Optimisation of siRNA transfection. ShhLIGHT-II cells were transfected with siRNAs to *Wdr35* (A and B) part of the IFT-A complex*, Dync2h1* (C and D) and *Kif3a* (E and F), subunits of the retrograde and anterograde IFT motors, respectively. The percentage of cells with cilia (identified by α-Arl13b staining) is plotted in A, C and E, compared to untransfected cells (transfection reagent added without siRNA) (Unt) and cells transfected with non-targeting siRNA (neg) (A-D) or non-targeting (Neg) and *GFP* siRNA (*GFP*) (E and F). The corresponding mRNA levels of the target gene are plotted in B, D and F. Despite all being involved in IFT and required for ciliogenesis, a consistent reduction in cilia numbers was not seen, highlighting noise in the system. Plotted is the mean of two biological duplicates and in B, D and F, three technical triplicates. Error bars show standard deviation. *p<0.05 **p<0.01 ***p<0.0001, calculated by Chi Squared for A, C and E, and student's t-test in B, D and F.

reduction in cilia numbers (Zhu et al., 2009). Since I designed the screen, two additional siRNA screens looking at cilia formation have used *Kif3a* and *Ift88* as positive controls (Kim et al., 2010; Lai et al., 2011). I also changed the type of siRNA used. Several companies have developed chemical modifications to siRNAs designed to reduce toxicity and reduce off-target effects of siRNAs (knockdown of gene(s) other than the target gene) (Birmingham et al., 2006; Doench et al., 2003; Fedorov et al., 2006). We switched to Dharmacon OnTarget*Plus*™ siRNAs which have modifications on both strands of the siRNA to reduce such off-target effects (Jackson et al., 2006).

In Figure 4.3 E and F mRNA levels and percentage of ciliated cells upon *Kif3a* siRNA addition are compared to cells transfected with a non-targeting scramble control siRNA (Neg) as well as a *GFP* siRNA. As these cells are GFP negative this essentially acts as a second non-targeting siRNA. Three siRNAs to *Kif3a* at 25nM concentration were analysed, as well as a "pool" which is the addition of all three siRNAs in one well, where the total concentration of siRNA is 25nM. This is thought to reduce off-target affects, by using lower concentrations of individual siRNAs, while maintaining a good knockdown by adding 3 or 4 different siRNAs to the same gene.

Kif3a knockdown gave a reduction in cilia numbers, although it did not always correlate with mRNA levels and it was not highly reproducible between experiments (Figure 4.3 E and F and data not shown).

In contrast, *Ift88* siRNA gave a robust, reproducible and highly significant reduction in cilia numbers (Figure 4.4, and 5.2A). The reduction in cilia numbers did not correlate with the reduction in mRNA levels, for example *Ift88* siRNA#1 shows a significant reduction in ciliated cells (from 50% in the neg control to 25%), but it does not show a reduction in mRNA level by qPCR (Figure 4.4 C and D). This could be due to inaccurate qPCR result, or off-target effects of the siRNA. Analysis of Ift88 protein show it is reduced by 80% using *Ift88*#3 and #4 respectively, whereas Ift81 is unaffected suggesting that IFT proteins are not generally affected by *Ift88* siRNA (Figure 4.4 A and B). As *Ift88* siRNA #3 and #4 show a strong phenotype correlating with a good knockdown of *Ift88* at the mRNA and protein

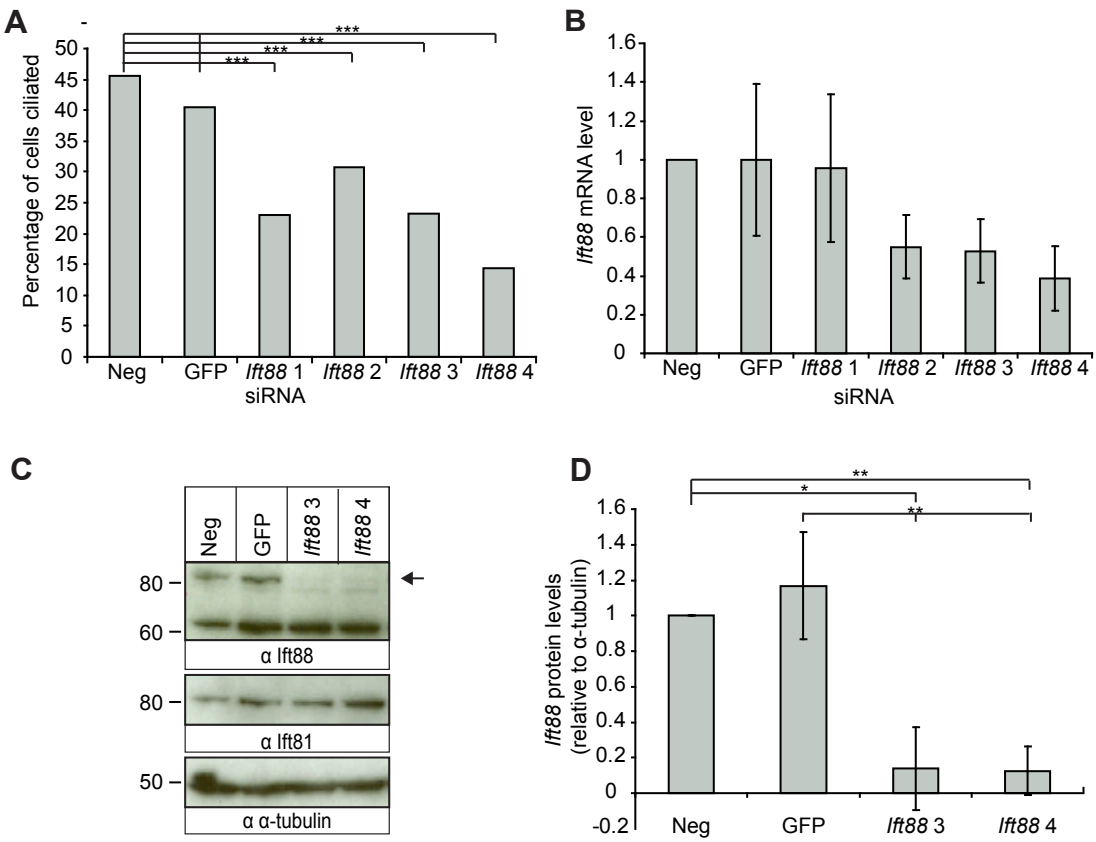

Figure 4.4 *Ift88* siRNA knockdown leads to reduced cilia numbers.
(A) The percentage of ciliated cells falls upon *Ift88* siRNA addition. Shown is the mean of biological duplicates (***p<0.001, Chi sqaured). (B) Addition of *Ift88* siRNA leads to a reduction in *Ift88* mRNA levels (relative to *Tbp*). Shown is mean +/- standard deviation of technical triplicates. (C) Ift88 protein levels are reduced upon *Ift88* siRNA treatment, but levels of another IFT B particle component, Ift81, are unaffected. (D) Quantification of Ift88 protein levels upon *Ift88* siRNA addition. Shown is the mean +/- standard deviation of three biological replicates. (*p<0.05 **p<0.01, students t test)

level, and most importantly, this phenotype is reproducible between experiments, these were chosen as positive controls for the screen.

4.1.3.2 *Ift88* siRNA knockdown leads to impaired Hh signalling

As well as analysing cilia formation upon *Ift88* knockdown, I also looked at cilia function in these cells, using Hh signalling as an indirect readout. As mentioned, ShhLIGHT-II cells have a *Gli-luciferase* transgene stably integrated, which consists of a multimerised Gli binding site driving firefly luciferase (Sasaki et al., 1997). These cells also have *Renilla* luciferase gene under the CMV promoter, to enable control for cell number and general transcription levels (Taipale et al., 2000). ShhLIGHT-II cells were transfected with negative controls (neg or *GFP*) or *Ift88* siRNA, serum starved for 48h and treated with DMSO or purmorphamine for 30h (see Figure 4.6 or 4.9 for diagram of timings). In some experiments, cyclopamine, a Hh antagonist, was added for 4h before the end of the experiment. Western blot confirmed Ift88 knockdown (Figure 4.5C). Luciferase levels were examined, and as expected, Gli-luciferase activity increases upon purmorphamine addition in the controls (Figure 4.5A and B). The basal levels of Gli-luciferase activity increases upon *Ift88* siRNA addition, whereas the levels of Gli-luciferase upon purmorphamine treatment remain unchanged. This leads to an overall decrease in the fold response to purmorphamine upon *Ift88* siRNA addition (Figure 4.5A and B).

Gli3 protein levels were examined in these cells. Upon *Ift88* siRNA knockdown, basal levels of the proteolytically processed $Gli3^{R}$ repressor form decrease, as seen for *Wdr35* mutant MEFs and *Ift88* mutant cells (Figure 3.4 and 4.5C and D, (Haycraft et al., 2005)). In addition to this it appears that $Gli3^{FL}$ is stabilised. In negative siRNA treated cells, purmorphamine leads to a decrease in $Gli3^{R}$ levels and an increase in $Gli3^{FL:R}$ ratio, a response which is lost in *Ift88* siRNA treated cells (Figure 4.5C-E). As in Figure 3.4, there is no evidence the cyclopamine treatment had an effect in my control cells, so perhaps the drug was not working correctly in these assays (Figure 4.5C).

The increase in basal levels of *Gli-luciferase* activity is likely to be due to impaired processing of $Gli3^{FL}$ to $Gli3^{R}$ and possibly stabilisation of $Gli3^{FL}$, leading to increased $Gli3^{FL:R}$ ratio and increased basal Hh target gene expression. This is

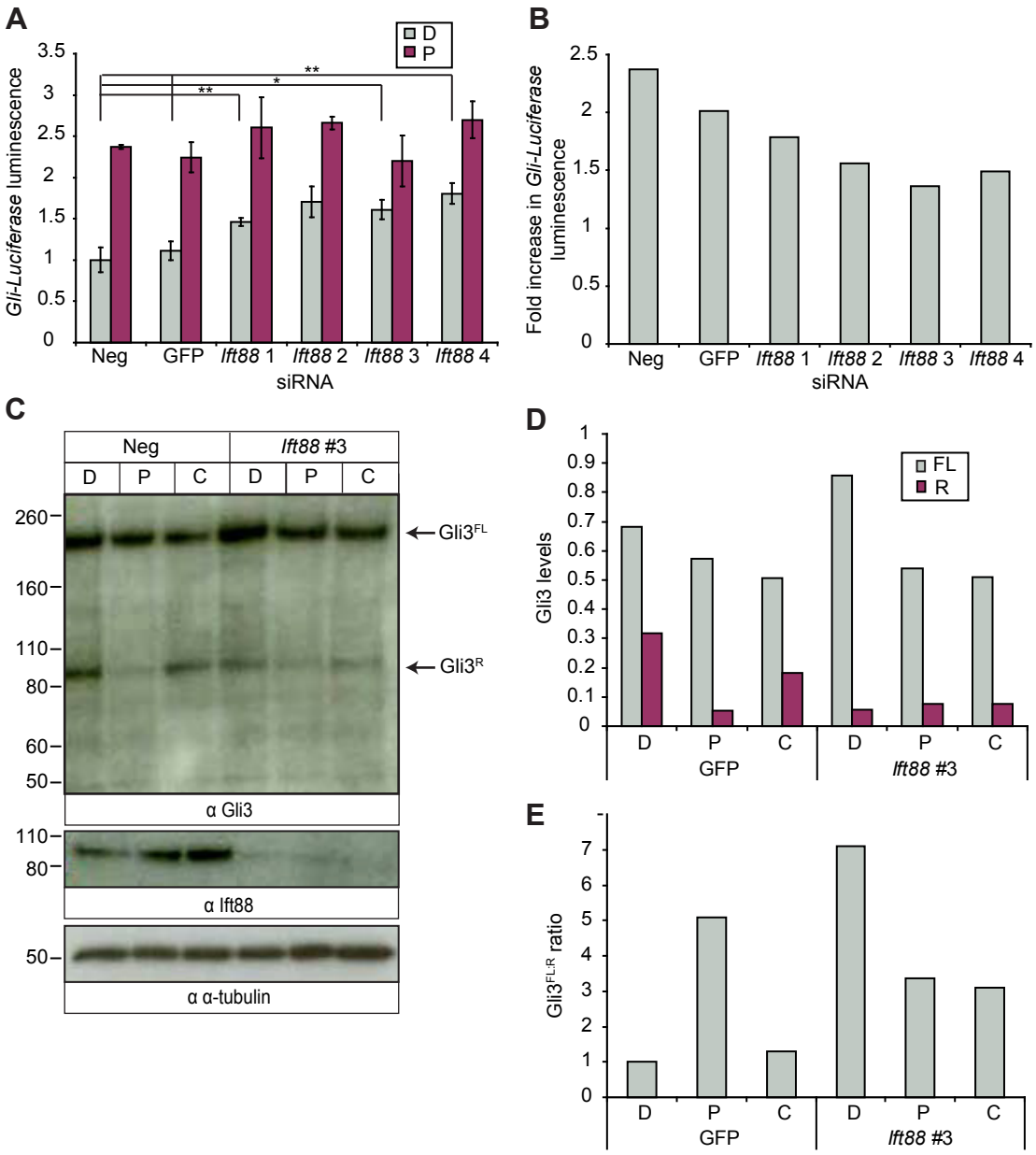

Figure 4.5 *Ift88* knockdown leads to aberrant Hh signalling
(A and B) ShhLIGHT-II cells were treated with *Ift88* siRNA plus DMSO or purmorphamine, and *Gli-Luciferase* luminescence was measured (relative to *CMV-Renilla Luciferase* luminescence). An increase in basal *Gli-luciferase* activity (A) lead to a decrease in the fold response to purmorphamine treatment upon *Ift88* siRNA addition (B). Shown is the mean of technical triplicates, error bars in (A) show standard deviation (*p<0.05, **p< 0.001 student's t-test). (C, D and E) Cells were treated with *GFP* or *Ift88* siRNA and either DMSO (D), Purmorphamine (P) or Cyclopamine (C). (C) Western blotting shows basal $Gli3^{R}$ levels are reduced and $Gli3^{FL}$ is stabilised upon *Ift88* siRNA addition, and the cells fail to respond to Purmorphamine (quantified in (D)). (E) $Gli3^{FL:R}$ ratio upon *Ift88* siRNA addition, increased basal $Gli3^{FL:R}$ ratio upon *Ift88* knockdown could explain the increased *Gli3-luciferase* activity in A. Cyclopamine treatment did not seem tp affect wild type or mutant cells, suggesting the drug failed to work.

similar to the results seen upon siRNA knockdown of *Ift88* in S12 cells (Wen et al., 2010), where a similar inability to process $Gli3^{FL}$ to $Gli3^{R}$ is seen, as well as a stabilisation of $Gli3^{FL}$. $Gli3^{FL}$ is stabilised upon addition of Hh to negative siRNA treated S12 cells (*Gli*-luciferase stably transfected C3H10T1/2 osteoblast cells) but this stabilisation is not seen upon purmorphamine addition in ShhLIGHT-II cells. This is likely to be due to the cell type, as Lai *et al* 2010 observed a lack of $Gli3^{FL}$ stabilisation in NIH-3T3 cells treated with Hh (the parental cell line of ShhLIGHT-II) although they saw it in S12 cells.

In summary, *Ift88* siRNA treatment leads to reduced numbers of cilia; this is expected because Ift88 is essential for anterograde IFT (Pazour et al., 2000). *Ift88* knockdown also increased basal Hh signalling levels due to, at least in part, an inability to process $Gli3^{FL}$ to Gli^{R}. Importantly, the phenotypes were highly reproducible between experiments. Of the four *Ift88* siRNAs tested, #3 and #4 gave the most robust and reproducible knockdown and phenotypes, therefore these siRNAs were chosen as positive controls for the screen.

4.1.4 Further attempts at siRNA transfection optimisation.

During optimisation, it was observed that genes known to be required for ciliogenesis did not give reproducible phenotypes upon siRNA knockdown (in particular *Wdr35,* and *Dync2h1*). It is possible this reflected variable transfection efficiency between cells, whereby the averaging of the phenotype across the whole (transfected and untransfected) population of cells diluted any phenotypic affects that occur. As the $Scan^{R}$ is designed for high content, cell by cell analysis, we attempted to utilise this to identify and analyse only the successfully transfected cells. ShhLIGHT-II cells stably expressing GFP were generated by transfecting with *pCAG-eGFP,* which express GFP under the CAG promoter, a relatively low expressing promoter. Clonal stable cell lines were generated and two clones with medium GFP expression levels and normal centrosome number were chosen for further analysis (ShhLIGHT-II-GFP).

4.1.4.1 Cells successfully transfected for one siRNA (i.e. *GFP*) are more likely to be transfected with a second siRNA.

The aim was to cotransfect siRNAs against *GFP* along with an siRNA to the gene of interest, the theory being cells which take up the *GFP* siRNA are more likely to have taken up the gene of interest (GOI) siRNA. Therefore by only analysing cells in which *GFP* was knocked down (GFP^{low} cells), this would select for cells transfected with the GOI siRNA (See Figure 4.6 for the planned screen design using this method). Essentially, cells would be transfected with the siRNA library, plus the *GFP* siRNA in every well. For the first readout for cilia formation, the Olympus $Scan^{R}$ microscope would automatically image the plates, identify cells, measure GFP fluorescence and assign cells to GFP^{high} and GFP^{low} populations. Only GFP^{low} cells (i.e. transfected) cells would be further analysed for cilia and centrosome numbers (via anti-Arl13b and -γ-tubulin staining). Readout two for cilia function, would require the cells to be FACS sorted into GFP^{high} and GFP^{low} populations and only the GFP^{low} (i.e. transfected) cells would be lysed and luciferase levels analysed to measure Hh response and therefore cilia function.

To investigate whether cells which are GFP^{low} also have lower GOI levels, cells were co-transfected with siRNAs against *GFP* and/or *Gapdh*, a housekeeping gene. Results are shown for one ShhLIGHT-II-GFP cell line but both clones analysed gave similar results (Figure 4.7). FACS profiles show the knockdown efficacy the *GFP* siRNA. ShhLIGHT-II cells which lack the GFP construct have no GFP positive cells (either high or low), whereas 93% of ShhLIGHT-II-GFP cells have high GFP levels. When ShhLIGHT-II-GFP cells are transfected with siRNAs to *GFP* and *GapdH,* 15.8% remain GFP^{high}, but 57% are now GFP^{low}, showing the *GFP* siRNA is effective (Figure 4.7A). Cells were sorted into GFP^{high} and GFP^{low} populations, RNA was extracted and the levels of *GapdH* mRNA were examined. *GapdH* siRNA alone decreased *GapdH* mRNA levels to 15% of control. Addition of *GapdH* and *GFP* siRNA, then analysis of only GFP^{low} cells reduced *GapdH* mRNA levels to 5% of control, whereas *GapdH* mRNA levels in GFP^{high} cells were 40% of control levels (Figure 4.7B). This suggests that cells which are transfected with *GFP* siRNA are more likely to be transfected with *GapdH* siRNA than those which are GFP^{high}, and

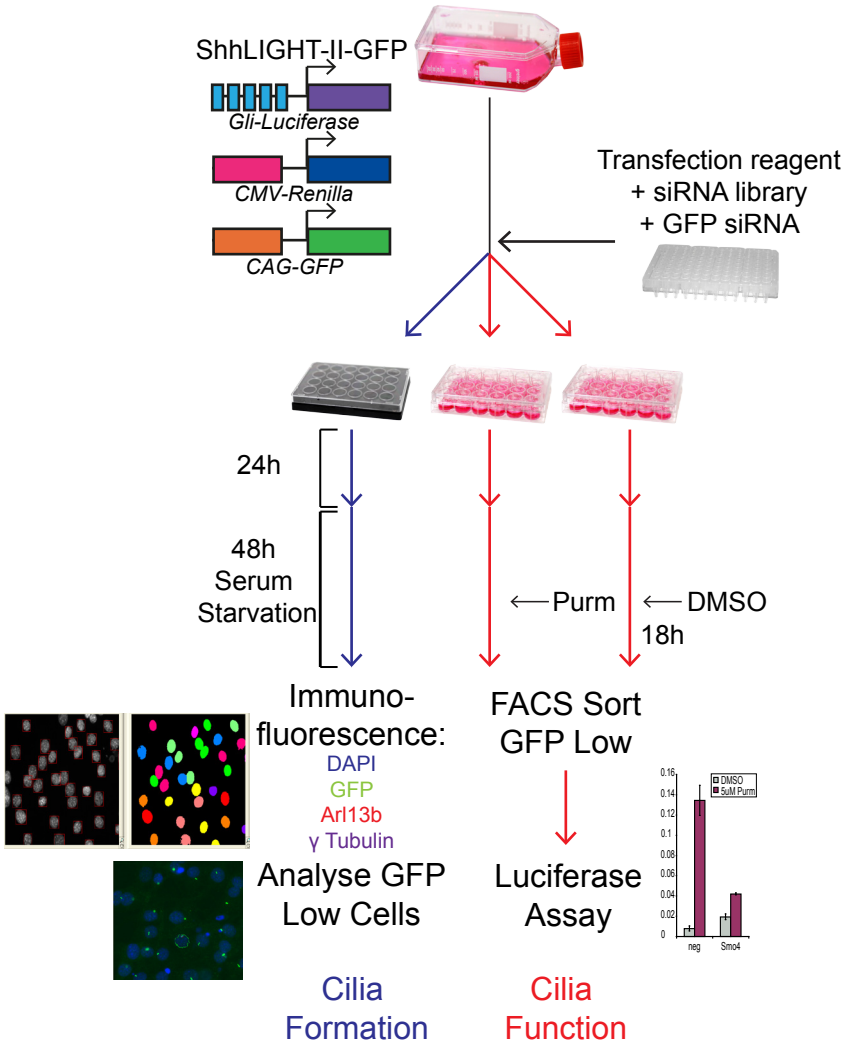

Figure 4.6 Overview of screen using GFP sorting to only analyse transfected cells. To try to optimise the screen, an attempt to only analyse transfected was made. This figure shows the plan for the new screening prototocol. Shh-LIGHT-II-GFP stably express *Gli-luciferase, CMV-Renilla* and *CAG-GFP.* Cells are transfected with an siRNA library, plus each well is transfected with *GFP* siRNA, and split to three plates, one glass and two plastic. After 24h, cells are serum starved for 48h. 30h in, the cilia function plates have DMSO or 5μM purmorphamine added for 18h. After 48h serum starvation, the glass plate is fixed and stained for cilia (α-Arl13b), centrosomes (α-γ-tubulin) and DAPI. The Scan^{R} micrsoscope automatically images the cells, measures the GFP fluorescence and splits the cells into GFP^{high} and GFP^{low} populations, and counts cilia and centrosome numbers GFP^{low} (transfected) population. After 48h serum starvation, the cells on the plastic plates are FACS sorted into GFP^{high} and GFP^{low} populations, the GFP^{low} (transfected) cells are lysed and luciferase activity is measured (with and without purmorphamine), as a readout of cilia function.

supports the idea that cells which take up one siRNA are more likely to have taken up a second siRNA. This is probably due to the way lipid based transfection protocols work; the siRNAs are packaged into liposomes which are delivered to the cell, and as each liposome has both siRNAs present, if a cell is successfully transfected it is likely it will be with both siRNAs. It is also possible some cells are inherently more amenable to transfection than others, or are exposed to conditions which improve transfection, such as ideal local transfection reagent and siRNA concentration. This experiment suggested it may be helpful to only analyse the GFP^{low} cells for cilia formation and function after siRNA transfection.

Therefore, I went on to combine *GFP* siRNA with *Ift88* or *Kif3a* siRNA and examine cilia numbers in GFP^{high} and GFP^{low} cells.

4.1.4.2 GFP^{low} cells show fewer cilia, regardless of which siRNA was cotransfected.

ShhLIGHT-II-GFP cells were transfected with negative siRNA, *GFP* siRNA alone, *GFP* and *Ift88* siRNA or *GFP* and *Kif3a* siRNA. Figure 4.8A shows the percentage of cells with cilia, demonstrating that all siRNAs to *Ift88* or *Kif3a* give some reduction in the number of cilia to varying degrees, compared with the negative and *GFP* siRNAs. As mentioned above, plates were imaged automatically using the Olympus $Scan^R$ microscope. Using the $Scan^R$ analysis software it was possible to analyse GFP intensity, "sort" the cells into GFP^{high} and GFP^{low} populations, and then count how many cells in each population have a cilium, marked by Arl13b. Figure 4.8B shows the percentage of cells classed as GFP^{low}. Upon addition of *GFP* siRNA, the percentage of GFP^{low} cells shifts from 3% to at least 23%, except in the well where *GFP* and *Kif3a* siRNA#2 was added, where no shift in GFP^{low} cells was seen, suggesting *GFP* siRNA transfection failed in this well. In some wells the percentage of GFP^{low} cells reached 55% (Figure 4.8B). This shift suggests transfection was successful in most wells.

However when I analysed the percentage of cilia in the GFP^{high} and GFP^{low} populations, problems with his approach are evident. As expected, addition of *Ift88* or *Kif3a* siRNA along with *GFP* siRNA lead to fewer cells with cilia in the GFP^{low}

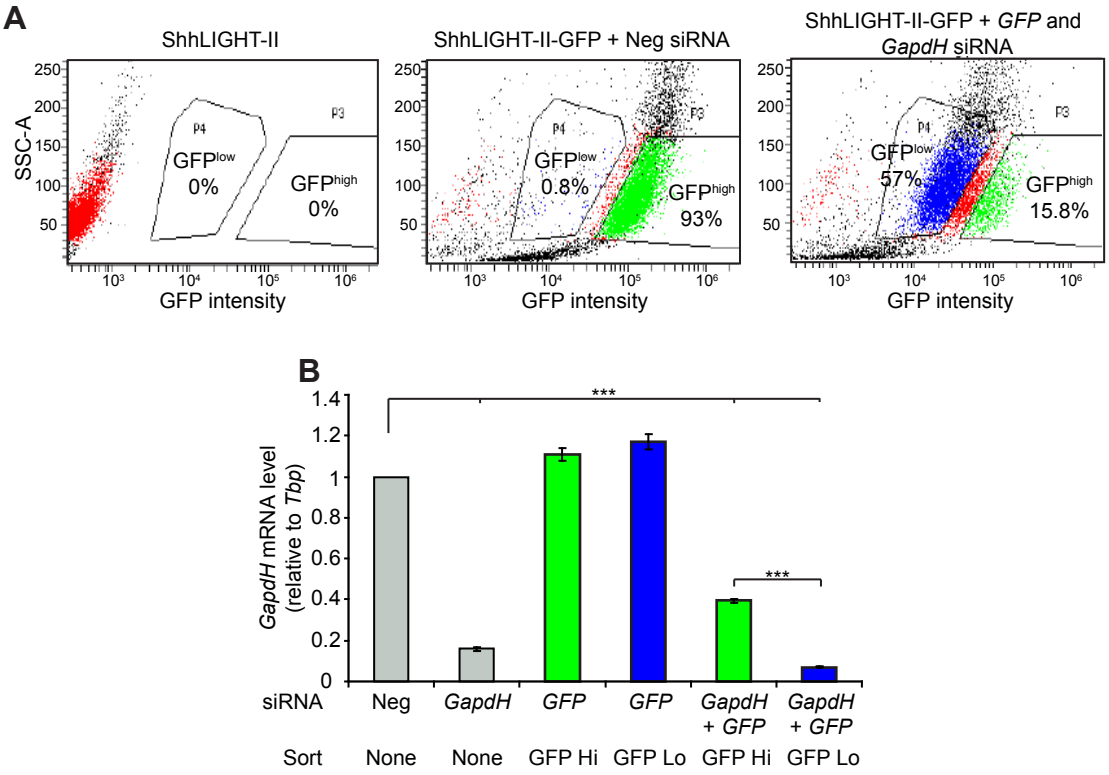

Figure 4.7 Screen Optimisation: sorting transfected cells by *GFP* siRNA knockdown. ShhLIGHT-II cells were stably transfected with *pCAG-GFP* and clonal lines were generated. (A) FACS plots of GFP intensity show that ShhLIGHT-II cells express no GFP, whereas 93% of ShhLIGHT-II-GFP cells express high levels of GFP. Upon *GFP* siRNA addition this drops to 15.8% of cells being GFP^{high} and 57% GFP^{low}. (B) ShhLIGHT-II-GFP cells were transfected with *GFP* siRNA and *GapdH* siRNA, FACS sorted into GFP^{high} and GFP^{low} populations and *GapdH* mRNA levels were examined. Cells with low GFP levels have lower *GapdH* mRNA levels. (***p<0.001 Student's t-test. Shown is mean of technical triplicates and biological duplicates +/- standard deviation).

cells compared to the GFP^{high} cells (Figure 4.8C), for example upon addition of *Ift88*#2 and *GFP* siRNA, 55% of cells are GFP^{low}, of these only 6% had cilia, compared to 40% of GFP^{high} cells having a cilium. However, upon addition of *GFP* siRNA alone GFP^{low} cells have fewer cilia than GFP^{high}: 30% of cells are GFP^{low} and of these 22% have a cilium, compared to the GFP^{high} cells where 50% have a cilium. Even upon addition of negative siRNA, where only 3% of cells are GFP^{low}, 18% of GFP^{low} cells have a cilium, compared with 47% of GFP^{high} cells (Figure 4.8B and C). This suggests that regardless of which siRNA is added, GFP^{low} cells have fewer cilia.

It is unclear why this would occur, we hypothesised that GFP levels could be linked to cell cycle, and as ciliogenesis and cilia resorbtion are closely linked with cell cycle this may explain these results. The Scan^R Analysis software is able to use DAPI intensity to identify whether cells are in G_1 or G_2. Therefore, to address this theory, the number of cells in G_1 and G_2 were analysed in the GFP^{high} and GFP^{low} cells. In most wells, 15-20% cells are in G_2, this number is fairly low because the cells have been serum starved for 48h, arresting the cells in G_1/G_0. The percent of cells in G_1 or G_2 was unchanged between the GFP^{high} and GFP^{low} populations in all wells, suggesting the GFP level was not linked to cell cycle, therefore this is unlikely to explain why GFP^{low} cells have fewer cilia (Figure 4.8D). We are unable to explain why, even in the control siRNA wells, GFP^{low} cells have fewer cilia.

Regardless of the explanation for this, sorting for co-transfected cells this way does not help in the analysis of cilia numbers, as the assay gains no power. If you compare unsorted cells transfected with non-targeting siRNA, 48% have a cilium, compared to 24% of cells having a cilium when transfected with *GFP* and *Ift88* #4 siRNA, a drop of 50%. If you sort the data for GFP^{low} cells, 18% of non-targeting siRNA treated GFP^{low} cells have cilia, compared to 9% of *Ift88*#4 siRNA treated GFP^{low} cells. Again this is a drop of 50%. This assay increases the amount of work and analysis required, but does not improve the power of the screen, so we did not pursue it further. As we were detecting a significant and reproducible reduction in cilia in the *Ift88* treated cells, we did not need to select for transfected cells to detect hits.

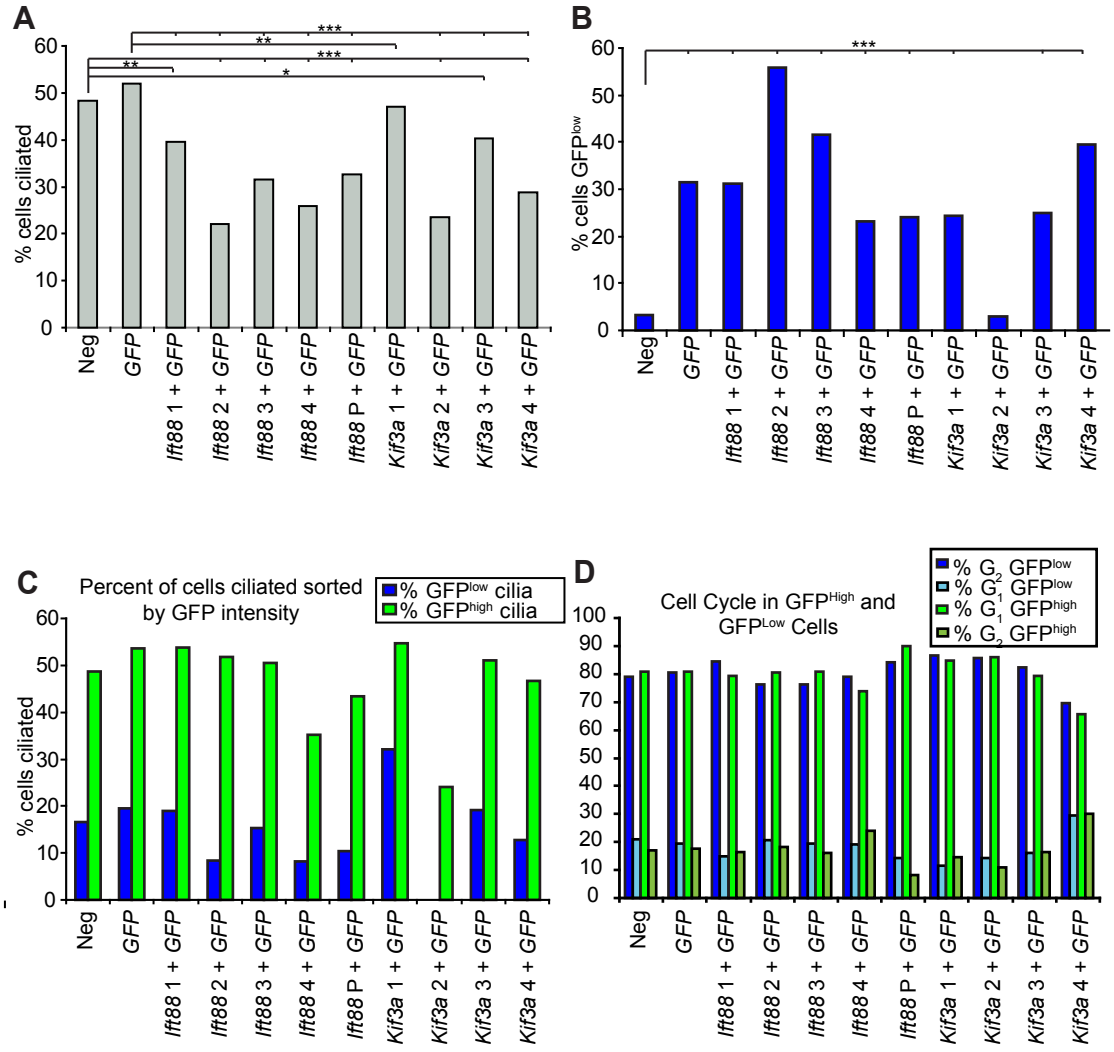

Figure 4.8 GFP^{low} cells have fewer cilia, regardless of the siRNAs added. ShhLIGHT-II-GFP cells were treated wth *GFP* and *Ift88* or *Kif3a* siRNAs. (A) The percent of ciliated cells falls upon addition of *Ift88* or *Kif3a* siRNA. (B, C and E) Automated image analysis separated cells into GFP^{high} and GFP^{low}. (B) Percentage of cells which are GFP^{low}. (C) Percentage of cells with cilia in GFP^{high} and GFP^{low} populations. Even treatment with negative or *GFP* siRNA leads to a decrease in the percentage of cells ciliated in GFP^{low} cells compared to GFP^{high} cells. (D) Percentage of cells in G_1 and G_2 in GFP^{high} and GFP^{low} populations. The cell cycle distribution doesn't change between GFP^{high} and GFP^{low} populations (*p<0.05, **p<0.01, ***p<0.001 Chi Squared).

4.2 Genes to screen

The original aim was to screen a large unbiased list of genes, for example using a genome-wide approach or a selected set of genes in the commercially available libraries such as the druggable genome or kinome, to identify novel ciliogenesis genes. However, having spent significant time and effort optimizing protocols, I decided to carry out a proof-of-principal screen of a relatively small number of candidate genes. This would allow the screening platform to be tested, while identifying possible novel ciliogenesis genes and permit some in-depth characterisation of candidates in cell culture and mouse *in vivo* models. The screen could then be scaled up at a later date.

We decided to knockdown a set of conserved genes identified as putative ciliary genes in *Drosophila* by our collaborators, Prof. Andrew Jarman (University of Edinburgh) (Cachero et al., 2011). Cachero *et al.* (2011) carried out an expression screen in *Drosophila* for genes highly expressed in the chordotonal mechanosensory neurons. Unlike mammals, sensory neurons and sperm are the only ciliated cell types in *Drosophila*. *Ato-GFP* flies express GFP under the *atonal* promoter, which is dynamically expressed during the development of ciliated chordotonal neuron precursors. Briefly, embryos were taken at varying time points, homogenised and GFP positive cells were isolated by FACs and subjected to microarray analysis. Expression analysis at the point examined just before ciliogenesis occurred showed 411 genes were upregulated, and these were significantly enriched for known ciliogenesis genes (Cachero et al., 2011). This gene list was further enriched for putative ciliary genes by bioinformatic methods to enrich for motifs which are common in ciliary genes, such as WD40 repeats, TPR domains and coiled-coil domains (Jekely and Arendt, 2006; Salisbury, 2003), as well as enriching for genes with X-boxes in their promoters, characteristic of cilia genes (Efimenko et al., 2005). Predicted mouse orthologues for these genes were identified, and a list of 41 putative ciliary genes was drawn up. Of these, four genes (*Arl3, Dync2li1, Dnaic1* and *Tekt2*)

Table 4.1 List of genes to screen from expression study in *Drosophila*

Drosophila gene	Mouse orthologue	Description	Included in screen?	In ciliome?
CG18472	Spag1	Sperm-associated antigen 1, Infertility in one human case, expressed in sperm [1,2]	Y	N
CG15701	Wdr60	WD repeat-containing protein 60	Y	Y
CG9313	Dnaic1	Cytoplasmic dynein mutated in 10% of primary ciliary dyskinesia patients. Mice lacking this gene in the lungs show chronic rhinosinusitus [3]	N	Y
CG13930	Wdr78	WD repeat domain 78	Y	Y
CG10064	Wdr16	WD repeat-containing protein 16, expressed in zebrafish kinocilia, morpholino knockdowns show hydrocephalus[4]	Y	Y
CG14353	Ppp3r1	Calcineurin subunit B type 1, mutant mice die early in embryogenesis due to cardiovascular defects[5]	Y	Y
CG14353	Wdr92	WD repeat-containing protein 92	Y	Y
CG4525	Ttc26	Tetratricopeptide repeat protein 26, orthologue of dyf13, gene required for cilia formation in *C. elegans*[6]	Y	Y
CG6915	Ttc28	Tetratricopeptide repeat protein 28	Y	N
Yrt (CG9764)	Epb4.1l5	Band 4.1-like protein 5, essential for left-right asymmetry, due to roles in node and midline morphogenesis but not ciliogenesis[7]	N	N
Yrt (CG9764)	Epb4.1l4b	Band 4.1-like protein 4B, orthologue of *Drosophila Yrt*, involved in cell polarity[8]	Y	N
CG14127	Ccdc151	Coiled-coil domain-containing protein 151	Y	N
CG14127	4921530D09Rik	Uncharacterized coiled-coil domain-containing protein KIAA1984	Y	N
CG31321	Slc46a2	Thymic stromal cotransporter protein (Tscot)	Y	N
CG3085	Tekt2	Tektin-2. Axonemal protein. Mice mutants have immotile cilia in airway epithelia and males are infertile[9]	N	Y

Drosophila gene	Mouse orthologue	Description	Included in screen?	In ciliome?
CG31291	Sdccag8	Centrosomal colon cancer autoantigen protein	Y	Y
CG13125	Lrrc48	Leucine-rich repeat-containing protein 48	Y	Y
CG6405	Fam92a	Family with sequence similarity 92, member a	Y	N
CG6405	Fam92b	Family with sequence similarity 92, member b	Y	N
CG3769	Dync2li1	Cytoplasmic dynein involved in retrograde IFT. Mouse mutants die at E115, lack nodal cilia, and show left-right asymmetry and aberrant Shh signalling	N	Y
CG1126	Bbs5	Bardet-Biedl syndrome 5 protein homolog, mutated in ciliopathy Bardet Biedl Syndrome[10], no mouse model published	Y	Y
CG5359	Tctex1d2	Tctex1 domain-containing protein 2, orthologue to *C elegans* dylt-2 which encodes a small putative dynein light chain subunit[11]	Y	N
CG5359	Tcte3	T-complex-associated testis expressed 3 isoform 1, light chain of the outer dynein arm of cilia and sperm flagella mutant mice show asthenozoospermia[12]	Y	N
CG5359	Tctex1d1	Tctex1 domain-containing protein 1, orthologue of *C elegans dylt-2* which encodes a small putative dynein light chain subunit[11]	Y	Y
CG5359	Tctex1d4	Tctex1 domain-containing protein 4 orthologue of *C elegans dylt-2* which encodes a small putative dynein light chain subunit[11]	Y	N
CG11253	Zmynd10	Zinc finger MYND domain-containing protein 10/BLU, tumour suppressor	Y	N
CG14905	Ccdc63	Coiled-coil domain-containing protein 63	Y	N
CG14905	Ccdc114	Coiled-coil domain-containing protein 114	Y	N

Drosophila gene	Mouse orthologue	Description	Included in screen?	In ciliome?
CG6560	Arl3	*Arl3* mutant mice die at 3 weeks with renal, pancreatic and hepatic cysts and retinal degeneration, ciliopathic phenotypes[13]	N	Y
Blimp-1	Prdm1	PR domain zinc finger protein 1 mutant mice embryonic lethal with primordial germ cell defects[14]	Y	Y
Blimp-1	Prdm2	Riz1 retinoblastoma protein-binding zinc finger protein, tumour suppressor	Y	N
CG1625	Azi1	5-azacytidine-induced protein 1/Centrosomal protein 131 Cep131. Expressed in spermatids[15]	Y	Y
CG5343	Gtl3	Gene trap locus 3 protein	Y	Y
Canoe	Mllt4	Afadin. Tight junction protein, mutant mice die at E10.5 with cell polarity defects[16]	Y	Y
CG11579	Ctnnb1	Beta-catenin. Mutant mice die at E7.5 with anterior-posterior axis formation anomalies[17]	Y	Y
CG3389	Pcdh24	Protocadherin 24, Involved in contact Inhibition	Y	N
CG31009	Pcdh15	Protocadherin 15. Associated with hearing loss and Usher syndrome in humans[18]. Mutant mice exhibit deafness, head tossing and hyperactivity[19]	Y	Y
CG5142	Ttc30b	TPR repeat protein 30B. Orthologue of *C. elegans Dyf-1* and zebrafish *flr*. Required for polyglutamylation of outer doublet microtubules, and IFT of Osm-3 kinesin.[20,21]	Y	Y
CG5142	Ttc30a1	TPR repeat protein 30A1.Orthologue of C. elegans Dyf-1 and zebrafish flr. Required for polyglutamylation of outer doublet microtubules, and IFT of Osm-3 kinesin.20,21	Y	Y

Drosophila gene	Mouse orthologue	Description	Included in screen?	In ciliome?
CG5142	Ttc30a2	TPR repeat protein 30A2. Orthologue of *C. elegans Dyf-1* and zebrafish *flr*. Required for polyglutamylation of outer doublet microtubules, and IFT of Osm-3 kinesin.[20,21]	Y	Y
CG8353	Cda	Cytidine deaminase	Y	N

Table 4.1 List of genes to screen from expression study in Drosophila. List of genes overexpressed in *Drosophila* ciliated sensory neurons after bioinformatic enrichment for ciliary genes. Genes highlighted in pink were not screened (see text 4.2 Genes to Screen). Description gives alternate and full names, and any functional data or mouse mutants published.
1 Neesse et al 2007; 2 Zhang et al 2002; 3 Ostrowski et al 2010; 4 Hirschner et al 2007; 5 Graef et al 2001; 6 Blacque et al 2005; 7 Lee et al. 2010; 8 Laprise et al 2009; 9 Tanaka et al 2004; 10 Li et al 2004; 11 O'Rourke et al 2007; 12 Rashid et al 2010; 13 Schrick et al 2006; 14 Vincent et al 2005; 15 Aoto et al 1995; 16 Zhadanov et al 1999; 17 Haegel et al 1995; 18 Ahmed et al 2001; 19 Alagramam et al 2001; 20 Dave et al 2009; 21 Ou et al 2005

were removed due to already well-characterised roles in mouse ciliogenesis and ciliary phenotypes previously described in mouse models (Table 4.1) (Ostrowski et al., 2010; Rana et al., 2004; Schrick et al., 2006; Tanaka et al., 2004). A further gene was removed because it was unlikely to have a ciliary role; Epb4.1l5 was described by Lee et al., (2010) to have a role in node and midline morphogenesis but not ciliogenesis. Table 4.1 shows the gene list with those removed highlighted, along with what was known about the genes at the time of the screen. The table states which genes featured in the ciliome (a database which compiles transcriptomic, proteomic and comparative genomic screens for ciliary genes (Inglis et al., 2006)) at the time the screen was started (July 2010). The list is highly enriched for genes involved in ciliogenesis; as well as the four genes removed because of well documented roles in ciliogenesis, a further 19 are reported in the ciliome, meaning more than 50% of genes in the final list are found in the ciliome. Importantly, many of these are uncharacterised in mouse. There are also 17 genes with no known link to cilia except the expression data (Cachero et al. 2011), which could have novel roles in mammalian ciliogenesis.

As well as screening these putative ciliary genes, we also added several control genes to the list. *Wdr35* was added, because although we had not seen a strong enough phenotype to use it as a positive control, we wanted to check whether we saw a phenotype when it was run as part of the screen, as an internal positive control. Finally, we added three genes with no roles in ciliogenesis as further negative controls, *Gapdh* and *Cyclophilin B* (both housekeeping genes that are highly and ubiquitously expressed but not essential for cell viability) and *Smo* (receptor involved in Hh signalling but not cilia structure). These genes were added for three main reasons. (i) The negative control siRNAs on each plate did not target specific endogenous genes (one was non-targeting and one targeted *GFP*) and we wanted to show specificity of the knockdown phenotype was restricted to genes affecting cilia. (ii) Adding additional controls gave us more data to calculate the amount of noise in the system and allow us to call a "hit" more confidently. (iii) *Smo* was used as a positive control for the second readout of Hh signalling (Figure 4.2E and F).

4.3 Final Screen Design

The final design for the first-pass screen is shown in Figure 4.9. To summarise, thirty-six putative ciliary genes identified by expression studies and cross-species analysis as described above were chosen for screening, plus *Wdr35*, a known ciliogenesis gene and three genes known not to be involved in ciliogenesis as further controls. Four genes were screened per plate, with four single siRNAs per gene and a pool of the four. Each plate also had two negative (non-targeting and *GFP*) and two positive (*Ift88* #3 and 4) control siRNAs. ShhLIGHT-II cells were transfected and then plated onto three 24-well plates (one glass plate for readout one, two plastic plates for readout two). The cells were left for 24h to recover, before changing to serum free conditions for 48 hours. For the cilia function assay, 30 hours into this 48 hour period, either DMSO or purmorphamine was added to the plastic plates for 18 hours. The two readouts were then analysed. Readout one assayed cilia formation on fixed cells, immunostaining for Arl13b, γ-tubulin and DAPI and using high-

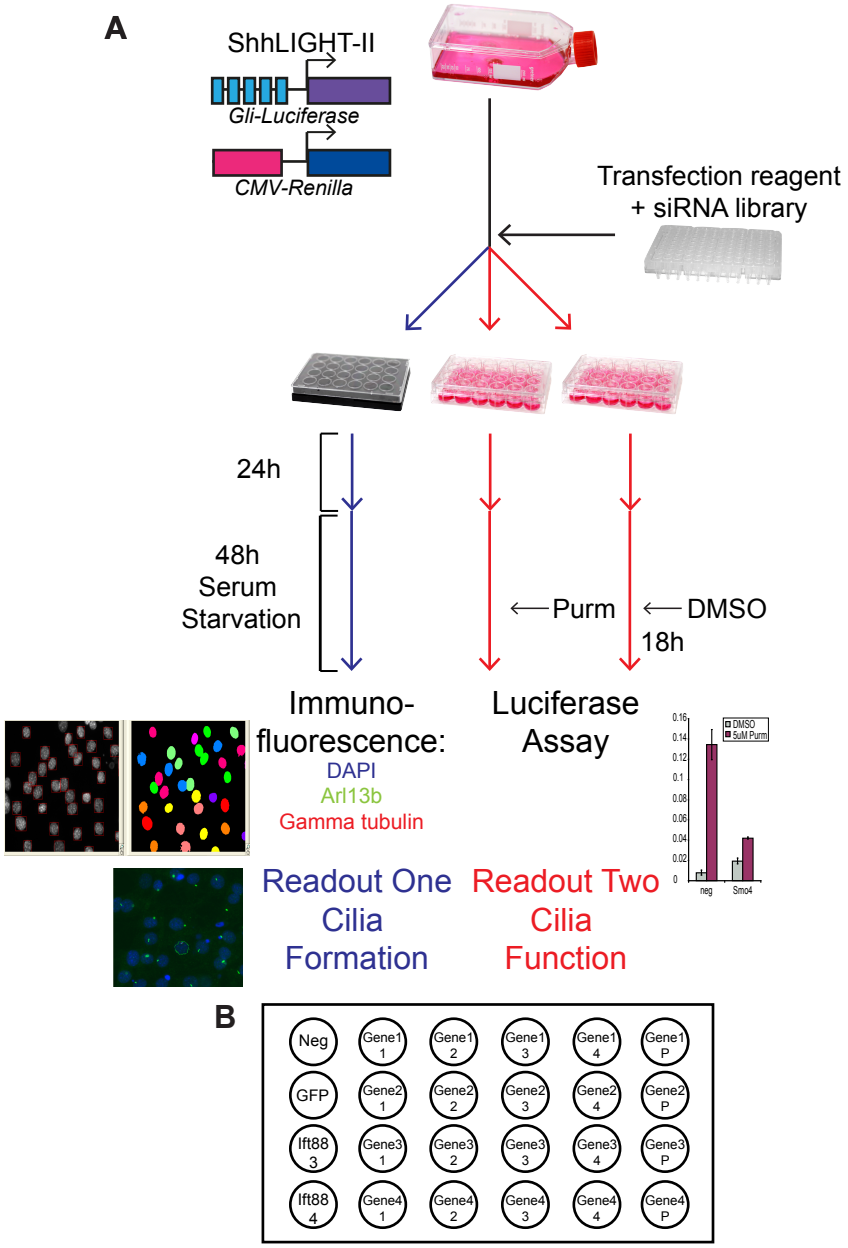

Figure 4.9 Final screen design. This figure shows the plan for the first-pass screen. (A) ShhLIGHT-II cells, stably expressing *Gli-luciferase* and *CMV-Renilla,* are transfected with an siRNA library containing 37 candidate ciliary genes identified in a *Drosophila* expression screen. Transfected cells are plated to three plates, one glass and two plastic. After 24h, cells are serum starved for 48h. After 30h the plastic plates have DMSO or 5μM purmorphamine added for 18h. After 48h serum starvation, the glass plate is fixed and stained for cilia (α-Arl13b), centrosomes (α-γ-tubulin) and nuclei (DAPI), for readout of cilia structure. The Scan^R micrsoscope automatically images the cells and counts cilia and centrosome numbers, as well as measuring cilia length and cell cycle status. The cells on the plastic plates are lysed and luciferase activity is measured (with and without purmorphamine, a Hh agonist), as a readout of cilia function. Candidates are taken forward for subsequent validation and characterisation. (B) Plan of each plate, containing two negative control siRNAs (Neg and *GFP*), two positive controls (*Ift88* #3 and 4), and siRNAs to four genes to be screened, four siRNAs per gene plus a pool of the siRNAs.

throughput image analysis to identify and count cells, cilia and basal bodies, as well as record cilia length and cell cycle status for each cell. Readout two utilised agonist-stimulated luciferase read-out of Hh transcriptional activation to analyse cilia function indirectly.

4.4 Discussion

In summary, a lot of time was initially spent optimising each step of the screen, and developing a robust protocol which gave reliable results with my positive control siRNAs to *Ift88*. Although attempts were made to further reduce noise in the screen by selecting for co-transfected cells by *GFP* knockdown, it did not enrich the proportion of cells showing reduction in cilia. As *Ift88* siRNA gave a robust phenotype even when analysing the cells as a whole population, it was not necessary to select for transfected cells.

The lack of reproducibility of phenotype when knocking down known ciliogenesis genes, *Dync2h1* and *Wdr35* highlights problems that can occur when screening using siRNAs. In the case of *Dync2h1,* the siRNAs did not reduce the *Dync2h1* mRNA levels, either due to inefficient transfection or more likely due to ineffective siRNAs which did not destabilize target mRNA. In the case of *Wdr35,* it seemed that level of transfection was important, suggesting a certain threshold of knockdown (<30% mRNA remaining) is needed to see a phenotype. This threshold will vary from gene to gene, and depends on many factors, including how much excess protein is in the cell and the half-life of the protein. Knockdown efficiency and stability of the siRNAs can be affected by chemical modifications. In the case of *Dync2h1,* the siRNAs were unmodified which may explain or at least contribute to the lack of knockdown. Chemical modification of siRNAs has been shown to improve the knockdown levels and reduce off-target effects (Jackson et al., 2006). *Wdr35* siRNAs were chemically modified Invitrogen Silencer Select siRNAs™, which may explain the slightly improved level of knockdown. Finally, *Kif3a* and *Ift88* were Dharmacon OnTarget*Plus* siRNAs™ which in our hands seemed to give the best

knockdown. Dharmacon OnTarget*Plus*™ were the siRNAs we used in the final screen. Despite extensive optimisation, this is ultimately a genetic screening tool to identify putative candidates involved in cilia formation or function. This means false positives are possible and need to be considered in the next phase of validation of potential hits. More likely are the false negatives, which mean the role of a particular gene in cilia biology cannot be definitively ruled out from this screen.

For these reasons and the technical limitations in the current set-up (transfection was carried out by hand, with four siRNAs plus a pool per gene, and each siRNA in triplicate for the two readouts (Figure 4.9)), it was decided that technical replicates would be carried out only on the hits of the first pass screen, in order to manage the workload. In retrospect, it may have been better to perform the technical repeats in parallel on all siRNAs to help identify true hits and reduce false negatives. This would require an automated high-throughput transfection platform to manage the workload, especially if the screen is scaled up to include more genes – this will be discussed further in Chapter Five.

Given the level of noise observed in the system, and the resource investment required (of both time and money) to perform a truly high-throughput siRNA screen, it was decided that it would be best to pilot a smaller-scale screen to judge the feasibility of scaling up to a genome-wide siRNA screening platform. We chose a unique test set of genes identified in a *Drosophila* ciliated sensory neuron expression screen (Cachero et al., 2011), which was further enriched for ciliary genes by bioinformatic approaches. This gene list was highly enriched for genes expressed in cilia but functionally uncharacterized, and importantly also had many genes with no known link to cilia. This approach gave us a unique set of genes to screen, at the time of the screen this list was unpublished, and it gave us a high chance of identifying ciliary genes. However, it must be considered that *Drosophila* cilia biology differs widely from mammalian systems. Hh signalling is cilia-independent in *Drosophila* and mutations in cilia genes give proprioception phenotypes in flies, as opposed to embryonic lethality. By our selection of candidates, we will overlook important mammalian genes are not expressed in *Drosophila* sensory neurons. Similarly, ciliated sensory neurons are highly specialised neuronal cells, therefore highly

expressed genes may have a role in neuronal processes, but no role in ciliogenesis specifically. Despite these caveats, it seemed this would be a novel and interesting gene list investigate further.

Chapter 5. A screen for genes involved in cilia formation and function.

After extensive optimisation of the screening protocol, described in Chapter Four, the first-pass screen was performed as described in Figure 4.9. In this chapter, results from the screen are described. Several candidate genes were identified in the first-pass screen; these were confirmed by follow-up screens, both by repeating in ShhLIGHT-II cells, and in a second ciliated mouse kidney cell line, IMCD3. Candidate genes were then further characterised by localisation studies as well as live imaging to dissect cilia phenotypes in real time.

5.1 First-pass screen: an imaging-based screen identifies several candidate cilia formation genes

The screen was performed as described in Chapter Four (Figure 4.9). To limit false positives, several additional technical "quality control" criteria for parameters which could indirectly affect cilia numbers were performed. Throughout the screen, any well in which the cells died, or had an abnormal morphology by DAPI or phase contrast microscopy were discarded. Any plates in which controls failed for this reason were also discarded. As cell density is known to affect ciliogenesis (Mori et al., 1979), any wells in which cell density fell below a certain threshold (10 cells/field) were discarded. Another key factor known to affect ciliogenesis is cell cycle – although cells are serum starved to arrest them in G_1/G_0, the window when ciliogenesis generally occurs, there can be variation in the efficacy of the cell cycle arrest. Cell cycle state was analysed using DAPI intensity with the Scan^R software, and any well with more than 20% of cells in G_2 is highlighted in Table 5.1. Optimisation experiments determined that wells with more than 20% of cells in G_2

began to show lower levels of ciliogenesis in ShhLIGHT-II cells (data not shown). This information was considered when analysing results.

5.1.1 Genes affecting cilia numbers

Figure 5.1A shows a box plot of the percentage of ciliated cells for the negative control (non-targeting and *GFP*) siRNAs, compared to the positive control *Ift88* siRNAs (#3 and 4) from all plates. There is a significant difference between negative and *Ift88* siRNA treatments ($p = 1.2 \times 10^{-8}$, Wilcoxon test with Bonferroni correction). Also plotted are all siRNAs to "genes not involved" (*GapdH, Cyc B2* and *Smo*) which were run as a further negative control to get an idea of the variation in the system. This is not significantly different to the negative controls, but is significantly different to *Ift88*, as expected. Finally, the percentage of ciliated cells upon addition of siRNAs to the ciliary gene list (Table 4.1) is shown. This is not significantly different from the negative control, probably due to the fact that some siRNAs do not give a successful knockdown, and not all genes screened are involved in cilia formation. However there is a much longer lower quartile whisker, suggesting there are siRNAs in our screen that give a reduction in the number of cilia (Figure 5.1A). Given the way the genes were chosen for our screen (being highly expressed in ciliated cells in *Drosophila*), we would expect siRNA knockdown to lead to a reduction in the number of cilia, therefore the increase in the lower quartile whisker is as expected. The results of the first-pass screen are shown in Table 5.1 (Note: Tables for Chapter Five are found at the end of the chapter).

In order to control for plate to plate variation, normalised percentage index (NPI) was calculated:

$$NPI = \frac{(\%\ NEG) - (\%\ GOI)}{(\%\ NEG) - (\%\ POS)}$$

% NEG = Mean % cells with cilia upon negative and *GFP* siRNA addition

% POS = Mean % cells with cilia upon *Ift88*#3 and *Ift88*#4 addition

% GOI = % cells with cilia upon addition of siRNA to gene of interest

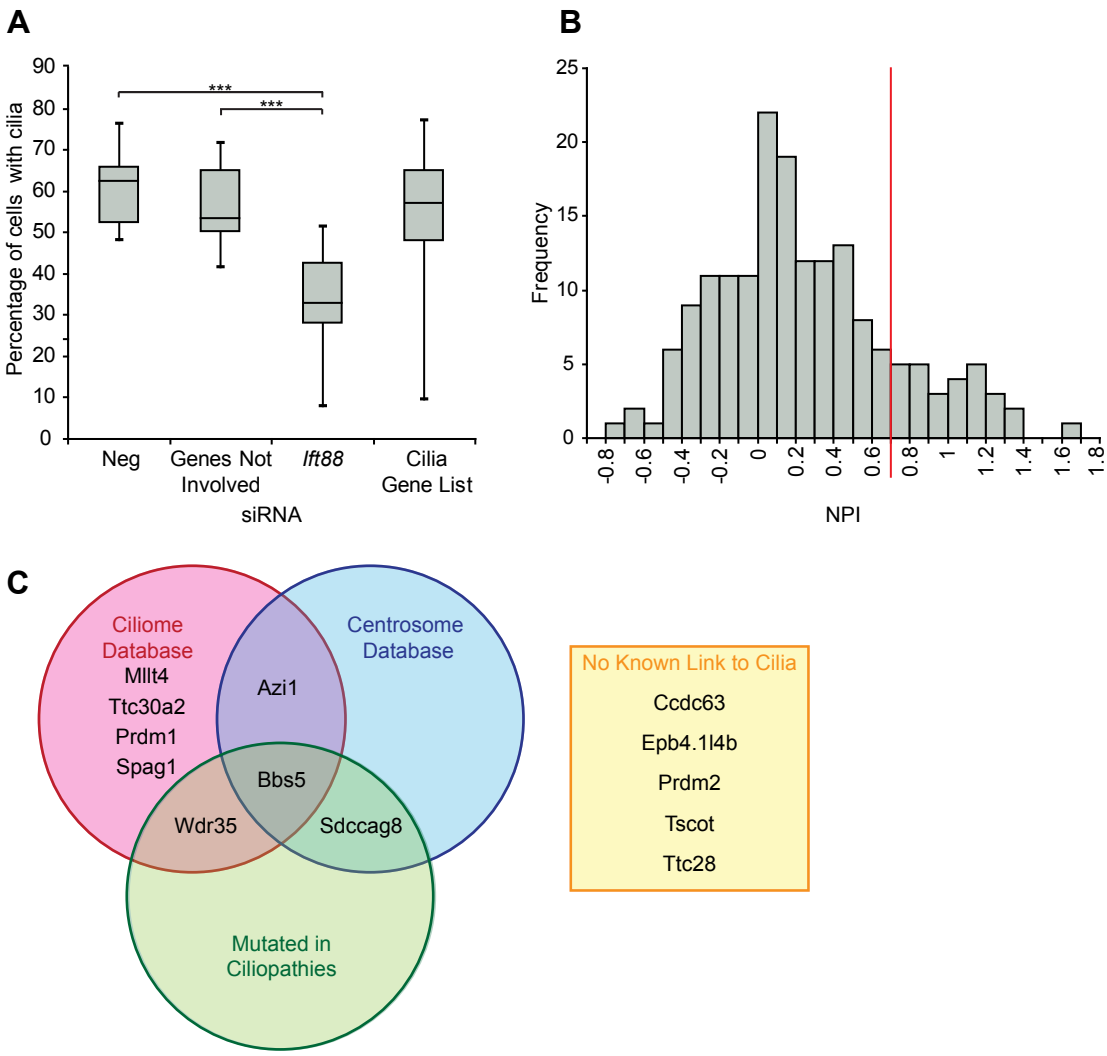

Figure 5.1 First pass screen results - cilia formation (A) Box plot shows the number of ciliated cells is significantly fewer upon *Ift88* siRNA addition compared to non-targeting or GFP siRNA (Neg) or siRNAs to genes known not to be involved in ciliogenesis (Genes not involved - *Smo, Gapdh* and *Cycb2*). The library of siRNAs against the list of putative ciliary genes (Gene list) did not give a significant reduction in the number of cilia, but several siRNAs did reduce cilia number as seen by the increased lower quartile whisker (*** $p<0.001$, Wilcoxon rank sum test). (B) Histogram of the normalised percentage index (NPI) scores of the siRNAs to the cilia gene list. An siRNA with an NPI score of more than two standard deviations from the mean of "genes not involved", i.e. NPI>0.7 (marked by the red line) was called as a hit. (C) Venn diagram showing the genes chosen for further study because siRNA knockdown lead to a reduction in cilia in the first pass screen, showing what was known about the genes at the time (2010). Ciliome database: www.ciliome.org (Inglis et al. 2006), centrosome database: http://centrosome.dacya.ucm.es/ (Andersen et al 2003) and ciliopathy genes were identified from literature searches and OMIM.

This score essentially scales the phenotype in the experimental well to the difference between the negative and positive controls on that plate, so if NPI = 1 this means the siRNA reduced the number of cilia by the same degree as the positive control, if NPI > 1 the siRNA caused a greater reduction in cilia than the positive control, and a minus NPI score indicates the number of cilia increased (Kim et al., 2010). Figure 5.1B shows a histogram of the NPI scores, which are listed in Table 5.1, for the siRNAs in the first-pass screen. The data seems to be bimodal with a peak of hits at an NPI of 1.2. In order to call hits using this score, the NPI values for the "genes not involved" were calculated. An siRNA which had an NPI score which was more than two standard deviations from the mean of this population, i.e. NPI > 0.7, was called as a hit. This gave a list of 24 siRNAs, which is 14% of all of those tested. From this list, five genes had at least two siRNAs called as a hit (*Sdccag8, Bbs5, Tscot, Mllt4* and *Epb4.1l4b.* Tables 5.1 and 5.2).

The NPI score is influenced by the degree of phenotype seen in the positive control on the plate, and in this way, assuming transfection efficiency is uniform across the plate, it corrects for transfection efficiency. However the assumption of equal transfection efficiency across the plate may not be true, therefore we also used another method to call hits, the Fisher's exact test. The mean of the number of ciliated cells upon negative and *GFP* siRNA addition on each plate was used to calculate the "expected" outcome, and Fishers test was used to calculate p values. This method does not depend on the effectiveness of the positive control (Table 5.1). To correct for multiple testing, Bonferonni correction was applied and a cut off of $p<0.01$ was used to call hits. This gave a hit rate of approximately 20% (34 siRNAs).

When considering statistical tests, Z score was also considered, as it is often used in the analysis of large scale screens (Birmingham et al. 2009, Zhang et al. 1999). However as the data is not normal (as it is percentage data) and this test assumes a normal distribution we decided to use the Fiscner's exact test as it is a non-parametric test.

By these two methods we had two lists of siRNAs that were called as a hit. These lists overlapped by 18 siRNAs (75%), significantly more than you would expect by

chance ($p = 8.8x10^{-10}$, hypergeometric test), indicating the two analysis methods are generating similar data sets. Although I had more confidence that hits called by both methods were true positives, those called by only one method could still be true, so I used both methods to call hits. Genes were ranked by the number of siRNAs giving a hit and then the strength of that hit by NPI or Fisher's test (Table 5.2 and 5.3). As mentioned above, the NPI method gives five genes with more than two siRNAs as a hit, whereas the Fisher's test gives 11 genes with more than two siRNAs as a hit. Interestingly, *Wdr35,* which was shown to be essential for ciliogenesis in Chapter Three, was ranked as fourth using the Fisher's Exact test method.

5.1.2 Genes affecting cilia length

The lengths of the cilia were also measured using maximum feret diameter (MFD, a measure of the longest dimension of the cilia) in the Scan^R Analysis software (Table 5.1). Overall, *Ift88* siRNA gives shorter cilia ($p<0.001$ Wilcoxon rank sum test). An siRNA was called as a hit if it changed the length significantly from both negative controls on the plate ($p<0.05$, Kruskall-Wallis test then Wilcoxon rank sum test with Bonferroni correction, highlighted in Table 5.1). siRNAs which gave a significantly different cilia length from just one negative control siRNA on the plate are also highlighted (Table 5.1). As the genes screened were chosen by high expression in a ciliated cell type, it is predicted that knockdown of these genes is more likely to give a reduction in cilia length and every siRNA which was significantly different to both negative controls in this first-pass screen decreases cilia length. Overall, 35 siRNAs reduced cilia length compared to both negative controls on the plate (roughly 20% of siRNAs screened). Of these, 15 also reduced cilia number, significantly more overlap than expected by chance ($p = 3.7x10^{-3}$, hypergeometric test), indicating, unsurprisingly that these phenotypes are related. In addition 20 siRNAs seemed to affect cilia length independent of cilia number. This gave a list of nine genes which had at least two siRNAs that reduced cilia length, of which four (*Spag1*, *Ebp4.1l4b*, *Bbs5* and *Tcte3*) also reduced cilia number and five (*Wdr60, Fam92b, Catnb, Tctex1d1* and *Tctex1d2*) which affect cilia length independently of number (Table 5.4).

5.1.3 Centrosome numbers

As well as imaging and quantifying cilia, centrosomes, stained with anti-γ-tubulin, were also imaged and quantified. Due to problems with antibody availability, this was not completed on every plate of the first-pass screen. The preliminary data from the first screen suggests that siRNAs to two genes, *Ccdc114* and *Zmynd10* may lead to supernumerary centrosome formation as we saw an increase in cells with more than two centrosomes. The data also suggest that siRNA to *Pp3r1, Wdr16* and *Wdr60* may reduce the number of centrosomes, as we observed a decrease in the number of cells with more than two centrosomes.

5.1.4 Selecting genes for second-pass screening.

It is important to note that up until this point in the screen, only one repeat for each siRNA had been carried out; repeats were needed in order to confirm these results. Therefore 12 genes were followed up with further study, which included repeating twice more in this cell type, whilst extracting RNA to correlate mRNA knockdown with phenotype, and repeating twice in a second cell line, IMCD3. Genes chosen for further study, based on siRNAs giving a reduction in cilia number are highlighted in Figure 5.1C, which summarises any links to ciliogenesis, such as presence in the ciliome database, known mutations in ciliopathies, or presence in the centrosome database. As the basal body at the cilia base is analogous to the centrosome, many centrosomal proteins have roles in cilia biology, therefore presence at the centrosome may indicate a ciliary role. It should be pointed out that we included three genes that only had one siRNA which reduced cilia number per gene, *Azi1, Prdm1,* and *Prdm2* for follow-up studies. It is more likely these are off-target effects and therefore false positives, than the other genes in the list which had more than one siRNA giving a phenotype. However we followed them up for two main reasons:

(i) ***Biological interest:*** *Azi1* had been followed up by Andrew Jarman after the initial expression screen (Cachero et al., 2011) and when the *Drosophila* homologue *Dila* was mutated in flies they showed a ciliary phenotype ((Ma and Jarman, 2011), See Chapter 6 for further information). *Prdm1/Blimp1* and *Prdm2/Riz1* are key

transcription regulators from the same family, and they were included in the screen as 1-to-many orthologues of the *Drosophila* gene. Although *Prdm1/Blimp1* has well characterised roles in germ cell development, and both genes are implicated in cancers (Cachero et al., 2011; Calado et al., 2010; He et al., 1998; Jiang et al., 1999; Schafer et al., 2011), nothing is functionally known about roles in cilia biology. Importantly, similar to the *Drosophila* expression studies (Cachero et al.), *Prdm1* was also identified in a transcriptomic study for genes highly expressed in ciliated cells in *C. elegans* (Blacque et al., 2005). Although these genes are unlikely to localize to cilia, they may play important and novel roles in the transcriptional control of ciliogenesis.

(ii) ***Robustness of the single hits:*** The siRNAs that did give a reduction in the number of cilia for these three genes gave the strongest phenotypes out of all the siRNAs in the screen, so although only one siRNA gave a phenotype, it was a very significant reduction in cilia number.

Wdr35 was not included in the second-pass screen because as shown in Chapter 3, we had already established that *Wdr35* is essential for ciliogenesis in mammals, and had characterised the ciliary defects in detail in the mutant cells.

In summary, I took twelve genes, nine of which had more than one siRNA giving a reduction in cilia numbers in the first-pass of the screen and carried out further screens to confirm these hits (Figure 5.1C).

5.2 Cilia Function Readout: Variation in controls and problems with cell death

The second readout of the screen examined Hh signalling as an indirect readout of cilia function. Figure 5.2A shows that as expected, the response of the cells to the Hh agonist purmorphamine is significantly reduced upon *Ift88* knockdown – plotted is the fold increase in luciferase activity upon purmorphamine addition across five

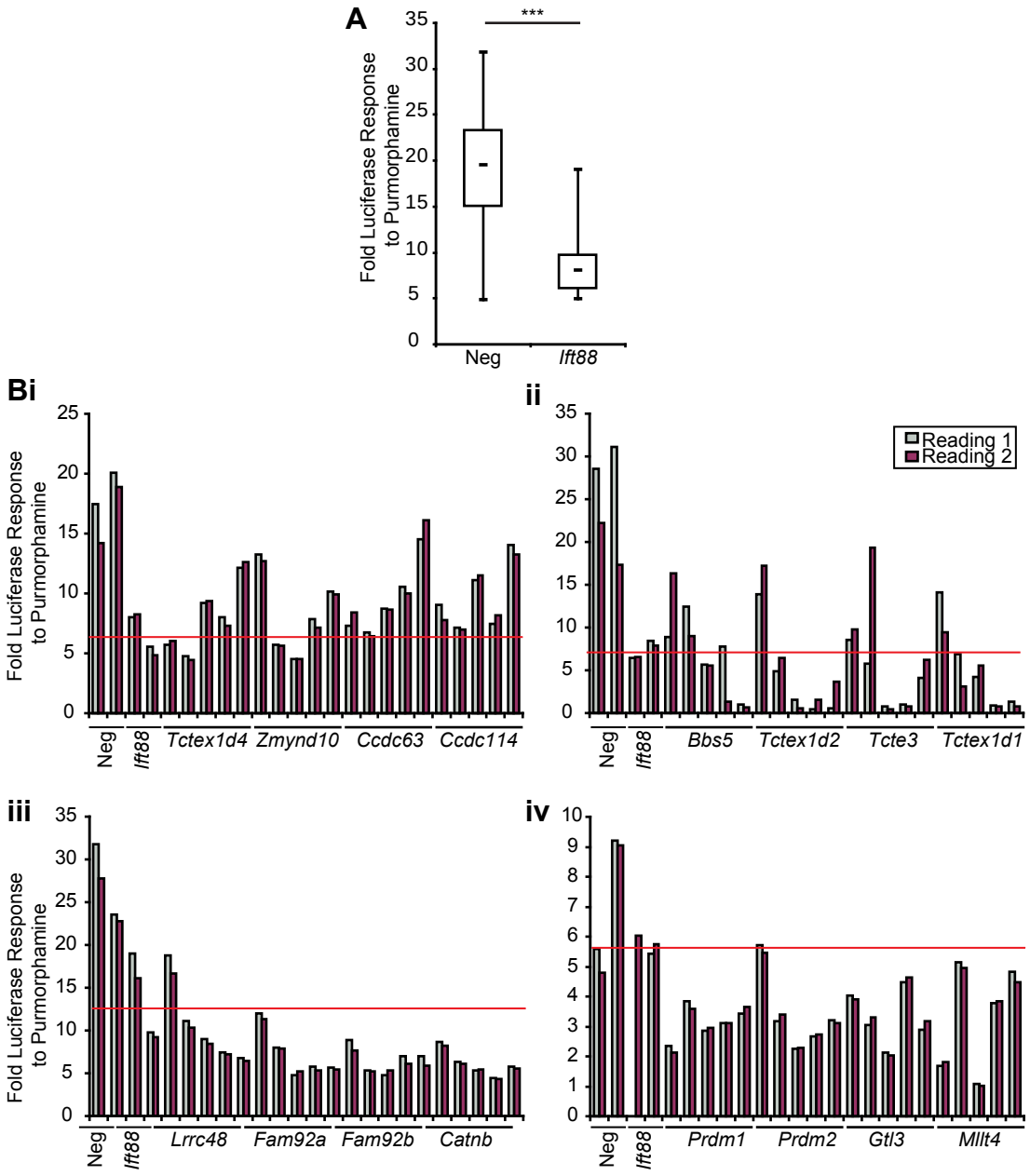

Figure 5.2 Variation in readout two - cilia function. (A) Fold *Gli-luciferase* activity increase in ShhLIGHT-II cells upon purmorphamine addition, relative to *Renilla-luciferase*, is attenuated upon addition of *Ift88* siRNA, compared to non-targeting or *GFP* siRNA (Neg) (*** p<0.001, students t-test) (B) Fold increases in *Gli-luciferase* activity upon purmorphamine addition is plotted across four plates. Each plate had two negative control siRNAs (Neg - Non-targeting and *GFP*), two positive control siRNAs (*Ift88* #3 and #4) and siRNAs to four genes to be screened (four siRNAs per genes plus an siRNA pool). Each luciferase reading was taken in technical duplicate (represented by grey and purple bars). 67% of siRNAs gave a stronger phenotype than the *Ift88* control (below red line) which is unlikely to be true as it is unlikely 67% of siRNAs knock down the target gene. Note the variation in controls (scale bars vary between graphs).

experiments. However as shown in Figure 5.2 B, the actual response was variable, with fold induction varying from 10 fold to 35 fold, which when compared to the responses seen in Figure 4.5A (2 fold), Figure 4.2C (4 fold) and 4.2 D (14 fold), highlights the variation in the assay. Further compounding problems with variability in results, there were also significant problems with cells dying after the combination of siRNA treatment, serum starvation and drug treatment, which was not seen in the optimisation experiments. This meant data was not successfully collected for every gene in the screen.

For the plates that were completed, calling a hit was difficult; 67% of siRNAs gave a signalling phenotype stronger than the *Ift88* siRNA, despite the *Ift88* siRNA giving a fairly robust phenotype in most plates. This lead to 14 out of 16 genes for which data was collected, giving more than two siRNAs with a lower *Gli-luciferase* response than *Ift88,* and therefore being called as a hit. It is possible that these genes truly affect Hh signalling, possibly through cilia function – in a screen published after I performed the first-pass screen, Lai et al. 2011 also reported a much higher number of siRNAs giving a phenotype with a *Gli-luciferase* readout than with the imaged-based readout. However, judging by the RNA knockdown levels seen upon siRNA addition (see Figure 4.3 and 5.4), it is unlikely that 70% of siRNAs would successfully knockdown the target gene. This uncertainty, combined with the problems with cell death, meant I concentrated on the results for cilia formation.

5.3 Validation: repeats of putative hits from the first-pass image-based screen in ShhLIGHT cells and IMCD3 cells

In order to validate the genes which had given a reduction in the number of cilia (and in some cases reduction in cilia length) upon siRNA knockdown from the first-pass of the screen, this assay was repeated in duplicate in ShhLIGHT-II cells, and RNA

was collected in order to correlate knockdown levels with phenotypes. The siRNAs to the genes chosen for validation were also transfected in duplicate into a second cell line, IMCD3. The box plot in Figure 5.3A shows the negative and positive controls worked in both cell lines (ShhLIGHT-II $p<0.001$, IMCD3 $p=0.044$, Kruskall Wallis). Table 5.5 shows the results from the repeat studies, with NPI scores and Fisher's Exact test p values indicating a significant reduction in cilia numbers highlighted in red. It shows that there is variation between repeats, no siRNA consistently gives a phenotype in all five repeats, although some siRNAs give a phenotype in 4 out of 5 repeats. Large variation in the NPI score is seen between repeats for the same siRNA in the same cell type, highlighting noise in the system, despite extensive optimisation. Table 5.7 shows the cell cycle results for the second-pass screen. A well called as a hit was no more likely to see an increase in the percentage of cells in G_2 than by chance ($p = 0.21$, hypergeometric test), which suggests two things: (i) the variation seen is probably not due to variation in cell cycle arrest and (ii) in general, the genes called as hits were not influencing ciliogenesis by influencing cell cycle.

Even with this variation, siRNAs to several genes show a much more reproducible phenotype than others, as shown in the Table 5.5 where the genes ranked in order of the reproducibility of the phenotype and the number of siRNAs giving a phenotype. As it is difficult to draw a line between genes which show reproducible phenotypes and those which do not, an arbitrary line was drawn which says 7 of the 12 genes give a fairly reproducible reduction in cilia number upon siRNA knockdown. These were *Ttc30a2, Sdccag8, Mllt4, Azi1, Ttc28, Ccdc63* and *Spag1*.

Figure 5.4 shows the correlation between the mRNA level and phenotype (measured by NPI score) in ShhLIGHT-II cells. The qPCR failed for four genes; this may be because the genes are not highly expressed, however only one primer pair was tried for each gene and no positive control RNA (i.e. from a tissue where the gene is known to be expressed) was included so we cannot rule out the technical possibility the primers failed. Two genes for which mRNA levels were detected did not give a reproducible reduction in cilia numbers so are not depicted. Of the remaining six genes, three (*Azi1, Ccdc63* and *Spag1*) gave a good correlation between knockdown

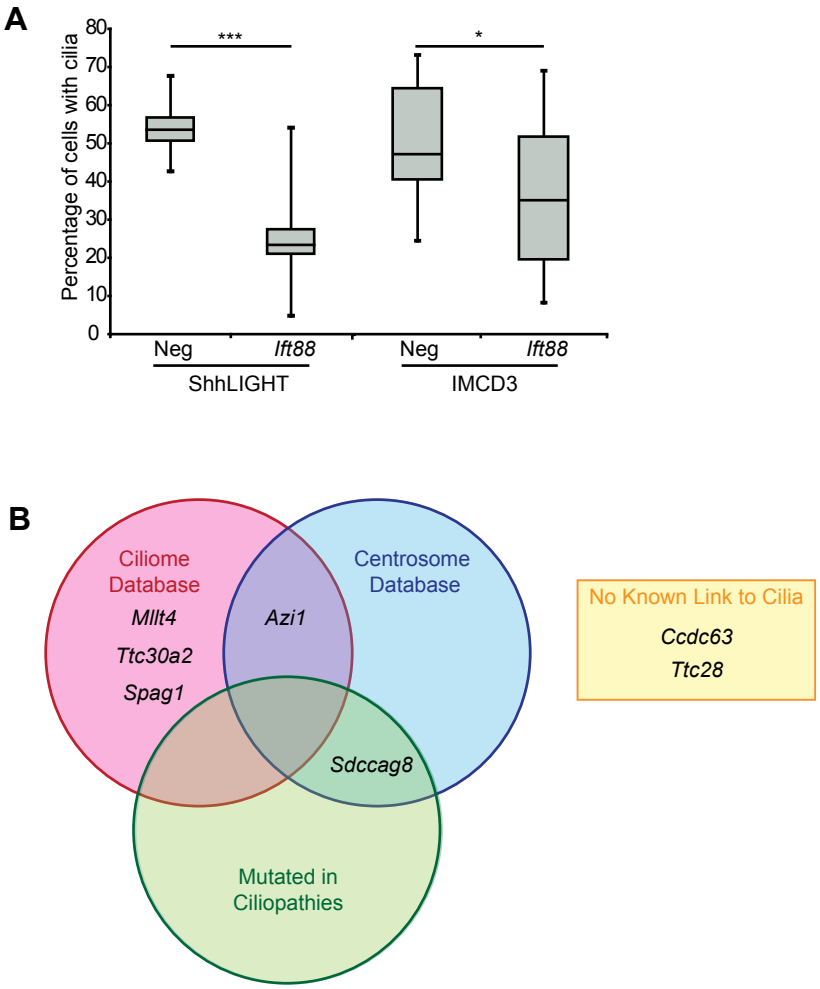

Figure 5.3 Second-pass validation screen. 7 out of 12 genes give a reproducible reduction in cilia number upon siRNA knock-down. 12 genes chosen from the first pass screen (Figure 5.1) were screened twice more in ShhLIGHT-II cells and twice in a second ciliated cell line, IMCD3. (A) Box plots show that the positive control *Ift88* siRNAs on these plates gaves a significant reduction in the percentage of cells with cilia (*p<0.05 ***p<0.001 Wilcoxon test). (B) 7 out of 12 genes gave a reproducible reduction in cilia number. The Venn diagram indicates whether the genes have any known link to cilia biology, Ciliome database: www.ciliome.org (Inglis et al. 2006), centrosome database: http://centrosome.dacya.ucm.es/ (Andersen et al 2003) and ciliopathy genes were identified from literature searches and OMIM.

levels and observed phenotype, i.e. as RNA levels dropped, NPI score increased. This suggests the reduction in cilia number is not due to off-target effects of the siRNAs. I also examined cell cycle arrest and although some wells in which ciliogenesis was impaired showed an increase in the percentage of cells in G_2, this was not consistently correlated with phenotype for any gene, suggesting they influence ciliogenesis by mechanisms other than influencing cell cycle arrest.

Therefore three genes (*Azi1, Spag1* and *Ccdc63*) give a fairly reproducible reduction in cilia numbers upon siRNA knockdown and this reduction correlates with mRNA level, suggesting it is not due to off target effects.

5.3.1 Cilia length

Table 5.6 shows the changes in cilia length in the second-pass screen. As seen with cilia number there is variation between repeats. In the first-pass screen, all significant changes in length constitute a reduction in length, and in the second-pass screen, this trend continued with most significant changes being a reduction in length, but there were also examples of significantly increased cilia length. There seemed to be more variation in IMCD3 cells, perhaps reflecting a cell-type specific effect. Three genes gave a fairly reproducible reduction in cilia length upon siRNA knockdown: *Azi1, Spag1* and *Ttc30a2*. Interestingly these also reduce cilia numbers, suggesting this represents different aspects or severity of the same phenotypes.

5.3.2 Centrosome number

Table 5.7 shows the data for centrosome numbers from the second-pass screen, with the percentage of cells with >2 centrosomes stated: siRNAs which lead to a significant increase or decrease in the number of cells with >2 centrosomes are highlighted in blue or pink respectively. No siRNAs give a reproducible phenotype, suggesting none of the genes screened affect centrosome number, at least not to an extent that can be reliably detected by this method.

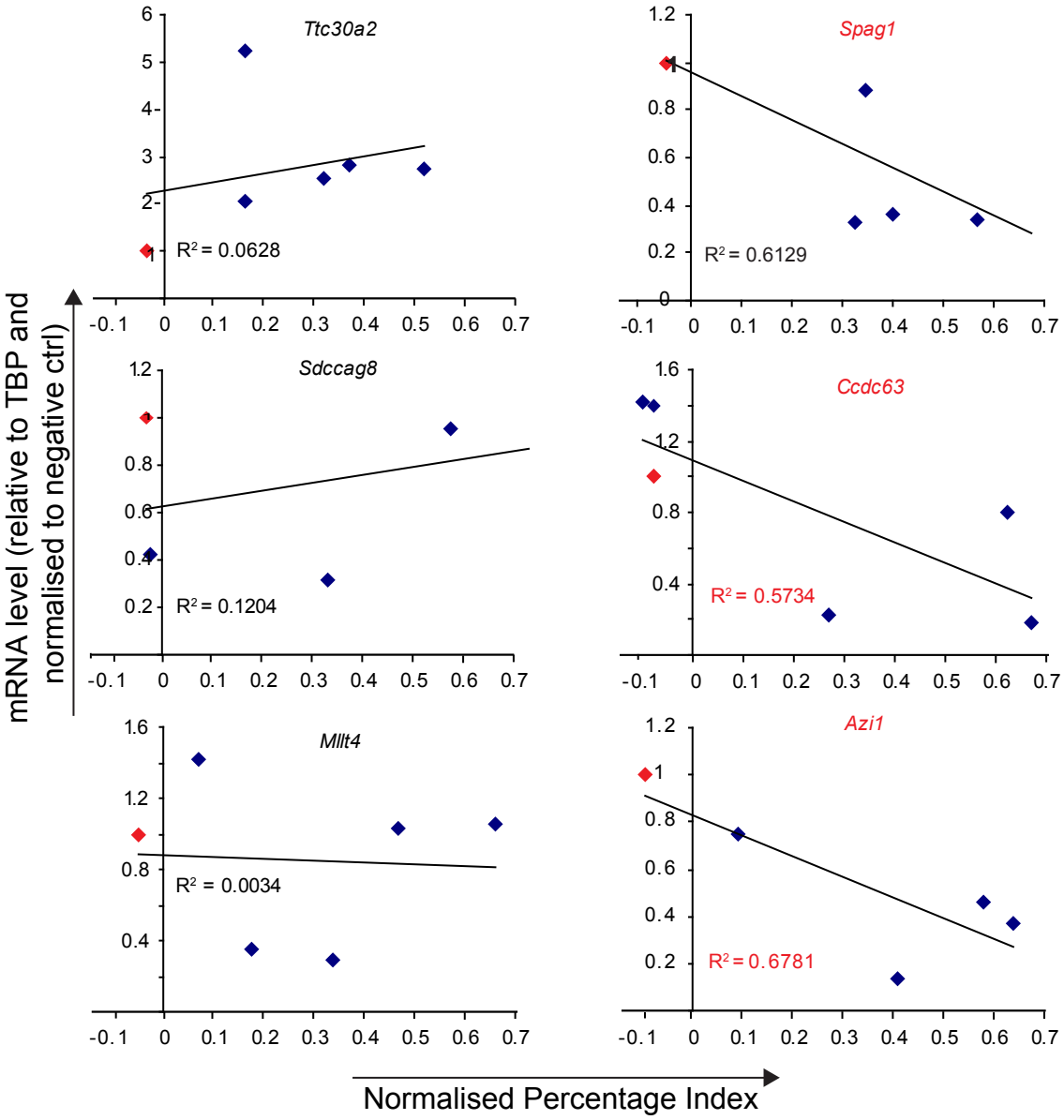

Figure 5.4 Determining siRNA knockdown with mRNA level:phenotype correlation. Plots show mRNA level, relative to the average of negative and *GFP* siRNAs in the corresponding plate, which is normalised to 1 against phenotype (measured by NPI score). qPCR results are the average of technical triplicates, and NPI score is the average of technical duplicates. The average score of the negative control siRNA and *GFP* siRNA is plotted as a red diamond. Genes highlighted in red (*Spag1, Ccdc63* and *Azi1*) give good mRNA to phenotype correlation, suggesting the phenotypes are not due to off-target effects.

5.4 Candidate characterization: Azi1, Sdccag8 and Ccdc63 localise to the base of the cilia/basal body

In order to investigate possible hits further, protein localisation was examined. Commercial antibodies to Azi1, Mllt4/Afadin, Sdccag8 and Ccdc63 were available. Azi1 had been reported to localise to the centrosome by proteomic studies (Andersen et al., 2003), and this localisation was confirmed (Figure 5.5A). As mentioned earlier, as the basal body is analogous to the centrosome, many centrosomally localised proteins have roles in ciliogenesis, so this supports the theory that Azi1 is involved in ciliogenesis. More detailed Azi1 localisation studies are included in Chapter Six of this thesis.

Sdccag8 also localised to the centrosome/basal body (Figure 5.5B), confirming a study published after the screen was started (Otto et al., 2010) which also showed *SDCCAG8* is mutated in nephronophthisis-related ciliopathies, validating it as a ciliary gene.

Ccdc63 is an uncharacterised coiled coil domain protein, which localised to the cilia and basal body (Figure 5.5C). Although the intensity of this localisation was faint, it was seen in several cilia, again supporting the theory that it could play role in cilia formation.

Finally, Mllt4/Afadin is a protein that is involved in cell-cell adhesion, specifically adherens junctions (Ikeda et al., 1999). We saw localisation to the cell membrane as expected (Figure 5.5D), but despite close inspection of the centrosome and cilia we never saw Mllt4/Afadin localising to these structures. This does not rule out a role of this protein in ciliogenesis, it could affect cilia without localising there. Examples exist where genes have roles in cell polarity which can indirectly affect basal body docking and cilia formation in some cells (Bossinger and Bachmann, 2004; Fan et

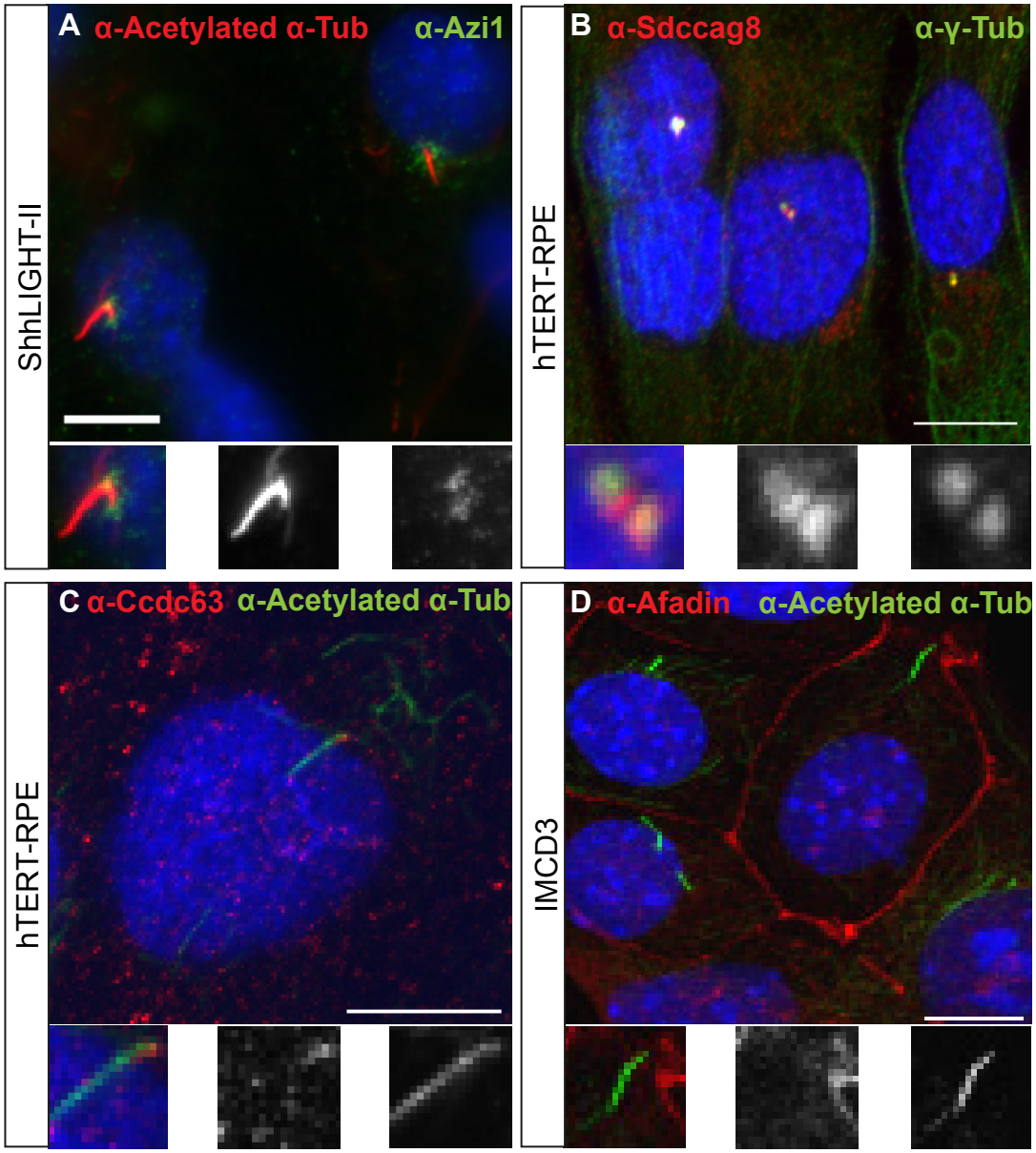

Figure 5.5 Azi1, Sdccag8 and Ccdc63 localise to the base of the cilia/basal body. (A) Azi1 localises to the base of the cilium (axoneme stained with α-acetylated α-tubulin (α-Acetylated α-Tub)) and in punctate staining around it the basal body. (B) Sdccag8 colocalises with the centrosomal marker γ-tubulin (γ-Tub). (C) Ccdc63 is slightly enriched at the base of the cilium (stained with α-acetylated α-tubulin). (D) Afadin localises to cell-cell junctions but does not localise to the cilia or basal body. Scale bars are 10μm. Enlargements of cilia are shown below each panel, with the red channel in the centre and the green channel on the right.

al., 2004a). It should be noted that although Mllt4 gave a fairly reproducible phenotype, it did not correlate with knockdown so may be due to off-target effects.

5.5 Live cell imaging: dissecting functional roles for ciliogenesis versus cilia maintenance

Up until this point, all the assays for ciliogenesis/cilia function have been carried out after 48h serum starvation, on fixed cells, giving an end-stage snapshot of the processes involved in ciliogenesis. In order to fully understand this process it is important to look in real time to see the dynamics involved. Therefore I developed two stable cell lines expressing Arl13b-mKate2, (full length mouse Arl13b with a C-terminal fluorescent tag mKate2, under the CMV promoter); a NIH-3T3 line (the parental line of ShhLIGHT-II cells) (3T3-Arl13b-mK2) and an IMCD3 line (IMCD3-Arl13b-mK2). Arl13b is a member of the Arl/Arf superfamily of small GTPases, which although poorly functionally characterized is known to be critical for cilia trafficking and localises exquisitely to the ciliary membrane. Overexpression of Arl13b-mKate2, similar to the endogenous antibody staining used in my screen, showed strong enrichment in ciliary membranes, and could be successfully used to track trafficking events in real-time. We examined the effect of *Ccdc63* knockdown on cilia dynamics in real time using the 3T3-Arl13b-mK2 cells. We chose *Ccdc63* as it is one of the top hits from the screen, with a reproducible reduction in cilia number upon siRNA knockdown, a good correlation between mRNA level and phenotype, and localisation to cilia. In this experiment, cells were transfected with siRNA, 24h later serum was removed and 6h later imaging began, taking an image every 30 min for 18h. It was noted that overexpression of Arl13b seems to have some effects on ciliary biology, for example, both of the stable lines have longer cilia than the corresponding parental line (Data not shown – also

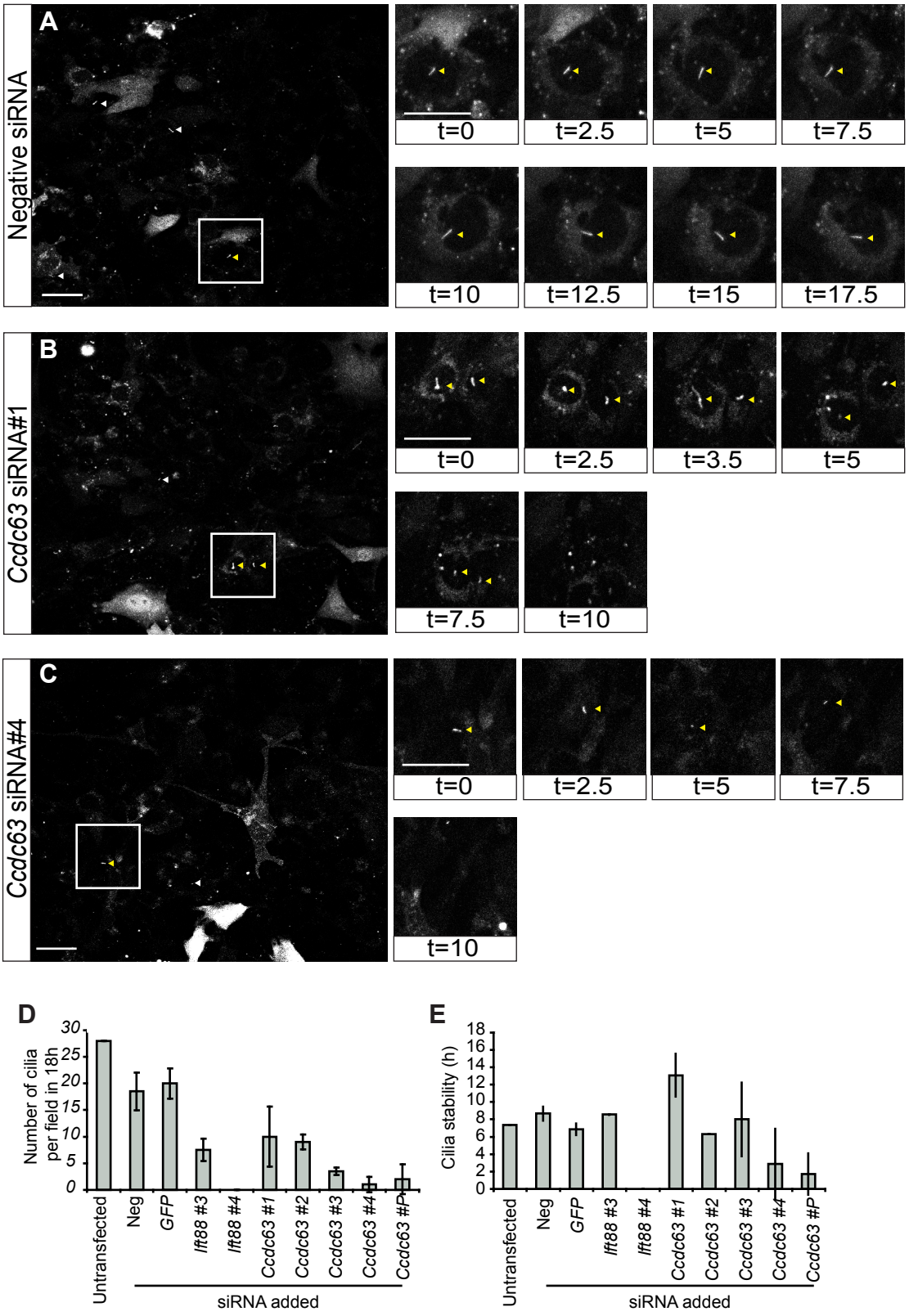

Figure 5.6 Live imaging of ciliogenesis suggests Ccdc63 has a role in cilia formation and possibly cilia stability

Figure 5.6 Live imaging of ciliogenesis suggests *Ccdc63* has a role in cilia formation and possibly cilia stability. 3T3-Arl13b-mK2 cells were transfected with negative control, *GFP*, *Ift88* or *Ccdc63* siRNA. Cells were imaged every 30 min for 18h. (A, B and C) Arl13b-mK2 marks the cilia as well as other vesicular structures, possibly due to overexpression. A whole field is shown with cilia highlighted (white and yellow arrows) and one cilium (yellow arrow, within a white box) is followed through time in the enlarged panels to the right. Scale bars show 50μm. (D) Cilia were counted per field. Addition of *Ift88* or *Ccdc63* siRNA reduces the number of cilia. (E) The stability of cilia was measured (i.e. the number of hours the cilia remained visible). *Ccdc63* siRNA may reduce cilia stability. Shown is the average of three fields of view +/- standard deviation. Note this preliminary, biological replicate n=1

reported in (Caspary et al., 2007)) and this must be considered when drawing conclusions from experiments using these cell lines.

Figure 5.6 A-C show screen shots of the initial time point for each siRNA treatment, and a close-up of one cilia followed through time (See Movies 5.1A-D). Figure 5.6 D shows the total number of cilia per field throughout the entire 18 hours. As a positive control, *Ift88* siRNAs were added, which gave a reduction in cilia numbers throughout all time points (Figure 5.5D). *Ccdc63* siRNA addition also leads to a reduction in cilia number (Figure 5.5D). This dynamic system allows many more parameters to be measured, such as cilia stability (the amount of time a cilia remains extended). Cilia stability is not reduced upon *Ift88* #3 siRNA addition (it could not be assayed upon *Ift88*#4 addition as no cilia were seen), however the data suggest it is reduced in some wells upon *Ccdc63* siRNA addition (Figure 5.5E). Cilia were seen to bulge and then collapse (Figure 5.5B enlarged figures) upon *Ccdc63* addition, which may be related to the instability seen. This data only represents one experiment, so further experiments are needed to confirm this finding, but it suggests Ccdc63 may be involved in both ciliogenesis and cilia stability.

Pairing such live imaging with complimentary approaches such as endogenous localisation studies allows us to probe the dynamic aspect of cilia biology. Certain caveats do exist for our live imaging approach. The effect of Arl13b overexpression on cilia biology could be controlled by reducing levels of expression, perhaps by generating cell lines with a single integration event.

5.6 Overexpression of *Azi1-GFP* resuces the reduction in ciliogenesis upon *Azi1* siRNA addition.

In order to further confirm the reduction in ciliogenesis upon addition of *Azi1* siRNA was not due to siRNA off-target effects, we attempted to rescue the phenotype by overexpression of a siRNA-insensitive version of the gene. *pAzi1-GFP* encodes *Azi1* cDNA tagged with *GFP* at the 3' end of the gene, and so lacks the *Azi1* 3'UTR. ShhLIGHT-II cells were cotransfected with a pool of four new siRNAs targeting the 3'UTR of *Azi1* along with a control *pCAG-eGFP* plasmid. This led to a reduction in *Azi1* mRNA levels to less than 10% of endogenous levels and Azi1 protein to less than 30% of endogenous levels (Figure 5.7 A-D). As with the siRNAs targeting the coding region of *Azi1* used in the screen (Table 5.5), this led to a significant reduction in cilia numbers in transfected (GFP positive) cells (Figure 5.7 E, G and I). This reproduction of the knockdown phenotype with new siRNAs targeting other regions of *Azi1* further strengthens the argument it is not due to off-target effects of the siRNAs. As final confirmation that the phenotype is due to a reduction in Azi1 levels and not off target effects, *pAzi1-GFP* plasmid was coransfected with the *Azi1* 3'UTR siRNA. This restored *Azi1* mRNA and protein levels and, importantly, restored the number of cilia in transfected cells to wild type levels. Therefore reduction in *Azi1* levels by siRNA leads to a reduction in ciliogenesis, supporting a conserved role for mammalian Azi1 in ciliogenesis.

5.7 Discussion

In this chapter, a reverse-genetic screen for genes involved in mammalian cilia formation and function was performed. In the first-pass screen, 37 genes, covered by

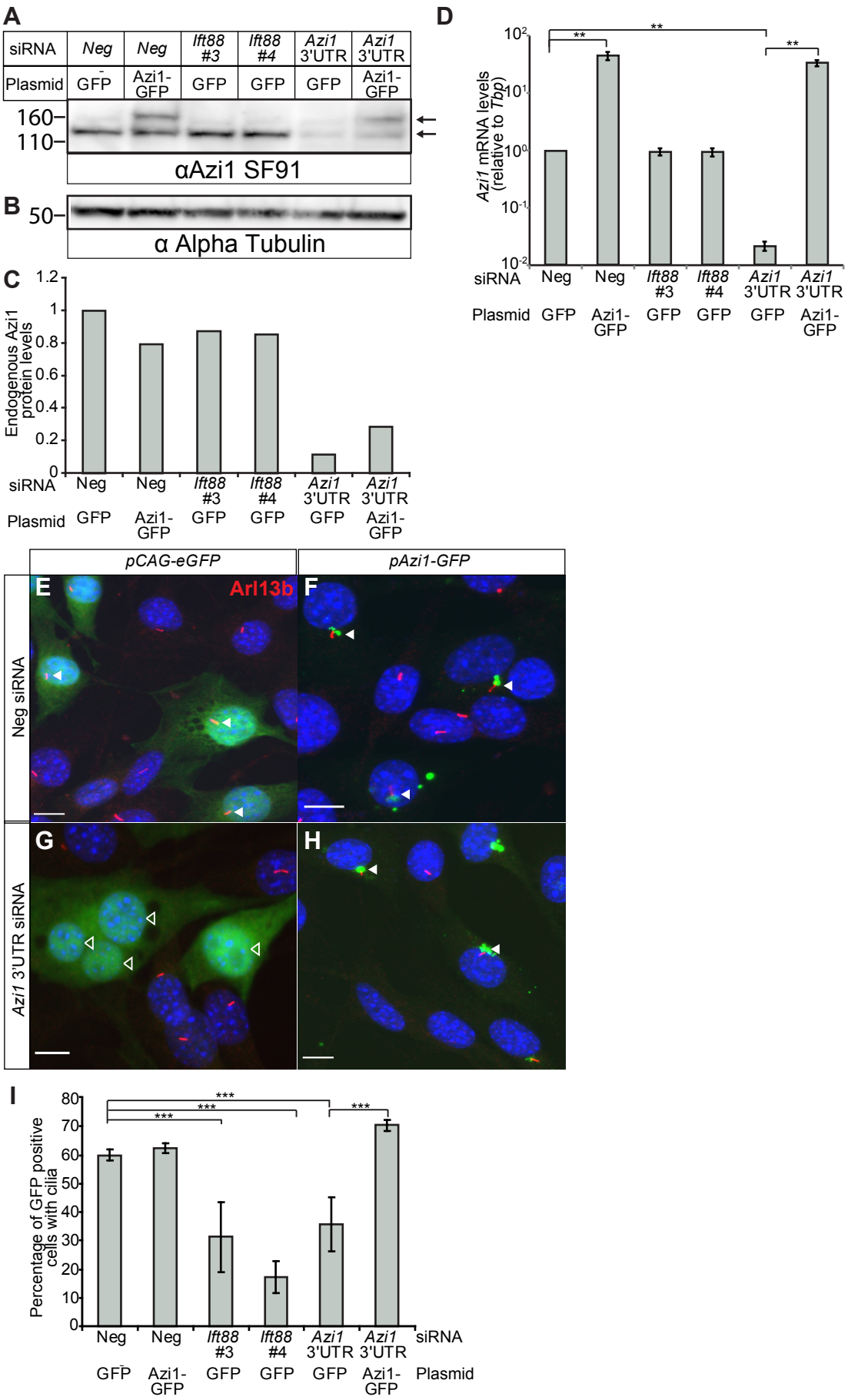

Figure 5.7Reduction of ciliogenesis upon Azi1 siRNA treatment is rescued by overexpression of Azi1-GFP.

Figure 5.7 Reduction of ciliogenesis upon *Azi1* siRNA treatment is rescued by overexpression of Azi1-GFP. ShhLIGHT-II cells were transfected with negative control (Neg), *GFP*, *Ift88* siRNA or a pool of four siRNAs to the 3' UTR of *Azi1* (*Azi1* 3'UTR), along with either pCAG-eGFP or pAzi1-GFP plasmids. As pAzi1-GFP lacks the 3'UTR of *Azi1,* this is predicted to be insensitive to targeting by the *Azi1* 3' UTR siRNA pool. (A) Western blot probed with α Azi1 SF91 shows Azi1 levels are reduced upon *Azi1* 3'UTR siRNA addition (Lower arrow, See Figure 6.3 for Azi1 antibody epitopes). The tagged Azi1-GFP protein is also detected, running slower due to the 27kDa GFP tag (Upper arrow). (B) The blot was reprobed with α Alpha tubulin as a loading control. (C) Quantification of endogenous Azi1 protein levels (relative to Alpha tubulin). (D) qPCR for *Azi1* relative to *Tbp* shows *Azi1* mRNA levels are reduced upon *Azi1* 3' UTR siRNA addition and this is rescued to above wild type levels upon transfection with *pAzi1-GFP*. Shown is the mean +/- standard deviation of two biological replicates and three technical replicates. ** $p<0.01$, student's t test. (E-H) Cells were stained with α Arl13b to mark cilia and GFP Booster (Chromotek) to enhance the GFP signal. Transfected, GFP positive cells with cilia are marked with a closed arrow, transfected GFP positive cells without a cilia are marked with an open arrow. (I) The percentage GFP positive cells with cilia quantified. Addition of *Azi1* 3'UTR siRNA significantly reduces the percentage of cells with cilia, and this reduction is rescued to wild type levels by cotransfection with *pAzi1-GFP*, indicatting the phenotype is not due to off-target effects of the siRNA. Shown is the mean +/- SEM of two technical and two biological duplicates. *** $p<0.001$ Chi Squared test.

four siRNAs per gene plus a pool, were screened. Putative hits from the first-pass screen were followed up by a second-pass screen, validating hits by repeats in the same cell type (ShhLIGHT-II) and a second ciliated cell line (IMCD3), identifying seven genes with reproducible phenotypes (*Ttc30a2, Sdccag8, Mllt4, Azi1, Ttc28, Ccdc63* and *Spag1).* Three of these showed correlation between mRNA levels and phenotype (*Azi1, Ccdc63* and *Spag1*), making them the top confidence hits from my screen, worthy of subsequent *in vivo* follow-up. Importantly, the reduction in cilia numbers upon *Azi1* siRNA addition was confirmed with further siRNAs to the 3' UTR of *Azi1* and this could be rescued by overexpression of tagged Azi1-GFP lacking the *Azi1* 3'UTR. *Azi1, Ttc30a2* and *Spag1* knockdown also lead to a significant reduction in cilia length.

5.7.1 Variation in cilia function readout.

The cilia function readout, which utilised the *Gli-luciferase* gene in ShhLIGHT-II cells, to analyse Hh signalling as an indirect readout of cilia function, proved too variable both within and between plates, and problems with cell death meant many plates could not be analysed. It appeared the assay worked to some extent because *Ift88* siRNA addition gave a significant reduction in fold response of *Gli-luciferase* to purmorphamine over five experiments (Figure 5.2A). On the plates which were

successfully analysed, 14 out of 16 genes lead to impaired Hh signalling upon knockdown (Figure 5.2B). This assay has proved very sensitive in other screens (Evangelista et al., 2008; Lai et al., 2011), however in our experience, this assay seemed to give a phenotype more often than siRNAs successfully knockdown mRNA (Figure 4.5A, 4.2C, 4.2D, 4.3, 5.2 and 5.4), so it is possible variation in the system is creating false-positive results. It is unclear why such variation in results and problems with cell death occurred. For any future screens, perhaps it would be worth considering a *Gli-GFP* reporter line (Stamataki et al., 2005). This would allow streamlining of the two readouts with my Arl13b-mKate2 construct such that analysis of ciliogenesis and cilia function could in the future be done in parallel on the Scan^{R} microscope. This would eliminate the need for replicate plates for the second readout, allowing cells and reagents to be used for technical triplicates that would help the statistical analysis (see below). Again this would have to be re-tested and optimised to gauge the degree of variation seen by this method. Also further optimisation to avoid cell death upon transfection and then drug treatment would be needed.

5.7.2 The first-pass screen identifies 12 candidate genes involved in cilia formation.

The imaging based analysis for cilia formation gave more reproducible results, with significant difference between negative and positive controls across plates. In the first-pass screen, using two statistical analyses to detect hits, thirteen genes had more than one siRNA called as a hit, with significant overlap between the methods used, suggesting they are calling hits correctly. Twelve genes were chosen for validation by follow-up screens. With hindsight, due to the variation in repeat rate, perhaps the screen would have been improved by performing all 37 genes with technical triplicates as the first-pass screen, to reduce the chance of false negatives. Candidates could then have been repeated in another cell line, such as IMCD3 for further validation. The fact the first-pass screen did not include technical replicates should not affect the false positive rate, so although we may have missed hits by not performing repeats at the time, any hits we do get are still valid.

Interestingly, *Wdr35* had two siRNAs which significantly reduced cilia number, one of which also reduced cilia length. This agrees with the results presented in Chapter Three showing *Wdr35* is essential for ciliogenesis, and acts as validation for the screen. This gene was not followed up with secondary screening as we have already analysed the phenotype of *Wdr35* mutant cilia in detail (Chapter 3).

5.7.3 Genes which affect cilia number

Twelve genes identified as giving a reduction in cilia numbers in the first-pass screen were followed up by repetition in the same cell line as well as in IMCD3 cells. No siRNA gave an entirely reproducible phenotype, showing there is still variation in the assay. Indeed, NPI scores in some cases varied greatly between repeats of the same siRNA in the same cell types (Table 5.5). This assay is inherently quite noisy, ciliogenesis can be influenced by many factors including cell density and the degree of cell cycle arrest, and although we tried to control for such variation this was not entirely successful. The data we have on the variation in cell cycle arrest (summarised in Table 5.1 and 5.8), however, suggests it is not linked to the variation in phenotype in many cases, suggesting there are other factors influencing variation which could also include differences in transfection efficiency. Despite this, as a screening tool the approach was successful as we were able to identify genes which gave a fairly reproducible phenotype with some siRNAs giving a hit in 4 out of 5 repeats.

Table 5.5 summarises the results of the second-pass screen, with the genes ordered roughly by the degree of reproducibility of the phenotype. It is difficult to decide what constitutes a reproducible phenotype, but a line was drawn and it was decided that knockdown of *Tscot, Prdm1, Bbs5, Epb4.1l4b* and *Prdm2* do not reproducibly reduce cilia numbers, as no individual siRNA gave a hit in more than 3/5 repeats.

Therefore seven genes, *Ttc30a2, Sdccag8, Mllt4, Azi1, Ttc28, Ccdc63* and *Spag1* give fairly reproducible results. mRNA levels were examined, eight out of the twelve genes in the second-pass screen had detectable expression in ShhLIGHT-II cells, by qPCR. The four that failed were *Prdm1, Prdm2, Ttc28* and *Tscot*; only one

primer pair/probe combination was tried so this could reflect technical problems. Alternately, it is possible that some of these genes are not expressed in ShhLIGHT-II, which would mean the observed reduction in cilia must be due to off target effects; this theory is supported by the fact that 3/4 genes for which no expression was detected did not give reproducible phenotypes. Three genes, *Azi1, Spag1* and *Ccdc63* showed mRNA: phenotype correlation, suggesting the phenotype is not due to off-target siRNA effects. In the case of knockdown by *Azi1* siRNA treatment, the reduction in cilia upon *Azi1* siRNA treatment was further confirmed with additional siRNAs to the 3'UTR of *Azi1,* which could be fully rescued by overexpression of Azi1-GFP lacking *Azi1* 3' UTR. Therefore the reduction in cilia is due to a reduction in Azi1 levels and not due to off-target effects of the siRNA. This identifies *Azi1* as a top-confidence hit from the screen and suggests *Azi1* has a role in mammalian ciliogenesis.

For two of the three genes which gave reproducible phenotypes but which did not correlate with mRNA (*Sdccag8* and *Ttc30a2*), there is published information to suggest they do have roles in ciliogenesis in other organisms (Dave et al., 2009; Fan et al., 2010; Otto et al., 2010; Ou et al., 2005; Pathak et al., 2007). As a single primer/probe set per gene was used, it is possible the qPCR results are inaccurate and these phenotypes do not result from off-target effects. This could be further investigated by checking if protein levels correlate with phenotype or by rescue experiments, overexpressing an siRNA insensitive version of the gene to see if it restores cilia number.

5.7.4 Genes which affect ciliary length

In the first-pass screen, nine genes which had at least two siRNAs that reduced cilia length were identified, of which four (*Spag1*, *Ebp4.1l4b*, *Bbs5* and *Tcte3*) also reduced cilia number and five (*Wdr60, Fam92b, Catnb, Tctex1d1* and *Tctex1d2*) which affect cilia length independently of number (Table 5.4). As the original aim of the screen was to identify genes involved in cilia formation, we only followed up hits which affected cilia number, or cilia number and cilia length. However in future it would be interesting to follow up hits which affect cilia length without affecting cilia number.

Cilia length is known to be a carefully controlled process, and many cell types have cilia of different average lengths. Cilia length control is important for motile cilia as it can affect the ability to generate flow (Ishikawa and Marshall, 2011). Length is also important in primary cilia: tuberous sclerosis *Tsc1* and *Tsc2* knockout mice develop kidney cysts with longer cilia (Bonnet et al., 2009; Hartman et al., 2009; Ishikawa and Marshall, 2011). Interestingly one of the genes identified as possibly affecting cilia length in the first-pass screen, *Catnnb,* encodes β-catenin, a key protein in the canonical Wnt signalling pathway. Many studies have suggested cilia may be involved in transducing the Wnt signalling pathway, although this link remains controversial (reviewed in (Wallingford and Mitchell, 2011) and see 1.3.2.2). It has also been suggested that non canonical Wnt signalling/PCP may have a role in controlling ciliogenesis (Heydeck et al., 2009; Oishi et al., 2006; Park et al., 2006; Park et al., 2008; Zeng et al., 2010). However, a role for β-Catenin and canonical Wnt signalling in the control of ciliogenesis is less well characterised, although one recent study suggests canonical Wnt signalling and β-Catenin may control ciliogenesis via Foxj1 (Caron et al., 2012). Therefore it would be interesting to follow up genes which affect cilia length and not number to see if the phenotype is reproducible.

Table 5.6 shows cilia length results from the second-pass screen. As seen with cilia number, there is variability between repeats, and some genes gave a more reproducible phenotypes than others. Most siRNAs which gave a significant change in cilia length lead to a reduction in cilia length, although unlike the first-pass screen, there were also examples of siRNAs giving an increase in length.

It should be noted that images from which the lengths were measured were only taken in one z plane, and this could affect the accuracy of measurements, especially in IMCD3 cells, in which cilia tend to project perpendicular to the glass, and so in future screens it may be worth taking images in several z planes to aid length measurements, and this may also aid cilia identification. As the Scan^{R} (Olympus) is a light microscope based system it may be worth considering systems such as the Opera High Content Screening System (Perkin-Elmer) which is a confocal microscope based system and so gives enhanced resolution in the z plane.

Three genes gave a fairly reproducible reduction in cilia length upon siRNA knockdown: *Azi1, Spag1* and *Ttc30a2*. Interestingly, these also gave reproducible reductions in cilia number, perhaps a reduction in cilia length is a milder version of the same phenotype that leads to reduction in cilia numbers. Of these, only *Spag1* was identified as a candidate for affecting cilia length in the first-pass screen, it was only with repeats that the effect of *Azi1* and *Ttc30a2* on length became apparent, thus highlighting the need for repeats in siRNA screens.

5.7.5 No genes reproducibly affected centrosome number

Centrosome numbers were also recorded. In the first-pass screen at least three siRNAs to *Ccdc114* and *Zmynd10* lead to an increase in the number of cells with more than two centrosomes, and conversely at least three siRNAs to *Pp3r1, Wdr15* and *Wdr60* lead to a decrease in the number of cells with more than two centrosomes (Table 5.1). However, as the focus of this screen was cilia not centrosomes these genes were not followed up in the second-pass screen. As many of these siRNAs were on the same plate it is possible this is due to another external factor and is not a result of the siRNA knockdown, nevertheless it would be interesting to perform repeats to address this. Of the genes that were followed up in the second-pass screen, no gene gave a reproducible change in the number of centrosomes (Table 5.7), and although we cannot rule out a role in centrosome biology, this suggests these genes are not involved in controlling centrosome number.

5.7.6 Screen identified novel genes with roles in cilia formation as well as known genes with new roles in ciliogenesis

5.7.6.1 Sdccag8 is mutated in ciliopathies

Sdccag8 siRNA knockdown gave a reproducible reduction in cilia numbers, however mRNA levels do not correlate with knockdown. *SDCCAG8* was subsequently shown to be mutated in retinal renal ciliopathy patients (Otto et al., 2010). Here, they

showed Sdccag8 may be involved in cell polarity; as well as localising to the centrosome, Sdccag8 also localised to the cell-cell junctions. siRNA knockdown of *Sdccag8* in spheroid cultures of IMCD3 cells disrupts formation of a correctly polarised ciliated lumen, and this defect is rescued by overexpressing human SDCCAG8. This is an interesting 3D system that could be utilised as a further way of investigating possible roles of some of the genes identified by this screen in cell polarity and ciliogenesis, such as *Afadin/Mllt4*.

If Sdccag8 is required for cell polarity, then it is possible the phenotype we observed in our monolayer culture could be due to off-target effects as suggested by the lack of mRNA-phenotype correlation. However, protein localization studies by myself and Otto et al., (2010) showed there is a strong pool of Sdccag8 in the base of primary cilia in monolayer RPE-1 and ShhLIGHT cells (Figure 5.5 and data not shown). Further fluorescent tagging experiments could be used to validate localization and siRNA knockdown.

5.7.6.2 Ttc30a2 is the orthologue of the IFT-B protein IFT70

Several genes included in this screen were one-to-many predicted orthologues from *D. melanogaster* to *M. musculus*. In such cases, all of these putative genes were targeted by siRNAs in our screen. *Ttc30a2* knockdown gave a reproducible reduction in cilia number and length, however, like *Sdccag8*, mRNA levels did not correlate with phenotype. Evidence from other organisms suggests Ttc30a2 may have a role in ciliogenesis (Dave et al., 2009; Fan et al., 2010; Ou et al., 2005; Pathak et al., 2007). In *C. elegans* the *Ttc30a2* orthologue *Dyf-1* it has a role in controlling the homodimeric Osm-3 kinesin motor (Ou et al., 2005), which is required for IFT of specialised cilia in *C. elegans*. In *D. rerio*, *Ttc30a2/Fleer* is thought to play a role in polyglutamylation of tubulin and is important for the B tubules of the outer doublet microtubules (Pathak et al., 2007). Finally in *C. reinhardtii* it was biochemically identified as a component of the IFT-B complex (Fan et al., 2010). However, nothing is known about the function of mammalian Dyf-1/IFT70 , and indeed there are three predicted mammalian orthologues , *Ttc30a1*, *Ttc30a2* and *TTc30b*. All were included in the initial screen, but only *Ttc30a2* knockdown gave a reduction in

cilia numbers and length suggesting *Ttc30a2* may be the functional orthologue of *Dyf-1/IFT70*. If the lack of phenotype/RNA correlation can be resolved by rescue experiments or examination of protein levels, it would be interesting to study this gene further, for example by localisation studies now that a commercial antibody is available. Furthermore, cloning and tagging the gene to perform rescue studies as well as live-imaging to see if it undergoes IFT would be useful. Finally functional analysis of other markers, particularly post-translational modifications of tubulin, upon siRNA knockdown would be very informative. These studies are on-going.

5.7.6.3 *Spag1* knockdown leads to a reduction in cilia number and length

Three genes, *Spag1, Azi1* and *Ccdc63* gave good correlation between mRNA level and phenotype, suggesting these results are not due to off target effects. *Spag1* and *Azi1* knockdown also reduces cilia length.

Spag1 is a sperm-associated gene with TPR repeats, which are commonly enriched in ciliary genes (Jekely and Arendt, 2006). *Spag1* is reported to only be expressed in the testes (Silina et al., 2011; Takaishi and Huh, 1999), although our detection of the mRNA in mouse fibroblasts suggest it may be more widely expressed. It was identified as a putative ciliary gene in a genome comparison screen (Li et al., 2004). Infertility, which is a possible ciliopathic phenotype (Neesse et al., 2007), was linked to *SPAG1* in a single case, however in this case the female patient expressed antibodies to Spag1 causing sperm agglutination, which does not fit clearly with a role for Spag1 in ciliogenesis. Little is known about the role of Spag1 in mouse and further work is needed to establish whether Spag1 plays a role in mammalian ciliogenesis.

5.7.6.4 Azi1 localises to ciliary base and knockdown affects ciliogenesis and cilia length.

The risk of false negatives in the screening strategy is highlighted by *Azi1*. Only one siRNA to *Azi1* gave a reduction in cilia number and cilia length in the first-pass screen, but despite this, we decided to pursue it in the second round of screening because it was biologically interesting (Ma and Jarman, 2011; Wilkinson et al.,

2009), and because the phenotype observed was one of the most significant decrease in cilia number seen in the screen. *Azi1* had been followed up by our collaborators who carried out the original expression screen in *Drosophila*, and had been shown to have ciliary role in fly (Ma and Jarman, 2011). It had also been published to have ciliary roles in zebrafish (Wilkinson et al., 2009), but little was known about the mouse protein

In the second-pass screen, it did repeat fairly well and the phenotypes observed correlated with mRNA levels (Figure 5.4). The phenotype was confirmed with further siRNAs to *Azi1* and was rescued by overexpressing an siRNA insensitive GFP tagged version of the gene (Figure 5.7). Azi1 localisation to the centrosome is consistent with a ciliary role in mouse (Figure 5.5). This gene is studied in more detail in Chapter Six of the thesis, by generating a mutant mouse line. However here, the single hit *of Azi1* in the first pass screen highlights the risk of false negatives inherent to such a screening strategy. The screen is, by design, not comprehensive, but despite this is a powerful means to identify genes of interest for future studies.

5.7.6.5 Ccdc63 is a novel coiled-coil domain containing protein which may be involved in cilia formation and cilia stability.

Ccdc63 is an uncharacterised coiled coil domain protein, with no known link to ciliogenesis. siRNA knockdown reproducibly leads to a reduction in cilia numbers and mRNA levels correlate with phenotype suggesting it is not due to off-target effects of siRNAs. Preliminary studies suggest it localises to the cilia and basal body, albeit with weak expression (Figure 5.5C). It would be useful to confirm this, either by further antibodies or by tagging the gene for overexpression studies. This could be useful to confirm the phenotype is not due to off-target effects by rescuing the phenotype with an siRNA insensitive cDNA version of the gene. The phenotype of *Ccdc63* siRNA treated cells was examined further by looking at ciliogenesis in real-time, suggesting *Ccdc63* affects cilia stability as well as cilia number. It would be interesting to study other hits using the live-imaging system as it may identify genes which affect the ciliogenesis process at different specific time points.

These results suggest that *Ccdc63* is a novel gene involved in cilia formation and stability and it would be interesting to study the role Ccdc63 plays in ciliogenesis further. Further studies could involve characterisation of the ciliary phenotype of siRNA knockdown in detail, with markers for different structures within the cilium such as the axoneme, transition zone and basal body. Longer-term strategies could include the generation of a mutant mouse line to assess the role of *Ccdc63 in vivo*.

5.7.6.6 Other possible hits

Other genes which gave reproducible reduction in cilia numbers when knocked down include *Mllt4/Afadin* and *Ttc28. Ttc28,* like *Ttc30a2* is a tetratricopeptide repeat protein of unknown function. Tetratricopetide repeats are protein interaction mediating domains enriched in ciliary proteins, including Ift88, Wdr35, Wdr19, Ift172 and Ift140 (Jekely and Arendt, 2006). No mRNA expression was detected for *Ttc28*, suggesting it may not be expressed in these cells, although only one primer set was tested so this could be a technical issue. A search of expression databases suggest *Ttc28* is fairly widely expressed, including in fibroblasts, reinforcing the suggestion that the lack of expression detection is due to technical issues. Further studies, such as more detailed expression studies, localisation studies, rescue experiments and live imaging studies are needed to confirm whether this gene is involved in cilia formation or function.

Mllt4 encodes afadin, an actin-filament binding protein that is essential for the structural organisation of adherens junctions, and has roles in apicobasal polarity (Takai et al., 2008). Interestingly, apicobasal polarity has been shown to have links to ciliogenesis. Transmembrane protein Crb3 has roles in establishing apicobasal polarity and tight junction formation, in a complex with Pals1 and Patj, along with the Par3-Par6-aPKC. Crb3 has also been shown to localise to the cilia, and either knockdown of *Crb3* or blocking aPKC inhibits ciliogenesis (Bossinger and Bachmann, 2004; Fan et al., 2004a). This is reminiscent to the proposed role in apicobasal polarity for Sdccag8 discussed earlier. Similarly, another set of renal retinal ciliopathy proteins, the Nphp1,4,6 complex also localize to cell-cell junctions, in addition to the transition zone (Delous et al., 2009; Sang et al., 2011). As mentioned, our Mllt4/Afadin mRNA levels did not correlate with phenotype so it is

possible the phenotypes are due to off-target effect. However, a recent knockdown study of *Afadin/Mllt4* in NIH-3T3 cells, validated at a protein level (Miyata et al., 2009), showed reorientation of the cells' Golgi leading edge was impaired and migration to PDGF ligand disrupted. Importantly, this mimics migratory defects seen when signalling through PDGFRα-cilia axis is perturbed (Schneider et al., 2010; Schneider et al., 2005). Future investigation into the role of Afadin/Mllt4 cross-talk between the actin cytoskeleton and cilia signalling could provide further links between apicobasal cell polarity and ciliogenesis.

5.7.7 Screen summary and future directions

In summary, the most interesting and promising hits identified in the screen are *Azi1* and *Ccdc63*. *Azi1* has some known links to ciliogenesis; it was identified in a proteomic and genomic screens for ciliary genes and zebrafish morphants and *Drosophila* mutants have ciliary phenotypes (Avidor-Reiss et al., 2004; Li et al., 2004; Ma and Jarman, 2011; Pazour et al., 2005; Wilkinson et al., 2009). However the role of mouse *Azi1* is not well characterised; it is published to be expressed in elongating spermatids and localises to the acrosome of the developing sperm (Aoto et al., 1995). The role of mouse Azi1 will be examined in more detail in Chapter Six of this thesis.

In contrast, little is known of *Ccdc63*. It has no known previous link to cilia, except for the fact it was identified as highly expressed in fly ciliated sensory neurons, and hence was included in this screen (Cachero et al., 2011). This demonstrates that this screen can both further characterise the role of suspected ciliary genes in mammalian ciliogenesis, and also identify novel ciliary genes, with no previous link to ciliogenesis.

Several improvements to the screen could be made if it were to be scaled up to screen new libraries or whole genome collections of knockdown reagents. Using 3T3-Arl13b-mK2 stable cell lines would enable the measurement of the dynamics of ciliogenesis in real time. By incorporating additional fluorescent readouts of cilia function such as *Gli-GFP* (Stamataki et al., 2005) or markers for centrioles/basal

bodies such as Centrin2-eGFP, several readouts could be measured at once in real-time. It may also be useful to include further controls for other factors which could influence ciliogenesis. Controls for cell cycle were included, using DAPI intensity as a readout of cell cycle status, however more accurate measaurements could be made by using markers of the cell cycle, or even using the Fucci construct (Invitrogen), a commercially available plasmid encoding fluorescently labelled, rapidly degraded cell cycle markers, which allows analysis of the cell cycle in real time. It may also be useful to analyse cell polarity, by adding markers of the apical or basal cell surface, for example laminin (basal) or phalloidin (which stains actin found at the basal surface of polarised cells), as cell polarity has been shown to influence ciliogenesis (Dawe et al. 2009; Bossinger and Bachmann 2004; Fan et al. 2004a). This would be more relevant in the IMCD3 cell line, as the ShhLIGHT-II cells are not a polarised cell line. Due to restraints of the number of colours that can be imaged simultaneously, decisions would need to be made about which controls are most relevant to be included in the first pass screen, and which would be included in follow-up, functional characterisation studies.

Use of short hairpin RNAs (shRNAs) would allow a longer window of knockdown and generation of stable lines for continued analysis. Regardless of the reagents used, in order to scale up, a faster, automated method of transfection or infection is needed to increase speed and decrease risk of human error. Imaging on an automated high content confocal system like the PerkinElmer's Opera® High Content Screening System would greatly improve resolution in 4D on live cells. A genome-wide siRNA screen of genes involved in cilia formation and function has yet to be published, and this would be a very interesting project, allowing unbiased discovery of novel ciliary genes.

Another point to consider is that the majority of screens, including mine, have focused on cells with primary cilia given their ease of culture. However, motile cilia are equally important to human health, as shown by mutations in primary cilia dyskinesia (PCD). As *D. melanogaster* chordotonal neurons have modified sensory motile cilia, it is possible some of the genes included in our screen are dispensable for primary cilia, but required for motile cilia function. This is true for *Zmynd10*

which did not give a hit for either cilia number or length. *Zmynd10* is enriched in testis, and very recently, human *ZMYND10* was one of 372 genes linked to motile cilia function by expression profiling of bronchial biopsies from patients with PCD (Geremek et al., 2011). In yeast 2 hybrid screens, the *Drosophila* orthologue interacts with *tilB*, a gene recently shown to be involved in axonemal dynein arm assembly (Kavlie et al., 2010). Although not amenable to a high–throughput screen pipeline, motile multi-ciliated tracheobronchial epithelial cultures infected with shRNAs could question the functional role of candidate genes

Our lab's expertise in mutant mouse generation and phenotyping, utilising the mutant mouse resources (such as Knockout Mouse Project (KOMP), the European Conditional Mouse Mutagenesis Program (EUCOMM) and Sanger Institute Gene Trap Resource (SIGTR)), to access mutant mouse lines, meant we were well aligned to analyse the role of candidate genes *in vivo*. This is demonstrated in the next chapter, where the *in vivo* role of one hit, *Azi1*, is examined in detail.

Table 5.1 First-Pass Screen Readout One Results

siRNA	Cilia number					Cilia length			Cell Cycle	Centrosome number	
	No. cells with 1 cilia	No. cells with 0 cilia	% cells with 1 cilia	NPI	Fisher's Test p value	MFD (arbitary units)	Wilcoxon p value to Neg	Wilcoxon p value to *GFP*	% Cells in G2	% cells with >2 cent	Fisher's Test p value
Neg	324	349	48.14264			14.10959			11.293	3.8462	
Gfp	308	261	54.13005			15.20573			11.478	6.229	
Ift88 3	78	385	16.84665		1.5E-29	10.71471	5E-09	5E-10	14.433	3.2328	
Cda 1	280	234	54.47471	-0.1282	1	14.05838	1	0.153	15.679	0	1
Cda 2	208	243	46.11973	0.1926	1	13.48507	1	0.004	16.068	2.5	1
Cda 3	144	228	38.70968	0.4771	0.083643	13.87677	1	0.437	17.016	4.9251	1
Cda 4	197	214	47.93187	0.12303	1	13.84547	1	0.129	14.151	4.2328	1
Cda Pool	58	61	48.7395	0.09202	1	13.46832	1	1	17.213	9.2857	1
Ttc30b 1	372	296	55.68862	-0.1748	1	14.45193	1	1	15.679	4.9587	1
Ttc30b 2	196	182	51.85185	-0.0275	1	14.15269	1	1	16.098	12.621	1
Ttc30b 3	368	242	60.32787	-0.3529	0.324378	15.46724	8E-06	1	13.473	6.015	1
Ttc30b 4	367	244	60.06547	-0.3428	0.485313	14.58764	1	1	12.371	3.4109	1
Ttc30b Pool	336	301	52.74725	-0.0618	1	14.50547	1	1	16.176	4.6225	1
Ttc30a1 1	220	208	51.40187	-0.0102	1	10.71471	5E-09	5E-10	33.333	2.8788	1
Ttc30a1 2	423	344	55.14993	-0.1541	1	14.83613	1	1	20.435	4.4843	1
Ttc30a1 3	died	died				15.05417			11.951	3.7221	
Ttc30a1 4	201	140	58.94428	-0.2998	1	15.49153	0.05	1	11.765	4.0541	1
Ttc30a1 Pool	113	99	53.30189	-0.0831	1	15.69003	0.088	1	12.917	4.4053	1
Neg	255	99	72.0339			16.85772			10.891	2.2099	
Gfp	195	84	69.89247			17.1318			13.652	1.0309	
Ift88 3	38	87	30.4		4.16E-12	17.83081	1	1	13.907	7.7465	
Ift88 4	33	184	15.20737		1.43E-36	11.53203	3E-07	3E-06	24.664	7.2398	
Ttc30a2 1	146	97	60.0823	0.22593	1	15.16451	0.318	0.28	15.538	1.1952	1
Ttc30a2 2	86	87	49.71098	0.44129	0.001386	15.36239	1	1	32.065	5.4348	1
Ttc30a2 3	300	141	68.02721	0.06096	9.54E-06	17.83405	1	1	12.551	4.7109	1

	Cilia number					Cilia length			Cell Cycle	Centrosome number	
Ttc30a2 4	71	112	38.79781	0.66789	1	13.83031	2E-04	5E-04	14.01	6.2827	1
Ttc30a2 Pool	157	109	59.02256	0.24794	1	16.68137	1	1	23.427	3.2143	1
Spag1 1	139	162	46.1794	0.51462	1.53E-07	14.43602	0.006	0.008	45.246	6.2295	1
Spag1 2	117	118	49.78723	0.4397	0.000223	16.21814	1	1	45.2	4.8	1
Spag1 3	175	69	71.72131	-0.0157	1	16.13807	1	1	6.4	1.6	1
Spag1 4	76	111	40.64171	0.62961	1.1E-08	14.96343	0.532	0.599	22.222	8.4656	0.1901819
Spag1 Pool	100	181	35.58719	0.73456	1.04E-15	14.27639	0.007	0.01	34.948	2.4221	1
Azi1 1	226	88	71.97452	-0.021	1	17.70132	1	1	10.843	1.2308	1
Azi1 2	232	83	73.65079	-0.0558	1	17.21959	1	1	8.2857	1.5576	1
Azi1 3	12	112	9.677419	1.27256	4.16E-31	10.51255	0.003	0.005	15.971	0	1
Azi1 4	124	92	57.40741	0.28148	0.577367	15.1876	0.7	0.675	23.077	8.1448	0.191
Azi1 Pool	198	143	58.06452	0.26783	0.227798	16.32718	1	1	18.457	3.6111	1
Wdr35 1	159	126	55.78947	0.31507	0.047377	15.7421	1	1	17.687	3.7415	1
Wdr35 2	85	132	39.17051	0.66015	1.08E-10	13.26047	2E-06	1E-05	13.913	3.1111	1
Wdr35 3	280	140	66.66667	0.08921	1	16.90496	1	1	10.577	2.746	1
Wdr35 4	138	128	51.8797	0.39626	0.000856	15.54382	1	1	12.367	5.3957	1
Wdr35 Pool	73	48	60.33058	0.22078	1	15.76453	1	1	18.121	10.87	1
Neg	304	95	76.19048			19.85645			9.8214	20.951	
Gfp	231	95	70.8589			18.45205			7.6789	21.16	
Ift88 3	30	348	7.936508		9.09E-80	10.67338	7E-15	5E-13	26.914	16.391	
Ift88 4	46	300	13.2948		7.89E-61	12.71943	5E-15	1E-12	33.511	32.042	
Wdr60 1	460	138	76.92308	-0.054	1	21.44257	0.076	5E-08	15.796	17.185	1
Wdr60 2	360	108	76.92308	-0.054	1	17.20274	2E-12	2E-04	12.592	8.3736	6.791E-12
Wdr60 3	150	83	64.37768	0.1454	1	17.43399	0.026	1	13.636	4.7244	7.873E-16
Wdr60 4	74	278	21.02273	0.83457	2.5E-37	13.12401	2E-16	2E-16	22.717	0	2.293E-73
Wdr60 Pool	392	117	77.01375	-0.0555	1	19.98569	1	0.138	10.145	1.4134	3.236E-42
Wdr78 1	451	172	72.39165	0.01801	1	19.19706	1	1	17.098	6.0606	9.142E-19
Wdr78 2	309	147	67.76316	0.09159	1	14.77088	0.198	1	22.251	14.804	0.0312193
Wdr78 3	died	died									
Wdr78 4	411	182	69.3086	0.06702	1	19.72801	1	0.598	12.394	0	1.056E-13
Wdr78 Pool	156	80	66.10169	0.118	1	17.65351	8E-04	1	11.549	2.9718	2.308E-48
Wdr16 1	288	133	68.40855	0.08133	1	19.84139	1	0.496	7.1197	3.2538	1.928E-10

	Cilia number					Cilia length			Cell Cycle	Centrosome number	
Wdr16 2	411	197	67.59868	0.0942	1	18.45044	0.388	1	11.856	6.383	2.049E-07
Wdr16 3	394	157	71.50635	0.03208	1	19.01102	1	1	11.628	9.0909	0.0904359
Wdr16 4	397	174	69.52715	0.06354	1	18.85321	1	1	13.343	5.9816	3.919E-11
Wdr16 Pool	430	148	74.39446	-0.0138	1	19.19706	1	1	8.0282	3.5088	1.903E-14
Pp3r1 1	492	199	71.20116	0.03693	1	18.94307	1	1	17.64	6.7925	8.394E-18
Pp3r1 2	476	162	74.60815	-0.0172	1	20.1418	1	0.129	12.114	5.0139	5.451E-28
Pp3r1 3	378	180	67.74194	0.09192	1	18.30226	0.148	1	14.562	8.4006	1.009E-07
Pp3r1 4	454	195	69.95378	0.05676	1	18.90506	1	1	15.006	6.5596	6.261E-25
Pp3r1 Pool	401	152	72.51356	0.01607	1	18.85224	1	1	12.142	5.3797	6.405E-21
Neg	426	264	61.73913			18.53102			17.082		
Gfp	291	273	51.59574			16.78051			22.036		
Ift88 3	214	443	32.5723		2.75E-16	14.23273	1E-13	0.001	27.151		
Ift88 4	84	195	30.10753		1.55E-11	16.75895	0.007	1	17.594		
Wdr92 1	324	195	62.42775	-0.2274	0.169633	17.89969	1	1	14.504		
Wdr92 2	287	170	62.80088	-0.2422	0.33991	18.66184	1	0.013	10.949		
Wdr92 3	228	214	51.58371	0.20072	4.29E-08	17.96729	1	1	15.324		
Wdr92 4	150	130	53.57143	0.12224	4.77E-05	16.11799	0.004	1	14.839		
Wdr92 Pool	203	232	46.66667	0.39486	2.45E-12	15.52606	2E-06	1	18.125		
Ttc26 1	195	238	45.03464	0.45929	0.038488	15.81302	5E-06	1	24.547		
Ttc26 2	421	235	64.17683	-0.2965	1	18.65951	1	0.027	18.4		
Ttc26 3	409	185	68.85522	-0.4812	0.009392	19.36882	1	2E-06	14.047		
Ttc26 4	96	137	41.20172	0.61063	0.011886	15.75926	0.005	1	28.163		
Ttc26 Pool	284	312	47.65101	0.35599	0.32712	16.07001	9E-07	1	15.873		
Ttc28 1	716	382	65.20947	-0.3373	1	17.35098	0.014	1			
Ttc28 2	433	291	59.80663	-0.1239	1	17.49008	0.875	1	21.945		
Ttc28 3	384	202	65.52901	-0.3499	0.428248	18.50958	1	0.026	12.981		
Ttc28 4	74	173	29.95951	1.0545	9.12E-08	15.11257	4E-04	1	31.621		
Ttc28 Pool	158	198	44.38202	0.48506	3.07E-09	15.05432	2E-08	0.354	30.376		
Epb4.1l4b 1	459	270	62.96296	-0.2486	1	17.7592	1	0.007	20.193		
Epb4.1l4b 2	201	153	56.77966	-0.0044	1	17.30048	1	1	19.241		
Epb4.1l4b 3	279	136	67.22892	-0.417	0.017407	17.67649	1	1	13.182		
Epb4.1l4b 4	134	235	36.31436	0.8036	0.017407	14.11635	2E-16	4E-07	31.983		

	Cilia number					Cilia length			Cell Cycle	Centrosome number	
Epb4.1l4b Pool	135	250	35.06494	0.85293	1	14.38646	3E-09	0.03	20.551		
Neg	176	171	50.72046			14.64734			10.571		
Gfp	241	139	63.42105			16.54388			11.026		
Ift88 1	107	211	33.6478		2.34E-07	13.85738	0.603	0.001	12.15		
Ift88 2	166	164	50.30303		1	14.54169	1	0.727	10.386		
Ccdc151 1	159	158	50.15773	0.45796	1	14.91581	1	1	9.2437		
Ccdc151 2	194	156	55.42857	0.10879	1	14.22803	1	0.022	14.674		
Ccdc151 3	123	166	42.56055	0.96124	0.017407	14.05469	1	0.105	16.563		
Ccdc151 4	died	died									
Ccdc151 Pool	134	111	54.69388	0.15746	1	15.61227	1	1	15.033		
Rp23-464C2.9 1	201	171	54.03226	0.20129	1	14.94773	1	1	12.5		
Rp23-464C2.9 2	188	148	55.95238	0.07409	1	15.40613	1	1	9.2697		
Rp23-464C2.9 3	died	died									
Rp23-464C2.9 4	218	183	54.36409	0.1793	1	14.68621	1	0.229	8.5158		
Rp23-464C2.9 Pool	died	died									
Tscot 1	123	168	42.26804	0.98061	0.057198	15.02808	1	0.256	15.385		
Tscot 2	170	103	62.27106	-0.3445	1	16.37578	1	1	19.257		
Tscot 3	died	died									
Tscot 4	123	164	42.85714	0.94159	0.102252	14.13265	1	0.009	16.216		
Tscot Pool	253	199	55.97345	0.07269	1	14.36616	1	0.003	14.017		
Sdccag8 1	148	211	41.22563	1.04967	0.005853	12.92702	0.003	2E-09	5.1351		
Sdccag8 2	223	122	64.63768	-0.5013	1	15.0659	1	1	10.989		
Sdccag8 3	111	170	39.50178	1.16387	0.003061	16.70281	1	1	19.672		
Sdccag8 4	99	141	41.25	1.04806	0.046877	17.81929	1	1	15.294		
Sdccag8 Pool	70	105	40	1.13086	0.081016	16.49609	1	1	15.676		
Neg	432	250	63.34311			15.82967			12.411		
Gfp	450	443	50.39194			15.65544			21.882		
Ift88 3	401	387	50.88832		1	14.26158	2E-08	1E-05	15.012		
Ift88 4	181	412	30.52277		1.17E-18	14.11745	9E-05	0.004	11.725		
Lrrc48 1	467	293	61.44737	-0.2674	1	16.04449	1	1	15.182		
Lrrc48 2	300	277	51.99307	0.31027	1	16.26742	1	1	12.137		
Lrrc48 3	340	367	48.09052	0.54874	0.814837	15.00241	0.204	1	12.859		

	Cilia number					Cilia length			Cell Cycle	Centrosome number	
Lrrc48 4	357	244	59.401	-0.1424	1	15.57664	1	1	10.112		
Lrrc48 Pool	died	died									
Fam92a 1	303	407	42.67606	0.87959	0.000106	15.12494	0.987	1	9.7222		
Fam92a 2	280	284	49.64539	0.45373	1	14.26524	7E-07	2E-04	17.463		
Fam92a 3	401	298	57.36767	-0.0181	1	15.25837	1	1	10.069		
Fam92a 4	died	died									
Fam92a Pool	died	died									
Fam92b 1	died	died									
Fam92b 2	375	358	51.15962	0.3612		15.30685	9E-09	5E-06	9.1877		
Fam92b 3	370	427	46.42409	0.65057	0.049109	14.12581	3E-09	2E-06	11.247		
Fam92b 4	394	337	53.89877	0.19383	1	14.04731	4E-07	2E-04	7.651		
Fam92b Pool	died	died									
Catnb 1	336	333	50.22422	0.41836	1	14.33254	1E-05	0.002	8.0409		
Catnb 2	513	272	65.35032	-0.5059	0.060024	16.359	0.856	0.002	13.51		
Catnb 3	died	died									
Catnb 4	307	355	46.37462	0.65359	0.099289	14.39411	2E-05	0.002	6.8554		
Catnb Pool	died	died									
Neg	411	375	52.29008			16.79041			16.918		
Gfp	275	278	49.72875			17.16542			8.9286		
Ift88 3	128	267	32.40506		6.58E-07	15.69603	1	0.174	19.154		
Ift88 4	93	171	35.22727		0.004273	16.54889	0.053	0.005	16.716		
Bbs5 1	111	227	32.84024	1.05676	8.99E-06	14.19982	8E-06	2E-07	24.26		
Bbs5 2	126	262	32.47423	1.07805	1.12E-06	14.9198	0.002	6E-05	16.113		
Bbs5 3	307	247	55.41516	-0.2562	1	15.61185	0.026	0.001	12.057		
Bbs5 4	271	216	55.64682	-0.2697	1	16.19729	1	1	9.9593		
Bbs5 Pool	216	164	56.84211	-0.3392	1	15.7153	0.456	0.02	11.458		
Tctex1d2 1	275	353	43.78981	0.41991	1	13.92214	8E-16	2E-16	8.4639		
Tctex1d2 2	84	194	30.21583	1.2094	8.44E-07	13.41502	1E-08	2E-10	13.167		
Tctex1d2 3	459	339	57.5188	-0.3786	1	14.76848	5E-11	7E-13	16.865		
Tctex1d2 4	369	242	60.3928	-0.5458	0.400555	16.87675	1	1	7.9872		

	Cilia number					Cilia length			Cell Cycle	Centrosome number	
Tctex1d2 Pool	271	184	59.56044	-0.4973	1	14.67309	1	1	8.6022		
Tcte3 1	289	378	43.32834	0.44675	1	14.67221	2E-16	2E-16	8.9153		
Tcte3 2	354	202	63.66906	-0.7363	0.004892	14.76136	4E-12	2E-14	4.4484		
Tcte3 3	232	319	42.10526	0.51789	0.56041	14.79683	2E-12	1E-14	12.926		
Tcte3 4	216	263	45.09395	0.34406	1	14.88387	1E-09	5E-11	9.0349		
Tcte3 Pool	258	419	38.10931	0.7503	0.000499	14.96547	5E-09	1E-10	14.516		
Tctex1d1 1	299	214	58.2846	-0.4231	1	15.02115	5E-05	6E-07	5.3743		
Tctex1d1 2	307	181	62.90984	-0.6922	0.034767	15.03172	5E-11	3E-13	4.878		
Tctex1d1 3	326	201	61.85958	-0.6311	0.100612	15.13351	0.019	4E-04	8.2243		
Tctex1d1 4	300	239	55.65863	-0.2704	1	14.62388	1E-06	1E-08	9.6364		
Tctex1d1 Pool	166	278	37.38739	0.79229	0.001978	14.03227	2E-10	4E-12	13.274		
Neg	354	178	66.54135			17.41405			4.9908	2.7778	
Gfp	595	376	61.27703			16.13233			6.0362	6.5392	
Ift88 3	499	473	51.33745		0.000438	15.89978	3E-04	1	8.498	7.4925	
Ift88 4	231	829	21.79245		6.93E-69	12.63726	2E-16	2E-16	14.128	14.888	
Tctex1d4 1	313	244	56.1939	0.28215	1	15.35609	3E-09	1	9.7938	6.1856	1
Tctex1d4 2	528	229	69.74901	-0.2136	1	16.61899	0.88	1	7.284	8.5185	1
Tctex1d4 3	146	115	55.9387	0.29149	1	16.00278	0.074	1	12.222	5.5556	1
Tctex1d4 4	404	187	68.35871	-0.1627	1	17.07596	1	0.073	7.5041	8.1566	1
Tctex1d4 Pool	408	286	58.78963	0.18723	1	16.35006	0.096	1	10.792	15.16	0.0001384
Zmynd10 1	169	184	47.87535	0.58637	0.00085	15.59257	0.011	1	7.2626	15.775	0.000349
Zmynd10 2	370	247	59.96759	0.14415	1	16.00518	0.005	1	10.252	17.143	6.89E-12
Zmynd10 3	478	356	57.31415	0.24119	1	15.33165	2E-12	0.674	14.664	24.294	1.869E-10
Zmynd10 4	389	309	55.73066	0.2991	1	16.55775	0.721	1	14.624	15.59	4.677E-07
Zmynd10 Pool	313	244	56.1939	0.28215	1	15.70296	9E-07	1	9.7938	6.1856	1
Ccdc63 1	365	180	66.97248	-0.112	1	17.23336	1	0.003	10.932	5.5556	1
Ccdc63 2	453	204	68.94977	-0.1843	1	17.03761	1	0.347	8.8365	2.3564	1
Ccdc63 3	237	271	46.65354	0.63105	3.31E-06	14.97347	1E-09	0.561	12.646	9.3385	1
Ccdc63 4	206	234	46.81818	0.62503	1.69E-05	14.28031	5E-14	1E-04	13.004	16.368	1.17E-07
Ccdc63 Pool	447	216	67.42081	-0.1284	1	16.15058	0.002	1	10.399		
Ccdc114 1	392	234	62.61981	0.04715	1	14.87158	2E-16	5E-04	6.5053	24.763	9.86E-17

	Cilia number					Cilia length			Cell Cycle	Centrosome number	
Ccdc114 2	302	311	49.26591	0.53552	0.000114	15.31188	2E-10	0.129	11.654	19.874	2.534E-12
Ccdc114 3	252	198	56	0.28925	1	16.00181	5E-04	1	9.6567	13.519	0.0054334
Ccdc114 4	183	157	53.82353	0.36884	1	16.17689	0.115	1	14.857	12.321	0.1348223
Ccdc114 Pool	453	204	68.94977	-0.1843	1	17.03761	1	0.347	8.8365	2.3564	0.5700494
Neg	403	211	65.63518			18.02085			5.6489	1.8547	
Gfp	407	219	65.01597			16.26343			9.6386	1.6794	
Ift88 3	305	371	45.11834		1.16E-10	16.20364	3E-04	1	7.2546	3.0347	
Ift88 4	242	319	43.13725		7.95E-12	16.26343	0.003	1	7.5862	1.0619	
Prdm1 1	132	281	31.96126	1.57395	1.29E-23	14.22074	1E-12	0.055	23.487	1.6949	1
Prdm1 2	310	242	56.15942	0.43241	0.539551	19.41649	1	1	13.677	1.9538	1
Prdm1 3	469	251	65.13889	0.00881	1	16.87447	0.017	1	7.9634	3.1332	1
Prdm1 4	398	223	64.09018	0.05828	1	17.64572	1	0.144	7.396	2.1739	1
Prdm1 Pool	292	159	64.74501	0.02739	1	17.85742	1	0.049	13.017	1.6913	1
Prdm2 1	258	399	39.26941	1.22919	3.32E-18	15.04239	5E-14	0.998	19.97	4.3413	1
Prdm2 2	330	224	59.56679	0.27167	1	16.11501	6E-07	1	10.396	2.3649	1
Prdm2 3	349	202	63.33938	0.0937	1	17.17588	0.275	1	14.261	3.2258	1
Prdm2 4	322	172	65.18219	0.00676	1	17.16697	1	1	7.1429	0.3968	1
Prdm2 Pool	344	262	56.76568	0.40381	0.848919	17.95854	1	0.096	11.823	3.3742	1
Gtl3 1	398	236	62.77603	0.12027	1	15.58686	1E-09	1	12.02	2.3155	1
Gtl3 2	345	185	65.09434	0.01091	1	15.14623	7E-11	1	14.871	0.1859	1
Gtl3 3	241	272	46.97856	0.86552	2.55E-07	15.11275	2E-13	1	15.094	1.711	1
Gtl3 4	712	478	59.83193	0.25916	1	17.56833	1	0.077	14.803	4.4728	1
Gtl3 Pool	363	227	61.52542	0.17927	1	16.80774	0.026	1	10.662	3.3003	1
Mllt4 1	278	305	47.68439	0.83222	3.21E-07	Failed				1.3468	1
Mllt4 2	197	254	43.68071	1.02109	8.42E-10	Failed				5.2516	1
Mllt4 3	273	130	67.74194	-0.114	1	16.90043	4E-11	1	9.1932	4.3152	1
Mllt4 4	457	171	72.7707	-0.3512	1	17.81631	1	0.009	6.0842	1.8721	1
Mllt4 Pool	357	238	60	0.25123	1	17.73219	1	0.078	7.9491	3.1797	1
Neg	428	251	63.03387			16.39039			12.674		
Gfp	382	254	60.06289			16.53937	1		9.716		
Ift88 3	146	249	36.96203		3.21E-12	15.31256	0.455	0.167	2.8986		
Ift88 4	196	265	42.51627		1.14E-07	14.90731	3E-04	2E-04	12.739		

	Cilia number					Cilia length			Cell Cycle	Centrosome number	
Cdhr2 1	534	228	70.07874	-0.2894	0.32927	16.21494	1	1	11.221		
Cdhr2 2	325	268	54.80607	0.35966	1	16.28262	1	1	15.435		
Cdhr2 3	428	251	63.03387	0.00998	1	16.39039	1	1	12.674		
Cdhr2 4	416	261	61.44756	0.0774	1	15.90975	1	1	12.248		
Cdhr2 Pool	577	291	66.47465	-0.1362	1	16.15588	1	1	17.672		
Abcd2 1	451	177	71.81529	-0.3632	0.043647	16.34428	1	1	7.6547		
Abcd2 2	433	234	64.91754	-0.0701	1	15.91589	1	1	10.882		
Abcd2 3	440	225	66.16541	-0.1231	1	16.06624	1	1	Failed		
Abcd2 4	417	179	69.96644	-0.2846	0.725345	15.69823	0.058	0.02	Failed		
Abcd2 Pool	435	213	67.12963	-0.1641	1	16.30097	1	1	Failed		

Table 5.1 First-Pass Screen Readout One Results. Results of the first pass screen are shown plate by plate, with the controls for each plate included. The number and percentage of ciliated cells for each siRNA is shown, as well as the NPI score and the p value from the Fisher's Exact test (with Bonferroni correction), highlighted in red if called as a hit which reduces cilia number or blue if it increases cilia number (NPI>0.7, or p<0.01). Average cilium length is shown for each well, calculated by maximum feret diameter MFD (arbitary units). Wells which show a significant reduction in length compared to both negative controls on that plate are highlighted in red, to one negative control are highlighted in orange. Those which gave a significant increase in length compared to one negative control are highlighted in light blue, no well gave a significant increase in length compared to both negative control (Wilcoxon rank sum with Bonferroni correction). P values compared to either negative siRNA or *GFP* siRNA on each plate are shown. The percentage of cells in G2 is shown and any well with more than 20% of cells in G2 is highlighted in red. T

Table 5.2 siRNA knockdown reduces cilia number (NPI)

Gene Name	No. siRNAs called
Sdccag8	4
Bbs5	2
Tscot	2
Mllt4	2
Epb4.1l4b	2
Prdm1	1
Azi1	1
Prdm2	1
Tcex1d2	1
Ttc28	1
Ccdc151	1
Fam92a	1
Gtl3	1
Wdr60	1
Tctex1d1	1
Tcte3	1
Spag1	1

Table 5.2 siRNA knockdown reduces cilia number (NPI). Any siRNA which lead to an NPI score of more than two standard deviations from the mean of the genes not involved (NPI>0.7) was called as a hit. Table lists the genes with siRNAs called as a hit and how many siRNAs targeting the gene were called.

Table 5.3 siRNA knockdown reduces cilia number (Fisher's)

Gene Name	No. siRNAs called
Spag1	4
Wdr92	3
Ttc28	2
Mllt4	2
Wdr35	2
Bbs5	2
Ttc30a2	2
Ccdc63	2
Tcte3	2
Sdccag8	2
Ttc26	2
Epb4.1l4b	2
Wdr60	1
Azi1	1
Prdm1	1
Prdm2	1
Spag1	1
Gtl3	1
Tctex1d2	1
Fm92a	1
Ccdc114	1
Zmynd10	1
Tctex1d1	1

Table 5.3 siRNA knockdown reduces cilia number (Fisher's). Any siRNA which gave a reduction in cilia number with $p<0.01$ (Fisher's Exact test with Bonferroni correction) was called as a hit. The table lists the genes with siRNAs called as hits and how many siRNAs targeting the gene were called

Table 5.6 Second-pass screen: cilia length (MFD)

	ShhLIGHT-II									IMCD3					
	Original			Repeat 1			Repeat 2			Repeat 1			Repeat 2		
	MFD	p value (Neg)	p value (*GFP*)	MFD	p value (Neg)	p value (*GFP*)	MFD	p value (Neg)	p value (*GFP*)	MFD	p value (Neg)	p value (*GFP*)	MFD	p value (Neg)	p value (*GFP*)
Ttc30a2 1	15.16	0.3175	0.2804	14.74	1	1	14.58	1	1	12.38	2E-16	2E-16	16.11	1E-13	0.1197
Ttc30a2 2	15.36	1	1	15.03	1	1	14.88	1	1	15.41	1	1	13.68	1	0.8832
Ttc30a2 3	17.83	1	1	14.7	0.1381	1	13.44	0.0978	0.0112	13.66	4E-12	0.0175	13.25	1	0.002
Ttc30a2 4	13.83	0.0002	0.0005	15	1	1	13.9	1	0.1829	12.2	2E-16	2E-16	13.98	0.0337	1
Ttc30a2 Pool	16.68	1	1	13.81	6E-06	0.2833	14.32	1	1	15.82	8E-15	3E-05			
Sdccag8 1	12.93	0.0029	2E-09	14.66	1	1	12.13		1	12.91	1	1	12.34	2E-16	0.0016
Sdccag8 2	15.07	1	1	15.19	0.0496	0.1091	14.07		1	11.56	1	0.0016	14.88	1	0.0003
Sdccag8 3	16.7	1	1	14.2	1	1	14.04		1	12.92	1	1	15.66	0.0182	2E-16
Sdccag8 4	17.82	1	1	12.97	1	1	12.36		1	13.62	1	1	16.12	0.0002	2E-16
Sdccag8 Pool	16.5	1	1	12.4	0.2124	0.0236	12.2		1	14.22	0.6427	1	17.6	2E-16	2E-16
Mllt4 1				12.74	0.0036	0.2884	13.09	1	1	12.44	1	1	17.39	2E-16	2E-16
Mllt4 2				12.93	0.0358	1	12.14	0.099	0.3408	11.83	1	0.8555	14.46	1	0.023
Mllt4 3	16.9	4E-11	1	13.84	1	1	13.4	1	1	13.11	1	1	14.24	0.0598	1
Mllt4 4	17.82	1	0.0092	13.91	1	1	11.76	0.0561	0.1937	12.11	1	1	14.6	1	0.1061
Mllt4 Pool	17.73	1	0.0784	14.02	1	1	13.99	1	1	15.93	0.0004	0.0341	17.55	2E-16	2E-16
Azi1 1	17.7	1	1	11.84	1	1	12.03		1	15.83	1	0.0169	13.14	1	0.0054
Azi1 2	17.22	1	1	12.49	0.1495	0.0762	13.65		1	15.94	1	0.0014	12.27	1	5E-10
Azi1 3	10.51	0.0027	0.0049	14.14	0.1469	0.0922	13.47		1	15.23	1	1	10.36	4E-06	4E-11
Azi1 4	15.19	0.6995	0.6751	10.69	0.033	0.0338	14.49		0.8781	15.4	1	1	9.69	3E-05	7E-09
Azi1 Pool	16.33	1	1	13.09	1	1	12.18		1	15.58	1	0.0273	12.52	1	3E-05
Ttc28 1	17.35	0.014	1	16.38	1	1	15.44	1	1	15.2	1	1	14.22	0.3678	1
Ttc28 2	17.49	0.8753	1	17.05	0.0132	0.0005	15.09	1	1	17.12	0.0335	1E-12	14.26	0.0334	1
Ttc28 3	18.51	1	0.0264	14.7	1	1	13.06	0.3486	0.0721	16.52	1	4E-09	13.26	1	0.0098
Ttc28 4	15.11	0.0004	1	15.92	1	1	14.1	1	1	14.83	0.0029	1	13.84	1	1
Ttc28 Pool	15.05	2E-08	0.3544	14.6	1	1	11.63	4E-05	6E-06	15.54	1	1	11.78	0.0849	2E-09
Ccdc63 1	17.23	1	0.0034	13.57	1	1	13.83	1	1	13.86	1	1	13.91	0.0012	1
Ccdc63 2	17.04	1	0.3472	12.63	1	1	12.83	1	1	13.85	1	1	14.21	0.1381	1

	ShhLIGHT-II									IMCD3					
	Original			Repeat 1			Repeat 2			Repeat 1			Repeat 2		
	MFD	p value (Neg)	p value (*GFP*)	MFD	p value (Neg)	p value (*GFP*)	MFD	p value (Neg)	p value (*GFP*)	MFD	p value (Neg)	p value (*GFP*)	MFD	p value (Neg)	p value (*GFP*)
Ccdc63 3	14.97	1E-09	0.5608	13.71	1	1	12.46	1	1	13.38	1	1	15.5	1	0.005
Ccdc63 4	14.28	5E-14	0.0001	12.22	0.1379	0.4197	12.5	1	1	13.27	1	1	17.22	2E-16	2E-16
Ccdc63 Pool	16.15	0.0015	1	13.92	1	1	13.35	1	1	13.36	1	1	17.21	3E-15	2E-16
Spag1 1	14.44	0.0059	0.0075	12.43	0.0003	0.0276	13.86	1	1	14.15	1	1	13.34	1	1
Spag1 2	16.22	1	1	13.6	1	1	13.7	1	1	13.29	0.0879	1	13.38	0.5369	1
Spag1 3	16.14	1	1	13.42	0.4482	1	12.94	1	1	13.73	0.5415	1	15.42	1	1
Spag1 4	14.96	0.5318	0.5989	13.66	0.509	1	13.58	1	1	13.66	5E-07	1	13.15	0.0126	1
Spag1 Pool	14.28	0.007	0.0102	12.82	0.0748	1	12.48	1	1	12.93	2E-16	8E-07	13.2	0.6479	1
Tscot 1	15.03	1	0.2556	13.99	1	1	13.44	1	1	14.79	0.0013	1	11.78	1	9E-05
Tscot 2	16.38	1	1	12.27	1	1	12.13	1	1	13.65	2E-14	0.0339	18.13	2E-16	3E-15
Tscot 3				12.64	1	1	12.64	1	1	15.25	1	1	14.22	0.0002	1
Tscot 4	14.13	1	0.0087	14.51	1	1	13.89	1	1	15.58	1	1	13.94	1	1
Tscot Pool	14.37	1	0.0029	13.6	1	1	13.91	1	1	16.05	1	2E-05	13.18	1	0.0176
Prdm1 1	14.22	1E-12	0.0546	15.96	1	1	14.87	1	1	16.32	2E-13	2E-16	13.47	0.081	1.00
Prdm1 2	19.42	1	1	16.4	1	1	15.15	1	1	13.74	0.1951	1			
Prdm1 3	16.87	0.0173	1	15.09	1	1	15.12	1	1	14.12	0.3457	1			
Prdm1 4	17.65	1	0.1438	16.27	1	1	14.88	1	1	13.35	9E-12	0.0003	16.71	1	0.2645
Prdm1 Pool	17.86	1	0.0487	15.51	1	1	13.96	1	0.3062	14.79	1	0.3158	16.86	1	0.1892
Bbs5 1	14.2	8E-06	2E-07	13.05	1	1	13.21	1	1	13.28	1	1	14.95	1	4E-08
Bbs5 2	14.92	0.002	6E-05	12.4	0.1495	0.0762	12.61	1	1	14.49	0.0376	1	15.51	0.2946	2E-16
Bbs5 3	15.61	0.026	0.0011	12.12	0.1469	0.0922	12.38	0.7676	0.1471	13.74	1	1	15.52	0.0462	2E-16
Bbs5 4	16.2	1	1	11.86	0.033	0.0338	11.17	2E-05	8E-07	14.02	1	1	14.34	1	2E-12
Bbs5 Pool	15.72	0.4561	0.0201	13.4	1	1	14.66	1	1	11.1	1	4E-07	12.34	2E-16	0.0016
Epb4.1l4b 1	17.76	0.0029	2E-09	12.74	1	1	12.71		1	15.33	4E-05	1E-13	13.23	0.1895	1
Epb4.1l4b 2	17.3	1	1	14.01	0.0496	0.1091	14.2		1	13.77	0.0037	1	12.63	0.9329	1
Epb4.1l4b 3	17.68	1	1	12.6	1	1	15.8		0.0082	14.22	0.9385	1	12.86	1	1
Epb4.1l4b 4	14.12	1	1	13.39	1	1	13.68		1	13.81	0.0035	1	16.37	0.5266	0.03
Epb4.1l4b Pool	14.39	1	1	12.86	0.2124	0.0236	13.45		1	12.69	2E-16	3E-14	13.47	1	1
Prdm2 1	15.04	5E-14	0.9984	15.78	1	1	14.34	1	1	14.56	1	0.0067	12.82	0.0101	1.00

	ShhLIGHT-II									IMCD3					
	Original			Repeat 1			Repeat 2			Repeat 1			Repeat 2		
	MFD	p value (Neg)	p value (*GFP*)	MFD	p value (Neg)	p value (*GFP*)	MFD	p value (Neg)	p value (*GFP*)	MFD	p value (Neg)	p value (*GFP*)	MFD	p value (Neg)	p value (*GFP*)
Prdm2 2	16.12	6E-07	1	15.83	1	1	14.96	1	1	15.14	1	1			
Prdm2 3	17.18	0.2748	1	16.59	1	0.9291	14	1	0.1181	14.82	1	1			
Prdm2 4	17.17	1	1	15.08	1	1	14.77	1	1	14.67	1	1	17.43	0.0003	8E-05
Prdm2 Pool	17.96	1	0.0958	15.1	1	1	14.87	1	1	13.52	1	1	15.77	0.9556	0.0278

Table 5.6 Second-Pass Screen Results: Cilia Length Genes chosen from the first-pass screen were screened twice more in ShhLIGHT-II and twice in IMCD3 cells. Shown is the cilia length measured using maximum feret diameter (MFD arbitrary units). Wells which show a significant reduction in length compared to both negative controls on that plate are highlighted in red, to one negative control are highlighted in orange (Wilcoxon rank sum test with Bonferroni correction). Those which gave a significant increase in length compared to one negative control are highlighted in light blue, those which gave a significant increase in length compared to both negative controls are highlighted in darker blue. P values from Wilcoxon rank sum test to whether the negative control siRNA or the *GFP* siRNA on that plate are shown.

Table 5.4 siRNA knockdown reduces cilia length

Gene Name	No. siRNAs called
*Tcte3 **	5
Tctex1d1	5
Tctex1d2	3
Fam92b	3
Wdr60	2
*Bbs5 **	2
*Epb4.1l4b **	2
Catnb	2
*Spag1 **	2
Ttc30a1	1
*Wdr35 **	1
*Ccdc63 **	1
Fam92a	1
Ccdc114	1
Ttc30a2	1
*Sdccag8 **	1
Azi1	1

Table 5.4 siRNA knockdown reduces cilia length. Cilia length was measured by max feret diameter MFD (Table 5.1) and Wilcoxon rank sum test was performed, with Bonferroni correction. Listed are the target genes of siRNAs which gave a significant reduction in cilia length, and the number of siRNAs targeting that gene which significantly reduced cilia length. Those marked with * also gave a reduction in cilia number.

Table 5.5 Second-Pass Screen Results: Cilia Number

	ShhLIGHT-II									IMCD3					
	Original screen			Repeat 1			Repeat 2			Repeat 1			Repeat 2		
	% cilia	NPI	Fisher Test p Value	% cilia	NPI	Fisher Test p Value	% cilia	NPI	Fisher Test p Value	% cilia	NPI	Fisher Test p Value	% cilia	NPI	Fisher Test p Value
Ttc30a2 1	60.1	0.23	1	53.9	0.73	1	62.0	0.13	1	36.2	1.32	4.3E-12	48.1	-0.45	7.1E+00
Ttc30a2 2	49.7	0.44	0.001386	69.5	-0.15	1	71.1	-0.12	1	39.9	0.96	1.13E-05	32.2	0.85	4.2E-03
Ttc30a2 3	68.0	0.06	9.54E-06	54.7	0.69	1	47.1	0.55	0.001021	33.2	1.61	2.76E-17	44.2	-0.08	2.5E+02
Ttc30a2 4	38.8	0.67	1	68.7	-0.10	1	38.6	0.78	2.35E-11	32.5	1.68	1.51E-20	49.9	-0.63	3.4E-01
Ttc30a2 Pool	59.0	0.25	1	65.0	0.11	1	49.1	0.49	0.00245	34.0	1.54	8.1E-13	42.1	0.12	2.1E+02
Sdccag8 1	41.2	1.05	0.005853	48.4	0.14	1	32.7	0.62	1.07E-06	22.3	0.63	0.004808	38.5	3.76	1.3E-39
Sdccag8 2	64.6	-0.50	1	64.4	-0.27	0.943078	47.1	0.26	1	35.4	-0.05	1	51.7	2.23	1.2E-17
Sdccag8 3	39.5	1.16	0.003061	59.3	-0.14	1	48.3	0.23	1	34.9	-0.03	1	74.2	-0.37	3.2E+01
Sdccag8 4	41.3	1.05	0.046877	44.5	0.24	0.877164	37.7	0.50	0.000119	34.5	0.00	1	70.4	0.08	2.6E+02
Sdccag8 Pool	40.0	1.13	0.081016	37.8	0.41	1.04E-05	33.4	0.61	1.08E-08	30.5	0.20	1	61.6	1.22	1.3E-07
Mllt4 1	47.7	0.83	3.21E-07	35.8	0.61	0.020612	40.2	0.42	1	15.3	0.99	2.55E-10	59.9	0.03	2.0E-04
Mllt4 2	43.7	1.02	8.42E-10	52.8	-0.02	1	42.9	0.32	1	23.4	0.57	0.693442	61.8	1.06	6.1E-04
Mllt4 3	67.7	-0.11	1	53.7	-0.05	1	41.4	0.37	1	24.7	0.50	0.877557	66.9	0.47	8.9E+00
Mllt4 4	72.8	-0.35	1	49.1	0.12	1	32.0	0.73	0.030482	11.1	1.21	1.22E-15	52.4	2.15	2.1E-16
Mllt4 Pool	60.0	0.25	1	40.5	0.43	1	49.1	0.08	1	40.0	-0.29	1	68.7	0.27	7.4E+01
Azi1 1	72.0	-0.02	1	41.2	0.25	1	29.7	0.70	7.2E-10	50.6	-0.08	1	20.7	2.18	5.9E-14
Azi1 2	73.7	-0.06	1	37.9	0.36	1	40.8	0.42	0.016763	44.0	0.56	1	50.1	-0.64	1.0E+00
Azi1 3	9.7	1.27	4.16E-31	48.3	0.03	1	34.9	0.57	3.72E-05	46.9	0.28	1	43.8	-0.04	3.1E+02
Azi1 4	57.4	0.28	0.577367	35.2	0.45	0.260664	41.3	0.41	0.000532	49.9	-0.01	1	35.5	0.76	1.1E-01
Azi1 Pool	58.1	0.27	0.227798	35.6	0.43	0.139421	26.0	0.80	4.5E-13	51.5	-0.17	1	38.1	0.50	6.5E+00
Ttc28 1	65.2	-0.34	1	78.2	-0.64	1	64.1	0.08	1	49.9	-0.01	1	49.4	-0.58	1.5E+00
Ttc28 2	59.8	-0.12	1	76.1	-0.52	1	56.1	0.30	1	45.2	0.44	1	45.1	-0.17	1.5E+02
Ttc28 3	65.5	-0.35	0.428248	71.6	-0.27	1	38.4	0.78	3.03E-06	48.8	0.09	1	47.0	-0.34	4.3E+01
Ttc28 4	30.0	1.05	9.12E-08	68.6	-0.10	1	42.4	0.68	2.9E-07	39.3	1.02	1.08E-06	51.6	-0.79	1.0E-01
Ttc28 Pool	44.4	0.49	3.07E-09	62.5	0.25	1	35.8	0.86	1.25E-09	44.5	0.52	1	22.7	1.99	2.2E-12
Ccdc63 1	67.0	-0.11	1	58.6	-0.29	1	44.3	0.02	0.108756	21.9	0.65	0.032555	64.0	0.81	1.2E-01
Ccdc63 2	68.9	-0.18	1	44.2	0.26	1	51.4	-0.30	1	39.1	-0.24	1	59.1	1.38	4.3E-06

	ShhLIGHT-II									IMCD3					
	Original screen			Repeat 1			Repeat 2			Repeat 1			Repeat 2		
	% cilia	NPI	Fisher Test p Value	% cilia	NPI	Fisher Test p Value	% cilia	NPI	Fisher Test p Value	% cilia	NPI	Fisher Test p Value	% cilia	NPI	Fisher Test p Value
Ccdc63 3	46.7	0.63	3.31E-06	43.2	0.30	1	30.0	0.67	0.077906	47.1	-0.66	0.078641	43.9	3.14	1.6E-23
Ccdc63 4	46.8	0.63	1.69E-05	33.7	0.67	0.003377	32.7	0.55	0.000854	21.4	0.67	0.012752	71.7	-0.08	2.9E+02
Ccdc63 Pool	67.4	-0.13	1	49.7	0.05	1	35.4	0.43	6.36E-07	35.4	-0.05	1	72.4	-0.15	1.9E+02
Spag1 1	46.2	0.51	1.53E-07	42.1	0.37	1	48.7	-0.18	1	64.8	0.09	1	45.3	-0.50	1.9E+00
Spag1 2	49.8	0.44	0.000223	39.7	0.46	1	45.5	-0.03	1	66.8	-0.07	1	28.9	0.23	5.9E+00
Spag1 3	71.7	-0.02	1	53.0	-0.03	1	54.2	-0.43	1	58.9	0.57	0.018792	25.3	0.39	2.5E-01
Spag1 4	40.6	0.63	1.1E-08	53.9	-0.06	1	32.5	0.56	1	71.5	-0.45	0.051232	19.8	0.64	4.3E-06
Spag1 Pool	35.6	0.73	1.04E-15	37.5	0.54	1	35.2	0.44	1	46.3	1.59	9.68E-31	20.3	0.61	6.4E-07
Tscot 1	42.3	0.98	0.057198	49.8	0.05	1	54.8	-0.45	1	43.1	0.65	0.066286	20.7	2.18	5.9E-14
Tscot 2	62.3	-0.34	1	22.6	1.09	1.09E-07	24.3	0.93	0.000737	50.1	-0.03	1	50.1	-0.64	1.0E+00
Tscot 3				34.5	0.64	0.23131	40.0	0.22	1	50.3	-0.05	1	43.8	-0.04	3.1E+02
Tscot 4	42.9	0.94	0.102252	47.0	0.16	1	50.4	-0.25	1	45.6	0.40	1	35.5	0.76	1.1E-01
Tscot Pool	56.0	0.07	1	37.8	0.51	0.809403	45.1	-0.01	1	53.4	-0.35	1	38.1	0.50	6.5E+00
Prdm1 1	32.0	1.57	1.29E-23	70.3	-0.19	1	66.5	0.01	1	63.0	0.23	1	30.3	0.17	3.6E+01
Prdm1 2	56.2	0.43	0.539551	75.1	-0.47	1	52.8	0.39	0.495351	28.9	3.01	1.13E-81			
Prdm1 3	65.1	0.01	1	65.1	0.10	1	60.9	0.17	1	61.5	0.36	1			
Prdm1 4	64.1	0.06	1	77.8	-0.62	1	47.4	0.54	0.000101	55.8	0.82	4.47E-07	24.9	0.41	7.3E-01
Prdm1 Pool	64.7	0.03	1	73.9	-0.40	1	45.5	0.59	6.57E-05	44.8	1.72	7.59E-36	32.2	0.08	3.6E+01
Bbs5 1	32.8	1.06	8.99E-06	47.8	0.04	1	52.8	0.02	1	20.5	0.72	0.036637	69.1	0.22	1.1E+02
Bbs5 2	32.5	1.08	1.12E-06	39.7	0.30	0.581377	41.0	0.32	0.35533	37.3	-0.15	1	72.1	-0.13	2.2E+02
Bbs5 3	55.4	-0.26	1	31.9	0.55	1.3E-05	46.6	0.18	1	42.4	-0.41	1	75.1	-0.47	8.2E+00
Bbs5 4	55.6	-0.27	1	25.6	0.75	7.52E-11	35.7	0.46	0.001704	32.5	0.10	1	74.1	-0.35	4.3E+01
Bbs5 Pool	56.8	-0.34	1	44.7	0.14	1	48.4	0.14	1	30.3	0.22	1	76.9	-0.68	4.8E-01
Epb4.1l4b 1	63.0	-0.25	1	48.4	0.14	1	43.1	0.36	0.277483	73.6	-0.63	4.82E-05	30.6	0.16	1.1E+01
Epb4.1l4b 2	56.8	0.00	1	60.4	-0.17	0.169517	46.6	0.27	0.60688	59.9	0.49	0.209184	30.4	0.16	6.5E+00
Epb4.1l4b 3	67.2	-0.42	0.017407	54.8	-0.03	0.823135	49.8	0.19	1	68.0	-0.17	1	33.6	0.02	1.1E+02
Epb4.1l4b 4	36.3	0.80	0.017407	62.0	-0.21	0.447742	42.7	0.37	0.036487	59.8	0.50	0.229856	35.0	-0.04	2.0E+02
Epb4.1l4b Pool	35.1	0.85	1	59.3	-0.14	1	51.3	0.15	1	45.4	1.67	6.93E-34	33.5	0.02	8.6E+01
Prdm2 1	39.3	1.23	3.32E-18	78.7	-0.67	0.723885	51.7	0.42	0.036352	71.8	-0.48	0.018616	31.6	0.11	3.3E+01

	ShhLIGHT-II									IMCD3					
	Original screen			Repeat 1			Repeat 2			Repeat 1			Repeat 2		
	% cilia	NPI	Fisher Test p Value	% cilia	NPI	Fisher Test p Value	% cilia	NPI	Fisher Test p Value	% cilia	NPI	Fisher Test p Value	% cilia	NPI	Fisher Test p Value
Prdm2 2	59.6	0.27	1	72.3	-0.31	1	61.1	0.16	1	74.2	-0.68	2.28E-05			
Prdm2 3	63.3	0.09	1	66.2	0.04	1	52.8	0.39	0.266379	49.5	1.34	7.34E-17			
Prdm2 4	65.2	0.01	1	75.3	-0.48	1	49.8	0.47	0.043672	32.0	2.75	1.4E-64	26.7	0.33	9.1E-01
Prdm2 Pool	56.8	0.40	0.848919	71.2	-0.24	1	66.5	0.01	1	64.8	0.09	1	34.6	-0.02	1.7E+02

Table 5.5 Second-Pass Screen Results: Cilia Number. Genes chosen from the first-pass screen were screened twice more in ShhLIGHT-II and twice in IMCD3 cells. Shown is the percentage of cells with cilia (% cilia), the NPI score and the p value from Fisher's exact test (with Bonferroni correction). Any siRNA called as a hit (NPI>0.7, p<0.01) which reduces cilia numbers is highlighted in red, or increases cilia numbers is highlighted in dark blue. Genes are organised roughly in order of reproducibility of phenotype. Those above the line were said to have successfully repeated, those below the line (in blue) did not repeat. Genes are highlighted alternately in yellow or blue to aid identification across the table.

Table 5.6 Second-pass screen: cilia length (MFD)

	ShhLIGHT-II									IMCD3					
	Original			Repeat 1			Repeat 2			Repeat 1			Repeat 2		
	MFD	p value (Neg)	p value (*GFP*)	MFD	p value (Neg)	p value (*GFP*)	MFD	p value (Neg)	p value (*GFP*)	MFD	p value (Neg)	p value (*GFP*)	MFD	p value (Neg)	p value (*GFP*)
Ttc30a2 1	15.16	0.3175	0.2804	14.74	1	1	14.58	1	1	12.38	2E-16	2E-16	16.11	1E-13	0.1197
Ttc30a2 2	15.36	1	1	15.03	1	1	14.88	1	1	15.41	1	1	13.68	1	0.8832
Ttc30a2 3	17.83	1	1	14.7	0.1381	1	13.44	0.0978	0.0112	13.66	4E-12	0.0175	13.25	1	0.002
Ttc30a2 4	13.83	0.0002	0.0005	15	1	1	13.9	1	0.1829	12.2	2E-16	2E-16	13.98	0.0337	1
Ttc30a2 Pool	16.68	1	1	13.81	6E-06	0.2833	14.32	1	1	15.82	8E-15	3E-05			
Sdccag8 1	12.93	0.0029	2E-09	14.66	1	1	12.13		1	12.91	1	1	12.34	2E-16	0.0016
Sdccag8 2	15.07	1	1	15.19	0.0496	0.1091	14.07		1	11.56	1	0.0016	14.88	1	0.0003
Sdccag8 3	16.7	1	1	14.2	1	1	14.04		1	12.92	1	1	15.66	0.0182	2E-16
Sdccag8 4	17.82	1	1	12.97	1	1	12.36		1	13.62	1	1	16.12	0.0002	2E-16
Sdccag8 Pool	16.5	1	1	12.4	0.2124	0.0236	12.2		1	14.22	0.6427	1	17.6	2E-16	2E-16
Mllt4 1				12.74	0.0036	0.2884	13.09	1	1	12.44	1	1	17.39	2E-16	2E-16
Mllt4 2				12.93	0.0358	1	12.14	0.099	0.3408	11.83	1	0.8555	14.46	1	0.023
Mllt4 3	16.9	4E-11	1	13.84	1	1	13.4	1	1	13.11	1	1	14.24	0.0598	1
Mllt4 4	17.82	1	0.0092	13.91	1	1	11.76	0.0561	0.1937	12.11	1	1	14.6	1	0.1061
Mllt4 Pool	17.73	1	0.0784	14.02	1	1	13.99	1	1	15.93	0.0004	0.0341	17.55	2E-16	2E-16
Azi1 1	17.7	1	1	11.84	1	1	12.03		1	15.83	1	0.0169	13.14	1	0.0054
Azi1 2	17.22	1	1	12.49	0.1495	0.0762	13.65		1	15.94	1	0.0014	12.27	1	5E-10
Azi1 3	10.51	0.0027	0.0049	14.14	0.1469	0.0922	13.47		1	15.23	1	1	10.36	4E-06	4E-11
Azi1 4	15.19	0.6995	0.6751	10.69	0.033	0.0338	14.49		0.8781	15.4	1	1	9.69	3E-05	7E-09
Azi1 Pool	16.33	1	1	13.09	1	1	12.18		1	15.58	1	0.0273	12.52	1	3E-05
Ttc28 1	17.35	0.014	1	16.38	1	1	15.44	1	1	15.2	1	1	14.22	0.3678	1
Ttc28 2	17.49	0.8753	1	17.05	0.0132	0.0005	15.09	1	1	17.12	0.0335	1E-12	14.26	0.0334	1
Ttc28 3	18.51	1	0.0264	14.7	1	1	13.06	0.3486	0.0721	16.52	1	4E-09	13.26	1	0.0098
Ttc28 4	15.11	0.0004	1	15.92	1	1	14.1	1	1	14.83	0.0029	1	13.84	1	1
Ttc28 Pool	15.05	2E-08	0.3544	14.6	1	1	11.63	4E-05	6E-06	15.54	1	1	11.78	0.0849	2E-09
Ccdc63 1	17.23	1	0.0034	13.57	1	1	13.83	1	1	13.86	1	1	13.91	0.0012	1
Ccdc63 2	17.04	1	0.3472	12.63	1	1	12.83	1	1	13.85	1	1	14.21	0.1381	1

	ShhLIGHT-II									IMCD3					
	Original			Repeat 1			Repeat 2			Repeat 1			Repeat 2		
	MFD	p value (Neg)	p value (*GFP*)	MFD	p value (Neg)	p value (*GFP*)	MFD	p value (Neg)	p value (*GFP*)	MFD	p value (Neg)	p value (*GFP*)	MFD	p value (Neg)	p value (*GFP*)
Ccdc63 3	14.97	1E-09	0.5608	13.71	1	1	12.46	1	1	13.38	1	1	15.5	1	0.005
Ccdc63 4	14.28	5E-14	0.0001	12.22	0.1379	0.4197	12.5	1	1	13.27	1	1	17.22	2E-16	2E-16
Ccdc63 Pool	16.15	0.0015	1	13.92	1	1	13.35	1	1	13.36	1	1	17.21	3E-15	2E-16
Spag1 1	14.44	0.0059	0.0075	12.43	0.0003	0.0276	13.86	1	1	14.15	1	1	13.34	1	1
Spag1 2	16.22	1	1	13.6	1	1	13.7	1	1	13.29	0.0879	1	13.38	0.5369	1
Spag1 3	16.14	1	1	13.42	0.4482	1	12.94	1	1	13.73	0.5415	1	15.42	1	1
Spag1 4	14.96	0.5318	0.5989	13.66	0.509	1	13.58	1	1	13.66	5E-07	1	13.15	0.0126	1
Spag1 Pool	14.28	0.007	0.0102	12.82	0.0748	1	12.48	1	1	12.93	2E-16	8E-07	13.2	0.6479	1
Tscot 1	15.03	1	0.2556	13.99	1	1	13.44	1	1	14.79	0.0013	1	11.78	1	9E-05
Tscot 2	16.38	1	1	12.27	1	1	12.13	1	1	13.65	2E-14	0.0339	18.13	2E-16	3E-15
Tscot 3				12.64	1	1	12.64	1	1	15.25	1	1	14.22	0.0002	1
Tscot 4	14.13	1	0.0087	14.51	1	1	13.89	1	1	15.58	1	1	13.94	1	1
Tscot Pool	14.37	1	0.0029	13.6	1	1	13.91	1	1	16.05	1	2E-05	13.18	1	0.0176
Prdm1 1	14.22	1E-12	0.0546	15.96	1	1	14.87	1	1	16.32	2E-13	2E-16	13.47	0.081	1.00
Prdm1 2	19.42	1	1	16.4	1	1	15.15	1	1	13.74	0.1951	1			
Prdm1 3	16.87	0.0173	1	15.09	1	1	15.12	1	1	14.12	0.3457	1			
Prdm1 4	17.65	1	0.1438	16.27	1	1	14.88	1	1	13.35	9E-12	0.0003	16.71	1	0.2645
Prdm1 Pool	17.86	1	0.0487	15.51	1	1	13.96	1	0.3062	14.79	1	0.3158	16.86	1	0.1892
Bbs5 1	14.2	8E-06	2E-07	13.05	1	1	13.21	1	1	13.28	1	1	14.95	1	4E-08
Bbs5 2	14.92	0.002	6E-05	12.4	0.1495	0.0762	12.61	1	1	14.49	0.0376	1	15.51	0.2946	2E-16
Bbs5 3	15.61	0.026	0.0011	12.12	0.1469	0.0922	12.38	0.7676	0.1471	13.74	1	1	15.52	0.0462	2E-16
Bbs5 4	16.2	1	1	11.86	0.033	0.0338	11.17	2E-05	8E-07	14.02	1	1	14.34	1	2E-12
Bbs5 Pool	15.72	0.4561	0.0201	13.4	1	1	14.66	1	1	11.1	1	4E-07	12.34	2E-16	0.0016
Epb4.1l4b 1	17.76	0.0029	2E-09	12.74	1	1	12.71		1	15.33	4E-05	1E-13	13.23	0.1895	1
Epb4.1l4b 2	17.3	1	1	14.01	0.0496	0.1091	14.2		1	13.77	0.0037	1	12.63	0.9329	1
Epb4.1l4b 3	17.68	1	1	12.6	1	1	15.8		0.0082	14.22	0.9385	1	12.86	1	1
Epb4.1l4b 4	14.12	1	1	13.39	1	1	13.68		1	13.81	0.0035	1	16.37	0.5266	0.03
Epb4.1l4b Pool	14.39	1	1	12.86	0.2124	0.0236	13.45		1	12.69	2E-16	3E-14	13.47	1	1
Prdm2 1	15.04	5E-14	0.9984	15.78	1	1	14.34	1	1	14.56	1	0.0067	12.82	0.0101	1.00

	ShhLIGHT-II									IMCD3					
	Original			Repeat 1			Repeat 2			Repeat 1			Repeat 2		
	MFD	p value (Neg)	p value (*GFP*)	MFD	p value (Neg)	p value (*GFP*)	MFD	p value (Neg)	p value (*GFP*)	MFD	p value (Neg)	p value (*GFP*)	MFD	p value (Neg)	p value (*GFP*)
Prdm2 2	16.12	6E-07	1	15.83	1	1	14.96	1	1	15.14	1	1			
Prdm2 3	17.18	0.2748	1	16.59	1	0.9291	14	1	0.1181	14.82	1	1			
Prdm2 4	17.17	1	1	15.08	1	1	14.77	1	1	14.67	1	1	17.43	0.0003	8E-05
Prdm2 Pool	17.96	1	0.0958	15.1	1	1	14.87	1	1	13.52	1	1	15.77	0.9556	0.0278

Table 5.6 Second-Pass Screen Results: Cilia Length Genes chosen from the first-pass screen were screened twice more in ShhLIGHT-II and twice in IMCD3 cells. Shown is the cilia length measured using maximum feret diameter (MFD arbitrary units). Wells which show a significant reduction in length compared to both negative controls on that plate are highlighted in red, to one negative control are highlighted in orange (Wilcoxon rank sum test with Bonferroni correction). Those which gave a significant increase in length compared to one negative control are highlighted in light blue, those which gave a significant increase in length compared to both negative controls are highlighted in darker blue. P values from Wilcoxon rank sum test to whether the negative control siRNA or the *GFP* siRNA on that plate are shown.

Table 5.7 Second-pass screen: centrosome number

	ShhLIGHT-II						IMCD3			
	Original		1		2		1		2	
	% >2 cent	p value	% >2 cent	p value	% >2 cent	p value	% >2 cent	p value	% >2 cent	p value
Ttc30a2 1	1.20	1	3.92	1	4.21	1	0.06	1	15.28	0.03354
Ttc30a2 2	5.43	1	0.49	1	1.04	1	0.00	1	16.04	0.03517
Ttc30a2 3	4.71	1	1.56	1	2.04	1	0.07	1	0.26	3E-09
Ttc30a2 4	6.28	1	0.28	1	3.71	1	0.17	1	1.56	0.01564
Ttc30a2 Pool	3.21	1	0.75	1	3.31	1	0.18	1	2.87	1
Sdccag8 1			10.45	1	2.19	1	0.96	1	8.02	1
Sdccag8 2			6.70	1	0.41	1	0.36	1	31.55	3.5E-16
Sdccag8 3			5.96	1	0.40	1	0.81	1	1.20	0.00037
Sdccag8 4			6.25	1	1.48	1	0.67	1	0.46	1.4E-05
Sdccag8 Pool			4.59	1	1.15	1	2.04	0.00531	1.08	0.00496
Mllt4 1	1.35	1	0.79	1	2.09	1	8.76	0.00038	24.39	1
Mllt4 2	5.25	1	0.51	1	1.71	1	2.66	0.30854		
Mllt4 3	4.32	1	0.00	1	4.58	1	2.07	0.01093		
Mllt4 4	1.87	1	0.30	1	0.35	1	1.65	0.00153	23.08	1
Mllt4 Pool	3.18	1	4.92	1	1.45	1	1.47	2.2E-06	29.66	1
Azi1 1	1.23	1	3.14	1	4.46	1	5.63	4.4E-18	0.32	3.7E-06
Azi1 2	1.56	1	5.08	1	0.41	0.00166	0.83	1	0.60	4.5E-05
Azi1 3	0.00	1	2.07	1	2.76	1	1.00	1	0.00	0.00013
Azi1 4	8.14	0.191	14.41	3.6E-10	2.82	0.31816	0.45	1	0.00	0.00098
Azi1 Pool	3.61	1	5.32	0.56453	1.17	0.03294	0.61	1	0.00	9.9E-07
Ttc28 1			7.40	1	6.14	1	6.08	1	22.73	1
Ttc28 2			3.83	1	1.95	1	3.56	1	14.46	1
Ttc28 3			4.32	1	1.79	1	4.78	1	18.31	1
Ttc28 4			6.27	1	0.89	1	9.54	4.9E-06	29.47	1
Ttc28 Pool			8.30	1	1.46	1	6.46	1	16.85	1
Ccdc63 1	5.5556	1	1.38	1	11.90	0.03412	1.12	1	33.87	1
Ccdc63 2	2.3564	1	3.25	1	8.70	1	1.69	1	28.40	1
Ccdc63 3	9.3385	1	1.87	1	9.66	1	0.44	1	1.40	1.2E-49

	ShhLIGHT-II						IMCD3			
	Original		1		2		1		2	
	% >2 cent	p value	% >2 cent	p value	% >2 cent	p value	% >2 cent	p value	% >2 cent	p value
Ccdc63 4	16.368	1.2E-07	2.97	1	20.09	9.7E-08	0.65	1	1.53	1E-37
Ccdc63 Pool			2.44	1	21.08	1.3E-12	2.71	1	46.67	0.00014
Tscot 1			7.38	1	2.48	0.59033	1.53	2.9E-07	16.91	1
Tscot 2			6.47	1	1.97	0.02549	3.44	1	20.41	1
Tscot 3			5.50	1	23.08	5.3E-05	0.70	3.5E-12	24.18	1
Tscot 4			3.77	1	50.21	3.2E-25	1.18	2.4E-07	26.55	1
Tscot Pool			16.19	1.9E-05	19.61	0.00636	1.52	4.2E-07	33.09	1
Prdm1 1	1.69	1	4.17	1	2.06	1	0.77	1	1.67	5.3E-42
Prdm1 2	1.95	1	4.82	1	1.68	1	0.96	1	0.84	5.9E-40
Prdm1 3	3.13	1	5.92	1	2.29	1	1.46	1	21.69	1
Prdm1 4	2.17	1	6.15	1	4.26	1	1.78	1	8.94	1.8E-09
Prdm1 Pool	1.69	1	4.42	1	1.33	1	3.76	1	29.70	1
Bbs5 1			21.08	1.3E-12	1.33	0.09355	4.49	0.46907	3.46	2.8E-23
Bbs5 2			3.47	1	2.88	0.58938	0.12	1	1.95	4.1E-34
Bbs5 3			8.89	1	7.65	1	0.00	1	8.26	1.3E-11
Bbs5 4			7.87	1	2.77	2.04114	0.86	1	30.33	1
Bbs5 Pool			7.80	1	1.42	0.0111	1.82	1	61.92	1.7E-19
Epb4.1l4b 1			1.22	1	3.40	1	0.18	1	13.43	0.72818
Epb4.1l4b 2			1.20	1	5.02	1	0.00	1	4.90	1
Epb4.1l4b 3			0.00	1	5.29	1	0.05	1	4.58	1
Epb4.1l4b 4			0.43	1	3.88	1	0.72	1	0.80	0.00182
Epb4.1l4b Pool			**0.77**	1	21.03	3E-15	0.88	1	0.00	0.00866
Prdm2 1	4.34	1	0.98	1	1.45	1	2.04	0.00047	10.53	1
Prdm2 2	2.36	1	1.32	1	3.09	1	0.73	8.7E-09		1
Prdm2 3	3.23	1	0.53	1	2.71	1	2.60	0.08962		
Prdm2 4	0.40	1	1.16	1	3.20	1	1.04	1.8E-10	13.64	
Prdm2 Pool	**3.37**	**1**	**0.00**	1	4.67	1	2.75	0.17986	32.67	1

Table 5.7 Second-Pass Screen Results: Centrosome numbers. Genes chosen from the first-pass screen were screened twice more in ShhLIGHT-II and twice in IMCD3 cells. Shown is the percentage of cells with >2 centrosomes, along with p value from Fisher's exact test. siRNAs which significantly reduce the number of cells with >2 centrosomes is highlighted in red, any which significantly increases the number of cells with >2 centrosomes is highlighted in dark blue (Fisher's exact with Bonferroni correction. Cent = centrosomes

Table 5.8 Second-pass screen: cell cycle (% G2)

	ShhLIGHT-II			IMCD3	
	Orig	1	2	1	2
Ttc30a2 1	15.53785	4.888889	11.57895	24.65675	
Ttc30a2 2	32.06522	3.846154	8.298755	24.15842	
Ttc30a2 3	12.55144	5.46875	19.04762	26.68588	
Ttc30a2 4	14.00966	7.692308	20.15915	24.27273	
Ttc30a2 Pool	23.42657	3.990025	17.8117		
Sdccag8 1	5.135135	27.25322	15.04425		24.14286
Sdccag8 2	10.98901	17.70833	11.00478		31.49905
Sdccag8 3	19.67213	17.77778	13.74269		27.5886
Sdccag8 4	15.29412	10.91371	17.46575		28.03419
Sdccag8 Pool	15.67568	27.80488	20.22792		31.32832
Mllt4 1		15.29412	7.983193		27.85088
Mllt4 2		11.5894	12.08791		30.10909
Mllt4 3	9.193246	11.30952	8.307692		24.7305
Mllt4 4	6.084243	12.35955	11.94969		24.69253
Mllt4 Pool	7.949126	13.09524	9.15493		29.86553
Azi1 1	10.84337	21.07623	19.78022	22.07053	
Azi1 2	8.285714	32.20339	12.70492	27.99114	
Azi1 3	35.97122	13.31361	16.58986	19.52233	
Azi1 4	23.07692	32.20339	15.15748	23.43595	
Azi1 Pool	18.4573	31.89369	27.30769	18.6019	
Ttc28 1		7.287449	8.586762	23.99527	
Ttc28 2	21.94514	10.57692	11.71548	23.33526	
Ttc28 3	12.98077	3.092784	20.58824	21.45833	
Ttc28 4	31.62055	3.797468	14.92537	22.94992	
Ttc28 Pool	30.37634	1.532567	17.28972	25.52486	
Ccdc63 1	10.9319	12.26415	9.465021		27.85235
Ccdc63 2	8.836524	19.60784	12.79461		24.34343
Ccdc63 3	12.64591	14.0056			32.3049
Ccdc63 4	13.00448	12.29773	17.7305		32.7335
Ccdc63 Pool	10.39886	13.88889	15.42553		25.83519
Spag1 1	45.2459	11.88406	13.65188	27.81881	32.60073
Spag1 2	45.2	10.30928	10.71429	22.91196	37.94712
Spag1 3	6.4	12.07865	11.65919	26.66297	29.91453
Spag1 4	22.22222	15.97052	12.16617	28.1583	27.30263
Spag1 Pool	34.9481	13.87755	15.04854	29.62255	26.58402
Tscot 1	15.38462	16.96429	18.18182	21.53187	
Tscot 2	19.25676	6.629834	10.33058	20.91072	
Tscot 3		10.52632	10.27668	22.70916	
Tscot 4	16.21622	13.72549	17.40741	22.78708	
Tscot Pool	14.01674	10.04566	11.0687	24.42188	
Prdm1 1	23.48668	4.390244	7.660455	27.19807	25.10638
Prdm1 2	13.67673	3.846154	11.11111	21.72859	
Prdm1 3	7.963446	3.535354	9.480813	26.51042	
Prdm1 4	7.395994	4.942966	19.86301	24.28941	29.7561
Prdm1 Pool	13.01653	6.498195	11.21495	23.74939	29.58861

Bbs5 1	24.26036	27.28238	24.86772		25.49697
	ShhLIGHT-II			IMCD3	
	Orig	1	2	1	2
Bbs5 Pool	11.45833	29.5122	27.25322		22.18978
Epb4.1l4b 1	20.19347	28.14208	16.06426	25.46992	27.79043
Epb4.1l4b 2	19.24051	25.86207	12.52654	22.81803	32.67045
Epb4.1l4b 3	13.18182	24.46483	13.65079	28.07018	26.55738
Epb4.1l4b 4	31.98294	19.24528	10.76923	26.8111	34.05995
Epb4.1l4b Pool	20.55138	24.7619	6.451613	24.92823	37.42204
Prdm2 1	19.97041	3.921569	12.5523	32.18218	29.54545
Prdm2 2	10.39604	2.487562	11.18012	28.64353	
Prdm2 3	14.26146	3.235294	17.55725	24.02448	
Prdm2 4	7.142857	2.686567		18.71658	41.36808
Prdm2 Pool	11.82336	4.166667	7.660455	17.70073	34.2246

Table 5.8 Second-Pass Screen Results: Cell Cycle Genes chosen from the first-pass screen were screened twice more in ShhLIGHT-II and twice in IMCD3 cells. Shown is the percentage of cells in G2. If a well has more than 20% of cells in G2 it is highlighted in red.

Chapter Six. The role of Azi1 in vivo

Azi1/Cep131 (*Induced upon 5-aza-cytidine treatment 1/Centrosomal protein 131*) is a coiled-coil domain protein, which was initially identified as a centrosomal protein by proteomics and immunofluorescence studies (Andersen et al., 2003; Jakobsen et al., 2011). The centrosomal localisation of Azi1 was confirmed in Chapter Five, and the localisation of Azi1 is studied in more detail in this chapter.

Azi1 is conserved in organisms with motile and compartmentalised cilia, termed "prototypical cilia" (cilia in which the formation depends on IFT) – *Azi1* is not found in the *P. Falciparum* genome, which form their flagellar in the cytosol, independent of IFT (Avidor-Reiss et al., 2004; Gabernet-Castello et al., 2011; Li et al., 2004). *Azi1* is also not found in the *C. elegans* genome, suggesting it may be involved in motile ciliogenesis, as *C. elegans* have only sensory ciliated neurons and lack sperm flagella (Gabernet-Castello et al., 2011). This is further supported by the recent study by Azimzadeh et al., (2012) which suggested Azi1 is required for cilia motility in planarians. However the data presented in Chapter Five of this thesis showing that siRNA knock down of *Azi1* in mammalian cells leads to a reduction in the number of primary, non-motile cilia, suggests Azi1 may also play a role in primary (non-motile) ciliogenesis.

Azi1 has been shown to have roles in ciliogenesis in flies and zebrafish; *Dila,* (the *Drosophila Azi1* orthologue) was shown to be highly expressed in chordotonal neurons as they undergo ciliogenesis (hence it was included in this siRNA screen (Chapter 4 and 5 (Cachero et al., 2011)). Moreover, *Dila* mutant flies have an uncoordinated phenotype similar to other ciliary mutants (Han et al., 2003; Lee et al., 2008), with the cilia of the chordotonal neurons showing shortened, disorganised axonemal ultrastructure (Ma and Jarman, 2011). Zebrafish morphant embryos for the *Azi1* orthologue, *cep131*, show characteristic ciliopathic phenotypes including aberrant kidney and ear development, laterality defects and shortened cilia (Wilkinson et al., 2009). As the cilia disrupted upon knockdown of *Azi1* in zebrafish

include motile and non-motile cilia, this supports a conserved role for Azi1 in both motile and non-motile ciliogenesis. Azi1 localises to the pre-acrosome region of spermatids in mouse testes (Aoto et al., 1995), but little is known about mammalian Azi1 function.

In this chapter the role of mammalian Azi1 is examined further, including detailed localisation studies and the generation and characterisation of *Azi1* mutant mice to investigate the role of Azi1 *in vivo*.

6.1 Azi1 localises to the transition zone, but is not trafficked into the cilium itself.

AZI1 was previously published to localise to the human centrosome (Andersen et al., 2003; Jakobsen et al., 2011), and localisation to the base of cilia and around the centrosome was independently confirmed and characterised with several antibodies in mammalian cells (Figure 5.5A and Figure 6.1A and B). The target sequence of these antibodies is shown in Figure 6.3B. Costaining with anti-polyglutamylated tubulin, which stains the ciliary axoneme and basal body but, importantly, is absent from the transition zone (Lechtreck and Geimer, 2000), shows Azi1 is specifically enriched at the transition zone (arrow Fig 6.1 A), an area at the base of the cilia involved in regulating what enters and leaves the cilium (Czarnecki and Shah, 2012 and references within) (Figure 6.1A). Upon 48h serum starvation, approximately 60% of ShhLIGHT-II cells have a cilium marked by anti-acetylated α-tubulin (Figure 5.1A). Punctate staining of anti-acetylated α-tubulin marks the basal body at the base of cilia or the centrosome in non-ciliated cells. Quantitative image analysis of the intensity of Azi1 at the centrosome in non-ciliated cells versus the basal body of ciliated cells, found higher intensity anti-Azi1 staining in ciliated cells, suggesting Azi1 localisation is dynamic and ciliary dependent (Figure 6.1B and C). Interestingly, total AZI1 protein levels remain unchanged in hTERT-RPE cells upon

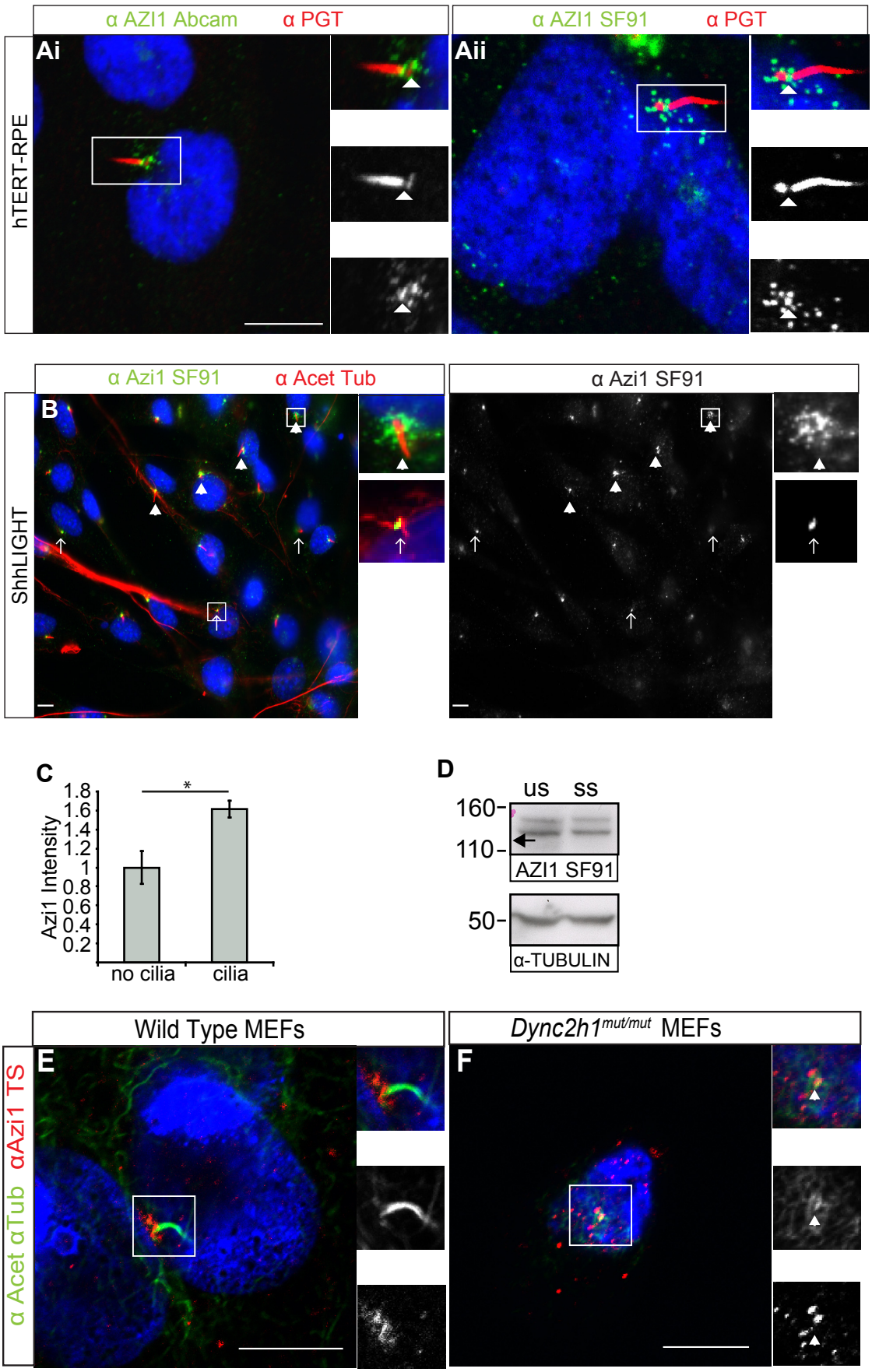

Figure 6.1 Azi1 localises around the basal body and to the transition zone, but is not trafficked into the cilium by IFT.

Figure 6.1 Azi1 localises around the basal body and to the transition zone, but is not trafficked into the cilium by IFT. (A) AZI1 localises around the basal body and is also enriched at the transition zone, identified as the gap in α-Poly-Glutamylated Tubulin (PGT) staining between the axoneme and the basal body (arrow on enlarged view). This is seen with both the Abcam (Ai) and the SF91 (Aii) antibodies to Azi1 (Antibody target sequences are shown in Figure 6.3) (C) α-acetylated α-tubulin stains the ciliary axoneme and basal bodies, and shows punctate staining at the centrosome of unciliated cells. α-Azi1 staining is more intense at the basal body in ciliated cells (closed arrows) than the centrosome of unciliated cells (open arrows) also see enlarged views as examples. (C) AZI1 intensity was quantified and scaled relative to Azi1 intensity in unciliated cells set at 1. (D) AZI1 levels remain unchanged upon 48h serum starvation (ss, compared to unsynchronised cells (us) in hTERT-RPE cells. The lower band runs closer to the expected size of 130kDa, the upper band could represent post translational modifications (E and F) Azi1 does not accumulate in *Dync2h1*$^{pol/pol}$ cilia, which lack retrograde IFT, suggesting Azi1 is not trafficked by IFT. Scale bars represent 10μm. * $p<0.05$ students t-test

48h serum starvation (ss), which induces ciliogenesis, suggesting it is Azi1 localisation as opposed to changes in expression levels which are altered in response to ciliogenesis (Figure 6.1D). These experiments were carried out in different cell lines (hTERT-RPE for the western and ShhLIGHT-II for the intensity calculations), so it would be useful to quantify Azi1 levels upon 48h ss in ShhLIGHT-II cells. These data suggest that Azi1 localisation but not expression levels changes during ciliogenesis.

Although Azi1 was not detected along the axoneme of cilia past the transition zone, it is possible a small amount (below the threshold of detection by antibody staining) could traffic into the cilium by IFT. To investigate this, we analysed Azi1 localisation in *Dync2h1*$^{pol/pol}$ MEFs, which lack retrograde IFT and show accumulation of IFT particles and cargo in shortened bulging cilia. We saw no build-up of Azi1; the localisation remained unchanged at the base of the cilia, suggesting it is not transported into the cilium by IFT (Figure 6.1 E and F).

6.2 Azi1 also localises to centriolar satellites and its centrosomal localisation is cell cycle and microtubule dependent.

As well as localising to the transition zone of cilia, Azi1 localised to punctuate spots around the centrosome and basal body. This localisation resembled centriolar satellite-marker PCM1 (Pericentriolar material 1) (Dammermann and Merdes, 2002; Kubo et al., 1999). Colocalisation studies showed that AZI1 does indeed colocalise very closely with PCM1 (Figure 6.2A). This colocalisation has since been confirmed by another group who also showed that AZI1 and PCM1 interact by immunoprecipitation (Akimov et al., 2011). Centriolar satellites are electron dense structures found near centrioles and basal bodies. The role of centriolar satellites is not well understood but it is suggested they may have a role in centriole maturation and/or ciliogenesis (Barenz et al., 2011; Dammermann and Merdes, 2002; Kim et al., 2004; Kubo et al., 1999).

PCM1 is dynamically localised throughout the cell cycle (Dammermann and Merdes, 2002) so I investigated the localisation of AZI1 throughout the cell cycle in HeLa cells. AZI1 also shows dynamic localisation throughout the cell cycle and in general, it colocalises with PCM1 throughout (Figure 6.2B). In S phase and G_2, PCM1 and AZI1 are enriched at or near the centrosome. In metaphase, AZI1 and PCM1 show weaker staining at the centrosome, along with punctuate staining throughout the cytoplasm; in many of these cytoplasmic puncta AZI1 and PCM1 remain colocalised (see Figure 6.2B metaphase inset). PCM1 but not AZI1 is seen at the spindle microtubules suggesting they do not always interact. During telophase, AZI1 and PCM1 re-concentrate around the centrosome and are both also found at the minus ends of midbody microtubules. Although PCM1 is seen at the midbody, AZI1 is absent from this structure (Figure 6.2B).

Centriolar satellites traffic along microtubules, and peri-centrosomal localisation of PCM1 has shown to be microtubule dependent. Therefore I investigated whether

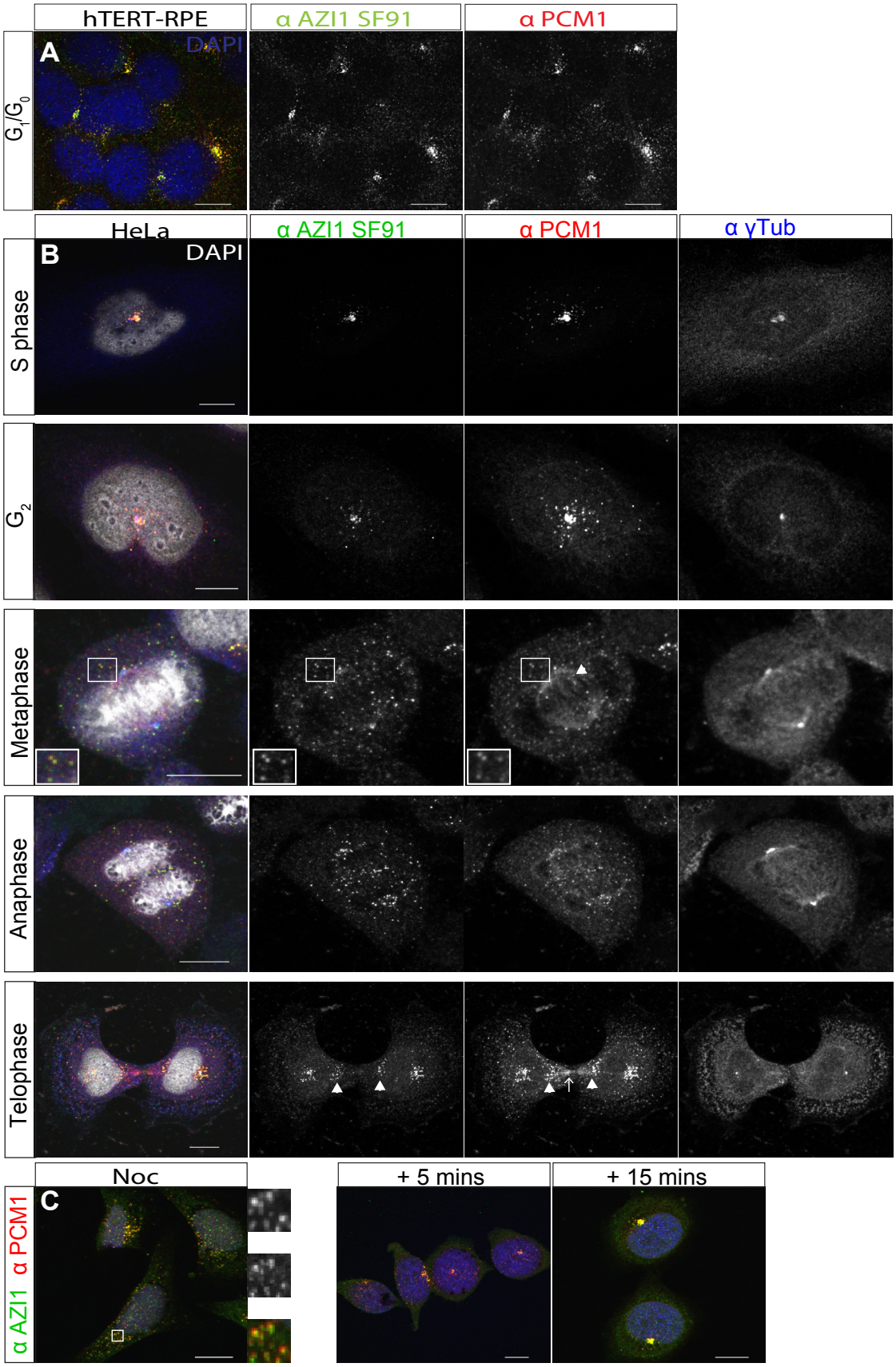

Figure 6.2 AZI1 colocalises with PCM1 at centriolar satellites, and localisation is cell cycle and microtubule dependent.

Figure 6.2 AZI1 colocalises with PCM1 at centriolar satellites, and localisation is cell cycle and microtubule dependent. (A) AZI1 colocalises with PCM1, a centriolar satellite marker, in hTERT-RPE cells which have been serum starved for 48h. (B) HeLa cell cycle was synchronised by double thymidine block to allow examination of AZI1 localisation throughout the cell cycle. AZI1 and PCM1 are found concentrated at the centrosome, marked by α-γ-Tubulin (α-γ-Tub), in S phase and G2. As the cells enter metaphase, PCM1 and AZI1 are found at the centrosome but at lower intensity. They are also dispersed throughout the cytoplasm, where they continue to colocalise (inset). PCM1 but not AZI1 is also found on the spindles (arrow, metaphase). During telophase, AZI1 and PCM1 re-concentrate at the centrosome, and are also seen at the minus ends of the midbody microtubules (closed arrow, telophase). PCM1 but not AZI1 localises to the midbody (open arrow, telophase). (C) Upon 30 min nocodazole treatment, microtubules are depolymerised (not shown) and PCM1 and AZI1 are dispersed throughout the cytoplasm, although they remain colocalised (panels to the right: PCM1 at top, AZI1 in middle, merged at bottom), showing that AZI1 centrosomal localisation is microtubule dependent. When nocodazole is washed out for 5 minutes, AZI1 and PCM1 begin to re-concentrate around the centrosome, and after 15 minutes localisation is peri-centrosomal again. Scale bars represent 10μm.

AZI1 localisation is microtubule dependent by nocodazole treating HeLa cells to induce microtubule depolymerisation. After 30 minutes of nocodazole treatment microtubules are depolymerised (data not shown), both AZI1 and PCM1 become dispersed throughout the cell and no longer concentrate at the centrosome (Figure 6.2C). Interestingly they remain colocalised within the cytoplasm, suggesting their interaction is not microtubule dependent (Figure 6.2C enlargement). Nocodazole was washed out and microtubules allowed to repolymerise for 5 and 15 minutes. After 5 minutes, AZI1 and PCM1 are still fairly dispersed throughout the cell although some cells show more focussed staining. After 15 minutes washout, AZI1 and PCM1 once again show more focussed, presumably peri-centrosomal staining (Figure 6.2C). No centrosomal marker was used in this experiment, however the focussed staining resembles the staining seen in untreated cells, so it is likely to be peri-centrosomal.

6.3 Generation of *Azi1* mutant mice

Previous studies in zebrafish and fruitfly show Azi1 is involved in cilia formation and/or function in these organisms (Ma and Jarman, 2011; Wilkinson et al., 2009).

The finding that siRNA knockdown of *Azi1* in mammalian cells leads to reduced cilia numbers, which can be rescued by overexpressing an siRNA insensitive version of the gene (Chapter 5), and the observation that Azi1 localises to the ciliary transition zone and centriolar satellites in mammalian cells (Figure 6.1 and 2) suggests Azi1 may have a conserved role in mammalian ciliogenesis. In order to investigate the *in vivo* role of mammalian Azi1 we generated *Azi1* mutant mice. We ordered $Azi1^{Gt(CCOG35)Wtsi}$ embryonic stem (ES) cells from the Sanger Institute Gene Trap Resource, which have a gene trap inserted into intron 2 of *Azi1* (Figure 6.3A). We confirmed the insertion was present in intron 2 of *Azi1* and then injected the ES cells into C57BL/6J blastocysts to generate chimeras. These chimeras were bred to C57Bl/6J females to determine germ-line transmission and produce heterozygote $Azi1^{+/Gt(CCOG35)Wtsi}$ mice, which were then intercrossed to generate $Azi1^{Gt(CCOG35)Wtsi/Gt(CCOG35)Wtsi}$ mice (referred to as $Azi1^{Gt/Gt}$ for this thesis). The gene trap inserts a strong splice acceptor and *β-Geo* gene into intron 2 of *Azi1,* which should force splicing from exon 2 onto the inserted splice acceptor, leading to premature termination of *Azi1* transcript on the β-Geo poly A. This leads to a severe truncation of the Azi1 protein to 69 amino acids (aa) (Figure 6.3 A and B). By examining the mRNA from $Azi1^{Gt/Gt}$ embryos I confirmed that no wild type *Azi1* transcript is detected from exons 3-13 in $Azi1^{Gt/Gt}$ animals, and also confirmed the expression of the gene trap allele (Figure 6.3C). Some low level expression of exons 20-24 was detected. This is likely to be non- translated, because when we probe protein extracts from $Azi1^{+/+}$, $Azi1^{+/Gt}$ and $Azi1^{Gt/Gt}$ testes with an antibody raised against the C-terminal of Azi1, we find Azi1 protein expression is reduced in $Azi1^{+/Gt}$ mice and completely absent in $Azi1^{Gt/Gt}$ mice (Figure 6.3C and D). Further supporting the theory that the mRNA we detect is non-translated, there are several non-coding transcripts detailed in ensembl at the 3' end of *Azi1*. Expression of these untranslated transcripts is predicted to be unaffected by the gene trap insertion.

Azi1 has several conserved coiled-coil domains, mostly in the C terminal half of the protein, some of which form a t-SNARE domain, a domain found in proteins involved in vesicular trafficking, which facilitates vesicular fusion (Li and Chin, 2003) (Figure 6.3B and 6.4). Alignment of *Azi1* orthologues in several organisms shows the C terminal of the protein is much more conserved than the N terminal

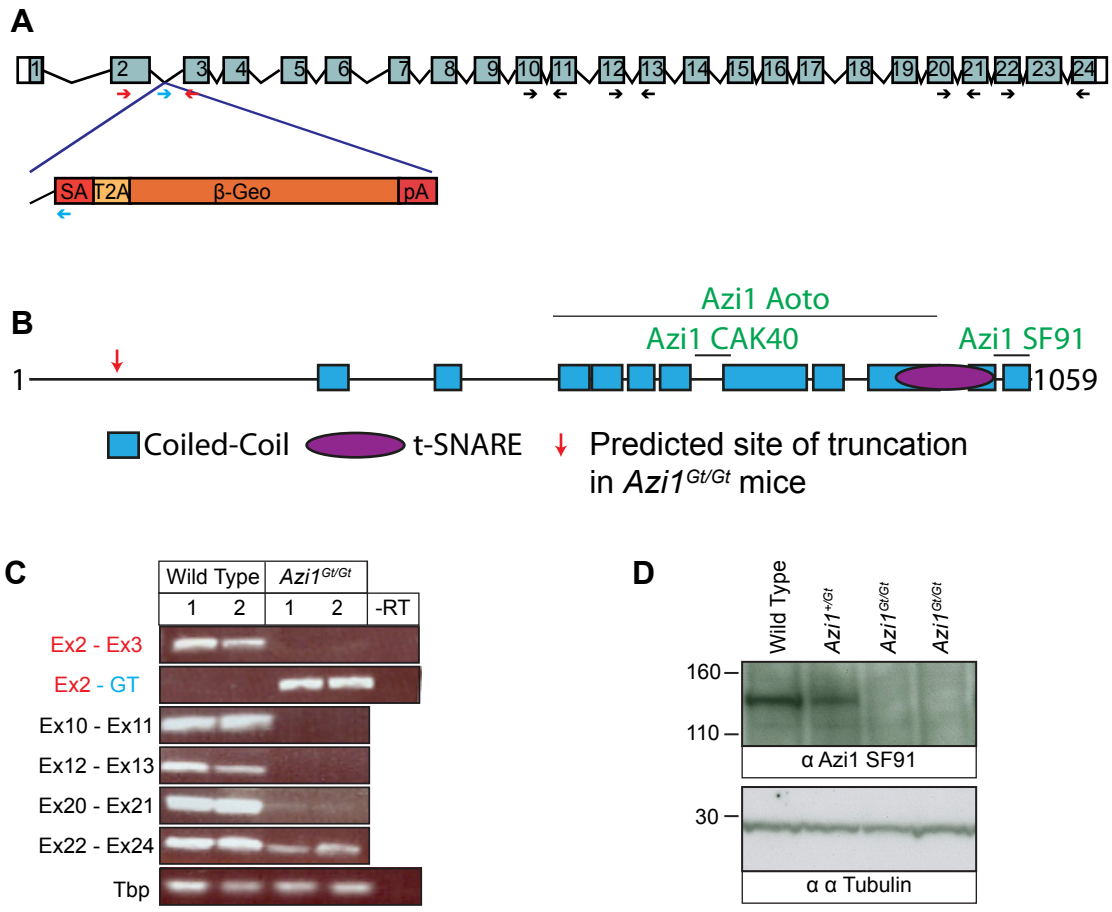

Figure 6.3 *Azi1*$^{Gt/Gt}$ mice are a null allele of *Azi1*. Gene trap mice were generated from ES cells obtained from the SIGTR. (A) The gene trap is inserted in intron 2 of *Azi1*. Exons are shown as boxes with translated transcript shown in blue. Arrows indicate primers used to characterise the mRNA expression in *Azi1*$^{Gt/Gt}$ mice. Blue and red arrows indicate primers used for genotyping. SA - Splice acceptor, T2A - self cleaving peptide, pA - polyA. (B) Schematic showing the predicted domain structure of Azi1 (predicted domains from www.ensembl.org). Red arrow indicates the predicted site of truncation in *Azi1*$^{Gt/Gt}$ mice. The truncated product lacks all the predicted domains. Shown in green are the sequences targetted by different antibodies, all of which have been used to confirm Azi1 localisation (Figure 5.5, 6.1, 6.2 and data not shown). Abcam does not give details of the target sequence of the antibody used in Figure 6.1A. (C) mRNA expression of *Azi1* in E 13.5 embryos was examined using primers depicted in (A). No expression of exons 3-13 was detected in *Azi1*$^{Gt/Gt}$ mice. The gene trap was expressed in *Azi1*$^{Gt/Gt}$ mice. Some low expression of exons 20-24 was detected but this is likely to be untranslated (see D). (D) No Azi1 protein expression was detected in *Azi1*$^{Gt/Gt}$ mutant testes, despite a strong band of the correct size being detected in wild type and at lower levels in *Azi1*$^{+/Gt}$ testes extract using an antibody to the C terminal of Azi1 (Azi1 SF91 B). Therefore it was concluded that *Azi1*$^{Gt/Gt}$ mice are a null allele of *Azi1*.

(Figure 6.4). The severely truncated 69 aa protein which is predicted to be expressed in *Azi1*$^{Gt/Gt}$ mice is lacking the t-SNARE domain and all the coiled coil domains, as well as several stretches of highly conserved residues suggesting it is most likely to be non-functional. We therefore concluded that *Azi1*$^{Gt/Gt}$ mice are null for Azi1.

6.4 *Azi1* null mice show male infertility

Surprisingly, *Azi1*$^{Gt/Gt}$ mice are born and survive. This suggests *Azi1* is not essential for ciliogenesis in mouse, as mouse mutants which lack cilia show early embryonic lethality and characteristic patterning defects (Huangfu et al., 2003). *Azi1*$^{Gt/Gt}$ mice are born at sub-mendelian ratios ($p < 0.01$ Chi squared, Table 6.1), and we also see significantly fewer *Azi1*$^{+/Gt}$ mice than expected. We are still backcrossing these mice onto C57BL6/J to get a more inbred line, but initial data suggest that litters from later generations do not show this loss of *Azi1*$^{Gt/Gt}$ or *Azi1*$^{+/Gt}$ mice (Table 6.1). Further backcrossing is needed, but this suggests the lethality was due to a linked lethal mutation, and not due to the gene trap insertion in *Azi1*. Therefore we conclude *Azi1* is not essential for ciliogenesis in mouse.

Interestingly, *Azi1*$^{Gt/Gt}$ males which survive are infertile. Six *Azi1*$^{Gt/Gt}$ males were observed to plug wild type females at least twice each, a total of 27 plugs were observed, but no female became visibly pregnant and no litters were born. This phenotype of male infertility was observed in all mutants tested and not seen in any heterozygotes, so although backcrossing is on-going, this suggests the male infertility is caused by the gene trap insertion into the *Azi1* gene. In contrast, females are fertile. An average litter of 8.2 pups was born to *Azi1*$^{Gt/Gt}$ females (5 litters from 3 *Azi1*$^{Gt/Gt}$ females) compared to an average litter of 9 pups born to *Azi1*$^{+/Gt}$ females (6 litters from 2 *Azi1*$^{+/Gt}$ females) which is not statistically different ($p = 0.38$, students t test).

As male infertility is a symptom of some ciliopathies, and can occur in conjunction with other, late-onset ciliopathic phenotypes such as retinal degeneration, kidney and

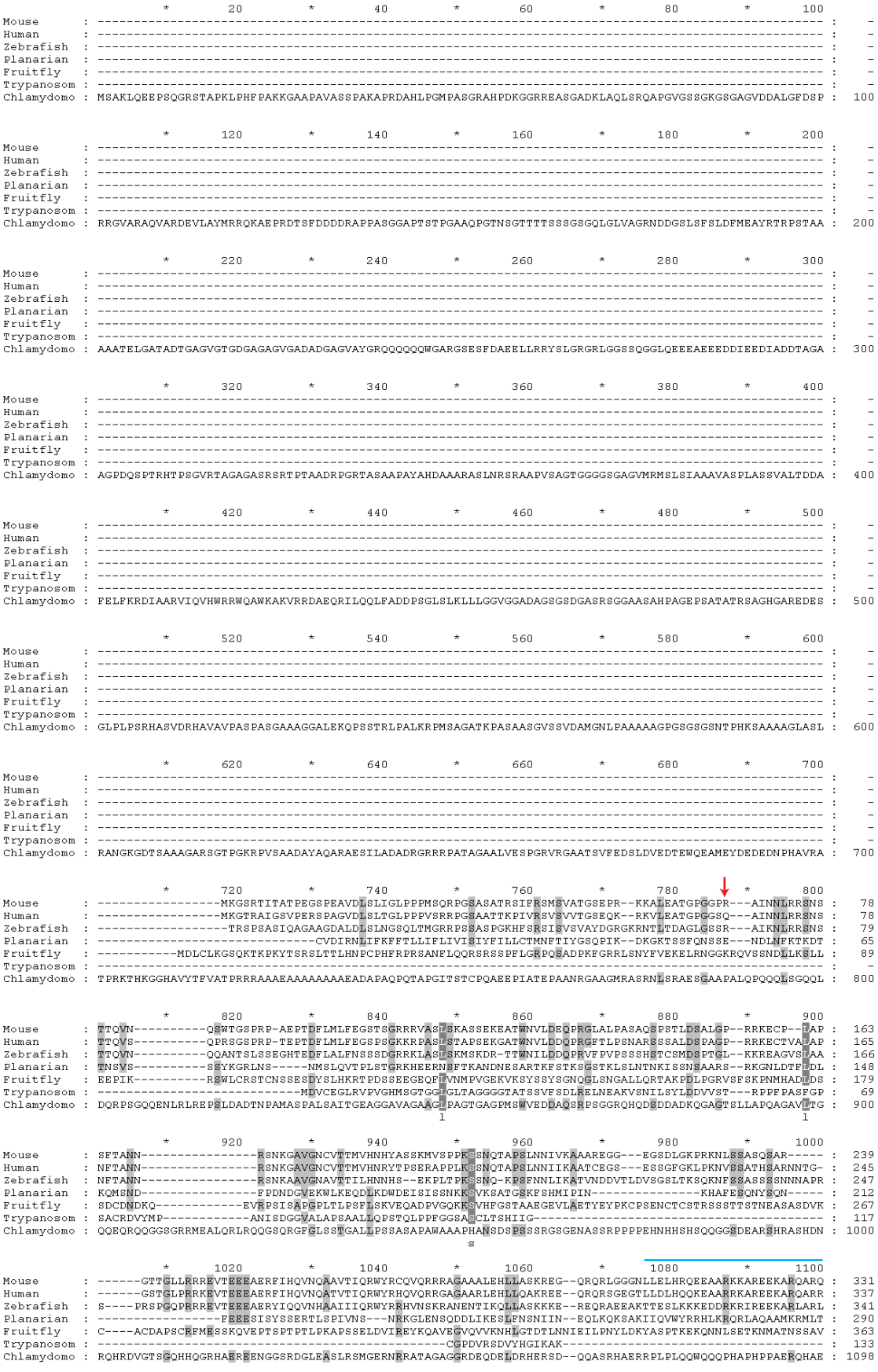
Mouse
Human
Zebrafish
Planarian
Fruitfly
Trypanosom
Chlamydomo

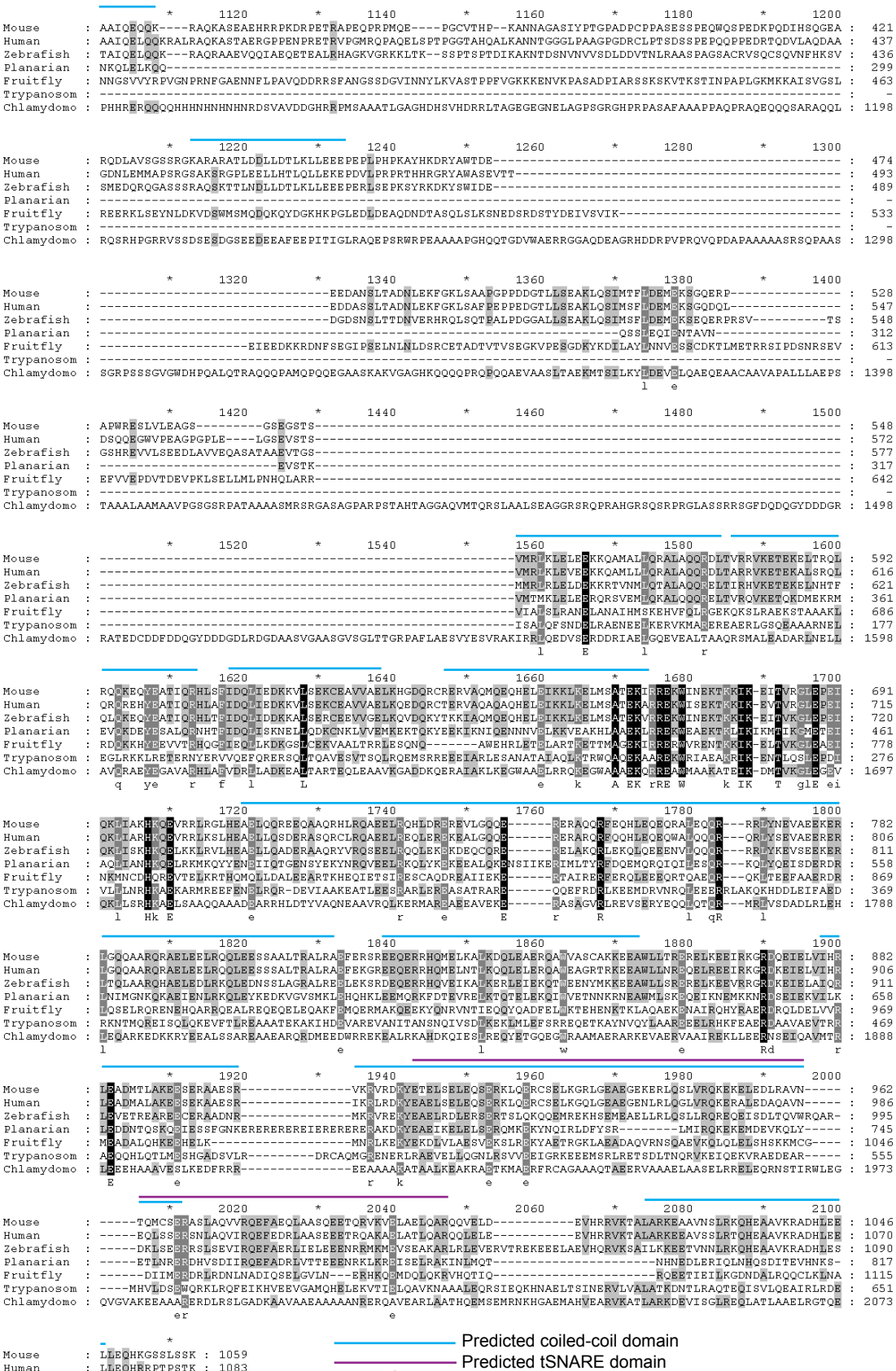

Figure 6.4 Conservation of *Azi1* orthologues.

Figure 6.4 Conservation of Azi1 orthologues Protein sequences of Azi1 orthologues in *H. sapiens, M. musculus, D. rerio, S. mediterranea, D. melanogaster, T. Bruceii* and *C. reinhardtii* were aligned using CLUSTALW (Philippe Gautier, MRC HGU). The predicted mouse coiled-coil domains and tSNARE domains are highlighted (predictions taken from www.ensembl.org). Also marked is the predicted site of truncation in Azi1Gt/Gt mice (red arrow 69 aa.) The predicted truncated protein lacks the more highly conserved C terminus and all the coiled coil and t-SNARE domains.

pancreatic cysts and obesity in mouse mutants of ciliopathy genes, we aged the mice and watched for late-onset phenotypes (Fath et al., 2005; Hildebrandt et al., 2011; Kim et al., 2004; Mykytyn et al., 2004). These studies are on-going, but so far, the eyes of seven *Azi1*$^{Gt/Gt}$ animals were examined by ophthalmoscope at 6 months of age and no retinal degeneration was observed. The lack of retinal degeneration was confirmed by histology in two mice (Figure 6.5 A-C). No pancreatic or kidney cysts have been observed at 6 months (Figure 6.5 D-F and data not shown). Preliminary results suggest that these mice do not suffer from obesity – no difference was observed in weights of mice at 9 months of age (Figure 6.5 G and H).

As mentioned, aging studies are preliminary and on-going, so although no late onset ciliopathic phenotypes have yet been observed in these mice, we cannot yet exclude such phenotypes. Interestingly other transition zone protein mutants show male infertility, and in the case of *Nphp1* mutant mice, male infertility is the only phenotype seen, despite the fact this gene is linked to cystic kidneys in humans (Jiang et al., 2008; Won et al., 2011).

Table 6.1 Genotypes of animals born from *Azi1* Het x Het matings

Genotype	*Azi1*$^{+/+}$	*Azi1*$^{+/Gt}$	*Azi1*$^{Gt/Gt}$	No. litters	Chi squared
All matings	52	68	21	17	P<0.01
F_1 or F_2	37	38	22	13	P<0.001
F_3	10	17	7	4	Not significant

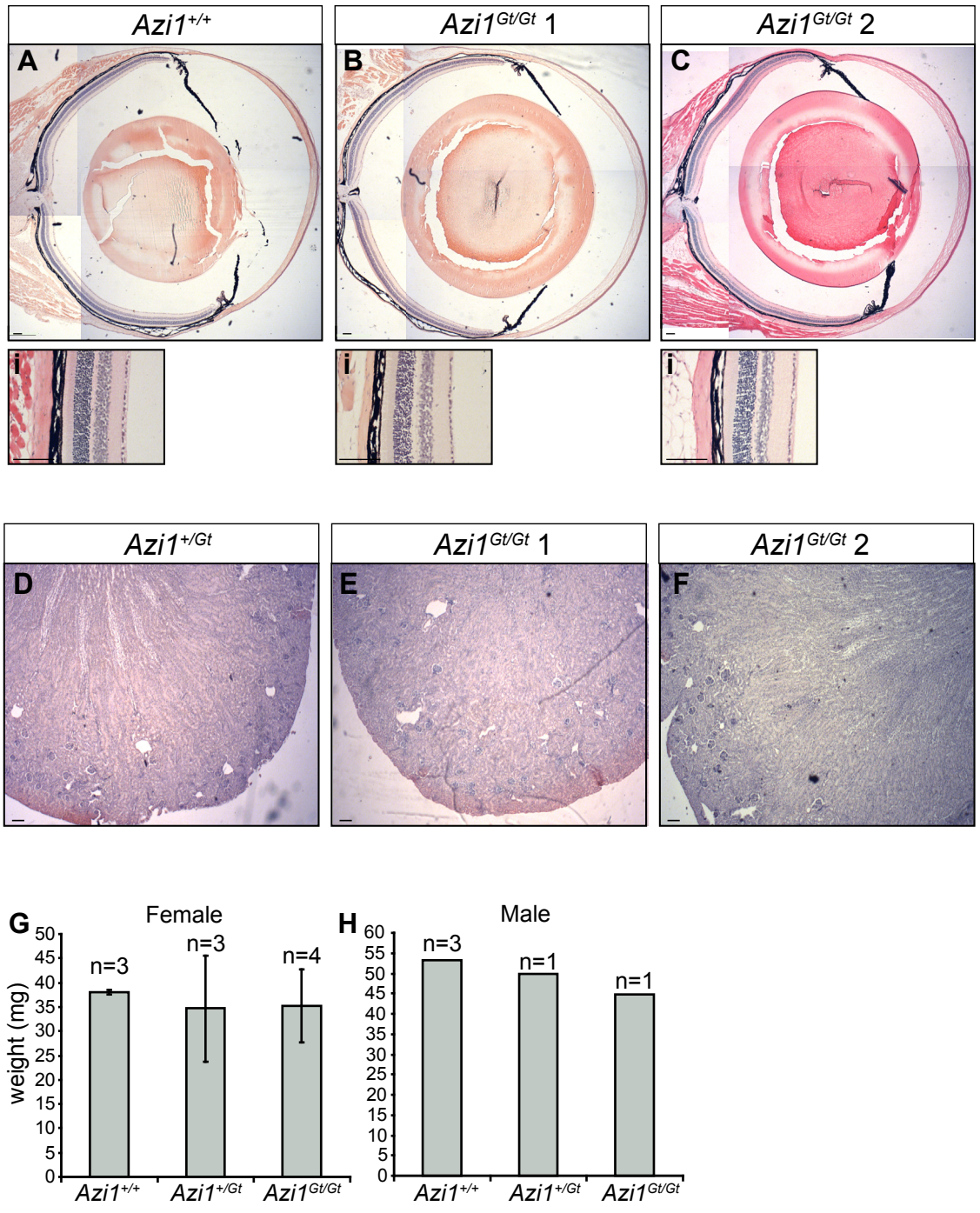

Figure 6.5 No late-onset ciliopathy phenotypes oberved in *Azi1*$^{Gt/Gt}$ mice.
(A - C) Eyes of seven mutant mice at 6 months of age were examined by opthalmoscope and no retinal degeneration was observed (data not shown). This was confirmed by examining histology on H&E stained wax sections in two mutants (B and C), which show no retinal degeneration (Bi and Ci). (A) shows the eye of a wild type litter mate. (D - E) H&E stained sections of kidney from 6 months old *Azi1*$^{+/Gt}$ (D) or *Azi1*$^{Gt/Gt}$ (E and F) mice, showing no cysts in the mutant kidneys. Scale bars represent 100µm. (G and H) Graph showing weight of mice at 9 months. (G) Female *Azi1*$^{Gt/Gt}$ mice do not differ significantly from *Azi1*$^{+/Gt}$ or wild type in weight at 9 months (students t test). (H) Preliminary results for males suggest mutants do not differ significantly from *Azi1*$^{+/Gt}$ or wild type in weight at 9 months old.

6.5 Azi1 is expressed in ciliated tissues

As the gene trap strategy inserts *β-Geo* under the control of the *Azi1* promoter, this enabled us to examine the expression pattern of *Azi1* by LacZ staining (Figure 6.3A). At E11.5, *Azi1* is fairly constitutively expressed at low levels with higher levels in the forebrain, limb, eye and the somites (Figure 6.6 A and B). In the adult, *Azi1* is expressed in ciliated tissues, such as the highly multiciliated epithelia of the oviduct where *Azi1* is very highly expressed (Figure 6.6 C and D). It is also expressed at lower levels throughout the ovary (Figure 6.6 C-E). Preliminary results in the testes seem consistent with previous studies which state Azi1 protein is expressed in late pachytene spermatocytes and round and elongating spermatids in the testes. On-going studies are underway to confirm the expression pattern as well as Azi1 protein localisation in the testes (Aoto et al., 1995) (Figure 6.6 F). *Azi1* is expressed in the retina, although surprisingly it is expressed in the ganglion cell layer, whereas *Azi1* was not expressed in the photoreceptors, which possess specialised cilia, at least not at levels detectable by LacZ staining (Figure 6.6 G). As mentioned, *Azi1* was identified as upregulated in *Atonal-GFP* positive chordotonal ciliated neurons in flies and interestingly the orthologue of *Atonal*, *Math5* is expressed in the ganglion cell layer (Brown et al., 2001; Wang et al., 2001). Perhaps this drives *Azi1* expression in the ganglion cell layer.

Expression was also detected in the brain, in the outer cortex and the cerebellum, as well as the kidney by whole-mount staining but it was difficult to get a strong enough signal for sectioning (Figure 6.6 I-K). In summary, *Azi1* is fairly ubiquitously expressed during development, but more highly in limbs, eyes, forebrain and somites, and is expressed in ciliated tissues such as the multiciliated oviduct epithelium and the kidney in adults (Figure 6.6).

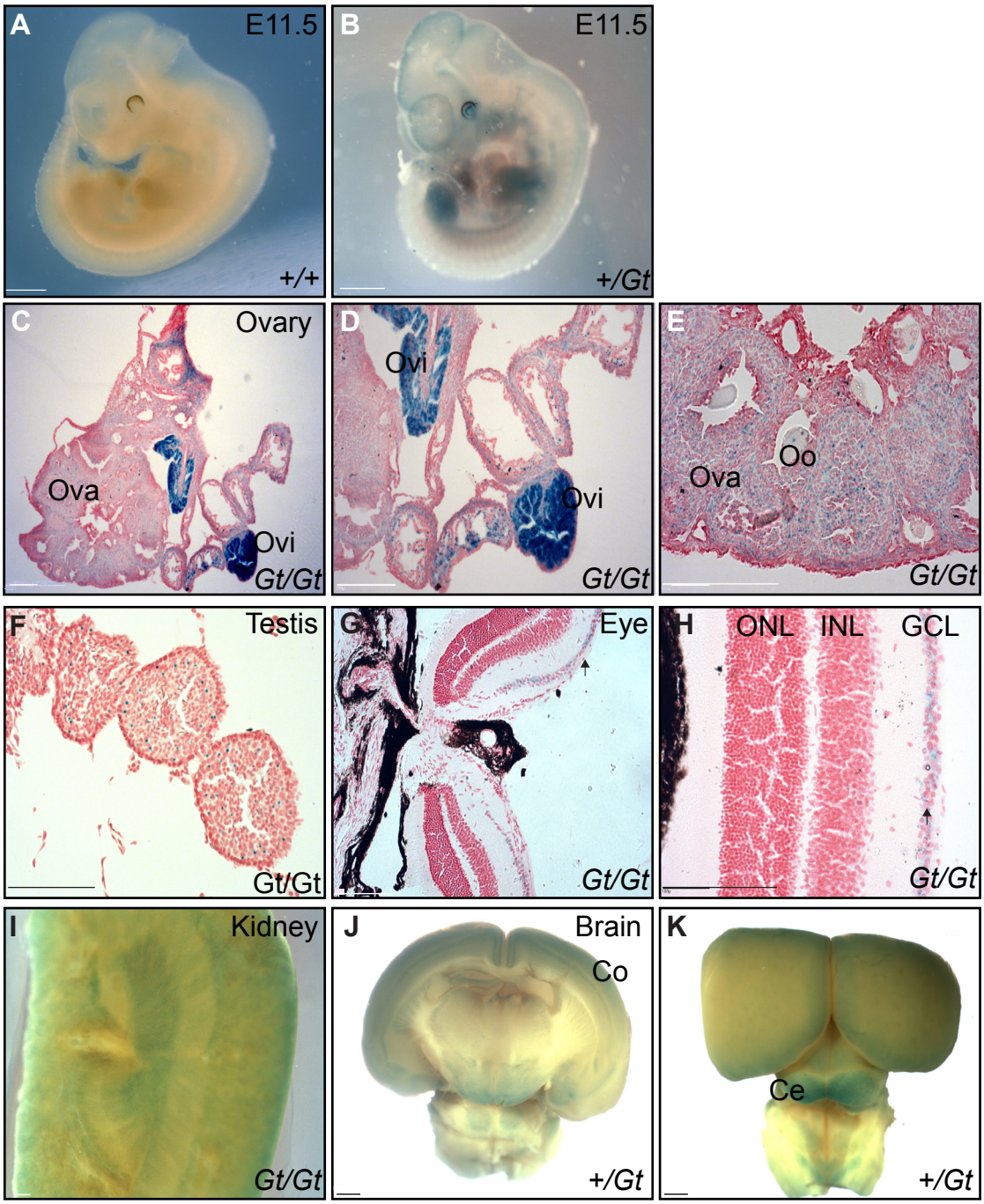

Figure 6.6 *Azi1* is expressed in ciliated tissues.

Figure 6.6 *Azi1* is expressed in ciliated tissues. The gene trap inserts *β-Geo* under the control of the *Azi1* promoter allowing the examination of *Azi1* expression pattern by LacZ staining, in both heterozygotes and mutants. Examination in mutants allows increased sensitivity due to two copies of the *β-Geo* being expressed. (A and B) *Azi1* is expressed fairly ubiquitously at low levels at E11.5, with higher expression in the limbs, forebrain, eye and somites (B). No staining is seen in wild type control embryos (A). (C-E) *Azi1* expression in the ovary (Ova) and oviduct (Ovi). *Azi1* is highly expressed in the multiciliated epithelium in the oviduct, and is expressed at lower levels in the ovary itself. (Oo = oocyte) (F) *Azi1* expression in $Azi1^{Gt/Gt}$ P28 testis. Histology is poor (see Figure 6.8 for histological analysis of $Azi1^{Gt/Gt}$ testes) but it seems *Azi1* may be expressed in round and elongating spermatids (G and H) P28 eye showing *Azi1* is expressed in the ganglion cell layer (GCL) of the retina, but surprisingly is not expressed in the photoreceptors (at least not at levels detectable by this method). (INL = inner nuclear layer, ONL = outer nuclear layer) (I) Wholemount LacZ staining shows *Azi1* is expressed in the kidney, but levels were too low to detect upon sectioning. (J and K) *Azi1* is expressed in the outer cortex (Co) and the cerebellum (Ce). Again staining is too faint to detect easily once sectioned. (A, B, J, K) Scale bar represents 1mm. (C-I) Scale bar represents 250μm.

6.6 Ciliary, centriolar duplication or centriolar satellite defects are not detected in *Azi1* null MEFs

In Chapter 5, I showed that siRNA knockdown of *Azi1* leads to a reduction in the number of cilia in the mouse fibroblast cell line ShhLIGHT-II. Therefore I examined the cilia of MEFs from $Azi1^{Gt/Gt}$ and wild type litter mates. Using anti-Arl13b to stain the ciliary membranes, and anti-γ-tubulin to stain the basal bodies, the number and length of cilia was counted in $Azi1^{+/+}$ and $Azi1^{Gt/Gt}$ MEFs. No change in the number of cells with cilia, or the length of the cilia was seen (Figure 6.7 A, F, K and data not shown). The number of cells with extra centrosomes, i.e. more than two γ-tubulin foci, was also counted, and again there was no difference between wild type and *Azi1* mutant MEFs. The localisation of Acetylated α-tubulin, an axoneme marker and Ift88, an IFT-B complex protein, was also examined but remained unchanged between wild type and *Azi1* mutant MEFs (Figure 6.7 B, G, E and J).

As Azi1 localises to the transition zone (Fig 6.1A), I examined a marker of the transition zone, Nphp1; localisation was identical in $Azi1^{+/+}$ and $Azi1^{Gt/Gt}$ cilia

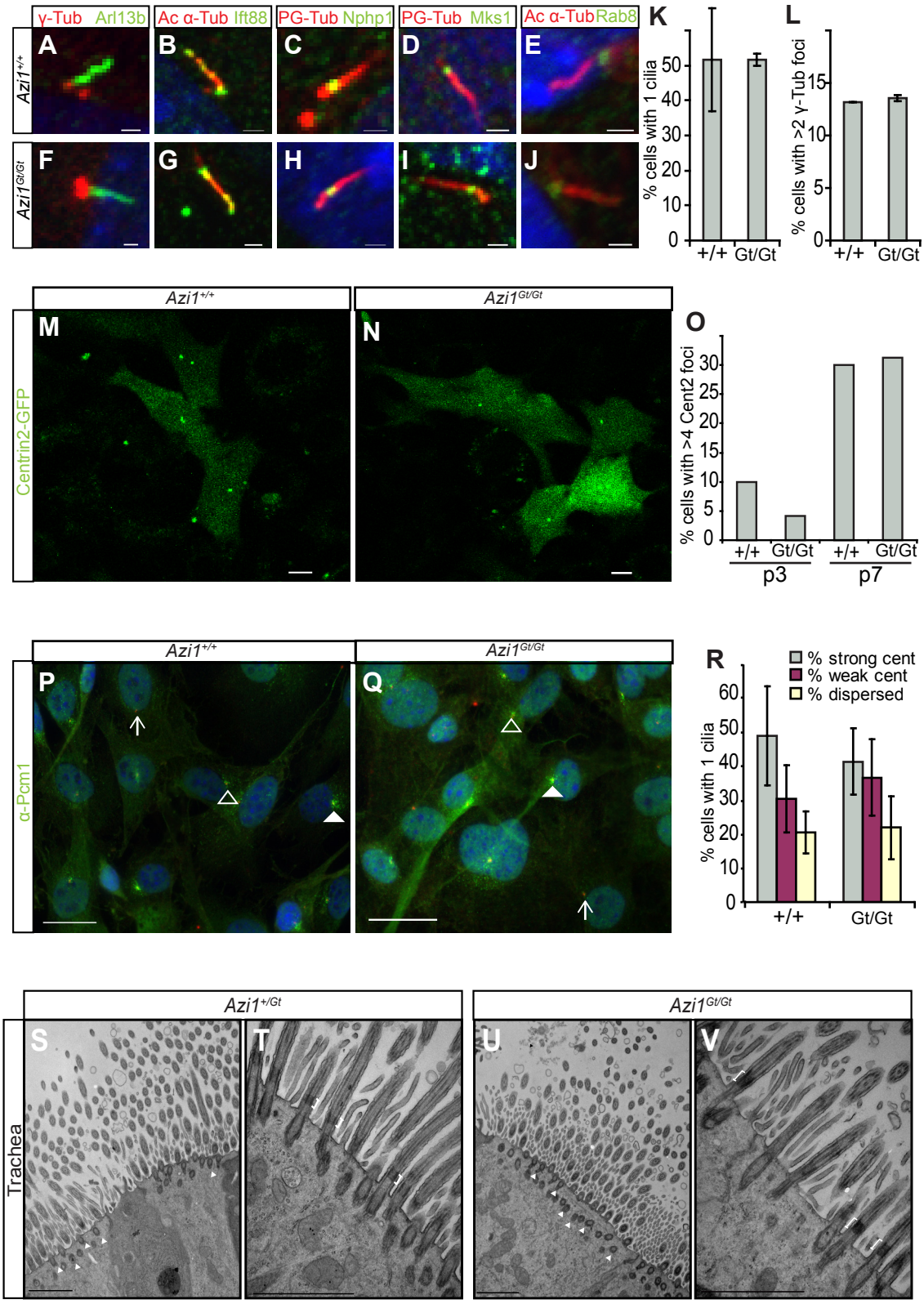

Figure 6.7 Azi1 is not required for primary ciliiogenesis, centriole maturation or basal body docking

Figure 6.7 Azi1 is not required for primary ciliiogenesis, centriole maturation or basal body docking (A-L) *Azi1*$^{Gt/Gt}$ MEFs have normal numbers of cilia and centrosomes and normal cilia compartmentalisation as shown by localisation of ciliary membrane protein Arl13b (A and F), IFT-B protein Ift88 (B and G), transition zone markers Nphp1 and Mks1 (C, D, H and I) and small GTPase Rab8 (E and J) (PG-Tub = Poly-glutamylated tubulin, Ac α-tub = Acetylated α-tubulin). (K) Quantification of the percentage of cells with cilia stained by α-Arl13b. (L) Quantification of the number of cells with >2 centrosomes stained by α-γ-Tubulin (γ-Tub). (K and L) n=2 cell lines per genotype. (M and N) Centrin-2-GFP was transfected into wild type and *Azi1*$^{Gt/Gt}$ MEFs to mark centrioles. (M) Although the percentage of cells with more than 4 Centrin-2 positive foci increases with passage number (p), there is no difference in centriole numbers between *Azi1*$^{+/+}$ and *Azi1*$^{Gt/Gt}$ MEFs. (P and Q) Unsynchronised MEFs were stained with α-Pcm1. The number of cells with strong centrosomal (strong cent, filled arrowhead), weak centrosomal (weak cent, open arrowhead) or dispersed Pcm1 staining (arrow) does not change between wild type and Azi1Gt/Gt MEFs (R). (S-V) TEM shows *Azi1*$^{Gt/Gt}$ multiciliated trachea have normal cilia numbers, basal body docking (arrows S and U) and transition zone morphology (brackets T and V). A-J scale bars 1μm, M-N scale bars 50μm, S-V scale bars 2μm.

(Figure 6.7 C and H). There are two main protein complexes found at the transition zone; the NPHP complex and the MKS complex (Sang et al., 2011; Williams et al., 2011; Williams et al., 2008). Nphp1 is part of the NPHP complex, so I also checked the localisation of a second transition zone protein, Mks1, which is a component of the MKS complex, and once again localisation remained unchanged (Figure 6.7 D and I). Together these data suggest the gross composition of the transition zone in *Azi1* mutants is unchanged.

Finally, two lines of evidence suggest Azi1 may have a role in vesicular trafficking: (i) Azi1 has a C-terminal t-SNARE domain, which is a domain found in proteins involved in vesicular trafficking and membrane fusion, such as Syntaxins (Li and Chin, 2003), and (ii) Azi1 has been shown in *T. brucei* to interact with the small GTPase Rab11, which is involved in vesicular trafficking to the cilium along with Rab8 (Gabernet-Castello et al., 2011; Knodler et al., 2010). Therefore I also examined the localisation of Rab8, a small GTPase involved in trafficking to the cilium, and saw it localised at the base of the cilium, as reported (Figure 6.7 E). However as with the various ciliary markers, localisation did not change in the *Azi1*$^{Gt/Gt}$ MEFs (Figure 6.7 J).

As Azi1 localises to centriolar satellites (Figure 6.2), which have been suggested to have a role in centriolar maturation (Dammermann and Merdes, 2002), I examined

the centriolar marker Centrin2-GFP, as well as the centriolar satellite marker Pcm1 in the *Azi1* mutant MEFs. To account for all stages of the centriole duplication cycle, cells with more than four centrin2-GFP foci were considered to have supernumerary centrioles. There was no difference in the number of cells with abnormal numbers of centrioles (>4 Centrin2-GFP foci) between wild type and mutant MEFs, although the number of MEFs with extra centrioles increased with passage number regardless of genotype (Figure 6.7M-O).

Pcm1 localisation was examined in unsynchronised MEFs, and the localisation of Pcm1 remained unchanged in the mutant MEFs, suggesting Azi1 is not required for recruitment of Pcm1 to centriolar satellites, or for the formation of centriolar satellites (Figure 6.7 P-R).

As it has been proposed that Azi1 is involved in motile ciliogenesis, we examined whether Azi1 is required for motile ciliogenesis and basal body docking *in vivo*, by performing transmission electron microscopy (TEM) on trachea from $Azi1^{+/Gt}$ and $Azi1^{Gt/Gt}$ mice. No difference was observed in the number of cilia or the docking of basal bodies, nor in the transition zone morphology or basal body appendages between $Azi1^{+/Gt}$ and $Azi1^{Gt/Gt}$ trachea, suggesting Azi1 is not involved in motile ciliogenesis in the mammalian trachea (Figure 6.7 S-V and data not shown).

These data suggests that Azi1 is not essential for cilia formation in MEFs, and seems to contradict the siRNA screen data which suggested a reduction of Azi1 lead to reduced ciliogenesis. This discrepancy will be discussed further below. It also suggests Azi1 is not required for centriolar duplication in MEFs, basal body maturation or motile ciliogenesis in the trachea.

6.7 *Azi1*$^{Gt/Gt}$ male infertility is due spermiogenesis arrest at Stage IX, just as the flagella is forming

Azi1$^{Gt/Gt}$ mutant males are completely infertile, with a 50 fold reduction in sperm density from the cauda epididymus (Figure 6.9A). The testes of *Azi1*$^{Gt/Gt}$ mice are significantly smaller than wild type testes (Figure 6.8A, p=0.037, student t test). To investigate the infertility phenotype further, histology of mutant testes was examined. *Azi1*$^{Gt/Gt}$ mutant testes have a reduced tubule diameter and a much reduced lumen diameter (Figure 6.8B). Mutant tubules show spermatogonia, spermatocytes and round spermatids of normal morphology. However there are reduced numbers of elongating spermatids and spermatozoa, and flagella are not visible in mutant tubules.

Spermiogenesis arrests at stage IX in *Azi1*$^{Gt/Gt}$ testes, just as several morphological changes are occurring in the elongating spermatids, including nuclear remodelling, cytoplasmic elongation and flagella formation (Oakberg, 1956; Yan, 2009). Sperm tails are absent/greatly reduced in mutant tubules and elongating spermatids show disorganised localisation within the tubule (Figure 6.8C and D). Residual cytoplasm is poorly condensed and there is also some evidence of phagocytosis of degenerating elongates in mutant tubules (Figure 6.8E and F). Much fewer sperm were observed in the epididymis of *Azi1*$^{Gt/Gt}$ mice compared to wild type (Figure 6.8G).

To investigate whether the elongating spermatids were undergoing apoptosis, we analysed activated Caspase3a (Casp3) staining in wild type and *Azi1*$^{Gt/Gt}$ mutant tubules. Some activated Casp3 was occasionally seen in wild type spermatogonia near the basement membrane of the tubule (Figure 6.8H), consistent with degeneration of spermatogonia in wild type testes during normal spermatogenesis (Huckins, 1978) (Figure 6.8H and I). In contrast, in the mutant tubules an elevated number of Casp3 positive cells were observed, with some tubules showing very high numbers of Casp3 positive elongating spermatids, suggesting they are undergoing apoptosis at a specific stage (Figure 6.8J). This data is preliminary (n=1 of each

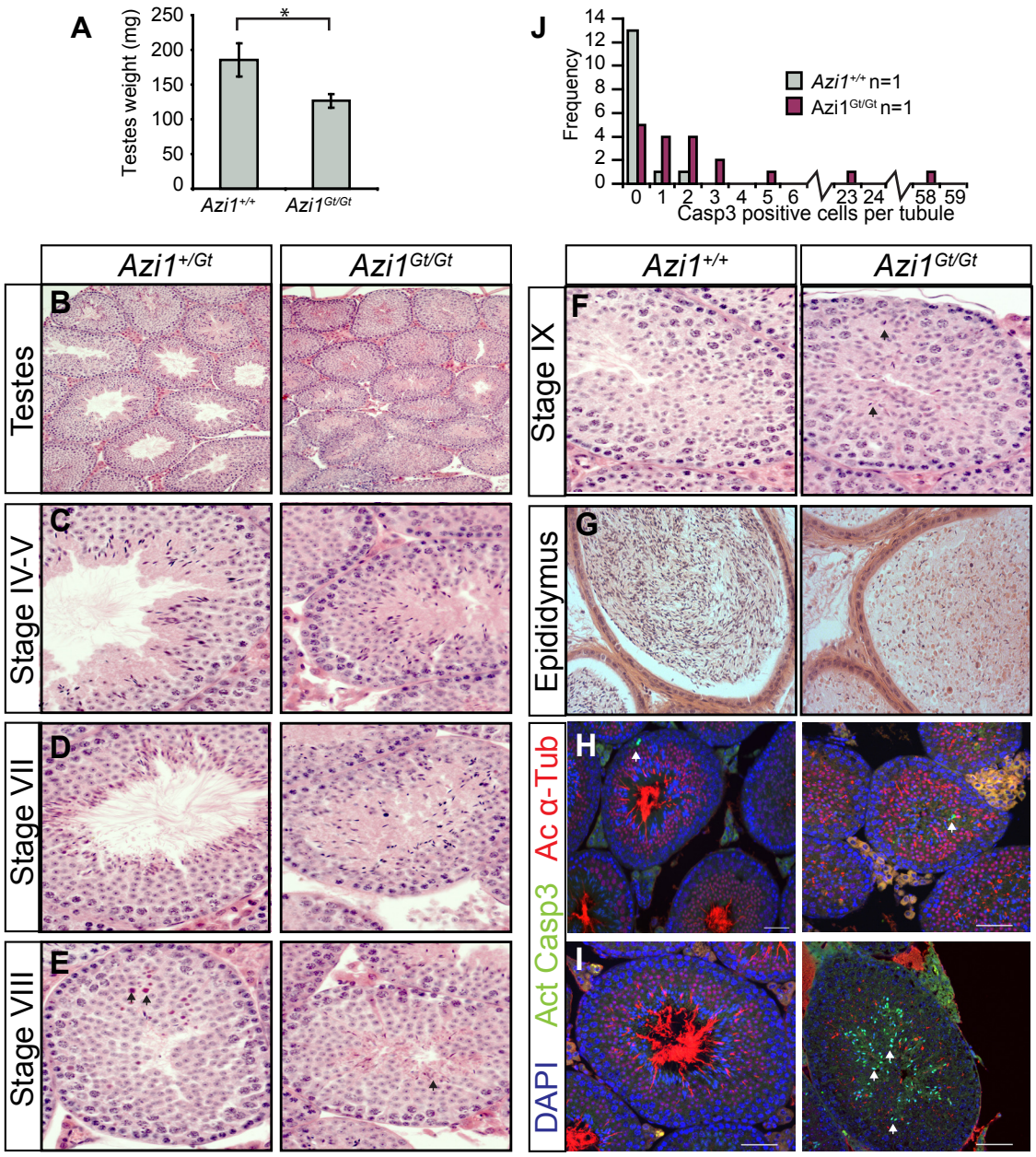

Figure 6.8 Spermiogenesis arrest at Stage IX in *Azi1*$^{Gt/Gt}$ males. (A) Testes of *Azi1*$^{Gt/Gt}$ males show significantly reduced weight compared with wild type littermates (* p<0.05, students t test, n=3 per genotype.) Shown is mean +/- standard deviation. (B - F) H&E stained sections of 6 month old *Azi1*$^{+/Gt}$ and *Azi1*$^{Gt/Gt}$ testes. (Note: samples were processed by Emma Hall and imaged by Dr Lee Smith). (B) *Azi1*$^{Gt/Gt}$ tubules have reduced lumen diameter. (C and D) Stage IV-V and Stage VII tubules. Sperm tails are clearly visible in *Azi1*$^{+/Gt}$ lumen but cannot be identified in *Azi1*$^{Gt/Gt}$ tubules. Sperm heads are disorganised in *Azi1*$^{Gt/Gt}$ tubules. (E) Stage VIII just after spermatazoa release in *Azi1*$^{+/Gt}$ tubules. Residual cytoplasm is poorly condensed in *Azi1*$^{Gt/Gt}$ (arrows show condensed residual bodies in *Azi1*$^{+/Gt}$). (F) Spermiogenesis arrests at stage IX in *Azi1*$^{Gt/Gt}$ mice. Phagocytosis of elongated spermatids is apparent in the *Azi1*$^{Gt/Gt}$ tubules (arrows). (G) H&E stained sections of *Azi1*$^{+/Gt}$ and *Azi1*$^{Gt/Gt}$ cauda epididymi, showing drastic reduction in sperm in *Azi1*$^{Gt/Gt}$ mutants. (H and I) *Azi1*$^{+/Gt}$ and *Azi1*$^{Gt/Gt}$ testes sections were stained with anti-activated Caspase3a (Act Casp3) to mark cells undergoing apoptosis and α-Acetylated α-tubulin (Ac α-Tub) to mark the sperm tail axoneme. Much fewer sperm tails are present in the mutant tubules, and those present appear shortened. Increased cell death is evidenced by increased numbers of activated Caspase3a positive cells in the mutant tubules (quantified in J) (n=1, studies ongoing)

genotype) so further investigation is needed to pinpoint exactly when the spermatids undergo apoptosis.

To investigate the infertility phenotype further, I examined whether *Azi1*$^{Gt/Gt}$ sperm are motile. *Azi1*$^{+/+}$ and *Azi1*$^{Gt/Gt}$ sperm were isolated from the cauda epididymus of littermates. For imaging clarity, *Azi1*$^{+/+}$ sperm were diluted 1:5 to track individual movements but due to the reduction in sperm count (Figure 6.9A), *Azi1*$^{Gt/Gt}$ sperm was not diluted. Methyl cellulose was added to increase viscosity and slow the sperm to allow imaging, and *Azi1*$^{+/+}$ and *Azi1*$^{Gt/Gt}$ sperm were imaged in glass capillaries. *Azi1*$^{+/+}$ sperm was highly motile (Movie 6.1A Figure 6.9B), whereas *Azi1*$^{Gt/Gt}$ sperm was completely immotile (data not shown). To see if *Azi1*$^{Gt/Gt}$ sperm were motile in the absence of methyl cellulose, *Azi1*$^{Gt/Gt}$ sperm in M2 medium was also imaged and although some slight flagella twitching was occasionally observed, the sperm were immotile (Movie 6.1B Figure 6.9C). Many abnormal sperm were observed in the *Azi1*$^{Gt/Gt}$ sperm preparations, including sperm with shortened tails, bent tails and sperm without tails, as well as sperm with abnormal head morphology (Figure 6.9C-E). An increase in cellular debris was also observed in Figure 6.9C: this could be due to the fact the ejaculate has not been diluted as in the wild type samples, or could be due to the increase in cell death in mutant testes (Figure 6.8H - I).

In order to characterise the mutant sperm flagella further, I isolated sperm from testes, caput and cauda epididymis to show progressively more mature sperm, and IFT particles respectively. Flagella length was measured using both anti-acetylated α-tubulin and transmitted light, and flagella were significantly shorter in the few remaining *Azi1* mutant sperm (Figure 6.9F).

Anti-acetylated α-tubulin marks the axoneme of the sperm whereas anti-Ift88 marks IFT trains along the sperm tail. Almost all *Azi1* mutant sperm flagella show a marked increase in the intensity of anti-acetylated α-tubulin staining, and some but not all flagella also show an increase in Ift88 staining intensity (Figure 6.9G and H).

We then conducted transmission electron microscope (TEM) studies on the testes and epididymus of *Azi1*$^{+/Gt}$ and *Azi1*$^{Gt/Gt}$ littermates, to identify any ultrastructural

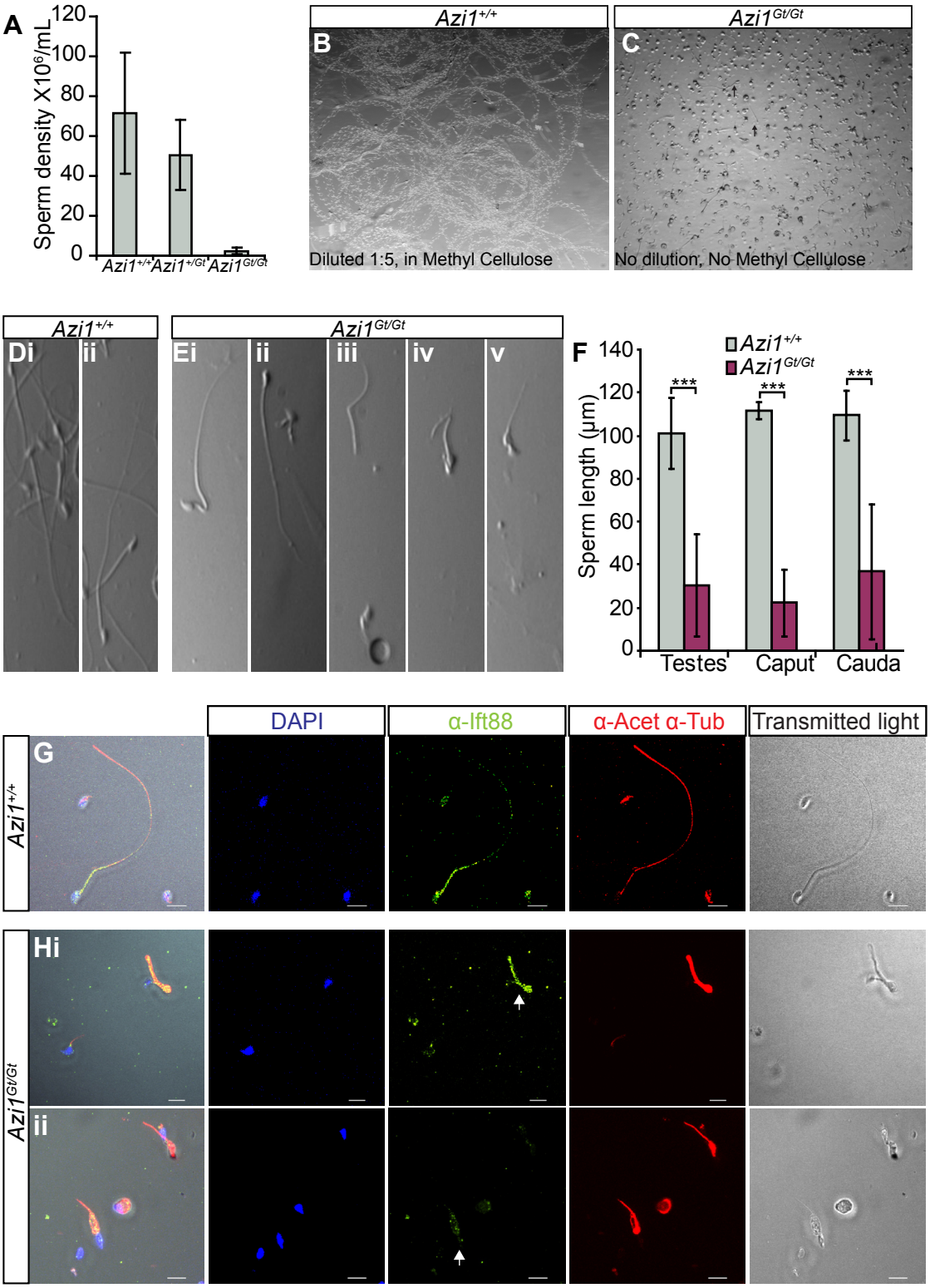

Figure 6.9 *Azi1*$^{Gt/Gt}$ mice have reduced sperm count and remaining sperm are immotile and morphologically abnormal.

Figure 6.9 Azi1Gt/Gt mice have reduced sperm count and remaining sperm are immotile and morphologically abnormal. (A) Sperm count taken from Cauda epididymus of *Azi1*$^{Gt/Gt}$ and *Azi1*$^{+/+}$ mice. *Azi1*$^{Gt/Gt}$ show a 50 fold reduction in sperm density. (B and C) Sperm was isolated from cauda epididymus and placed in glass capillary tubes and imaged with a super fast camera to determine motility. Wild type sperm was diluted 1:5 and put in methyl cellulose to slow sperm to allow imaging (see Movie 6.1A). (B) Movie stills superimposed to give the trails of the motile sperm. Mutant sperm was not diluted (due to the 50 fold reduction in numbers) and showed no motility in methyl cellulose (not shown). Without methyl cellulose, some sperm twitched (See Move 6.1B) but still remained immotile (C). Increased debris could be due to the lack of dilution or the increased cell death observed in Azi1Gt/Gt testes. (D and E) Sperm from the cauda epididymus were placed on slides and imaged without fixation. *Azi1*$^{Gt/Gt}$ sperm show abnormalities including bent tail (Ei) malformed head (Eii, iv and v) separated tails and heads (Eii) and shortened flagella (Eiii, iv, v and F). (F-H) Sperm was isolated from testes, caput epididymus and cauda epididymis, fixed on slides and stained with α-Acetylated α-tubulin and α-Ift88 and the length of the tail was measured using α-Acetylated α-tubulin staining and transmitted light. *Azi1*$^{Gt/Gt}$ sperm have significantly shorter tails (F), and show increased staining for α-Acetylated α-tubulin and sometimes Ift88 suggesting axonemal abnormalities (Hi and ii arrows).

defects. As in the histological sections, a build-up of proteinaceous and cellular debris was present in the lumen of *Azi1*$^{Gt/Gt}$ tubules, with many dark, vacuolar cells consistent with increased cell death in these mutants (Figure 6.10A and B). There was a reduced number of sperm heads visible in mutant tubules and a marked reduction in sperm flagella. We could not identify any intact sperm in the cauda epididymus by TEM (Figure 6.10C and D).

The remaining flagella in the testes appear to have relatively normal axonemal ultrastructure, with all those imaged having the expected (9+2) microtubule structure (Figure 6.10F, G, H, K and L). However, defects in outer dense fibre organisation was observed. Outer dense fibres are electron dense structures found in association with microtubule doublets; there are nine outer dense fibres visible in the midpiece of the flagella, 7 in the principal piece and 2 in the endpiece (Fawcett, 1966; Ferreira and Dolder, 2003). However, in *Azi1* mutant sperm we saw supernumerary outer dense fibres, once in the principal piece (Figure 6.10F) and in the end piece of most flagella imaged (Figure 6.10K and L). We also saw loss of outer dense fibres in the principal piece of some mutant sperm (Figure 6.10G and H). Abnormalities in mitochondrial organisation were observed in some cases (Figure 6.10M-O). This suggests Azi1 is not required for axonemal formation in sperm flagella but it may have a role in regulating the formation or termination of outer dense fibres.

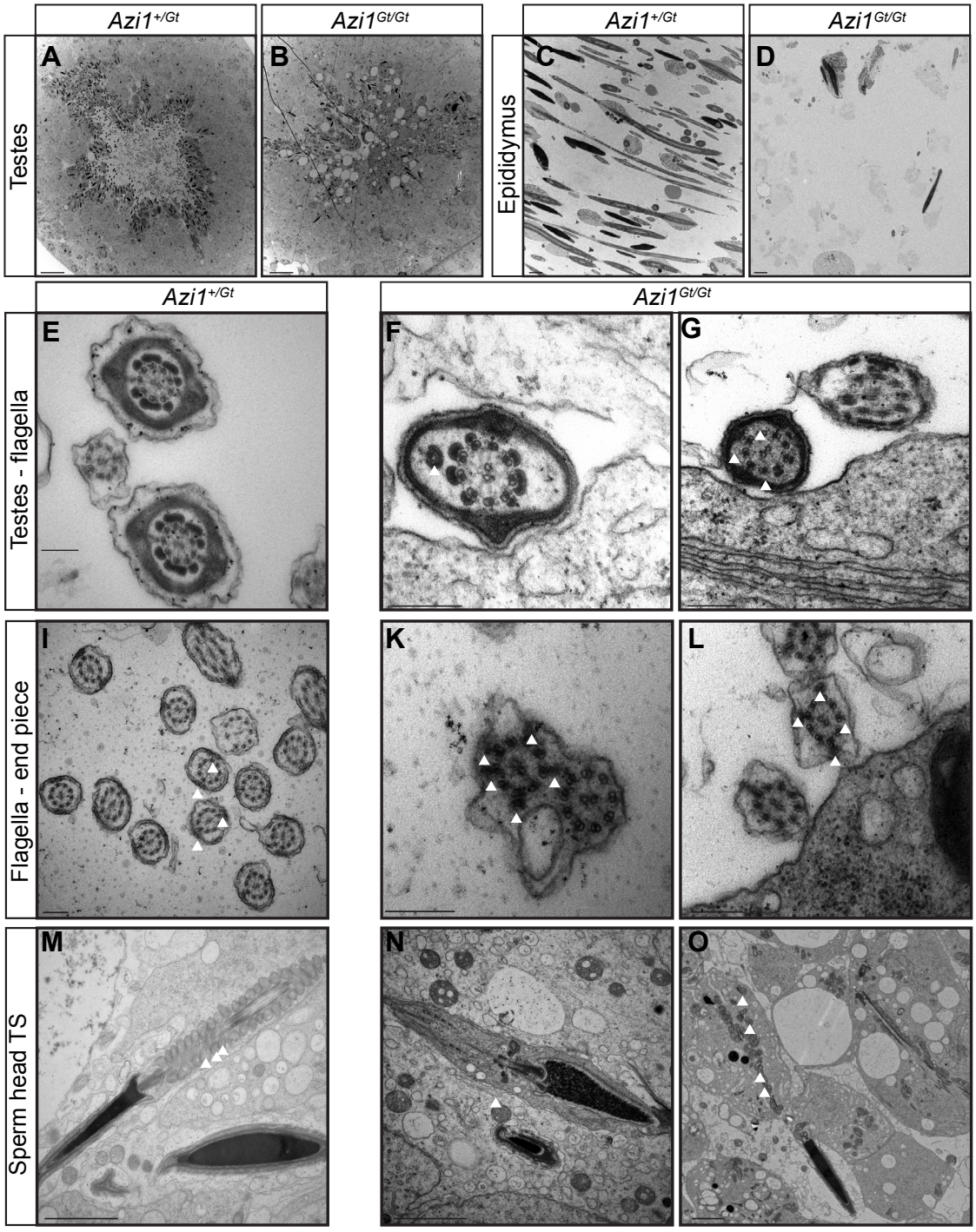

Figure 6.10 TEM confirms reduced number of flagella in Azi1Gt/Gt testes; but remaining flagella have normal microtubule axonemes with abnormalities in outer dense fibres, and disorganised mitochondria.

Figure 6.10 TEM confirms reduced number of flagella in *Azi1*$^{Gt/Gt}$ testes; but remaining flagella have normal microtubule axonemes with abnormalities in outer dense fibres, and disorganised mitochondria. (A and B) *Azi1*$^{+/Gt}$ tubules have lumens filled with sperm flagella (A), whereas mutant lumens are filled with proteinaceious debris and vacuolar dying cells and very few sperm flagella (B). (C and D) Longitudinal sections through sperm flagella in the cauda epididymus of *Azi1*$^{+/Gt}$ (C) whereas in *Azi1*$^{Gt/Gt}$ no normal sperm is present (D). (E-O) Closer examination of sperm in *Azi1*$^{+/Gt}$ and *Azi1*$^{Gt/Gt}$ testes. (E-H) In *Azi1*$^{+/Gt}$, the principal piece of the sperm flagella shows 7 outer dense fibres (ODFs) and two longitudinal columns. In mutants, flagella axonemes appeared normal with the expected (9+2) arrangement of microtubule doublets, but we observed what appeared to be extra ODFs (arrow F) or fewer than 7 ODFs in the principal piece (arrows mark microtubule pairs lacking associated ODFs G and H). (I-L) In the end piece of the *Azi1*$^{+/Gt}$ sperm flagellar, two ODFs continue (arrows I), whereas in the mutant we often saw 3 or more ODFs, suggesting they do not terminate at the principal piece (arrows K and L). (K) also shows fused flagella. (M-O) In the midpiece of the sperm flagella, mitochondria are arranged around the axoneme (arrows M) but in the mutant flagella, mitochondria appeared disorganised (N - no mitochondria and O - disorganised mitochondria (arrows)). A-D M-O Scale bar represents 2μm, E-L Scale bars represent 200nm. TS = transverse section.

In summary, *Azi1*$^{Gt/Gt}$ males show a dramatic reduction in sperm count, due to spermiogenesis arrests at Stage IX and increased cell death in *Azi1*$^{Gt/Gt}$ tubules. *Azi1*$^{Gt/Gt}$ sperm which reach the epididymus are immotile, and any remaining sperm isolated from the testes, cauda or caput epididymis show shortened tails and other structural abnormalities. The sperm flagella that remain in mutant tubules have normal axonemal structure but defects in outer dense fibre and mitochondrial organisation.

6.8 Discussion

In this chapter, the role of mammalian Azi1 was examined. Azi1 was shown to localise to the transition zone and centriolar satellites, and its localisation was shown to be dynamic. The role of Azi1 in mouse was examined by the generation of *Azi1*$^{Gt/Gt}$ mice, which were shown to be null for Azi1. Some *Azi1*$^{Gt/Gt}$ mice survive, although they are born at sub-mendelian ratios. Adult mutant males display infertility, with a severe reduction in sperm count due to an arrest in spermiogenesis at stage IX.

6.8.1 Azi1 localises to the transition zone of cilia and centriolar satellites.

Azi1 localises in punctuate staining around the base of the cilium, as well as to the transition zone of the cilium but is not trafficked by IFT into cilia, as demonstrated the absence of accumulations of Azi1 in *Dync2h1*$^{pol/pol}$ cilia, which lack retrograde IFT (Figure 6.1E and F). Azi1 dynamically localises to the centriolar satellites, as demonstrated by colocalisation with Pcm1 (Figure 6.2), and has been shown by another study to interact with the centriolar satellite marker Pcm1 (Akimov et al., 2011).

The localisation of Azi1 is shown to be dynamic, and is cell cycle and microtubule dependent (Figure 6.2). Azi1 does not always colocalise with Pcm1. For example Azi1 is not found at the spindles or midbody during mitosis, whereas Pcm1 is (Figure 6.2B). This suggests the interaction with Pcm1 may also be dynamic and cell-cycle dependent, although further studies are needed to investigate this further.

Centriolar satellites have been shown to traffic along microtubules and their centrosomal localisation is microtubule dependent. Consistent with Azi1 being a centriolar satellite component, microtubule depolymerisation leads to Azi1 mislocalisation (Figure 6.2C). Interestingly, although microtubule depolymerisation causes mislocalisation of both Pcm1 and Azi1, they remain colocalised, suggesting the interaction is not microtubule dependent, although further studies are needed to confirm this. Super-high resolution imaging at the transition zone and centriolar satellites will help to further dissect the exact localisation of Azi1, particularly with respect to the membrane and microtubules at the transition zone. In addition, immunogold TEM studies would elucidate the sub cellular localisation of Azi1 at the ultrastructural level. There are hints that Azi1 may be involved in vesicular trafficking, such as the presence of the t-SNARE domain, found in proteins involved in vesicular fusion, and the demonstration that Azi1 interacts with Rab11 (a small GTPase involved in vesicular trafficking to the cilium) in *T. Bruceii*. Therefore it would be interesting to see whether Azi1 localises to periciliary vesicles by TEM.

Total Azi1 levels do not change upon 48 h of serum starvation, which arrests cells in G_1/G_0 and promotes ciliogenesis, suggesting regulation of Azi1 levels is not cell cycle related, although more detailed analysis of Azi1 levels and post translational modifications during the cell cycle is on-going. Akimov et al., (2011) suggested that Azi1 is ubiquitinated and Azi1 has been reported to be highly phosphorylated (Olsen et al., 2006); in both cases these post translational modifications were shown to be dynamic. Investigations into the function of these post translational modifications may give insight into the role of Azi1 in mammals.

It would also be interesting to further characterise Azi1 interactors, to confirm whether it interacts with vesicular transport proteins, such as Rab11, in mammals and investigate whether it interacts with other ciliary, basal body or centriolar satellite proteins.

6.8.2 *Azi1* is not required for mammalian ciliogenesis.

Azi1 mutant mice were generated; mutants are born and survive, although mutant males show infertility. In earlier generations it appeared we were losing $Azi1^{Gt/Gt}$ and $Azi1^{+/Gt}$ mice, however as backcrossing onto C57BL6/J continued, the numbers of mutants and heterozygotes returned to the expected Mendellian ratios (Table 6.1). Backcrossing is still on-going, but these data suggest the initial loss of $Azi1^{Gt/Gt}$ and $Azi1^{+/Gt}$ mice may have been due to a lethal allele present in the colony linked to the *Azi1* locus.

Considering the involvement of Azi1 in ciliogenesis in other species (Ma and Jarman, 2011; Wilkinson et al., 2009), and the reduction in ciliogenesis in mouse cells upon siRNA knockdown (Chapter 5), the fact that *Azi1* mutant mice are born and survive without any developmental phenotypes was surprising to us, as cilia are required for mammalian development (Huangfu et al., 2003). We demonstrated that the allele is most likely to be null, as it is predicted to truncate the protein at 69 aa, before the more highly conserved C terminal including the coiled-coil and t-SNARE domains. We show the gene trap is not leaky as we see no mRNA expression just after the gene trap insertion, and no protein expression with an antibody directly

against the C terminal of Azi1. Therefore these mice are most likely to be null for Azi1, suggesting that Azi1 is not required for mammalian ciliogenesis. Backcrossing onto C57BL/6 is on-going in order to confirm whether the observed loss of *Azi1*$^{Gt/Gt}$ mutants was due to a linked lethal allele, but preliminary results suggests this is the case.

Characterisation of many ciliary markers, including markers of ciliary axoneme, membrane proteins, IFT proteins, transition zone proteins and ciliary trafficking proteins, in *Azi1* mutant MEFs demonstrated there is no detectable defect in ciliogenesis in these cells. This is in contrast to the siRNA data presented in Chapter 5 of this thesis, in which it was shown that siRNA knockdown of *Azi1* in mouse fibroblast cell line ShhLIGHT-II and mouse kidney cell line IMCD3 leads to a decreased ciliogenesis and a reduction in cilia length. This is unlikely to be due to off target effects of the siRNAs as it was confirmed with a further pool of siRNAs to the 3'UTR of *Azi1* and the reduction in ciliogenesis was rescued by overexpressing Azi1-GFP.

As we have demonstrated that the mice are highly likely to be null for Azi1, the mild phenotype is unlikely to be due to residual Azi1 function in the mutant mice (Figure 5.3). Equally the reduction in ciliogenesis seen upon siRNA knockdown is unlikely to be due to off-target effects of the siRNAs as the phenotype correclates with knockdown, it was confirmed with a further pool of siRNAs to the 3'UTR of *Azi1* and the reduction in ciliogenesis was rescued by overexpressing Azi1-GFP (Figure 5.4 and 5.7).

It is difficult to reconcile these contradicting results. One theory which may explain this discrepancy is that acute loss of Azi1 over 48h in cells which previously expressed the gene could give a more severe ciliogenesis phenotype than seen in MEFs which constitutively lack Azi1 and so may have compensated in some way for this loss. There are examples of transient siRNA knockdown giving different or more severe phenotypes than complete knock out in the literature (Freudenberg et al., 2011; Pulvers et al., 2010). Here, it has been suggested that acute loss can sometimes give a more severe phenotype than long term lack of a protein (Freudenberg et al., 2011). For example if a protein is part of a complex, acute loss

could destabilise the complex, whereas long term lack of the protein could allow time for the complex to form, and so loss could be overcome. This could be addressed by using an inducible system, such as the Cre-Lox system, to generate an acute loss of Azi1 *in vivo* to see if acute loss produces phenotypes not seen in complete loss of function models. Unfortunately our gene-trap allele is non-conditional, although another EUCOMM conditional "Knockout first" allele has since become available.

6.8.3 *Azi1* mutant males are infertile due to spermiogenesis arrest at stage IX.

Azi1$^{Gt/Gt}$ males display male infertility, with severely reduced sperm count; remaining sperm are immotile and many show morphological defects such as shortened flagella or disrupted head morphology. Male infertility is associated with ciliopathies such as Bardet-Biedl syndrome, and mouse models of several ciliopathy proteins also display male infertility (Fath et al., 2005; Hildebrandt et al., 2011; Jiang et al., 2008; Mykytyn et al., 2004; Nishimura et al., 2004; Won et al., 2011). Spermiogenesis arrests at stage IX in *Azi1*$^{Gt/Gt}$ mice, which is similar to the arrest seen in *Nphp1* and *Nphp4* mutant mice. Interestingly, for *Nphp1*, this is the only phenotype observed, despite the association of this gene with kidney disease in humans (Jiang et al., 2008; Won et al., 2011). Nphp1 and 4 localise to the transition zone of primary cilia, along with Azi1 (Figure 6.1 and 6.7 (Mollet et al., 2005)). Nphp4 was shown to colocalise with γ-tubulin at the neck of the sperm tail (Won et al., 2011); localisation studies of Azi1 in testes and sperm are still being optimised.

The axonemal structures of the remaining flagella in *Azi1*$^{Gt/Gt}$ testes show the normal (9+2) morphology. By immunofluorescence we saw a consistent increase in intensity of α-acetylated α-tubulin staining at the flagella, and sometimes an accumulation of Ift88. However by EM we did not clearly observe swelling of flagella in transverse sections, which would be expected upon an accumulation of IFT particles. Therefore it is unclear whether axonemal subunits or IFT particles accumulate in *Azi1* mutant flagella.

Loss of flagellar components, or disrupted flagellar axonemal structure usually leads to male infertility with normal sperm count, no arrest in spermiogenesis, but reduced motility (Escalier, 2006). As *Azi1* mutants arrest spermiogenesis at stage IX, show reduced sperm count and a largely normal albeit truncated flagellar axonemal structure, this suggests Azi1 is not essential for formation of flagella axonemal structure.

We observed defects in outer dense fibres in the flagella. Outer dense fibres are found closely associated with each microtubule doublet in the sperm, and are thought to be involved in structural reinforcement and possibly in the generation of increased force upon flagellar beating (Baltz et al., 1990; Lindemann, 1996). Other mutants which display defects in outer dense fibres do not show an arrest in spermiogenesis and show normal sperm counts, although do show sperm motility defects (Sapiro et al., 2002; Tarnasky et al., 2010). This suggests the defects in outer dense fibres observed in the $Azi1^{Gt/Gt}$ mice may not explain the arrest in spermiogenesis.

During spermiogenesis, many dramatic morphological changes occur, including nuclear elongation, flagellar formation, acrosome formation and formation and disassembly of the transient microtubule based structure, known as the manchette. The manchette forms transiently and is thought to be involved in the control of the shaping of the nucleus, as well as being involved in trafficking of proteins to the developing sperm tail (Kierszenbaum, 2001; Kierszenbaum and Tres, 2004). The acrosome is a Golgi-derived cap-like structure important for sperm head morphology and is also involved in penetrating the zona pellicuda of the oocyte, enabling fertilisation.

Ift88 has been shown to localise to the manchette and it has been suggested that intramanchette transport, which is thought to transport proteins to the sperm flagella, may involve similar motors to IFT. $Ift88^{orpk}$ hypomorphic mutant mice show male infertility, and Kierszenbaum et al., (2011) suggest this is due to defective acrosome formation, as well as ineffective intramanchette transport leading to defects in flagellar formation. Interestingly, Azi1 has been shown to localise to the pre-acrosome in round and elongating spermatids (Aoto et al., 1995). Defects in acrosome formation can lead to arrests early in spermiogenesis and reduced sperm

counts (Kang-Decker et al., 2001). Therefore it would be worth examining the structure of the manchette and acrosome in *Azi1*$^{Gt/Gt}$ mutant spermatids, as well as to look again at the localisation of Azi1 during spermatogenesis. Perhaps a defect in acrosome or manchette formation or function could lead to the morphological changes seen in *Azi1*$^{Gt/Gt}$ sperm and explain the arrest in spermiogenesis, and investigations into these structures in *Azi1*$^{Gt/Gt}$ testes are on-going.

It would also be interesting to examine what proteins Azi1 interacts directly with in the testes, for instance, is the interaction with Pcm1 maintained, and if so where do Pcm1, and other centriolar satellite proteins localise during spermatogenesis? There is no mouse mutant of Pcm1 published so it would be useful to determine whether loss of Pcm1 leads to male infertility, whether there are other phenotypes observed, and finally whether Azi1 and Pcm1 interact genetically as well as physically.

6.8.4 Analysis of late-onset ciliopathic phenotypes

Many mouse mutants of cilia-associated genes display male infertility associated with other, late-onset ciliopathic phenotypes such as kidney and pancreatic cysts, obesity and retinal degeneration. These phenotypes are generally observed at 2-3 months, becoming more severe by 6 months of age (Fath et al., 2005; Mykytyn et al., 2004; Nishimura et al., 2004; Won et al., 2011). As yet, no late-onset ciliopathic phenotypes have been detected in *Azi1*$^{Gt/Gt}$ mice: we see no increase in weight at 9 months and no retinal degeneration or kidney cysts at 6 months of age, although these studies are on-going.

6.8.5 Genetic interaction studies with IFT genes

Genetic interaction studies between *Azi1*$^{Gt/Gt}$ mice and the retrograde mutants *Dync2h1*$^{pol/pol}$ as well as *Wdr35*$^{yet/yet}$ ciliary mutants are on-going. These studies will address the question of whether Azi1 interacts genetically with IFT proteins to regulate traffic through the transition zone.

In summary, Azi1 is not required for ciliogenesis in mouse, although it is required for spermiogenesis, and *Azi1*$^{Gt/Gt}$ mutants display a significant reduction in sperm

density. Remaining sperm show defects in head and flagellar morphology, with shortened and immotile flagella.

Chapter Seven. *Azi1*$^{Gt/Gt}$ mice do not show increased DNA damage.

An independent study by the Collis group identified *Azi1/Cep131* in an siRNA screen for genes involved in DNA damage repair, in which they saw increased phospho-H2AX (pH2AX) staining upon siRNA knockdown of *Azi1* (S. Collis, personal communication). pH2AX (s139), known as γH2AX, marks DNA double strand breaks (DSBs), and, as such, is a measure of DNA damage (Mah et al., 2010; Sedelnikova et al., 2002). Several DNA damage components, including Atm/Atr kinases, Brca1 and Brca2 have been shown to localise to centrosomes (Nakanishi et al., 2007; Sankaran and Parvin, 2006; Shimada and Komatsu, 2009; Zhang et al., 2007a). Aberrant DNA damage repair can lead to mutations, genomic instability, centrosome amplification and multipolar spindles (Dodson et al., 2004; Lord and Ashworth, 2012). In this brief chapter, I summarise data which suggests Azi1 is not necessary for the DNA damage response *in vivo*.

7.1 No increase in γH2AX staining or defects in cell cycle progression observed in *Azi1*$^{Gt/Gt}$ MEFs

As an extension to the Collis knock-down study, we also analysed γH2AX staining, as an indicator of DNA damage (Mah et al., 2010; Sedelnikova et al., 2002), in wild type and *Azi1*$^{Gt/Gt}$ MEFs in order to examine whether DNA damage is similarly altered in the absence of *Azi1*. No difference in the number of cells with γH2AX foci, or the intensity of γH2AX staining was observed, suggesting no increase in DNA damage in *Azi1* mutant cells (Figure 7.1 A and B and data not shown), which we prove are a genetic null allele (Chapter 6). This is in contrast to the siRNA data

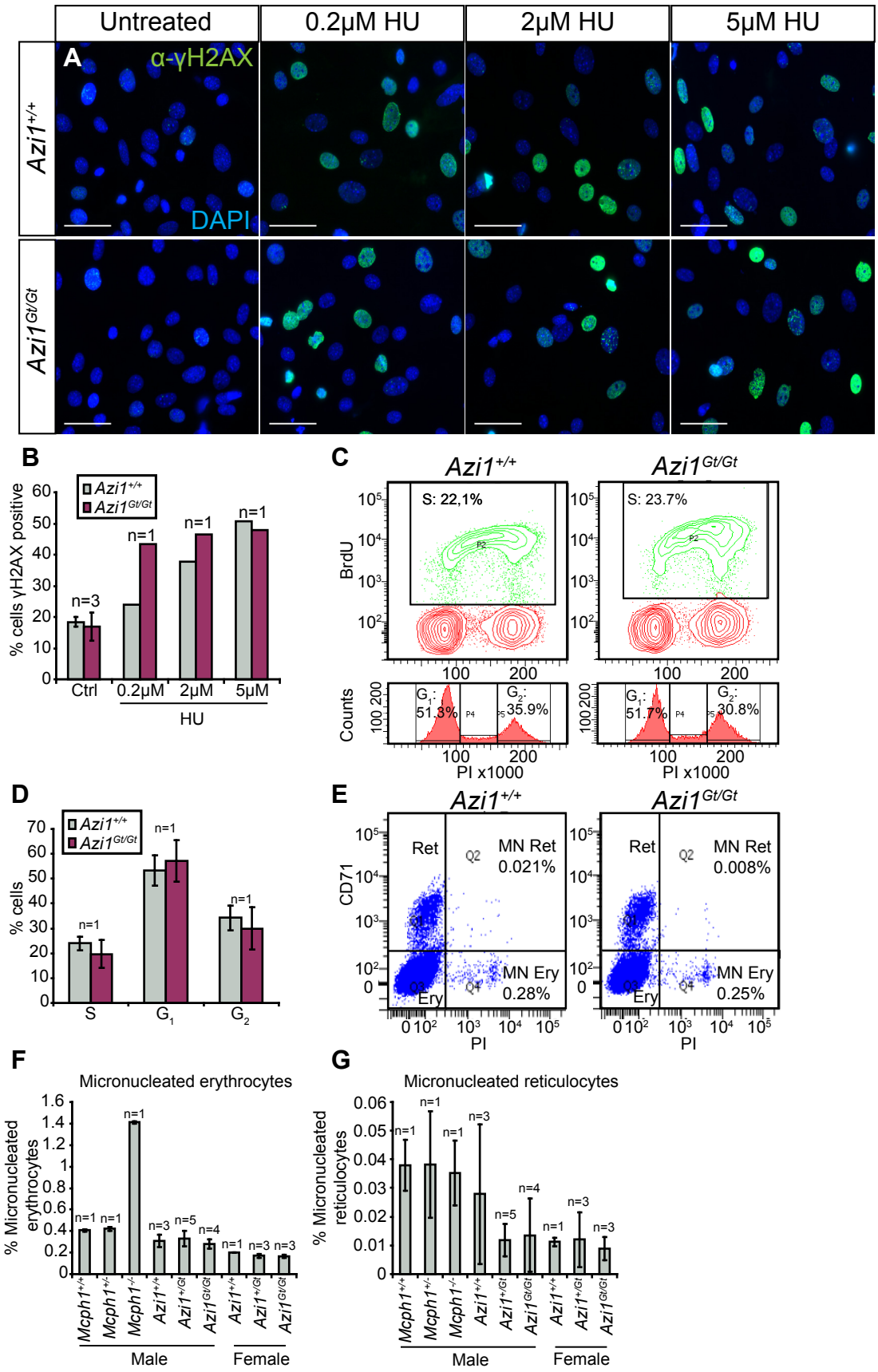

Figure 7.1 *Azi1*$^{Gt/Gt}$ mice do not show evidence of increased DNA damage.

Figure 7.1 *Azi1*$^{Gt/Gt}$ mice do not show evidence of increased DNA damage. (A) The amount of DNA damage, measured by anti-γH2AX staining, was assessed in *Azi1*$^{+/+}$ and *Azi1*$^{Gt/Gt}$ MEFs, both with and without challenge with hydroxyurea (HU), and is quantified in (B), showing the % cells which were γH2AX positive. Without HU, the number of cells staining positive for γH2AX is equal between wild type and mutants (n=3 MEF lines). Upon treatment with increasing concentrations of HU, the number of γH2AX positive cells increases. There is a slight increase in γH2AX positive cells in *Azi1*$^{Gt/Gt}$ MEFs treated with 0.2μM HU, however there is no difference in γH2AX positive cells between wild type and mutant MEFs treated with 2μM and 5μM HU. The HU treatment was only carried as one biological replicate so results are preliminary. For the Ctrl treated cells, plotted is the mean +/- standard deviation. (C and D) BrdU pulse then propidium iodide (PI) staining followed by flow cytometry was used to analyse the cell cycle time in *Azi1*$^{+/+}$ and *Azi1*$^{Gt/Gt}$ MEFs, showing there is no difference between cell cycle timing in mutant or wild type MEFs. Plotted is the mean of technical duplicates +/- standard deviation. (E, F and G) To assess DNA damage in vivo the percentage of micronuclei in peripheral blood was assessed by flow cytometry. (E) Example FACS data gated to show erythrocytes (Ery, CD71 negative) and reticulocytes (ret, CD71 positive), the high PI containing cells are micronucleated (MN). (F and G) plot the percentage of erythrocytes or reticulocytes which were micronucleated respectively. *Mcph1*$^{-/-}$ mice, which had previously been shown to have elevated numbers of micronucleated erythrocytes (http://www.sanger.ac.uk/mouseportal/phenotyping/MBGX/micronuclei/) were run as a control. As expected, they show an increased number of micronucleated erythrocytes (D) but not reticulocytes (E). In contrast, *Azi1*$^{Gt/Gt}$ mice show no change in the number of micronucleated erythrocytes or reticulocytes, suggesting no increase in DNA damage *in vivo*.

which suggests robust knockdown of *Azi1* leads to increased γH2AX staining (Spencer Collis, personal communication). To see if *Azi1*$^{Gt/Gt}$ MEFs show increased DNA damage when challenged, I treated wild type and *Azi1*$^{Gt/Gt}$ MEFs with increasing concentrations of Hydroxyurea (HU). HU treatment leads to stalled replication forks and DNA damage (Tanaka et al., 2007; Ward and Chen, 2001). Both wild type and *Azi1* mutant MEFs show an increase in γH2AX staining upon treatment with HU to similar extents, although *Azi1*$^{Gt/Gt}$ MEFs seemed to have more DNA damage in response to low HU concentrations than wild type MEFs (Figure 7.1A and B). The HU treatment was only carried out once so data is preliminary.

As DNA damage repair problems can lead to defects in mitosis and cell cycle arrest (Clarke and Allan, 2009), we examined the cell cycle in unsynchronised wild type and *Azi1*$^{Gt/Gt}$ MEFs. A 1 h pulse of BrdU was followed by fixation, propidium iodide staining and flow cytometric analysis. Preliminary data suggests no difference between wild type and *Azi1*$^{Gt/Gt}$ MEFs in cell cycle progression, although this was only performed in technical duplicate, so biological repeats are needed to confirm this result (Figure 7.1 C and D)..

7.2 *Azi1*$^{Gt/Gt}$ mice show no increase in DNA damage *in vivo*

In order to assess the degree of DNA damage *in vivo* we performed a micronucleus assay on peripheral blood (Heddle, 1973; Reinholdt et al., 2004). This assay is a very sensitive *in vivo* measure of chromosome damage; micronuclei can arise from acentric chromosomal fragments or whole chromosomes which are not incorporated into the main nucleus during cell division and as such is a measure of DNA DSBs and abnormal chromosome segregation. Mice with mutations in DNA damage repair genes show increased micronuclei (Crossan et al., 2011; Shima et al., 2003). Therefore we performed micronuclei tests on peripheral blood of 7 *Azi1*$^{Gt/Gt}$, 8 *Azi1*$^{+/Gt}$ and 4 wild type mice from 4 litters. As a positive control, we also performed micronuclei tests on wild type, *Mcph1*$^{+/-}$ and *Mcph1*$^{-/-}$ mutant littermates, as Mcph1 is involved in DNA damage repair, and these mice show increased levels of micronucleated reticulocytes ((Liang et al., 2010) http://www.sanger.ac.uk/mouseportal/phenotyping/MBGX/micronuclei/). As previously shown, *Mcph*$^{-/-}$ mice show increased levels of micronucleated erythrocytes but normal levels of micronucleated reticulocytes, but in contrast *Azi1*$^{Gt/Gt}$ mice show no increase in micronucleated reticulocytes or normochromatic erythrocytes, suggesting there is no increase in *in vivo* DNA damage in *Azi1*$^{Gt/Gt}$ mice (Figure 7.1 E, F and G).

7.3 Discussion

In this chapter, I show that *Azi1*$^{Gt/Gt}$ mice do not have increased levels of DNA damage, either *ex vivo* in MEF cell lines or *in vivo* in peripheral blood (Figure 7.1). This is in contrast to siRNA data by another group which suggests that siRNA knockdown of Azi1 leads to increased pH2AX staining, a marker of DNA DSBs (S

Collis, personal communication). This is another example of a phenotype which is detected by siRNA knockdown of *Azi1* but is not observed in our null $Azi1^{Gt/Gt}$ mutants. One possible explanation involves differences in the cell types analysed; the Collis screen was carried out in epithelial cell lines, whereas I analysed primary mutant fibroblasts and blood cells. Although tissue-specific differences in Azi1 control of genome integrity seem unlikely, γH2AX staining on embryonic sections from $Azi1^{Gt}$ intercrosses are under way. Interestingly, they also reported a decrease in ciliogenesis upon *Azi1* knockdown in their epithelial cell lines (S Collis, personal communication). Apart from cell type specific effects, two main possibilities exist to explain the discrepancy between siRNA and knockout data: either the siRNA data are due to off-target effects, or there is a difference in response of cells to acute loss of *Azi1* by siRNA as opposed to long term loss of *Azi1* in the mouse mutant (Freudenberg et al., 2011; Pulvers et al., 2010). This study did not attempt to rescue the the DNA damage phenotypes by overexpressing an siRNA-insensitive version of the gene. It would be interesting to see if, in their system, the phenotype is reproduced with the siRNAs to the 3'UTR of *Azi1* and whether this phenotype can be rescued by overexpressing Azi1-GFP. As discussed in Chapter 6 further experiments involving acute knockdown of *Azi1 in vivo* using the Cre-lox system would also help to distinguish between these possibilities.

Chapter Eight Discussion.

8.1 Summary of thesis findings

The aim of this thesis was to perform an RNAi screen to identify genes involved in mammalian cilia formation and function.

Whilst optimising screening protocols, I first carried out an analysis of the ciliary phenotypes of mouse embryonic fibroblasts (MEFs) isolated from two novel ciliary mouse mutants, *Wdr35*$^{yet/yet}$ and *Dync2h1*$^{pol/pol}$ (Chapter 3). Dync2h1 is a component of the retrograde IFT motor, whereas Wdr35 is a member of the IFT-A complex which binds the retrograde dynein motor and is involved in retrograde IFT (Blacque et al., 2006; Criswell et al., 1996; Huangfu and Anderson, 2005; Mill et al., 2011; Mukhopadhyay et al., 2010; Porter et al., 1999; Signor et al., 1999). I show that *Dync2h1* and *Wdr35* are required for ciliogenesis; both mutant cell lines show a drastic reduction in ciliogenesis (Figure 3.1). *Dync2h1*$^{pol/pol}$ cilia show the classic retrograde phenotype of shortened bulging cilia with a build-up of IFT-B protein Ift88 and ciliary membrane protein Arl13b. Interestingly, *Wdr35*$^{yet/yet}$ cilia show a distinct phenotype, in which no build-up of Ift88 or Arl13b is seen. Although Ift88 is localised to the basal bodies of *Wdr35*$^{yet/yet}$ cilia, in contrast Arl13b is not localised at the basal body in these cilia (Figure 3.2). This suggests Wdr35 has additional novel roles in mammalian ciliogenesis; as well as roles in retrograde IFT as predicted by the *Chlamydomonas* phenotype, it may also have roles in anterograde IFT and/or traffic of proteins to the ciliary base. Short Rib Polydactyly (SRP) patient fibroblasts with mutations in *WDR35* show a similar ciliary phenotype, suggesting this non-retrograde role is conserved in humans (Figure3.3). Finally, I show that *Dync2h1*$^{pol/pol}$ and *Wdr35*$^{yet/yet}$ have defects in Hh signalling (Figure 3.4).

Screening protocols were optimised in mouse cells, including optimisation of siRNA transfection, and of two readouts, one immunofluorescence-based readout for cilia formation, and one Hh-responsive luciferase-based readout for cilia function (Chapter 4). A cohort of thirty-six genes were chosen for screening, which were identified as highly expressed in ciliated neurons in *Drosophila,* just as they undergo ciliogenesis. The list was further enriched for putative ciliary genes by bioinformatics, including enriching for genes with motifs common in ciliogenesis genes such as WD, coiled coil and TPR domains, and for genes with X-boxes in their promoters, a signature of ciliary genes. We also included *Wdr35* in the first pass screen as a further control (Table 4.1).

The first-pass screen was carried out using 4 siRNAs plus a pool for each of the thirty-seven genes using both readouts of cilia formation and function in ShhLIGHT-II mouse fibroblast cells. These cells have a stably integrated Hh-responsive *Gli-luciferase* transgene, utilised in the second readout for cilia function. However, problems with cell death and the ability to call hits with the cilia function readout meant this assay was not pursued further. In contrast, the immunofluorescent readout of cilia formation allowed us to identify 12 of 37 genes which gave a significant reduction in ciliogenesis upon siRNA knockdown in the first pass screen, including the ciliopathy gene *Wdr35* as a positive control (Chapter 5).

A second pass screen was carried out on these 12 genes, in which the immunofluorescent readout was performed twice more in ShhLIGHT-II cells and twice in mouse ciliated kidney cell line IMCD3. Although no siRNA gave an entirely reproducible phenotype across the five repeats, probably due to inherent noise in the system, seven genes gave a fairly reproducible reduction in ciliogenesis upon siRNA knockdown, of which three (*Azi1, Spag1* and *Ttc30a2*) also gave a fairly reproducible reduction in cilia length (Table 5.5 and 5.6, Figure 5.3). *Azi1, Ccdc63* and *Spag1* showed a correlation between mRNA knockdown and phenotype (Figure 5.4), suggesting these phenotypes are not due to off-target effects. The reduction in ciliogenesis upon *Azi1* knockdown was confirmed with further siRNAs to the 3'UTR of *Azi1* and this phenotype was rescued by overexpressing Azi1-GFP which lacks the 3'UTR, thereby confirming that the phenotype is not due to off-target effects of the

siRNA, and suggesting that *Azi1* is involved in mammalian ciliogenesis. Localisation studies identified Azi1 at the base of the cilia and Ccdc63 at the base and along the axoneme of the cilia, further supporting a ciliary roles for these proteins (Figure 5.5). Live imaging of ciliary dynamics showed Ccdc63 may have a role in cilia stability as well as cilia formation (Figure 5.6).

Finally, *Azi1*, which was confirmed to reduce cilia number upon siRNA knockdown was followed up in detail. Azi1 localises to the transition zone of cilia, but is not trafficked into cilia by IFT (Figure 6.1). It also localises to centriolar satellites, colocalising with Pcm1, and AZI1 and PCM1 have recently been shown to interact in human cells (Akimov et al., 2011). I show Azi1 localisation is cell cycle and microtubule dependent, and is similar to centriolar satellite marker Pcm1 throughout the cell cycle and upon microtubule depolymerisation, suggesting Azi1 is a core component of centriolar satellites (Figure 6.2).

Previously published work in zebrafish and fly suggested Azi1 was required for ciliogenesis in these model organisms (Ma and Jarman, 2011; Wilkinson et al., 2009). Therefore the *in vivo* role of mammalian Azi1 was investigated by generation and characterisation of $Azi1^{Gt/Gt}$ mutant mice, a null gene-trap allele of *Azi1*. Surprisingly, these mice are born without developmental defects and survive. This suggests Azi1 is not required for mammalian ciliogenesis. However males display infertility, with drastically reduced sperm count due to an arrest in spermiogenesis at stage IX (Figure 6.7 and 6.8). Remaining sperm show pronounced morphological defects, including shortened, immotile flagella, and although the axonemal (9+2) microtubule arrangement of these runted structures seems intact, there are marked defects in outer dense fibre and mitochondrial organisation (Figure 6.9). Male infertility is observed in several mouse mutants of ciliopathy-associated genes such as *Bbs2*, *4* and *6* and *Nphp1* and *Nphp4* (Fath et al., 2005; Jiang et al., 2008; Mykytyn et al., 2004; Nishimura et al., 2004; Won et al., 2011). Interestingly *Nphp1* mutant mice display male infertility as the only phenotype, despite an association with kidney disease in humans (Jiang et al., 2008).

This data suggests Azi1 is not essential for ciliogenesis in mouse, contradicting the siRNA data, but suggests Azi1 is necessary for the formation key of structures in the highly specialised motile sperm flagella.

In addition to a role in ciliogenesis, Azi1 has been suggested to be involved in DNA damage response, with an increase in γH2AX staining upon *Azi1* siRNA treatment (S Collis, personal communication). However we see no increase in γH2AX staining in $Azi1^{Gt/Gt}$ MEFs compared to wild type controls, even when challenged with hydroxyurea to induce DNA DSBs (Figure 7.1). We also observed no increase in micronuclei in peripheral blood, which is a highly sensitive measure of DNA damage *in vivo*. This suggests Azi1 is not required the DNA damage response *in vivo*.

8.2 siRNA screening

This thesis highlights both advantages and disadvantages of siRNA screening. The real strengths of siRNA screening is the ability to perform reverse genetics in mammalian systems in a rapid, high-throughput way. A key advantage is it gives functional data, unlike previous attempts to define ciliary genes such as proteomics, transcriptomics and genomic comparison studies, which lack such functional information (see Chapter 1.6). To this end we have identified several genes with putative novel roles in ciliogenesis.

However, as with all screening protocols, success depends on the signal-to-noise ratio of the readouts used. There is a fair amount of fluctuation in the percentage of ciliated cells after 48h serum starvation even when cells are plated at equal densities (Figure 5.1). When we transfect *Ift88* siRNA we see a significant reduction in ciliogenesis overall, although the degree of this reduction can vary from plate to plate (Figure 5.1). The fact that we had to try several siRNAs to several genes known to be required for ciliogenesis (*Wdr35, Dync2h1* and *Kif3a*) to identify *Ift88* as a suitable positive control highlights insensitivities in the screening protocol and

suggests we will encounter false negative results. Noise in the system is also demonstrated by the variability between repeats (Table 5.5).

Despite these problems, this remains a powerful screening tool and so, although not perfect, with careful analysis of the data and, importantly, follow-up studies, siRNA screening can identify novel and interesting functions for genes.

8.3 siRNA versus knockout of *Azi1* – reconciling conflicting loss of function phenotypes?

In this thesis I report on inconsistencies between the phenotypes observed by transient siRNA knockdown and genetic null mutation of *Azi1*. I see a reduction in ciliogenesis in mouse fibroblast cell line upon *Azi1* siRNA treatment, but no defects in primary ciliogenesis in $Azi1^{Gt/Gt}$ mice or $Azi1^{Gt/Gt}$ primary null fibroblasts. Additionally, a role for *Azi1* in DNA damage response suggested by another group upon siRNA knockdown, was not observed in the $Azi1^{Gt/Gt}$ mice.

Interestingly, the group that reported the increase in DNA damage also reported a decrease in ciliogenesis upon *Azi1* siRNA knockdown in epithelial cells (S Collis, unpublished data). Why are we seeing such different results between siRNA knockdown and loss of *Azi1* by genetic mutation? We have shown that the $Azi1^{Gt/Gt}$ mice are null, as no protein expression is detected with a C-terminal antibody and any remaining truncated 69aa protein expressed before the gene trap insertion lacks all the predicted functional domains and conserved residues of Azi1. Moreover, mRNA transcript analysis shows that all of the *Azi1* transcripts from exon 2 is efficiently forced onto the strong splice acceptor of the gene-trap insertion, which uses the strong polyA "trapping" sepuence to prematurely terminate *Azi1* transcription.

I have proven that the siRNA kncokdown data is not due to off-target effects of the siRNAs used. Although the phenotype is not entirewly reproducible throughout

repeats of the screen, it was highly reproducible when we used an additional pool of siRNAs to the 3'UTR of *Azi1*, giving a significant reduction in cilia number in 4 of 4 repeats (Table 5.5, Figure 5.7 and data not shown). The higher degree of reproducibility could be due to the fact only transfected cells were counted (as judged by cotransfection with pCAG-eGFP) when analysing the phenotype upon treatment with *Azi1* 3' UTR siRNAs and/or due to increased knockdown using the pool of siRNAs to the *Azi1* 3'UTR compared to the siRNAs used in the screen. Importantly, we were able to fully rescue this strong reduction in ciliogenesis back to wild type levels by overexpressing Azi1-GFP, suggesting the phenotype is not due to off-target effects of the siRNAs.

Other groups have suggested that acute loss of a protein can lead to more severe phenotype than chronic lack of a protein in mouse mutants (Freudenberg et al., 2011; Pulvers et al., 2010). One way to test this theory would be to use inducible systems, such as a Cre-deleter and floxed *Azi1* allele strategy, to acutely delete *Azi1* in mouse mutants and assess whether any ciliogenesis phenotypes are observed.

8.4 Azi1 and male infertility

Azi1$^{Gt/Gt}$ mice show male infertility due to an arrest in spermiogenesis at stage IX. The exact role of ciliary proteins in spermiogenesis is not well understood. Genes essential for ciliogenesis are embryonic lethal, precluding investigations into their role in spermiogenesis, but as the sperm tail is a highly modified motile flagella it is likely many ciliary proteins play key roles in flagella formation. Investigations into male infertility in the hypomorphic allele of *Ift88*, *Ift88*^{orpk} suggest IFT proteins could play roles in intramanchette trafficking and acrosome formation, as well as directly affecting flagellar formation by IFT (Kierszenbaum et al., 2011). It will be important to examine testes-specific knockouts of genes essential for ciliogenesis to further investigate the roles of ciliary genes in the complex morphological changes which occur during spermiogenesis. Several mouse mutants of ciliopathy-associated genes show male infertility but the exact phenotypes are not always explored in detail, and

the exact role of these proteins in spermiogenesis has not been addressed (Fath et al., 2005; Jiang et al., 2008; Mykytyn et al., 2004; Nishimura et al., 2004; Won et al., 2011). As male infertility is associated with human ciliopathies, it is important to increase our understanding of the role of these proteins in spermiogenesis.

8.5 Azi1 and human disease?

To our knowledge, no mutations in human *AZI1* have yet been identified. Judging by the mouse mutant phenotype it is possible that *AZI1* mutation would be associated with male infertility due to reduced sperm count, and so these patients would not be considered part of the ciliopathy disease cohorts. However the difference in phenotype between some mouse mutants of ciliopathy genes and human disease phenotypes, (eg. *NPHP1* is mutated in nephronopthisis, a recessive cystic kidney disease in humans, but the mouse mutants display no kidney defects and only male infertility (Jiang et al., 2008)) suggests it is possible that *AZI1* could still be associated with human ciliopathies. Interestingly, *AZI1* was included on ciliopathy candidate exon capture array used to screen ciliopathy patients for causative mutations, but as yet no human mutations have been reported (Otto et al., 2010).

8.6 Future plans

8.6.1 Large-scale screening

This screen was a pilot for a larger scale RNAi screen of an unbiased list of genes, such as genome-wide. Although the protocols were extensively optimised, further modifications and automation will be needed before this screening method can be scaled up. The cell culture and transfection protocols would need to be automated in

order to allow genome-wide or large scale coverage. It would also be interesting to explore the possibility of recording readouts in real-time using, for example, the 3T3-Arl13bmK2 cell line I developed, and possibly introducing other markers such as centriolar markers, or fluorescent readouts of Hh signalling. Live imaging plus high-throughput screening would, however, generate vast amounts of data so consideration for how this data would be stored and analysed is needed. It would also be interesting to investigate whether a reduction in noise in the screening protocol could be achieved by using shRNA libraries. Although more expensive than siRNA libraries, perhaps the increased knockdown efficiencies of such methods would increase reproducibility.

8.6.2 Follow up of other hits

As well as *Azi1,* several other genes gave a reduction in cilia numbers upon siRNA knockdown in the screen, including *Spag1*, *Ccdc63* and *Ttc30a2*. In order to further characterise the roles of these genes in ciliogenesis, it would be interesting to look at other ciliary markers upon siRNA knockdown such as the axoneme marker acetylated α-tubulin, to determine whether it is truly a loss of cilia we are seeing or whether it is a loss of Arl13b, (the ciliary membrane protein used as a ciliary marker during the screen) specifically. Ttc30a2 is a homologue of IFT70/Fleer, which has been shown to be involved in ciliogenesis in zebrafish and to have a role in tubulin polyglutamylation and tubulin glycylation, therefore it would be interesting to look at the level of polyglutamylation of tubulin upon siRNA knockdown of Ttc30a2. Localisation studies of Ttc30a2 are underway.

The role of *Ccdc63* in ciliogenesis was investigated in real time, and preliminary data suggested it has an additional role in the stabilisation of cilia. It will be interesting to confirm this result and also investigate the phenotypes in real time of other candidate ciliary genes from the screen.

8.6.2 Azi1 function

As mentioned, it will be interesting to investigate the role of Azi1, and perhaps other ciliary genes in spermiogenesis.

To further understand Azi1 function and localisation we are currently using the GFP-booster/GFP-Trap system (a high quality GFP binding protein coupled to agarose beads, magnetic particles or a fluorescent dye ATTO488, Chromotek), together with overexpressed Azi1-GFP, which we have shown to be functional (Figure 5.7), for biochemistry and super-resolution imaging. This sensitive and specific system will allow us to cleanly pull down over-expressed Azi1 and perform mass spectrometry to identify interactors. The GFP-booster platform would also allow live-imaging studies; combined with Arl13b-mKate2 it would be possible to study Azi1 localisation in real time during ciliogenesis, and during the cell cycle. The GFP-booster system will allow us to perform super-resolution imaging using the OMX system (Dundee) to better spatially define Azi1 localisation at the centriolar satellites and transition zone. We are currently modifying the GFP-booster system for immunogold transmission electron microscopy so we can undertake ultraresolution studies to pinpoint what structures Azi1 interacts with, such as whether it localises primarily to membranes or microtubules. Given the dynamic localisation of Azi1 it will be important to investigate post-translational modifications of Azi1 – it has been reported to be phosphorylated and ubiquitinated (Akimov et al., 2011; Olsen et al., 2006). Understanding whether these modifications are dynamic during the cell cycle, ciliogenesis or spermatogenesis, and what the functional significance of such post translational modification are, will help in the understanding of the role of Azi1 in these processes.

8.7 Conclusion

In conclusion, I have successfully designed, optimised and performed a siRNA screen for genes involved mammalian cilia formation, and identified several candidate ciliary genes. The requirement for cilia in mammalian development highlights their many roles, including transduction of developmental signalling pathways, sensory functions and generation of motility. Disruption of these organelles leads to a spectrum of human diseases, presenting with wide-ranging

phenotypes from embryonic lethality to male infertility. Identification of the genes which modulate the formation or function of these structures in mammals is key to understanding their complex biology.

Bibliography

Adams, M., Simms, R. J., Abdelhamed, Z., Dawe, H. R., Szymanska, K., Logan, C. V., Wheway, G., Pitt, E., Gull, K., Knowles, M. A., Blair, E., Cross, S. H., Sayer, J. A., Johnson, C. A., 2012. A meckelin-filamin A interaction mediates ciliogenesis. Hum Mol Genet. 21**,** 1272-86.

Afzelius, B. A., 1976. A human syndrome caused by immotile cilia. Science. 193**,** 317-9.

Ahmed, N. T., Gao, C., Lucker, B. F., Cole, D. G., Mitchell, D. R., 2008. ODA16 aids axonemal outer row dynein assembly through an interaction with the intraflagellar transport machinery. J Cell Biol. 183**,** 313-22.

Akimov, V., Rigbolt, K. T., Nielsen, M. M., Blagoev, B., 2011. Characterization of ubiquitination dependent dynamics in growth factor receptor signaling by quantitative proteomics. Mol Biosyst. 7**,** 3223-33.

Andersen, J. S., Wilkinson, C. J., Mayor, T., Mortensen, P., Nigg, E. A., Mann, M., 2003. Proteomic characterization of the human centrosome by protein correlation profiling. Nature. 426**,** 570-4.

Anderson, C. T., Stearns, T., 2009. Centriole age underlies asynchronous primary cilium growth in mammalian cells. Curr Biol. 19**,** 1498-502.

Anderson, R. G., 1972. The three-dimensional structure of the basal body from the rhesus monkey oviduct. J Cell Biol. 54**,** 246-65.

Aoto, H., Tsuchida, J., Nishina, Y., Nishimune, Y., Asano, A., Tajima, S., 1995. Isolation of a novel cDNA that encodes a protein localized to the pre-acrosome region of spermatids. Eur J Biochem. 234**,** 8-15.

Avidor-Reiss, T., Maer, A. M., Koundakjian, E., Polyanovsky, A., Keil, T., Subramaniam, S., Zuker, C. S., 2004. Decoding cilia function: defining specialized genes required for compartmentalized cilia biogenesis. Cell. 117**,** 527-39.

Aza-Blanc, P., Ramirez-Weber, F. A., Laget, M. P., Schwartz, C., Kornberg, T. B., 1997. Proteolysis that is inhibited by hedgehog targets Cubitus interruptus protein to the nucleus and converts it to a repressor. Cell. 89**,** 1043-53.

Azimzadeh, J., Wong, M. L., Downhour, D. M., Sanchez Alvarado, A., Marshall, W. F., 2012. Centrosome loss in the evolution of planarians. Science. 335**,** 461-3.

Baala, L., Audollent, S., Martinovic, J., Ozilou, C., Babron, M. C., Sivanandamoorthy, S., Saunier, S., Salomon, R., Gonzales, M., Rattenberry, E., Esculpavit, C., Toutain, A., Moraine, C., Parent, P., Marcorelles, P., Dauge, M. C., Roume, J., Le Merrer, M., Meiner, V., Meir, K., Menez, F., Beaufrere, A. M., Francannet, C., Tantau, J., Sinico, M., Dumez, Y., MacDonald, F., Munnich, A., Lyonnet, S., Gubler, M. C., Genin, E., Johnson, C. A., Vekemans, M., Encha-Razavi, F., Attie-Bitach, T., 2007. Pleiotropic effects of CEP290 (NPHP6) mutations extend to Meckel syndrome. Am J Hum Genet. 81**,** 170-9.

Balczon, R., Varden, C. E., Schroer, T. A., 1999. Role for microtubules in centrosome doubling in Chinese hamster ovary cells. Cell Motil Cytoskeleton. 42**,** 60-72.

Baltz, J. M., Williams, P. O., Cone, R. A., 1990. Dense fibers protect mammalian sperm against damage. Biol Reprod. 43**,** 485-91.

Barenz, F., Mayilo, D., Gruss, O. J., 2011. Centriolar satellites: busy orbits around the centrosome. Eur J Cell Biol. 90**,** 983-9.

Baron Gaillard, C. L., Pallesi-Pocachard, E., Massey-Harroche, D., Richard, F., Arsanto, J. P., Chauvin, J. P., Lecine, P., Kramer, H., Borg, J. P., Le Bivic, A., 2011. Hook2 is involved in the morphogenesis of the primary cilium. Mol Biol Cell. 22**,** 4549-62.

Basto, R., Lau, J., Vinogradova, T., Gardiol, A., Woods, C. G., Khodjakov, A., Raff, J. W., 2006. Flies without centrioles. Cell. 125**,** 1375-86.

Benzing, T., Simons, M., Walz, G., 2007. Wnt signaling in polycystic kidney disease. J Am Soc Nephrol. 18**,** 1389-98.

Berbari, N. F., Johnson, A. D., Lewis, J. S., Askwith, C. C., Mykytyn, K., 2008a. Identification of ciliary localization sequences within the third intracellular loop of G protein-coupled receptors. Mol Biol Cell. 19**,** 1540-7.

Berbari, N. F., Lewis, J. S., Bishop, G. A., Askwith, C. C., Mykytyn, K., 2008b. Bardet-Biedl syndrome proteins are required for the localization of G protein-coupled receptors to primary cilia. Proc Natl Acad Sci U S A. 105**,** 4242-6.

Bettencourt-Dias, M., Rodrigues-Martins, A., Carpenter, L., Riparbelli, M., Lehmann, L., Gatt, M. K., Carmo, N., Balloux, F., Callaini, G., Glover, D. M., 2005. SAK/PLK4 is required for centriole duplication and flagella development. Curr Biol. 15**,** 2199-207.

Bielas, S. L., Silhavy, J. L., Brancati, F., Kisseleva, M. V., Al-Gazali, L., Sztriha, L., Bayoumi, R. A., Zaki, M. S., Abdel-Aleem, A., Rosti, R. O., Kayserili, H., Swistun, D., Scott, L. C., Bertini, E., Boltshauser, E., Fazzi, E., Travaglini, L., Field, S. J., Gayral, S., Jacoby, M., Schurmans, S., Dallapiccola, B., Majerus, P. W., Valente, E. M., Gleeson, J. G., 2009. Mutations in INPP5E, encoding inositol polyphosphate-5-phosphatase E, link phosphatidyl inositol signaling to the ciliopathies. Nat Genet. 41**,** 1032-6.

Birmingham, A., Anderson, E. M., Reynolds, A., Ilsley-Tyree, D., Leake, D., Fedorov, Y., Baskerville, S., Maksimova, E., Robinson, K., Karpilow, J., Marshall, W. S., Khvorova, A., 2006. 3' UTR seed matches, but not overall identity, are associated with RNAi off-targets. Nat Methods. 3**,** 199-204.

Blacque, O. E., Li, C., Inglis, P. N., Esmail, M. A., Ou, G., Mah, A. K., Baillie, D. L., Scholey, J. M., Leroux, M. R., 2006. The WD repeat-containing protein IFTA-1 is required for retrograde intraflagellar transport. Mol Biol Cell. 17**,** 5053-62.

Blacque, O. E., Perens, E. A., Boroevich, K. A., Inglis, P. N., Li, C., Warner, A., Khattra, J., Holt, R. A., Ou, G., Mah, A. K., McKay, S. J., Huang, P., Swoboda, P., Jones, S. J., Marra, M. A., Baillie, D. L., Moerman, D. G., Shaham, S., Leroux, M. R., 2005. Functional genomics of the cilium, a sensory organelle. Curr Biol. 15**,** 935-41.

Blaineau, C., Tessier, M., Dubessay, P., Tasse, L., Crobu, L., Pages, M., Bastien, P., 2007. A novel microtubule-depolymerizing kinesin involved in length control of a eukaryotic flagellum. Curr Biol. 17**,** 778-82.

Blatt, E. N., Yan, X. H., Wuerffel, M. K., Hamilos, D. L., Brody, S. L., 1999. Forkhead transcription factor HFH-4 expression is temporally related to ciliogenesis. Am J Respir Cell Mol Biol. 21**,** 168-76.

Bobinnec, Y., Khodjakov, A., Mir, L. M., Rieder, C. L., Edde, B., Bornens, M., 1998. Centriole disassembly in vivo and its effect on centrosome structure and function in vertebrate cells. J Cell Biol. 143**,** 1575-89.

Boesger, J., Wagner, V., Weisheit, W., Mittag, M., 2009. Analysis of flagellar phosphoproteins from Chlamydomonas reinhardtii. Eukaryot Cell. 8**,** 922-32.

Boisvieux-Ulrich, E., Laine, M. C., Sandoz, D., 1990. Cytochalasin D inhibits basal body migration and ciliary elongation in quail oviduct epithelium. Cell Tissue Res. 259**,** 443-54.

Bonnafe, E., Touka, M., AitLounis, A., Baas, D., Barras, E., Ucla, C., Moreau, A., Flamant, F., Dubruille, R., Couble, P., Collignon, J., Durand, B., Reith, W., 2004. The transcription factor RFX3 directs nodal cilium development and left-right asymmetry specification. Mol Cell Biol. 24**,** 4417-27.

Bonnet, C. S., Aldred, M., von Ruhland, C., Harris, R., Sandford, R., Cheadle, J. P., 2009. Defects in cell polarity underlie TSC and ADPKD-associated cystogenesis. Hum Mol Genet. 18**,** 2166-76.

Bossinger, O., Bachmann, A., 2004. Ciliogenesis: polarity proteins on the move. Curr Biol. 14**,** R844-6.

Brancati, F., Iannicelli, M., Travaglini, L., Mazzotta, A., Bertini, E., Boltshauser, E., D'Arrigo, S., Emma, F., Fazzi, E., Gallizzi, R., Gentile, M., Loncarevic, D., Mejaski-Bosnjak, V., Pantaleoni, C., Rigoli, L., Salpietro, C. D., Signorini, S., Stringini, G. R., Verloes, A., Zabloka, D., Dallapiccola, B., Gleeson, J. G., Valente, E. M., International, J. S. G., 2009. MKS3/TMEM67 mutations are a major cause of COACH Syndrome, a Joubert Syndrome related disorder with liver involvement. Hum Mutat. 30**,** E432-42.

Bre, M. H., de Nechaud, B., Wolff, A., Fleury, A., 1994. Glutamylated tubulin probed in ciliates with the monoclonal antibody GT335. Cell Motil Cytoskeleton. 27**,** 337-49.

Breslow, D. K., Nachury, M. V., 2011. Primary cilia: how to keep the riff-raff in the plasma membrane. Curr Biol. 21**,** R434-6.

Broadhead, R., Dawe, H. R., Farr, H., Griffiths, S., Hart, S. R., Portman, N., Shaw, M. K., Ginger, M. L., Gaskell, S. J., McKean, P. G., Gull, K., 2006. Flagellar motility is required for the viability of the bloodstream trypanosome. Nature. 440**,** 224-7.

Brocker, C., Engelbrecht-Vandre, S., Ungermann, C., 2010. Multisubunit tethering complexes and their role in membrane fusion. Curr Biol. 20**,** R943-52.

Brody, S. L., Yan, X. H., Wuerffel, M. K., Song, S. K., Shapiro, S. D., 2000. Ciliogenesis and left-right axis defects in forkhead factor HFH-4-null mice. Am J Respir Cell Mol Biol. 23**,** 45-51.

Brown, N. L., Patel, S., Brzezinski, J., Glaser, T., 2001. Math5 is required for retinal ganglion cell and optic nerve formation. Development. 128**,** 2497-508.

Cachero, S., Simpson, T. I., Zur Lage, P. I., Ma, L., Newton, F. G., Holohan, E. E., Armstrong, J. D., Jarman, A. P., 2011. The gene regulatory cascade linking proneural specification with differentiation in Drosophila sensory neurons. PLoS Biol. 9**,** e1000568.

Calado, D. P., Zhang, B., Srinivasan, L., Sasaki, Y., Seagal, J., Unitt, C., Rodig, S., Kutok, J., Tarakhovsky, A., Schmidt-Supprian, M., Rajewsky, K., 2010. Constitutive canonical NF-kappaB activation cooperates with disruption of BLIMP1 in the pathogenesis of activated B cell-like diffuse large cell lymphoma. Cancer Cell. 18**,** 580-9.

Calvert, P. D., Schiesser, W. E., Pugh, E. N., Jr., 2010. Diffusion of a soluble protein, photoactivatable GFP, through a sensory cilium. J Gen Physiol. 135**,** 173-96.

Calvert, P. D., Strissel, K. J., Schiesser, W. E., Pugh, E. N., Jr., Arshavsky, V. Y., 2006. Light-driven translocation of signaling proteins in vertebrate photoreceptors. Trends Cell Biol. 16**,** 560-8.

Camner, P., Mossberg, B., Afzelius, B. A., 1975. Evidence of congenitally nonfunctioning cilia in the tracheobronchial tract in two subjects. Am Rev Respir Dis. 112**,** 807-9.

Caron, A., Xu, X., Lin, X., 2012. Wnt/beta-catenin signaling directly regulates Foxj1 expression and ciliogenesis in zebrafish Kupffer's vesicle. Development. 139**,** 514-24.

Carthew, R. W., Sontheimer, E. J., 2009. Origins and Mechanisms of miRNAs and siRNAs. Cell. 136**,** 642-55.

Carvalho-Santos, Z., Azimzadeh, J., Pereira-Leal, J. B., Bettencourt-Dias, M., 2011. Evolution: Tracing the origins of centrioles, cilia, and flagella. J Cell Biol. 194**,** 165-75.

Caspary, T., Larkins, C. E., Anderson, K. V., 2007. The graded response to Sonic Hedgehog depends on cilia architecture. Dev Cell. 12**,** 767-78.

Cavalier-Smith, T., 2002. The phagotrophic origin of eukaryotes and phylogenetic classification of Protozoa. Int J Syst Evol Microbiol. 52**,** 297-354.

Chang, B., Khanna, H., Hawes, N., Jimeno, D., He, S., Lillo, C., Parapuram, S. K., Cheng, H., Scott, A., Hurd, R. E., Sayer, J. A., Otto, E. A., Attanasio, M., O'Toole, J. F., Jin, G., Shou, C., Hildebrandt, F., Williams, D. S., Heckenlively, J. R., Swaroop, A., 2006. In-frame deletion in a novel centrosomal/ciliary protein CEP290/NPHP6 perturbs its interaction with RPGR and results in early-onset retinal degeneration in the rd16 mouse. Hum Mol Genet. 15**,** 1847-57.

Chauvet, V., Tian, X., Husson, H., Grimm, D. H., Wang, T., Hiesberger, T., Igarashi, P., Bennett, A. M., Ibraghimov-Beskrovnaya, O., Somlo, S., Caplan, M. J., 2004. Mechanical stimuli induce cleavage and nuclear translocation of the polycystin-1 C terminus. J Clin Invest. 114**,** 1433-43.

Chen, J. K., Taipale, J., Cooper, M. K., Beachy, P. A., 2002a. Inhibition of Hedgehog signaling by direct binding of cyclopamine to Smoothened. Genes Dev. 16**,** 2743-8.

Chen, M. H., Gao, N., Kawakami, T., Chuang, P. T., 2005. Mice deficient in the fused homolog do not exhibit phenotypes indicative of perturbed hedgehog signaling during embryonic development. Mol Cell Biol. 25**,** 7042-53.

Chen, M. H., Wilson, C. W., Li, Y. J., Law, K. K., Lu, C. S., Gacayan, R., Zhang, X., Hui, C. C., Chuang, P. T., 2009. Cilium-independent regulation of Gli protein function by Sufu in Hedgehog signaling is evolutionarily conserved. Genes Dev. 23**,** 1910-28.

Chen, Z., Indjeian, V. B., McManus, M., Wang, L., Dynlacht, B. D., 2002b. CP110, a cell cycle-dependent CDK substrate, regulates centrosome duplication in human cells. Dev Cell. 3**,** 339-50.

Chih, B., Liu, P., Chinn, Y., Chalouni, C., Komuves, L. G., Hass, P. E., Sandoval, W., Peterson, A. S., 2012. A ciliopathy complex at the transition zone protects the cilia as a privileged membrane domain. Nat Cell Biol. 14**,** 61-72.

Clarke, P. R., Allan, L. A., 2009. Cell-cycle control in the face of damage--a matter of life or death. Trends Cell Biol. 19**,** 89-98.

Cole, D. G., Chinn, S. W., Wedaman, K. P., Hall, K., Vuong, T., Scholey, J. M., 1993. Novel heterotrimeric kinesin-related protein purified from sea urchin eggs. Nature. 366**,** 268-70.

Cole, D. G., Diener, D. R., Himelblau, A. L., Beech, P. L., Fuster, J. C., Rosenbaum, J. L., 1998. Chlamydomonas kinesin-II-dependent intraflagellar transport (IFT): IFT particles contain proteins required for ciliary assembly in Caenorhabditis elegans sensory neurons. J Cell Biol. 141**,** 993-1008.

Colosimo, M. E., Brown, A., Mukhopadhyay, S., Gabel, C., Lanjuin, A. E., Samuel, A. D., Sengupta, P., 2004. Identification of thermosensory and olfactory neuron-specific genes via expression profiling of single neuron types. Curr Biol. 14**,** 2245-51.

Cooper, A. F., Yu, K. P., Brueckner, M., Brailey, L. L., Johnson, L., McGrath, J. M., Bale, A. E., 2005. Cardiac and CNS defects in a mouse with targeted disruption of suppressor of fused. Development. 132**,** 4407-17.

Coppieters, F., Lefever, S., Leroy, B. P., De Baere, E., 2010. CEP290, a gene with many faces: mutation overview and presentation of CEP290base. Hum Mutat. 31**,** 1097-108.

Corbit, K. C., Aanstad, P., Singla, V., Norman, A. R., Stainier, D. Y., Reiter, J. F., 2005. Vertebrate Smoothened functions at the primary cilium. Nature. 437**,** 1018-21.

Craige, B., Tsao, C. C., Diener, D. R., Hou, Y., Lechtreck, K. F., Rosenbaum, J. L., Witman, G. B., 2010. CEP290 tethers flagellar transition zone microtubules to the membrane and regulates flagellar protein content. J Cell Biol. 190**,** 927-40.

Criswell, P. S., Ostrowski, L. E., Asai, D. J., 1996. A novel cytoplasmic dynein heavy chain: expression of DHC1b in mammalian ciliated epithelial cells. J Cell Sci. 109 (Pt 7)**,** 1891-8.

Crossan, G. P., van der Weyden, L., Rosado, I. V., Langevin, F., Gaillard, P. H., McIntyre, R. E., Sanger Mouse Genetics, P., Gallagher, F., Kettunen, M. I., Lewis, D. Y., Brindle, K., Arends, M. J., Adams, D. J., Patel, K. J., 2011. Disruption of mouse Slx4, a regulator of structure-specific nucleases, phenocopies Fanconi anemia. Nat Genet. 43**,** 147-52.

Czarnecki, P. G., Shah, J. V., 2012. The ciliary transition zone: from morphology and molecules to medicine. Trends Cell Biol.

Dagoneau, N., Goulet, M., Genevieve, D., Sznajer, Y., Martinovic, J., Smithson, S., Huber, C., Baujat, G., Flori, E., Tecco, L., Cavalcanti, D., Delezoide, A. L., Serre, V., Le Merrer, M., Munnich,

A., Cormier-Daire, V., 2009. DYNC2H1 mutations cause asphyxiating thoracic dystrophy and short rib-polydactyly syndrome, type III. Am J Hum Genet. 84**,** 706-11.

Dammermann, A., Merdes, A., 2002. Assembly of centrosomal proteins and microtubule organization depends on PCM-1. J Cell Biol. 159**,** 255-66.

Danilov, A. I., Gomes-Leal, W., Ahlenius, H., Kokaia, Z., Carlemalm, E., Lindvall, O., 2009. Ultrastructural and antigenic properties of neural stem cells and their progeny in adult rat subventricular zone. Glia. 57**,** 136-52.

Dave, D., Wloga, D., Sharma, N., Gaertig, J., 2009. DYF-1 Is required for assembly of the axoneme in Tetrahymena thermophila. Eukaryot Cell. 8**,** 1397-406.

Davenport, J. R., Watts, A. J., Roper, V. C., Croyle, M. J., van Groen, T., Wyss, J. M., Nagy, T. R., Kesterson, R. A., Yoder, B. K., 2007. Disruption of intraflagellar transport in adult mice leads to obesity and slow-onset cystic kidney disease. Curr Biol. 17**,** 1586-94.

Dawe, H. R., Adams, M., Wheway, G., Szymanska, K., Logan, C. V., Noegel, A. A., Gull, K., Johnson, C. A., 2009. Nesprin-2 interacts with meckelin and mediates ciliogenesis via remodelling of the actin cytoskeleton. J Cell Sci. 122**,** 2716-26.

Dawe, H. R., Farr, H., Gull, K., 2007. Centriole/basal body morphogenesis and migration during ciliogenesis in animal cells. J Cell Sci. 120**,** 7-15.

Dawson, S. C., Sagolla, M. S., Mancuso, J. J., Woessner, D. J., House, S. A., Fritz-Laylin, L., Cande, W. Z., 2007. Kinesin-13 regulates flagellar, interphase, and mitotic microtubule dynamics in Giardia intestinalis. Eukaryot Cell. 6**,** 2354-64.

Deane, J. A., Cole, D. G., Seeley, E. S., Diener, D. R., Rosenbaum, J. L., 2001. Localization of intraflagellar transport protein IFT52 identifies basal body transitional fibers as the docking site for IFT particles. Curr Biol. 11**,** 1586-90.

Debec, A., Sullivan, W., Bettencourt-Dias, M., 2010. Centrioles: active players or passengers during mitosis? Cell Mol Life Sci. 67**,** 2173-94.

Delaval, B., Bright, A., Lawson, N. D., Doxsey, S., 2011. The cilia protein IFT88 is required for spindle orientation in mitosis. Nat Cell Biol. 13**,** 461-8.

Delous, M., Hellman, N. E., Gaude, H. M., Silbermann, F., Le Bivic, A., Salomon, R., Antignac, C., Saunier, S., 2009. Nephrocystin-1 and nephrocystin-4 are required for epithelial morphogenesis and associate with PALS1/PATJ and Par6. Hum Mol Genet. 18**,** 4711-23.

Deretic, D., Schmerl, S., Hargrave, P. A., Arendt, A., McDowell, J. H., 1998. Regulation of sorting and post-Golgi trafficking of rhodopsin by its C-terminal sequence QVS(A)PA. Proc Natl Acad Sci U S A. 95**,** 10620-5.

Deretic, D., Williams, A. H., Ransom, N., Morel, V., Hargrave, P. A., Arendt, A., 2005. Rhodopsin C terminus, the site of mutations causing retinal disease, regulates trafficking by binding to ADP-ribosylation factor 4 (ARF4). Proc Natl Acad Sci U S A. 102**,** 3301-6.

Dirksen, E. R., 1971. Centriole morphogenesis in developing ciliated epithelium of the mouse oviduct. J Cell Biol. 51**,** 286-302.

Dishinger, J. F., Kee, H. L., Jenkins, P. M., Fan, S., Hurd, T. W., Hammond, J. W., Truong, Y. N., Margolis, B., Martens, J. R., Verhey, K. J., 2010. Ciliary entry of the kinesin-2 motor KIF17 is regulated by importin-beta2 and RanGTP. Nat Cell Biol. 12**,** 703-10.

Dodson, H., Bourke, E., Jeffers, L. J., Vagnarelli, P., Sonoda, E., Takeda, S., Earnshaw, W. C., Merdes, A., Morrison, C., 2004. Centrosome amplification induced by DNA damage occurs during a prolonged G2 phase and involves ATM. EMBO J. 23**,** 3864-73.

Doench, J. G., Petersen, C. P., Sharp, P. A., 2003. siRNAs can function as miRNAs. Genes Dev. 17**,** 438-42.

Dubruille, R., Laurencon, A., Vandaele, C., Shishido, E., Coulon-Bublex, M., Swoboda, P., Couble, P., Kernan, M., Durand, B., 2002. Drosophila regulatory factor X is necessary for ciliated sensory neuron differentiation. Development. 129**,** 5487-98.

Efimenko, E., Bubb, K., Mak, H. Y., Holzman, T., Leroux, M. R., Ruvkun, G., Thomas, J. H., Swoboda, P., 2005. Analysis of xbx genes in C. elegans. Development. 132**,** 1923-34.

Eggenschwiler, J. T., Anderson, K. V., 2007. Cilia and developmental signaling. Annu Rev Cell Dev Biol. 23**,** 345-73.

Endoh-Yamagami, S., Evangelista, M., Wilson, D., Wen, X., Theunissen, J. W., Phamluong, K., Davis, M., Scales, S. J., Solloway, M. J., de Sauvage, F. J., Peterson, A. S., 2009. The mammalian Cos2 homolog Kif7 plays an essential role in modulating Hh signal transduction during development. Curr Biol. 19**,** 1320-6.

Escalier, D., 2006. Knockout mouse models of sperm flagellum anomalies. Hum Reprod Update. 12**,** 449-61.

Evangelista, M., Lim, T. Y., Lee, J., Parker, L., Ashique, A., Peterson, A. S., Ye, W., Davis, D. P., de Sauvage, F. J., 2008. Kinome siRNA screen identifies regulators of ciliogenesis and hedgehog signal transduction. Sci Signal. 1**,** ra7.

Evans, J. E., Snow, J. J., Gunnarson, A. L., Ou, G., Stahlberg, H., McDonald, K. L., Scholey, J. M., 2006. Functional modulation of IFT kinesins extends the sensory repertoire of ciliated neurons in Caenorhabditis elegans. J Cell Biol. 172**,** 663-9.

Fan, S., Hurd, T. W., Liu, C. J., Straight, S. W., Weimbs, T., Hurd, E. A., Domino, S. E., Margolis, B., 2004a. Polarity proteins control ciliogenesis via kinesin motor interactions. Curr Biol. 14**,** 1451-61.

Fan, Y., Esmail, M. A., Ansley, S. J., Blacque, O. E., Boroevich, K., Ross, A. J., Moore, S. J., Badano, J. L., May-Simera, H., Compton, D. S., Green, J. S., Lewis, R. A., van Haelst, M. M., Parfrey, P. S., Baillie, D. L., Beales, P. L., Katsanis, N., Davidson, W. S., Leroux, M. R., 2004b. Mutations in a member of the Ras superfamily of small GTP-binding proteins causes Bardet-Biedl syndrome. Nat Genet. 36**,** 989-93.

Fan, Z. C., Behal, R. H., Geimer, S., Wang, Z., Williamson, S. M., Zhang, H., Cole, D. G., Qin, H., 2010. Chlamydomonas IFT70/CrDYF-1 is a core component of IFT particle complex B and is required for flagellar assembly. Mol Biol Cell. 21**,** 2696-706.

Farzan, S. F., Ascano, M., Jr., Ogden, S. K., Sanial, M., Brigui, A., Plessis, A., Robbins, D. J., 2008. Costal2 functions as a kinesin-like protein in the hedgehog signal transduction pathway. Curr Biol. 18**,** 1215-20.

Fath, M. A., Mullins, R. F., Searby, C., Nishimura, D. Y., Wei, J., Rahmouni, K., Davis, R. E., Tayeh, M. K., Andrews, M., Yang, B., Sigmund, C. D., Stone, E. M., Sheffield, V. C., 2005. Mkks-null mice have a phenotype resembling Bardet-Biedl syndrome. Hum Mol Genet. 14**,** 1109-18.

Fawcett, D. W., 1966. An atlas of fine structure: the cell, its organelles, and inclusions. W. B. Saunders Co., Philadelphia,.

Fedorov, Y., Anderson, E. M., Birmingham, A., Reynolds, A., Karpilow, J., Robinson, K., Leake, D., Marshall, W. S., Khvorova, A., 2006. Off-target effects by siRNA can induce toxic phenotype. RNA. 12**,** 1188-96.

Ferrante, M. I., Romio, L., Castro, S., Collins, J. E., Goulding, D. A., Stemple, D. L., Woolf, A. S., Wilson, S. W., 2009. Convergent extension movements and ciliary function are mediated by ofd1, a zebrafish orthologue of the human oral-facial-digital type 1 syndrome gene. Hum Mol Genet. 18**,** 289-303.

Ferrante, M. I., Zullo, A., Barra, A., Bimonte, S., Messaddeq, N., Studer, M., Dolle, P., Franco, B., 2006. Oral-facial-digital type I protein is required for primary cilia formation and left-right axis specification. Nat Genet. 38**,** 112-7.

Ferreira, A., Dolder, H., 2003. Sperm ultrastructure and spermatogenesis in the lizard, Tropidurus itambere. Biocell. 27**,** 353-62.

Field, M. C., Carrington, M., 2009. The trypanosome flagellar pocket. Nat Rev Microbiol. 7**,** 775-86.

Fire, A., Xu, S., Montgomery, M. K., Kostas, S. A., Driver, S. E., Mello, C. C., 1998. Potent and specific genetic interference by double-stranded RNA in Caenorhabditis elegans. Nature. 391**,** 806-11.

Fliegauf, M., Benzing, T., Omran, H., 2007. When cilia go bad: cilia defects and ciliopathies. Nat Rev Mol Cell Biol. 8**,** 880-93.

Follit, J. A., Li, L., Vucica, Y., Pazour, G. J., 2010. The cytoplasmic tail of fibrocystin contains a ciliary targeting sequence. J Cell Biol. 188**,** 21-8.

Follit, J. A., San Agustin, J. T., Xu, F., Jonassen, J. A., Samtani, R., Lo, C. W., Pazour, G. J., 2008. The Golgin GMAP210/TRIP11 anchors IFT20 to the Golgi complex. PLoS Genet. 4**,** e1000315.

Follit, J. A., Tuft, R. A., Fogarty, K. E., Pazour, G. J., 2006. The intraflagellar transport protein IFT20 is associated with the Golgi complex and is required for cilia assembly. Mol Biol Cell. 17**,** 3781-92.

Francis, S. S., Sfakianos, J., Lo, B., Mellman, I., 2011. A hierarchy of signals regulates entry of membrane proteins into the ciliary membrane domain in epithelial cells. J Cell Biol. 193**,** 219-33.

Freudenberg, J. M., Ghosh, S., Lackford, B. L., Yellaboina, S., Zheng, X., Li, R., Cuddapah, S., Wade, P. A., Hu, G., Jothi, R., 2011. Acute depletion of Tet1-dependent 5-hydroxymethylcytosine levels impairs LIF/Stat3 signaling and results in loss of embryonic stem cell identity. Nucleic Acids Res.

Gabernet-Castello, C., Dubois, K. N., Nimmo, C., Field, M. C., 2011. Rab11 function in Trypanosoma brucei: identification of conserved and novel interaction partners. Eukaryot Cell. 10**,** 1082-94.

Gaertig, J., Cruz, M. A., Bowen, J., Gu, L., Pennock, D. G., Gorovsky, M. A., 1995. Acetylation of lysine 40 in alpha-tubulin is not essential in Tetrahymena thermophila. J Cell Biol. 129**,** 1301-10.

Gagnon, C., White, D., Cosson, J., Huitorel, P., Edde, B., Desbruyeres, E., Paturle-Lafanechere, L., Multigner, L., Job, D., Cibert, C., 1996. The polyglutamylated lateral chain of alpha-tubulin plays a key role in flagellar motility. J Cell Sci. 109 (Pt 6)**,** 1545-53.

Gao, C., Wang, G., Amack, J. D., Mitchell, D. R., 2010. Oda16/Wdr69 is essential for axonemal dynein assembly and ciliary motility during zebrafish embryogenesis. Dev Dyn. 239**,** 2190-7.

Garcia-Gonzalo, F. R., Corbit, K. C., Sirerol-Piquer, M. S., Ramaswami, G., Otto, E. A., Noriega, T. R., Seol, A. D., Robinson, J. F., Bennett, C. L., Josifova, D. J., Garcia-Verdugo, J. M., Katsanis, N., Hildebrandt, F., Reiter, J. F., 2011. A transition zone complex regulates mammalian ciliogenesis and ciliary membrane composition. Nat Genet. 43**,** 776-84.

Geng, L., Okuhara, D., Yu, Z., Tian, X., Cai, Y., Shibazaki, S., Somlo, S., 2006. Polycystin-2 traffics to cilia independently of polycystin-1 by using an N-terminal RVxP motif. J Cell Sci. 119**,** 1383-95.

Gerdes, J. M., Liu, Y., Zaghloul, N. A., Leitch, C. C., Lawson, S. S., Kato, M., Beachy, P. A., Beales, P. L., DeMartino, G. N., Fisher, S., Badano, J. L., Katsanis, N., 2007. Disruption of the basal body compromises proteasomal function and perturbs intracellular Wnt response. Nat Genet. 39**,** 1350-60.

Geremek, M., Bruinenberg, M., Zietkiewicz, E., Pogorzelski, A., Witt, M., Wijmenga, C., 2011. Gene expression studies in cells from primary ciliary dyskinesia patients identify 208 potential ciliary genes. Hum Genet. 129**,** 283-93.

Gherman, A., Davis, E. E., Katsanis, N., 2006. The ciliary proteome database: an integrated community resource for the genetic and functional dissection of cilia. Nat Genet. 38**,** 961-2.

Gilissen, C., Arts, H. H., Hoischen, A., Spruijt, L., Mans, D. A., Arts, P., van Lier, B., Steehouwer, M., van Reeuwijk, J., Kant, S. G., Roepman, R., Knoers, N. V., Veltman, J. A., Brunner, H.

G., 2010. Exome sequencing identifies WDR35 variants involved in Sensenbrenner syndrome. Am J Hum Genet. 87**,** 418-23.

Gilula, N. B., Satir, P., 1972. The ciliary necklace. A ciliary membrane specialization. J Cell Biol. 53**,** 494-509.

Goetz, S. C., Anderson, K. V., 2010. The primary cilium: a signalling centre during vertebrate development. Nat Rev Genet. 11**,** 331-44.

Gonzalez-Perrett, S., Kim, K., Ibarra, C., Damiano, A. E., Zotta, E., Batelli, M., Harris, P. C., Reisin, I. L., Arnaout, M. A., Cantiello, H. F., 2001. Polycystin-2, the protein mutated in autosomal dominant polycystic kidney disease (ADPKD), is a Ca2+-permeable nonselective cation channel. Proc Natl Acad Sci U S A. 98**,** 1182-7.

Goodrich, L. V., Milenkovic, L., Higgins, K. M., Scott, M. P., 1997. Altered neural cell fates and medulloblastoma in mouse patched mutants. Science. 277**,** 1109-13.

Graser, S., Stierhof, Y. D., Lavoie, S. B., Gassner, O. S., Lamla, S., Le Clech, M., Nigg, E. A., 2007. Cep164, a novel centriole appendage protein required for primary cilium formation. J Cell Biol. 179**,** 321-30.

Habedanck, R., Stierhof, Y. D., Wilkinson, C. J., Nigg, E. A., 2005. The Polo kinase Plk4 functions in centriole duplication. Nat Cell Biol. 7**,** 1140-6.

Hackett, B. P., Brody, S. L., Liang, M., Zeitz, I. D., Bruns, L. A., Gitlin, J. D., 1995. Primary structure of hepatocyte nuclear factor/forkhead homologue 4 and characterization of gene expression in the developing respiratory and reproductive epithelium. Proc Natl Acad Sci U S A. 92**,** 4249-53.

Hagiwara, H., Shibasaki, S., Ohwada, N., 1992. Ciliogenesis in the human oviduct epithelium during the normal menstrual cycle. J Electron Microsc (Tokyo). 41**,** 321-9.

Han, Y. G., Kwok, B. H., Kernan, M. J., 2003. Intraflagellar transport is required in Drosophila to differentiate sensory cilia but not sperm. Curr Biol. 13**,** 1679-86.

Hartman, T. R., Liu, D., Zilfou, J. T., Robb, V., Morrison, T., Watnick, T., Henske, E. P., 2009. The tuberous sclerosis proteins regulate formation of the primary cilium via a rapamycin-insensitive and polycystin 1-independent pathway. Hum Mol Genet. 18**,** 151-63.

Haycraft, C. J., Banizs, B., Aydin-Son, Y., Zhang, Q., Michaud, E. J., Yoder, B. K., 2005. Gli2 and Gli3 localize to cilia and require the intraflagellar transport protein polaris for processing and function. PLoS Genet. 1**,** e53.

He, L., Yu, J. X., Liu, L., Buyse, I. M., Wang, M. S., Yang, Q. C., Nakagawara, A., Brodeur, G. M., Shi, Y. E., Huang, S., 1998. RIZ1, but not the alternative RIZ2 product of the same gene, is underexpressed in breast cancer, and forced RIZ1 expression causes G2-M cell cycle arrest and/or apoptosis. Cancer Res. 58**,** 4238-44.

Heddle, J. A., 1973. A rapid in vivo test for chromosomal damage. Mutat Res. 18**,** 187-90.

Heisenberg, C. P., Tada, M., Rauch, G. J., Saude, L., Concha, M. L., Geisler, R., Stemple, D. L., Smith, J. C., Wilson, S. W., 2000. Silberblick/Wnt11 mediates convergent extension movements during zebrafish gastrulation. Nature. 405**,** 76-81.

Helou, J., Otto, E. A., Attanasio, M., Allen, S. J., Parisi, M. A., Glass, I., Utsch, B., Hashmi, S., Fazzi, E., Omran, H., O'Toole, J. F., Sayer, J. A., Hildebrandt, F., 2007. Mutation analysis of NPHP6/CEP290 in patients with Joubert syndrome and Senior-Loken syndrome. J Med Genet. 44**,** 657-63.

Heydeck, W., Zeng, H., Liu, A., 2009. Planar cell polarity effector gene Fuzzy regulates cilia formation and Hedgehog signal transduction in mouse. Dev Dyn. 238**,** 3035-42.

Hildebrandt, F., Benzing, T., Katsanis, N., 2011. Ciliopathies. N Engl J Med. 364**,** 1533-43.

Hildebrandt, F., Otto, E., 2005. Cilia and centrosomes: a unifying pathogenic concept for cystic kidney disease? Nat Rev Genet. 6**,** 928-40.

Hinchcliffe, E. H., Cassels, G. O., Rieder, C. L., Sluder, G., 1998. The coordination of centrosome reproduction with nuclear events of the cell cycle in the sea urchin zygote. J Cell Biol. 140**,** 1417-26.

Hirokawa, N., Tanaka, Y., Okada, Y., 2009. Left-right determination: involvement of molecular motor KIF3, cilia, and nodal flow. Cold Spring Harb Perspect Biol. 1**,** a000802.

Hou, Y., Qin, H., Follit, J. A., Pazour, G. J., Rosenbaum, J. L., Witman, G. B., 2007. Functional analysis of an individual IFT protein: IFT46 is required for transport of outer dynein arms into flagella. J Cell Biol. 176**,** 653-65.

Hoyer-Fender, S., 2010. Centriole maturation and transformation to basal body. Semin Cell Dev Biol. 21**,** 142-7.

Hu, Q., Milenkovic, L., Jin, H., Scott, M. P., Nachury, M. V., Spiliotis, E. T., Nelson, W. J., 2010. A septin diffusion barrier at the base of the primary cilium maintains ciliary membrane protein distribution. Science. 329**,** 436-9.

Huang, K., Diener, D. R., Mitchell, A., Pazour, G. J., Witman, G. B., Rosenbaum, J. L., 2007. Function and dynamics of PKD2 in Chlamydomonas reinhardtii flagella. J Cell Biol. 179**,** 501-14.

Huang, P., Schier, A. F., 2009. Dampened Hedgehog signaling but normal Wnt signaling in zebrafish without cilia. Development. 136**,** 3089-98.

Huang, T., You, Y., Spoor, M. S., Richer, E. J., Kudva, V. V., Paige, R. C., Seiler, M. P., Liebler, J. M., Zabner, J., Plopper, C. G., Brody, S. L., 2003. Foxj1 is required for apical localization of ezrin in airway epithelial cells. J Cell Sci. 116**,** 4935-45.

Huangfu, D., Anderson, K. V., 2005. Cilia and Hedgehog responsiveness in the mouse. Proc Natl Acad Sci U S A. 102**,** 11325-30.

Huangfu, D., Liu, A., Rakeman, A. S., Murcia, N. S., Niswander, L., Anderson, K. V., 2003. Hedgehog signalling in the mouse requires intraflagellar transport proteins. Nature. 426**,** 83-7.

Hubbert, C., Guardiola, A., Shao, R., Kawaguchi, Y., Ito, A., Nixon, A., Yoshida, M., Wang, X. F., Yao, T. P., 2002. HDAC6 is a microtubule-associated deacetylase. Nature. 417**,** 455-8.

Huckins, C., 1978. The morphology and kinetics of spermatogonial degeneration in normal adult rats: an analysis using a simplified classification of the germinal epithelium. Anat Rec. 190**,** 905-26.

Ikeda, W., Nakanishi, H., Miyoshi, J., Mandai, K., Ishizaki, H., Tanaka, M., Togawa, A., Takahashi, K., Nishioka, H., Yoshida, H., Mizoguchi, A., Nishikawa, S., Takai, Y., 1999. Afadin: A key molecule essential for structural organization of cell-cell junctions of polarized epithelia during embryogenesis. J Cell Biol. 146**,** 1117-32.

Ingham, P. W., McMahon, A. P., 2001. Hedgehog signaling in animal development: paradigms and principles. Genes Dev. 15**,** 3059-87.

Inglis, P. N., Boroevich, K. A., Leroux, M. R., 2006. Piecing together a ciliome. Trends Genet. 22**,** 491-500.

Insinna, C., Humby, M., Sedmak, T., Wolfrum, U., Besharse, J. C., 2009. Different roles for KIF17 and kinesin II in photoreceptor development and maintenance. Dev Dyn. 238**,** 2211-22.

Insinna, C., Pathak, N., Perkins, B., Drummond, I., Besharse, J. C., 2008. The homodimeric kinesin, Kif17, is essential for vertebrate photoreceptor sensory outer segment development. Dev Biol. 316**,** 160-70.

Iomini, C., Babaev-Khaimov, V., Sassaroli, M., Piperno, G., 2001. Protein particles in Chlamydomonas flagella undergo a transport cycle consisting of four phases. J Cell Biol. 153**,** 13-24.

Iomini, C., Li, L., Esparza, J. M., Dutcher, S. K., 2009. Retrograde intraflagellar transport mutants identify complex A proteins with multiple genetic interactions in Chlamydomonas reinhardtii. Genetics. 183**,** 885-96.

Ishikawa, H., Kubo, A., Tsukita, S., Tsukita, S., 2005. Odf2-deficient mother centrioles lack distal/subdistal appendages and the ability to generate primary cilia. Nat Cell Biol. 7**,** 517-24.

Ishikawa, H., Marshall, W. F., 2011. Ciliogenesis: building the cell's antenna. Nat Rev Mol Cell Biol. 12**,** 222-34.

Ishikawa, H., Thompson, J., Yates, J. R., 3rd, Marshall, W. F., 2012. Proteomic analysis of Mammalian primary cilia. Curr Biol. 22**,** 414-9.

Jackson, A. L., Burchard, J., Leake, D., Reynolds, A., Schelter, J., Guo, J., Johnson, J. M., Lim, L., Karpilow, J., Nichols, K., Marshall, W., Khvorova, A., Linsley, P. S., 2006. Position-specific chemical modification of siRNAs reduces "off-target" transcript silencing. RNA. 12**,** 1197-205.

Jacoby, M., Cox, J. J., Gayral, S., Hampshire, D. J., Ayub, M., Blockmans, M., Pernot, E., Kisseleva, M. V., Compere, P., Schiffmann, S. N., Gergely, F., Riley, J. H., Perez-Morga, D., Woods, C. G., Schurmans, S., 2009. INPP5E mutations cause primary cilium signaling defects, ciliary instability and ciliopathies in human and mouse. Nat Genet. 41**,** 1027-31.

Jacquet, B. V., Salinas-Mondragon, R., Liang, H., Therit, B., Buie, J. D., Dykstra, M., Campbell, K., Ostrowski, L. E., Brody, S. L., Ghashghaei, H. T., 2009. FoxJ1-dependent gene expression is required for differentiation of radial glia into ependymal cells and a subset of astrocytes in the postnatal brain. Development. 136**,** 4021-31.

Jakobsen, L., Vanselow, K., Skogs, M., Toyoda, Y., Lundberg, E., Poser, I., Falkenby, L. G., Bennetzen, M., Westendorf, J., Nigg, E. A., Uhlen, M., Hyman, A. A., Andersen, J. S., 2011. Novel asymmetrically localizing components of human centrosomes identified by complementary proteomics methods. EMBO J. 30**,** 1520-35.

Janke, C., Rogowski, K., Wloga, D., Regnard, C., Kajava, A. V., Strub, J. M., Temurak, N., van Dijk, J., Boucher, D., van Dorsselaer, A., Suryavanshi, S., Gaertig, J., Edde, B., 2005. Tubulin polyglutamylase enzymes are members of the TTL domain protein family. Science. 308**,** 1758-62.

Jekely, G., Arendt, D., 2006. Evolution of intraflagellar transport from coated vesicles and autogenous origin of the eukaryotic cilium. Bioessays. 28**,** 191-8.

Jenkins, P. M., Hurd, T. W., Zhang, L., McEwen, D. P., Brown, R. L., Margolis, B., Verhey, K. J., Martens, J. R., 2006. Ciliary targeting of olfactory CNG channels requires the CNGB1b subunit and the kinesin-2 motor protein, KIF17. Curr Biol. 16**,** 1211-6.

Jia, J., Kolterud, A., Zeng, H., Hoover, A., Teglund, S., Toftgard, R., Liu, A., 2009. Suppressor of Fused inhibits mammalian Hedgehog signaling in the absence of cilia. Dev Biol. 330**,** 452-60.

Jiang, G., Liu, L., Buyse, I. M., Simon, D., Huang, S., 1999. Decreased RIZ1 expression but not RIZ2 in hepatoma and suppression of hepatoma tumorigenicity by RIZ1. Int J Cancer. 83**,** 541-6.

Jiang, S. T., Chiou, Y. Y., Wang, E., Lin, H. K., Lee, S. P., Lu, H. Y., Wang, C. K., Tang, M. J., Li, H., 2008. Targeted disruption of Nphp1 causes male infertility due to defects in the later steps of sperm morphogenesis in mice. Hum Mol Genet. 17**,** 3368-79.

Jin, H., White, S. R., Shida, T., Schulz, S., Aguiar, M., Gygi, S. P., Bazan, J. F., Nachury, M. V., 2010. The conserved Bardet-Biedl syndrome proteins assemble a coat that traffics membrane proteins to cilia. Cell. 141**,** 1208-19.

Kaneshiro, E. S., 1987. Lipids of Paramecium. J Lipid Res. 28**,** 1241-58.

Kang-Decker, N., Mantchev, G. T., Juneja, S. C., McNiven, M. A., van Deursen, J. M., 2001. Lack of acrosome formation in Hrb-deficient mice. Science. 294**,** 1531-3.

Kang, R. S., Folsch, H., 2009. An old dog learns new tricks: novel functions of the exocyst complex in polarized epithelia in animals. F1000 Biol Rep. 1**,** 83.

Kannu, P., McFarlane, J. H., Savarirayan, R., Aftimos, S., 2007. An unclassifiable short rib-polydactyly syndrome with acromesomelic hypomineralization and campomelia in siblings. Am J Med Genet A. 143A**,** 2607-11.

Kaplan, O. I., Doroquez, D. B., Cevik, S., Bowie, R. V., Clarke, L., Sanders, A. A., Kida, K., Rappoport, J. Z., Sengupta, P., Blacque, O. E., 2012. Endocytosis Genes Facilitate Protein and Membrane Transport in C. elegans Sensory Cilia. Curr Biol. 22**,** 451-60.

Kavlie, R. G., Kernan, M. J., Eberl, D. F., 2010. Hearing in Drosophila requires TilB, a conserved protein associated with ciliary motility. Genetics. 185**,** 177-88.

Kee, H. L., Dishinger, J. F., Lynne Blasius, T., Liu, C. J., Margolis, B., Verhey, K. J., 2012. A size-exclusion permeability barrier and nucleoporins characterize a ciliary pore complex that regulates transport into cilia. Nat Cell Biol.

Keller, L. C., Romijn, E. P., Zamora, I., Yates, J. R., 3rd, Marshall, W. F., 2005. Proteomic analysis of isolated chlamydomonas centrioles reveals orthologs of ciliary-disease genes. Curr Biol. 15**,** 1090-8.

Khodjakov, A., Rieder, C. L., Sluder, G., Cassels, G., Sibon, O., Wang, C. L., 2002. De novo formation of centrosomes in vertebrate cells arrested during S phase. J Cell Biol. 158**,** 1171-81.

Kierszenbaum, A. L., 2001. Spermatid manchette: plugging proteins to zero into the sperm tail. Mol Reprod Dev. 59**,** 347-9.

Kierszenbaum, A. L., Rivkin, E., Tres, L. L., Yoder, B. K., Haycraft, C. J., Bornens, M., Rios, R. M., 2011. GMAP210 and IFT88 are present in the spermatid golgi apparatus and participate in the development of the acrosome-acroplaxome complex, head-tail coupling apparatus and tail. Dev Dyn. 240**,** 723-36.

Kierszenbaum, A. L., Tres, L. L., 2004. The acrosome-acroplaxome-manchette complex and the shaping of the spermatid head. Arch Histol Cytol. 67**,** 271-84.

Kim, J., Kato, M., Beachy, P. A., 2009. Gli2 trafficking links Hedgehog-dependent activation of Smoothened in the primary cilium to transcriptional activation in the nucleus. Proc Natl Acad Sci U S A. 106**,** 21666-71.

Kim, J., Lee, J. E., Heynen-Genel, S., Suyama, E., Ono, K., Lee, K., Ideker, T., Aza-Blanc, P., Gleeson, J. G., 2010. Functional genomic screen for modulators of ciliogenesis and cilium length. Nature. 464**,** 1048-51.

Kim, J. C., Badano, J. L., Sibold, S., Esmail, M. A., Hill, J., Hoskins, B. E., Leitch, C. C., Venner, K., Ansley, S. J., Ross, A. J., Leroux, M. R., Katsanis, N., Beales, P. L., 2004. The Bardet-Biedl protein BBS4 targets cargo to the pericentriolar region and is required for microtubule anchoring and cell cycle progression. Nat Genet. 36**,** 462-70.

Klinghoffer, R. A., Hamilton, T. G., Hoch, R., Soriano, P., 2002. An allelic series at the PDGFalphaR locus indicates unequal contributions of distinct signaling pathways during development. Dev Cell. 2**,** 103-13.

Klotz, C., Bordes, N., Laine, M. C., Sandoz, D., Bornens, M., 1986. Myosin at the apical pole of ciliated epithelial cells as revealed by a monoclonal antibody. J Cell Biol. 103**,** 613-9.

Knodler, A., Feng, S., Zhang, J., Zhang, X., Das, A., Peranen, J., Guo, W., 2010. Coordination of Rab8 and Rab11 in primary ciliogenesis. Proc Natl Acad Sci U S A. 107**,** 6346-51.

Kohlmaier, G., Loncarek, J., Meng, X., McEwen, B. F., Mogensen, M. M., Spektor, A., Dynlacht, B. D., Khodjakov, A., Gonczy, P., 2009. Overly long centrioles and defective cell division upon excess of the SAS-4-related protein CPAP. Curr Biol. 19**,** 1012-8.

Kovacs, J. J., Murphy, P. J., Gaillard, S., Zhao, X., Wu, J. T., Nicchitta, C. V., Yoshida, M., Toft, D. O., Pratt, W. B., Yao, T. P., 2005. HDAC6 regulates Hsp90 acetylation and chaperone-dependent activation of glucocorticoid receptor. Mol Cell. 18**,** 601-7.

Kozminski, K. G., Beech, P. L., Rosenbaum, J. L., 1995. The Chlamydomonas kinesin-like protein FLA10 is involved in motility associated with the flagellar membrane. J Cell Biol. 131**,** 1517-27.

Kozminski, K. G., Diener, D. R., Rosenbaum, J. L., 1993a. High level expression of nonacetylatable alpha-tubulin in Chlamydomonas reinhardtii. Cell Motil Cytoskeleton. 25**,** 158-70.

Kozminski, K. G., Johnson, K. A., Forscher, P., Rosenbaum, J. L., 1993b. A motility in the eukaryotic flagellum unrelated to flagellar beating. Proc Natl Acad Sci U S A. 90**,** 5519-23.

Kubo, A., Sasaki, H., Yuba-Kubo, A., Tsukita, S., Shiina, N., 1999. Centriolar satellites: molecular characterization, ATP-dependent movement toward centrioles and possible involvement in ciliogenesis. J Cell Biol. 147**,** 969-80.

Kulaga, H. M., Leitch, C. C., Eichers, E. R., Badano, J. L., Lesemann, A., Hoskins, B. E., Lupski, J. R., Beales, P. L., Reed, R. R., Katsanis, N., 2004. Loss of BBS proteins causes anosmia in humans and defects in olfactory cilia structure and function in the mouse. Nat Genet. 36**,** 994-8.

Lai, C. K., Gupta, N., Wen, X., Rangell, L., Chih, B., Peterson, A. S., Bazan, J. F., Li, L., Scales, S. J., 2011. Functional characterization of putative cilia genes by high-content analysis. Mol Biol Cell. 22**,** 1104-19.

Lancaster, M. A., Gopal, D. J., Kim, J., Saleem, S. N., Silhavy, J. L., Louie, C. M., Thacker, B. E., Williams, Y., Zaki, M. S., Gleeson, J. G., 2011. Defective Wnt-dependent cerebellar midline fusion in a mouse model of Joubert syndrome. Nat Med. 17**,** 726-31.

Lancaster, M. A., Louie, C. M., Silhavy, J. L., Sintasath, L., Decambre, M., Nigam, S. K., Willert, K., Gleeson, J. G., 2009. Impaired Wnt-beta-catenin signaling disrupts adult renal homeostasis and leads to cystic kidney ciliopathy. Nat Med. 15**,** 1046-54.

Lechtreck, K. F., Delmotte, P., Robinson, M. L., Sanderson, M. J., Witman, G. B., 2008. Mutations in Hydin impair ciliary motility in mice. J Cell Biol. 180**,** 633-43.

Lechtreck, K. F., Geimer, S., 2000. Distribution of polyglutamylated tubulin in the flagellar apparatus of green flagellates. Cell Motil Cytoskeleton. 47**,** 219-35.

LeDizet, M., Piperno, G., 1991. Detection of acetylated alpha-tubulin by specific antibodies. Methods Enzymol. 196**,** 264-74.

Lee, E., Sivan-Loukianova, E., Eberl, D. F., Kernan, M. J., 2008. An IFT-A protein is required to delimit functionally distinct zones in mechanosensory cilia. Curr Biol. 18**,** 1899-906.

Lee, J. D., Migeotte, I., Anderson, K. V., 2010. Left-right patterning in the mouse requires Epb4.1l5-dependent morphogenesis of the node and midline. Dev Biol. 346**,** 237-46.

Leitch, C. C., Zaghloul, N. A., Davis, E. E., Stoetzel, C., Diaz-Font, A., Rix, S., Alfadhel, M., Lewis, R. A., Eyaid, W., Banin, E., Dollfus, H., Beales, P. L., Badano, J. L., Katsanis, N., 2008. Hypomorphic mutations in syndromic encephalocele genes are associated with Bardet-Biedl syndrome. Nat Genet. 40**,** 443-8.

Lemullois, M., Klotz, C., Sandoz, D., 1987. Immunocytochemical localization of myosin during ciliogenesis of quail oviduct. Eur J Cell Biol. 43**,** 429-37.

Li, J. B., Gerdes, J. M., Haycraft, C. J., Fan, Y., Teslovich, T. M., May-Simera, H., Li, H., Blacque, O. E., Li, L., Leitch, C. C., Lewis, R. A., Green, J. S., Parfrey, P. S., Leroux, M. R., Davidson, W. S., Beales, P. L., Guay-Woodford, L. M., Yoder, B. K., Stormo, G. D., Katsanis, N., Dutcher, S. K., 2004. Comparative genomics identifies a flagellar and basal body proteome that includes the BBS5 human disease gene. Cell. 117**,** 541-52.

Li, L., Chin, L. S., 2003. The molecular machinery of synaptic vesicle exocytosis. Cell Mol Life Sci. 60**,** 942-60.

Li, T., Snyder, W. K., Olsson, J. E., Dryja, T. P., 1996. Transgenic mice carrying the dominant rhodopsin mutation P347S: evidence for defective vectorial transport of rhodopsin to the outer segments. Proc Natl Acad Sci U S A. 93**,** 14176-81.

Liang, Y., Gao, H., Lin, S. Y., Peng, G., Huang, X., Zhang, P., Goss, J. A., Brunicardi, F. C., Multani, A. S., Chang, S., Li, K., 2010. BRIT1/MCPH1 is essential for mitotic and meiotic recombination DNA repair and maintaining genomic stability in mice. PLoS Genet. 6**,** e1000826.

Liem, K. F., Jr., He, M., Ocbina, P. J., Anderson, K. V., 2009. Mouse Kif7/Costal2 is a cilia-associated protein that regulates Sonic hedgehog signaling. Proc Natl Acad Sci U S A. 106**,** 13377-82.

Lim, L., Zhou, H., Costa, R. H., 1997. The winged helix transcription factor HFH-4 is expressed during choroid plexus epithelial development in the mouse embryo. Proc Natl Acad Sci U S A. 94**,** 3094-9.

Lindemann, C. B., 1996. Functional significance of the outer dense fibers of mammalian sperm examined by computer simulations with the geometric clutch model. Cell Motil Cytoskeleton. 34**,** 258-70.

Litingtung, Y., Chiang, C., 2000. Specification of ventral neuron types is mediated by an antagonistic interaction between Shh and Gli3. Nat Neurosci. 3**,** 979-85.

Liu, A., Wang, B., Niswander, L. A., 2005. Mouse intraflagellar transport proteins regulate both the activator and repressor functions of Gli transcription factors. Development. 132**,** 3103-11.

Liu, Q., Tan, G., Levenkova, N., Li, T., Pugh, E. N., Jr., Rux, J. J., Speicher, D. W., Pierce, E. A., 2007. The proteome of the mouse photoreceptor sensory cilium complex. Mol Cell Proteomics. 6**,** 1299-317.

Loktev, A. V., Zhang, Q., Beck, J. S., Searby, C. C., Scheetz, T. E., Bazan, J. F., Slusarski, D. C., Sheffield, V. C., Jackson, P. K., Nachury, M. V., 2008. A BBSome subunit links ciliogenesis, microtubule stability, and acetylation. Dev Cell. 15**,** 854-65.

Lord, C. J., Ashworth, A., 2012. The DNA damage response and cancer therapy. Nature. 481**,** 287-94.

Ma, L., Jarman, A. P., 2011. Dilatory is a Drosophila protein related to AZI1 (CEP131) that is located at the ciliary base and required for cilium formation. J Cell Sci. 124**,** 2622-30.

Mah, L. J., El-Osta, A., Karagiannis, T. C., 2010. gammaH2AX: a sensitive molecular marker of DNA damage and repair. Leukemia. 24**,** 679-86.

Marion, V., Stoetzel, C., Schlicht, D., Messaddeq, N., Koch, M., Flori, E., Danse, J. M., Mandel, J. L., Dollfus, H., 2009. Transient ciliogenesis involving Bardet-Biedl syndrome proteins is a fundamental characteristic of adipogenic differentiation. Proc Natl Acad Sci U S A. 106**,** 1820-5.

Marose, T. D., Merkel, C. E., McMahon, A. P., Carroll, T. J., 2008. Beta-catenin is necessary to keep cells of ureteric bud/Wolffian duct epithelium in a precursor state. Dev Biol. 314**,** 112-26.

Marshall, W. F., Rosenbaum, J. L., 2001. Intraflagellar transport balances continuous turnover of outer doublet microtubules: implications for flagellar length control. J Cell Biol. 155**,** 405-14.

Marszalek, J. R., Ruiz-Lozano, P., Roberts, E., Chien, K. R., Goldstein, L. S., 1999. Situs inversus and embryonic ciliary morphogenesis defects in mouse mutants lacking the KIF3A subunit of kinesin-II. Proc Natl Acad Sci U S A. 96**,** 5043-8.

Maruta, H., Greer, K., Rosenbaum, J. L., 1986. The acetylation of alpha-tubulin and its relationship to the assembly and disassembly of microtubules. J Cell Biol. 103**,** 571-9.

May, S. R., Ashique, A. M., Karlen, M., Wang, B., Shen, Y., Zarbalis, K., Reiter, J., Ericson, J., Peterson, A. S., 2005. Loss of the retrograde motor for IFT disrupts localization of Smo to cilia and prevents the expression of both activator and repressor functions of Gli. Dev Biol. 287**,** 378-89.

Mayer, U., Ungerer, N., Klimmeck, D., Warnken, U., Schnolzer, M., Frings, S., Mohrlen, F., 2008. Proteomic analysis of a membrane preparation from rat olfactory sensory cilia. Chem Senses. 33**,** 145-62.

Mazelova, J., Astuto-Gribble, L., Inoue, H., Tam, B. M., Schonteich, E., Prekeris, R., Moritz, O. L., Randazzo, P. A., Deretic, D., 2009a. Ciliary targeting motif VxPx directs assembly of a trafficking module through Arf4. EMBO J. 28**,** 183-92.

Mazelova, J., Ransom, N., Astuto-Gribble, L., Wilson, M. C., Deretic, D., 2009b. Syntaxin 3 and SNAP-25 pairing, regulated by omega-3 docosahexaenoic acid, controls the delivery of rhodopsin for the biogenesis of cilia-derived sensory organelles, the rod outer segments. J Cell Sci. 122**,** 2003-13.

Mazet, F., Yu, J. K., Liberles, D. A., Holland, L. Z., Shimeld, S. M., 2003. Phylogenetic relationships of the Fox (Forkhead) gene family in the Bilateria. Gene. 316**,** 79-89.

McClintock, T. S., Glasser, C. E., Bose, S. C., Bergman, D. A., 2008. Tissue expression patterns identify mouse cilia genes. Physiol Genomics. 32**,** 198-206.

McGrath, J., Somlo, S., Makova, S., Tian, X., Brueckner, M., 2003. Two populations of node monocilia initiate left-right asymmetry in the mouse. Cell. 114**,** 61-73.

Meder, D., Shevchenko, A., Simons, K., Fullekrug, J., 2005. Gp135/podocalyxin and NHERF-2 participate in the formation of a preapical domain during polarization of MDCK cells. J Cell Biol. 168**,** 303-13.

Merchant, M., Evangelista, M., Luoh, S. M., Frantz, G. D., Chalasani, S., Carano, R. A., van Hoy, M., Ramirez, J., Ogasawara, A. K., McFarland, L. M., Filvaroff, E. H., French, D. M., de Sauvage, F. J., 2005. Loss of the serine/threonine kinase fused results in postnatal growth defects and lethality due to progressive hydrocephalus. Mol Cell Biol. 25**,** 7054-68.

Merrill, A. E., Merriman, B., Farrington-Rock, C., Camacho, N., Sebald, E. T., Funari, V. A., Schibler, M. J., Firestein, M. H., Cohn, Z. A., Priore, M. A., Thompson, A. K., Rimoin, D. L., Nelson, S. F., Cohn, D. H., Krakow, D., 2009. Ciliary abnormalities due to defects in the retrograde transport protein DYNC2H1 in short-rib polydactyly syndrome. Am J Hum Genet. 84**,** 542-9.

Mikule, K., Delaval, B., Kaldis, P., Jurcyzk, A., Hergert, P., Doxsey, S., 2007. Loss of centrosome integrity induces p38-p53-p21-dependent G1-S arrest. Nat Cell Biol. 9**,** 160-70.

Milenkovic, L., Scott, M. P., Rohatgi, R., 2009. Lateral transport of Smoothened from the plasma membrane to the membrane of the cilium. J Cell Biol. 187**,** 365-74.

Mill, P., Lockhart, P. J., Fitzpatrick, E., Mountford, H. S., Hall, E. A., Reijns, M. A., Keighren, M., Bahlo, M., Bromhead, C. J., Budd, P., Aftimos, S., Delatycki, M. B., Savarirayan, R., Jackson, I. J., Amor, D. J., 2011. Human and mouse mutations in WDR35 cause short-rib polydactyly syndromes due to abnormal ciliogenesis. Am J Hum Genet. 88**,** 508-15.

Miyata, M., Ogita, H., Komura, H., Nakata, S., Okamoto, R., Ozaki, M., Majima, T., Matsuzawa, N., Kawano, S., Minami, A., Waseda, M., Fujita, N., Mizutani, K., Rikitake, Y., Takai, Y., 2009. Localization of nectin-free afadin at the leading edge and its involvement in directional cell movement induced by platelet-derived growth factor. J Cell Sci. 122**,** 4319-29.

Mohr, S., Bakal, C., Perrimon, N., 2010. Genomic screening with RNAi: results and challenges. Annu Rev Biochem. 79**,** 37-64.

Molla-Herman, A., Ghossoub, R., Blisnick, T., Meunier, A., Serres, C., Silbermann, F., Emmerson, C., Romeo, K., Bourdoncle, P., Schmitt, A., Saunier, S., Spassky, N., Bastin, P., Benmerah, A., 2010. The ciliary pocket: an endocytic membrane domain at the base of primary and motile cilia. J Cell Sci. 123**,** 1785-95.

Mollet, G., Silbermann, F., Delous, M., Salomon, R., Antignac, C., Saunier, S., 2005. Characterization of the nephrocystin/nephrocystin-4 complex and subcellular localization of nephrocystin-4 to primary cilia and centrosomes. Hum Mol Genet. 14**,** 645-56.

Mori, Y., Akedo, H., Tanigaki, Y., Tanaka, K., Okada, M., 1979. Ciliogenesis in tissue-cultured cells by the increased density of cell population. Exp Cell Res. 120**,** 435-9.

Moritz, M., Braunfeld, M. B., Guenebaut, V., Heuser, J., Agard, D. A., 2000. Structure of the gamma-tubulin ring complex: a template for microtubule nucleation. Nat Cell Biol. 2**,** 365-70.

Moritz, M., Braunfeld, M. B., Sedat, J. W., Alberts, B., Agard, D. A., 1995. Microtubule nucleation by gamma-tubulin-containing rings in the centrosome. Nature. 378**,** 638-40.

Moritz, O. L., Tam, B. M., Hurd, L. L., Peranen, J., Deretic, D., Papermaster, D. S., 2001. Mutant rab8 Impairs docking and fusion of rhodopsin-bearing post-Golgi membranes and causes cell death of transgenic Xenopus rods. Mol Biol Cell. 12**,** 2341-51.

Moser, J. J., Fritzler, M. J., Ou, Y., Rattner, J. B., 2010. The PCM-basal body/primary cilium coalition. Semin Cell Dev Biol. 21**,** 148-55.

Mukhopadhyay, S., Lu, Y., Qin, H., Lanjuin, A., Shaham, S., Sengupta, P., 2007. Distinct IFT mechanisms contribute to the generation of ciliary structural diversity in C. elegans. EMBO J. 26**,** 2966-80.

Mukhopadhyay, S., Wen, X., Chih, B., Nelson, C. D., Lane, W. S., Scales, S. J., Jackson, P. K., 2010. TULP3 bridges the IFT-A complex and membrane phosphoinositides to promote trafficking of G protein-coupled receptors into primary cilia. Genes Dev. 24**,** 2180-93.

Murcia, N. S., Richards, W. G., Yoder, B. K., Mucenski, M. L., Dunlap, J. R., Woychik, R. P., 2000. The Oak Ridge Polycystic Kidney (orpk) disease gene is required for left-right axis determination. Development. 127**,** 2347-55.

Mykytyn, K., Mullins, R. F., Andrews, M., Chiang, A. P., Swiderski, R. E., Yang, B., Braun, T., Casavant, T., Stone, E. M., Sheffield, V. C., 2004. Bardet-Biedl syndrome type 4 (BBS4)-null mice implicate Bbs4 in flagella formation but not global cilia assembly. Proc Natl Acad Sci U S A. 101**,** 8664-9.

Nachury, M. V., Loktev, A. V., Zhang, Q., Westlake, C. J., Peranen, J., Merdes, A., Slusarski, D. C., Scheller, R. H., Bazan, J. F., Sheffield, V. C., Jackson, P. K., 2007. A core complex of BBS proteins cooperates with the GTPase Rab8 to promote ciliary membrane biogenesis. Cell. 129**,** 1201-13.

Nachury, M. V., Seeley, E. S., Jin, H., 2010. Trafficking to the ciliary membrane: how to get across the periciliary diffusion barrier? Annu Rev Cell Dev Biol. 26**,** 59-87.

Nair, K. S., Hanson, S. M., Mendez, A., Gurevich, E. V., Kennedy, M. J., Shestopalov, V. I., Vishnivetskiy, S. A., Chen, J., Hurley, J. B., Gurevich, V. V., Slepak, V. Z., 2005. Light-dependent redistribution of arrestin in vertebrate rods is an energy-independent process governed by protein-protein interactions. Neuron. 46**,** 555-67.

Nakanishi, A., Han, X., Saito, H., Taguchi, K., Ohta, Y., Imajoh-Ohmi, S., Miki, Y., 2007. Interference with BRCA2, which localizes to the centrosome during S and early M phase, leads to abnormal nuclear division. Biochem Biophys Res Commun. 355**,** 34-40.

Nauli, S. M., Alenghat, F. J., Luo, Y., Williams, E., Vassilev, P., Li, X., Elia, A. E., Lu, W., Brown, E. M., Quinn, S. J., Ingber, D. E., Zhou, J., 2003. Polycystins 1 and 2 mediate mechanosensation in the primary cilium of kidney cells. Nat Genet. 33**,** 129-37.

Neesse, A., Gangeswaran, R., Luettges, J., Feakins, R., Weeks, M. E., Lemoine, N. R., Crnogorac-Jurcevic, T., 2007. Sperm-associated antigen 1 is expressed early in pancreatic tumorigenesis and promotes motility of cancer cells. Oncogene. 26**,** 1533-45.

Nigg, E. A., Stearns, T., 2011. The centrosome cycle: Centriole biogenesis, duplication and inherent asymmetries. Nat Cell Biol. 13**,** 1154-60.

Nishimura, D. Y., Fath, M., Mullins, R. F., Searby, C., Andrews, M., Davis, R., Andorf, J. L., Mykytyn, K., Swiderski, R. E., Yang, B., Carmi, R., Stone, E. M., Sheffield, V. C., 2004. Bbs2-null mice have neurosensory deficits, a defect in social dominance, and retinopathy associated with mislocalization of rhodopsin. Proc Natl Acad Sci U S A. 101**,** 16588-93.

Nishio, S., Tian, X., Gallagher, A. R., Yu, Z., Patel, V., Igarashi, P., Somlo, S., 2010. Loss of oriented cell division does not initiate cyst formation. J Am Soc Nephrol. 21**,** 295-302.

Nonaka, S., Tanaka, Y., Okada, Y., Takeda, S., Harada, A., Kanai, Y., Kido, M., Hirokawa, N., 1998. Randomization of left-right asymmetry due to loss of nodal cilia generating leftward flow of extraembryonic fluid in mice lacking KIF3B motor protein. Cell. 95**,** 829-37.

Oakberg, E. F., 1956. A description of spermiogenesis in the mouse and its use in analysis of the cycle of the seminiferous epithelium and germ cell renewal. Am J Anat. 99**,** 391-413.

Ocbina, P. J., Eggenschwiler, J. T., Moskowitz, I., Anderson, K. V., 2011. Complex interactions between genes controlling trafficking in primary cilia. Nat Genet. 43**,** 547-53.

Ocbina, P. J., Tuson, M., Anderson, K. V., 2009. Primary cilia are not required for normal canonical Wnt signaling in the mouse embryo. PLoS One. 4**,** e6839.

Ohlmeyer, J. T., Kalderon, D., 1998. Hedgehog stimulates maturation of Cubitus interruptus into a labile transcriptional activator. Nature. 396**,** 749-53.

Oishi, I., Kawakami, Y., Raya, A., Callol-Massot, C., Izpisua Belmonte, J. C., 2006. Regulation of primary cilia formation and left-right patterning in zebrafish by a noncanonical Wnt signaling mediator, duboraya. Nat Genet. 38**,** 1316-22.

Okada, Y., Nonaka, S., Tanaka, Y., Saijoh, Y., Hamada, H., Hirokawa, N., 1999. Abnormal nodal flow precedes situs inversus in iv and inv mice. Mol Cell. 4**,** 459-68.

Okada, Y., Takeda, S., Tanaka, Y., Izpisua Belmonte, J. C., Hirokawa, N., 2005. Mechanism of nodal flow: a conserved symmetry breaking event in left-right axis determination. Cell. 121**,** 633-44.

Olsen, J. V., Blagoev, B., Gnad, F., Macek, B., Kumar, C., Mortensen, P., Mann, M., 2006. Global, in vivo, and site-specific phosphorylation dynamics in signaling networks. Cell. 127**,** 635-48.

Orozco, J. T., Wedaman, K. P., Signor, D., Brown, H., Rose, L., Scholey, J. M., 1999. Movement of motor and cargo along cilia. Nature. 398**,** 674.

Ostrowski, L. E., Blackburn, K., Radde, K. M., Moyer, M. B., Schlatzer, D. M., Moseley, A., Boucher, R. C., 2002. A proteomic analysis of human cilia: identification of novel components. Mol Cell Proteomics. 1**,** 451-65.

Ostrowski, L. E., Yin, W., Rogers, T. D., Busalacchi, K. B., Chua, M., O'Neal, W. K., Grubb, B. R., 2010. Conditional deletion of dnaic1 in a murine model of primary ciliary dyskinesia causes chronic rhinosinusitis. Am J Respir Cell Mol Biol. 43**,** 55-63.

Otto, E. A., Hurd, T. W., Airik, R., Chaki, M., Zhou, W., Stoetzel, C., Patil, S. B., Levy, S., Ghosh, A. K., Murga-Zamalloa, C. A., van Reeuwijk, J., Letteboer, S. J., Sang, L., Giles, R. H., Liu, Q., Coene, K. L., Estrada-Cuzcano, A., Collin, R. W., McLaughlin, H. M., Held, S., Kasanuki, J. M., Ramaswami, G., Conte, J., Lopez, I., Washburn, J., Macdonald, J., Hu, J., Yamashita, Y., Maher, E. R., Guay-Woodford, L. M., Neumann, H. P., Obermuller, N., Koenekoop, R. K., Bergmann, C., Bei, X., Lewis, R. A., Katsanis, N., Lopes, V., Williams, D. S., Lyons, R. H., Dang, C. V., Brito, D. A., Dias, M. B., Zhang, X., Cavalcoli, J. D., Nurnberg, G., Nurnberg, P., Pierce, E. A., Jackson, P. K., Antignac, C., Saunier, S., Roepman, R., Dollfus, H., Khanna, H., Hildebrandt, F., 2010. Candidate exome capture identifies mutation of SDCCAG8 as the cause of a retinal-renal ciliopathy. Nat Genet. 42**,** 840-50.

Otto, E. A., Schermer, B., Obara, T., O'Toole, J. F., Hiller, K. S., Mueller, A. M., Ruf, R. G., Hoefele, J., Beekmann, F., Landau, D., Foreman, J. W., Goodship, J. A., Strachan, T., Kispert, A., Wolf, M. T., Gagnadoux, M. F., Nivet, H., Antignac, C., Walz, G., Drummond, I. A., Benzing, T., Hildebrandt, F., 2003. Mutations in INVS encoding inversin cause nephronophthisis type 2, linking renal cystic disease to the function of primary cilia and left-right axis determination. Nat Genet. 34**,** 413-20.

Ou, G., Blacque, O. E., Snow, J. J., Leroux, M. R., Scholey, J. M., 2005. Functional coordination of intraflagellar transport motors. Nature. 436**,** 583-7.

Paintrand, M., Moudjou, M., Delacroix, H., Bornens, M., 1992. Centrosome organization and centriole architecture: their sensitivity to divalent cations. J Struct Biol. 108**,** 107-28.

Pan, X., Ou, G., Civelekoglu-Scholey, G., Blacque, O. E., Endres, N. F., Tao, L., Mogilner, A., Leroux, M. R., Vale, R. D., Scholey, J. M., 2006. Mechanism of transport of IFT particles in C. elegans cilia by the concerted action of kinesin-II and OSM-3 motors. J Cell Biol. 174**,** 1035-45.

Papermaster, D. S., Schneider, B. G., Besharse, J. C., 1985. Vesicular transport of newly synthesized opsin from the Golgi apparatus toward the rod outer segment. Ultrastructural immunocytochemical and autoradiographic evidence in Xenopus retinas. Invest Ophthalmol Vis Sci. 26**,** 1386-404.

Park, T. J., Haigo, S. L., Wallingford, J. B., 2006. Ciliogenesis defects in embryos lacking inturned or fuzzy function are associated with failure of planar cell polarity and Hedgehog signaling. Nat Genet. 38**,** 303-11.

Park, T. J., Mitchell, B. J., Abitua, P. B., Kintner, C., Wallingford, J. B., 2008. Dishevelled controls apical docking and planar polarization of basal bodies in ciliated epithelial cells. Nat Genet. 40**,** 871-9.

Pathak, N., Austin, C. A., Drummond, I. A., 2011. Tubulin tyrosine ligase-like genes ttll3 and ttll6 maintain zebrafish cilia structure and motility. J Biol Chem. 286**,** 11685-95.

Pathak, N., Obara, T., Mangos, S., Liu, Y., Drummond, I. A., 2007. The zebrafish fleer gene encodes an essential regulator of cilia tubulin polyglutamylation. Mol Biol Cell. 18**,** 4353-64.

Pazour, G. J., Agrin, N., Leszyk, J., Witman, G. B., 2005. Proteomic analysis of a eukaryotic cilium. J Cell Biol. 170**,** 103-13.

Pazour, G. J., Dickert, B. L., Vucica, Y., Seeley, E. S., Rosenbaum, J. L., Witman, G. B., Cole, D. G., 2000. Chlamydomonas IFT88 and its mouse homologue, polycystic kidney disease gene tg737, are required for assembly of cilia and flagella. J Cell Biol. 151**,** 709-18.

Pazour, G. J., Dickert, B. L., Witman, G. B., 1999. The DHC1b (DHC2) isoform of cytoplasmic dynein is required for flagellar assembly. J Cell Biol. 144**,** 473-81.

Pazour, G. J., San Agustin, J. T., Follit, J. A., Rosenbaum, J. L., Witman, G. B., 2002. Polycystin-2 localizes to kidney cilia and the ciliary level is elevated in orpk mice with polycystic kidney disease. Curr Biol. 12**,** R378-80.

Pazour, G. J., Wilkerson, C. G., Witman, G. B., 1998. A dynein light chain is essential for the retrograde particle movement of intraflagellar transport (IFT). J Cell Biol. 141**,** 979-92.

Pechart, I., Kann, M. L., Levilliers, N., Bre, M. H., Fouquet, J. P., 1999. Composition and organization of tubulin isoforms reveals a variety of axonemal models. Biol Cell. 91**,** 685-97.

Pennekamp, P., Karcher, C., Fischer, A., Schweickert, A., Skryabin, B., Horst, J., Blum, M., Dworniczak, B., 2002. The ion channel polycystin-2 is required for left-right axis determination in mice. Curr Biol. 12**,** 938-43.

Phillips, C. L., Miller, K. J., Filson, A. J., Nurnberger, J., Clendenon, J. L., Cook, G. W., Dunn, K. W., Overbeek, P. A., Gattone, V. H., 2nd, Bacallao, R. L., 2004. Renal cysts of inv/inv mice resemble early infantile nephronophthisis. J Am Soc Nephrol. 15**,** 1744-55.

Phirke, P., Efimenko, E., Mohan, S., Burghoorn, J., Crona, F., Bakhoum, M. W., Trieb, M., Schuske, K., Jorgensen, E. M., Piasecki, B. P., Leroux, M. R., Swoboda, P., 2011. Transcriptional profiling of C. elegans DAF-19 uncovers a ciliary base-associated protein and a CDK/CCRK/LF2p-related kinase required for intraflagellar transport. Dev Biol. 357**,** 235-47.

Piao, T., Luo, M., Wang, L., Guo, Y., Li, D., Li, P., Snell, W. J., Pan, J., 2009. A microtubule depolymerizing kinesin functions during both flagellar disassembly and flagellar assembly in Chlamydomonas. Proc Natl Acad Sci U S A. 106**,** 4713-8.

Pigino, G., Geimer, S., Lanzavecchia, S., Paccagnini, E., Cantele, F., Diener, D. R., Rosenbaum, J. L., Lupetti, P., 2009. Electron-tomographic analysis of intraflagellar transport particle trains in situ. J Cell Biol. 187**,** 135-48.

Pinson, K. I., Brennan, J., Monkley, S., Avery, B. J., Skarnes, W. C., 2000. An LDL-receptor-related protein mediates Wnt signalling in mice. Nature. 407**,** 535-8.

Piperno, G., Siuda, E., Henderson, S., Segil, M., Vaananen, H., Sassaroli, M., 1998. Distinct mutants of retrograde intraflagellar transport (IFT) share similar morphological and molecular defects. J Cell Biol. 143**,** 1591-601.

Poole, C. A., Zhang, Z. J., Ross, J. M., 2001. The differential distribution of acetylated and detyrosinated alpha-tubulin in the microtubular cytoskeleton and primary cilia of hyaline cartilage chondrocytes. J Anat. 199**,** 393-405.

Porter, M. E., Bower, R., Knott, J. A., Byrd, P., Dentler, W., 1999. Cytoplasmic dynein heavy chain 1b is required for flagellar assembly in Chlamydomonas. Mol Biol Cell. 10**,** 693-712.

Praetorius, H. A., Spring, K. R., 2001. Bending the MDCK cell primary cilium increases intracellular calcium. J Membr Biol. 184**,** 71-9.

Praetorius, H. A., Spring, K. R., 2003. Removal of the MDCK cell primary cilium abolishes flow sensing. J Membr Biol. 191**,** 69-76.

Pugacheva, E. N., Golemis, E. A., 2005. The focal adhesion scaffolding protein HEF1 regulates activation of the Aurora-A and Nek2 kinases at the centrosome. Nat Cell Biol. 7**,** 937-46.

Pugacheva, E. N., Jablonski, S. A., Hartman, T. R., Henske, E. P., Golemis, E. A., 2007. HEF1-dependent Aurora A activation induces disassembly of the primary cilium. Cell. 129**,** 1351-63.

Pulvers, J. N., Bryk, J., Fish, J. L., Wilsch-Brauninger, M., Arai, Y., Schreier, D., Naumann, R., Helppi, J., Habermann, B., Vogt, J., Nitsch, R., Toth, A., Enard, W., Paabo, S., Huttner, W. B., 2010. Mutations in mouse Aspm (abnormal spindle-like microcephaly associated) cause not only microcephaly but also major defects in the germline. Proc Natl Acad Sci U S A. 107**,** 16595-600.

Qian, C. N., Knol, J., Igarashi, P., Lin, F., Zylstra, U., Teh, B. T., Williams, B. O., 2005. Cystic renal neoplasia following conditional inactivation of apc in mouse renal tubular epithelium. J Biol Chem. 280**,** 3938-45.

Qian, F., Germino, F. J., Cai, Y., Zhang, X., Somlo, S., Germino, G. G., 1997. PKD1 interacts with PKD2 through a probable coiled-coil domain. Nat Genet. 16**,** 179-83.

Qin, H., Burnette, D. T., Bae, Y. K., Forscher, P., Barr, M. M., Rosenbaum, J. L., 2005. Intraflagellar transport is required for the vectorial movement of TRPV channels in the ciliary membrane. Curr Biol. 15**,** 1695-9.

Qin, H., Diener, D. R., Geimer, S., Cole, D. G., Rosenbaum, J. L., 2004. Intraflagellar transport (IFT) cargo: IFT transports flagellar precursors to the tip and turnover products to the cell body. J Cell Biol. 164**,** 255-66.

Qin, H., Wang, Z., Diener, D., Rosenbaum, J., 2007. Intraflagellar transport protein 27 is a small G protein involved in cell-cycle control. Curr Biol. 17**,** 193-202.

Qin, J., Lin, Y., Norman, R. X., Ko, H. W., Eggenschwiler, J. T., 2011. Intraflagellar transport protein 122 antagonizes Sonic Hedgehog signaling and controls ciliary localization of pathway components. Proc Natl Acad Sci U S A. 108**,** 1456-61.

Rana, A. A., Barbera, J. P., Rodriguez, T. A., Lynch, D., Hirst, E., Smith, J. C., Beddington, R. S., 2004. Targeted deletion of the novel cytoplasmic dynein mD2LIC disrupts the embryonic organiser, formation of the body axes and specification of ventral cell fates. Development. 131**,** 4999-5007.

Randall, J., Warr, J. R., Hopkins, J. M., McVittie, A., 1964. A Single-Gene Mutation of Chlamydomonas Reinhardii Affecting Motility: A Genetic and Electron Microscope Study. Nature. 203**,** 912-4.

Reinholdt, L., Ashley, T., Schimenti, J., Shima, N., 2004. Forward genetic screens for meiotic and mitotic recombination-defective mutants in mice. Methods Mol Biol. 262**,** 87-107.

Rieder, C. L., Jensen, C. G., Jensen, L. C., 1979. The resorption of primary cilia during mitosis in a vertebrate (PtK1) cell line. J Ultrastruct Res. 68**,** 173-85.

Rink, J. C., Gurley, K. A., Elliott, S. A., Sanchez Alvarado, A., 2009. Planarian Hh signaling regulates regeneration polarity and links Hh pathway evolution to cilia. Science. 326**,** 1406-10.

Robbins, D. J., Nybakken, K. E., Kobayashi, R., Sisson, J. C., Bishop, J. M., Therond, P. P., 1997. Hedgehog elicits signal transduction by means of a large complex containing the kinesin-related protein costal2. Cell. 90**,** 225-34.

Robert, A., Margall-Ducos, G., Guidotti, J. E., Bregerie, O., Celati, C., Brechot, C., Desdouets, C., 2007. The intraflagellar transport component IFT88/polaris is a centrosomal protein regulating G1-S transition in non-ciliated cells. J Cell Sci. 120**,** 628-37.

Rogers, K. K., Wilson, P. D., Snyder, R. W., Zhang, X., Guo, W., Burrow, C. R., Lipschutz, J. H., 2004. The exocyst localizes to the primary cilium in MDCK cells. Biochem Biophys Res Commun. 319**,** 138-43.

Rohatgi, R., Milenkovic, L., Scott, M. P., 2007. Patched1 regulates hedgehog signaling at the primary cilium. Science. 317**,** 372-6.

Rosenbaum, J. L., Moulder, J. E., Ringo, D. L., 1969. Flagellar elongation and shortening in Chlamydomonas. The use of cycloheximide and colchicine to study the synthesis and assembly of flagellar proteins. J Cell Biol. 41**,** 600-19.

Rosenbaum, J. L., Witman, G. B., 2002. Intraflagellar transport. Nat Rev Mol Cell Biol. 3**,** 813-25.

Ross, A. J., May-Simera, H., Eichers, E. R., Kai, M., Hill, J., Jagger, D. J., Leitch, C. C., Chapple, J. P., Munro, P. M., Fisher, S., Tan, P. L., Phillips, H. M., Leroux, M. R., Henderson, D. J., Murdoch, J. N., Copp, A. J., Eliot, M. M., Lupski, J. R., Kemp, D. T., Dollfus, H., Tada, M., Katsanis, N., Forge, A., Beales, P. L., 2005. Disruption of Bardet-Biedl syndrome ciliary proteins perturbs planar cell polarity in vertebrates. Nat Genet. 37**,** 1135-40.

Ruiz-Perez, V. L., Blair, H. J., Rodriguez-Andres, M. E., Blanco, M. J., Wilson, A., Liu, Y. N., Miles, C., Peters, H., Goodship, J. A., 2007. Evc is a positive mediator of Ihh-regulated bone growth that localises at the base of chondrocyte cilia. Development. 134**,** 2903-12.

Ruiz i Altaba, A., Palma, V., Dahmane, N., 2002. Hedgehog-Gli signalling and the growth of the brain. Nat Rev Neurosci. 3**,** 24-33.

Saadi-Kheddouci, S., Berrebi, D., Romagnolo, B., Cluzeaud, F., Peuchmaur, M., Kahn, A., Vandewalle, A., Perret, C., 2001. Early development of polycystic kidney disease in transgenic mice expressing an activated mutant of the beta-catenin gene. Oncogene. 20**,** 5972-81.

Saarikangas, J., Barral, Y., 2011. The emerging functions of septins in metazoans. EMBO Rep. 12**,** 1118-26.

Saburi, S., Hester, I., Fischer, E., Pontoglio, M., Eremina, V., Gessler, M., Quaggin, S. E., Harrison, R., Mount, R., McNeill, H., 2008. Loss of Fat4 disrupts PCP signaling and oriented cell division and leads to cystic kidney disease. Nat Genet. 40**,** 1010-5.

Salisbury, J. L., 2003. Centrosomes: coiled-coils organize the cell center. Curr Biol. 13**,** R88-90.

Sang, L., Miller, J. J., Corbit, K. C., Giles, R. H., Brauer, M. J., Otto, E. A., Baye, L. M., Wen, X., Scales, S. J., Kwong, M., Huntzicker, E. G., Sfakianos, M. K., Sandoval, W., Bazan, J. F., Kulkarni, P., Garcia-Gonzalo, F. R., Seol, A. D., O'Toole, J. F., Held, S., Reutter, H. M., Lane, W. S., Rafiq, M. A., Noor, A., Ansar, M., Devi, A. R., Sheffield, V. C., Slusarski, D. C., Vincent, J. B., Doherty, D. A., Hildebrandt, F., Reiter, J. F., Jackson, P. K., 2011.

Mapping the NPHP-JBTS-MKS protein network reveals ciliopathy disease genes and pathways. Cell. 145**,** 513-28.

Sankaran, S., Parvin, J. D., 2006. Centrosome function in normal and tumor cells. J Cell Biochem. 99**,** 1240-50.

Sapiro, R., Kostetskii, I., Olds-Clarke, P., Gerton, G. L., Radice, G. L., Strauss, I. J., 2002. Male infertility, impaired sperm motility, and hydrocephalus in mice deficient in sperm-associated antigen 6. Mol Cell Biol. 22**,** 6298-305.

Sasaki, H., Hui, C., Nakafuku, M., Kondoh, H., 1997. A binding site for Gli proteins is essential for HNF-3beta floor plate enhancer activity in transgenics and can respond to Shh in vitro. Development. 124**,** 1313-22.

Sasaki, H., Nishizaki, Y., Hui, C., Nakafuku, M., Kondoh, H., 1999. Regulation of Gli2 and Gli3 activities by an amino-terminal repression domain: implication of Gli2 and Gli3 as primary mediators of Shh signaling. Development. 126**,** 3915-24.

Sato, T., Mushiake, S., Kato, Y., Sato, K., Sato, M., Takeda, N., Ozono, K., Miki, K., Kubo, Y., Tsuji, A., Harada, R., Harada, A., 2007. The Rab8 GTPase regulates apical protein localization in intestinal cells. Nature. 448**,** 366-9.

Schafer, S., Anschlag, J., Nettersheim, D., Haas, N., Pawig, L., Schorle, H., 2011. The role of BLIMP1 and its putative downstream target TFAP2C in germ cell development and germ cell tumours. Int J Androl. 34**,** e152-8; discussion e158-9.

Schmidt, T. I., Kleylein-Sohn, J., Westendorf, J., Le Clech, M., Lavoie, S. B., Stierhof, Y. D., Nigg, E. A., 2009. Control of centriole length by CPAP and CP110. Curr Biol. 19**,** 1005-11.

Schneider, L., Cammer, M., Lehman, J., Nielsen, S. K., Guerra, C. F., Veland, I. R., Stock, C., Hoffmann, E. K., Yoder, B. K., Schwab, A., Satir, P., Christensen, S. T., 2010. Directional cell migration and chemotaxis in wound healing response to PDGF-AA are coordinated by the primary cilium in fibroblasts. Cell Physiol Biochem. 25**,** 279-92.

Schneider, L., Clement, C. A., Teilmann, S. C., Pazour, G. J., Hoffmann, E. K., Satir, P., Christensen, S. T., 2005. PDGFRalphaalpha signaling is regulated through the primary cilium in fibroblasts. Curr Biol. 15**,** 1861-6.

Schrick, J. J., Vogel, P., Abuin, A., Hampton, B., Rice, D. S., 2006. ADP-ribosylation factor-like 3 is involved in kidney and photoreceptor development. Am J Pathol. 168**,** 1288-98.

Sedelnikova, O. A., Rogakou, E. P., Panyutin, I. G., Bonner, W. M., 2002. Quantitative detection of (125)IdU-induced DNA double-strand breaks with gamma-H2AX antibody. Radiat Res. 158**,** 486-92.

Sedmak, T., Wolfrum, U., 2010. Intraflagellar transport molecules in ciliary and nonciliary cells of the retina. J Cell Biol. 189**,** 171-86.

Shalom, O., Shalva, N., Altschuler, Y., Motro, B., 2008. The mammalian Nek1 kinase is involved in primary cilium formation. FEBS Lett. 582**,** 1465-70.

Shima, N., Hartford, S. A., Duffy, T., Wilson, L. A., Schimenti, K. J., Schimenti, J. C., 2003. Phenotype-based identification of mouse chromosome instability mutants. Genetics. 163**,** 1031-40.

Shimada, M., Komatsu, K., 2009. Emerging connection between centrosome and DNA repair machinery. J Radiat Res. 50**,** 295-301.

Signor, D., Wedaman, K. P., Orozco, J. T., Dwyer, N. D., Bargmann, C. I., Rose, L. S., Scholey, J. M., 1999. Role of a class DHC1b dynein in retrograde transport of IFT motors and IFT raft particles along cilia, but not dendrites, in chemosensory neurons of living Caenorhabditis elegans. J Cell Biol. 147**,** 519-30.

Silflow, C. D., Lefebvre, P. A., 2001. Assembly and motility of eukaryotic cilia and flagella. Lessons from Chlamydomonas reinhardtii. Plant Physiol. 127**,** 1500-7.

Silina, K., Zayakin, P., Kalnina, Z., Ivanova, L., Meistere, I., Endzelins, E., Abols, A., Stengrevics, A., Leja, M., Ducena, K., Kozirovskis, V., Line, A., 2011. Sperm-associated antigens as targets for cancer immunotherapy: expression pattern and humoral immune response in cancer patients. J Immunother. 34**,** 28-44.

Simons, M., Gloy, J., Ganner, A., Bullerkotte, A., Bashkurov, M., Kronig, C., Schermer, B., Benzing, T., Cabello, O. A., Jenny, A., Mlodzik, M., Polok, B., Driever, W., Obara, T., Walz, G., 2005. Inversin, the gene product mutated in nephronophthisis type II, functions as a molecular switch between Wnt signaling pathways. Nat Genet. 37**,** 537-43.

Singla, V., Reiter, J. F., 2006. The primary cilium as the cell's antenna: signaling at a sensory organelle. Science. 313**,** 629-33.

Sinha, S., Chen, J. K., 2006. Purmorphamine activates the Hedgehog pathway by targeting Smoothened. Nat Chem Biol. 2**,** 29-30.

Sisson, J. C., Ho, K. S., Suyama, K., Scott, M. P., 1997. Costal2, a novel kinesin-related protein in the Hedgehog signaling pathway. Cell. 90**,** 235-45.

Smith, J. C., Northey, J. G., Garg, J., Pearlman, R. E., Siu, K. W., 2005. Robust method for proteome analysis by MS/MS using an entire translated genome: demonstration on the ciliome of Tetrahymena thermophila. J Proteome Res. 4**,** 909-19.

Snow, J. J., Ou, G., Gunnarson, A. L., Walker, M. R., Zhou, H. M., Brust-Mascher, I., Scholey, J. M., 2004. Two anterograde intraflagellar transport motors cooperate to build sensory cilia on C. elegans neurons. Nat Cell Biol. 6**,** 1109-13.

Sokol, S. Y., 1996. Analysis of Dishevelled signalling pathways during Xenopus development. Curr Biol. 6**,** 1456-67.

Song, L., Dentler, W. L., 2001. Flagellar protein dynamics in Chlamydomonas. J Biol Chem. 276**,** 29754-63.

Soriano, P., 1997. The PDGF alpha receptor is required for neural crest cell development and for normal patterning of the somites. Development. 124**,** 2691-700.

Sorokin, S., 1962. Centrioles and the formation of rudimentary cilia by fibroblasts and smooth muscle cells. J Cell Biol. 15**,** 363-77.

Sorokin, S. P., 1968. Reconstructions of centriole formation and ciliogenesis in mammalian lungs. J Cell Sci. 3**,** 207-30.

Spektor, A., Tsang, W. Y., Khoo, D., Dynlacht, B. D., 2007. Cep97 and CP110 suppress a cilia assembly program. Cell. 130**,** 678-90.

Stamataki, D., Ulloa, F., Tsoni, S. V., Mynett, A., Briscoe, J., 2005. A gradient of Gli activity mediates graded Sonic Hedgehog signaling in the neural tube. Genes Dev. 19**,** 626-41.

Stephens, R. E., 1997. Synthesis and turnover of embryonic sea urchin ciliary proteins during selective inhibition of tubulin synthesis and assembly. Mol Biol Cell. 8**,** 2187-98.

Stewart, M., 2007. Molecular mechanism of the nuclear protein import cycle. Nat Rev Mol Cell Biol. 8**,** 195-208.

Stolc, V., Samanta, M. P., Tongprasit, W., Marshall, W. F., 2005. Genome-wide transcriptional analysis of flagellar regeneration in Chlamydomonas reinhardtii identifies orthologs of ciliary disease genes. Proc Natl Acad Sci U S A. 102**,** 3703-7.

Stubbs, J. L., Oishi, I., Izpisua Belmonte, J. C., Kintner, C., 2008. The forkhead protein Foxj1 specifies node-like cilia in Xenopus and zebrafish embryos. Nat Genet. 40**,** 1454-60.

Sun, Z., Amsterdam, A., Pazour, G. J., Cole, D. G., Miller, M. S., Hopkins, N., 2004. A genetic screen in zebrafish identifies cilia genes as a principal cause of cystic kidney. Development. 131**,** 4085-93.

Sung, C. H., Makino, C., Baylor, D., Nathans, J., 1994. A rhodopsin gene mutation responsible for autosomal dominant retinitis pigmentosa results in a protein that is defective in localization to the photoreceptor outer segment. J Neurosci. 14**,** 5818-33.

Swoboda, P., Adler, H. T., Thomas, J. H., 2000. The RFX-type transcription factor DAF-19 regulates sensory neuron cilium formation in C. elegans. Mol Cell. 5**,** 411-21.

Taipale, J., Chen, J. K., Cooper, M. K., Wang, B., Mann, R. K., Milenkovic, L., Scott, M. P., Beachy, P. A., 2000. Effects of oncogenic mutations in Smoothened and Patched can be reversed by cyclopamine. Nature. 406**,** 1005-9.

Takai, Y., Ikeda, W., Ogita, H., Rikitake, Y., 2008. The immunoglobulin-like cell adhesion molecule nectin and its associated protein afadin. Annu Rev Cell Dev Biol. 24**,** 309-42.

Takaishi, M., Huh, N., 1999. A tetratricopeptide repeat-containing protein gene, tpis, whose expression is induced with differentiation of spermatogenic cells. Biochem Biophys Res Commun. 264**,** 81-5.

Takeda, S., Yonekawa, Y., Tanaka, Y., Okada, Y., Nonaka, S., Hirokawa, N., 1999. Left-right asymmetry and kinesin superfamily protein KIF3A: new insights in determination of laterality and mesoderm induction by kif3A-/- mice analysis. J Cell Biol. 145**,** 825-36.

Tam, B. M., Moritz, O. L., Hurd, L. B., Papermaster, D. S., 2000. Identification of an outer segment targeting signal in the COOH terminus of rhodopsin using transgenic Xenopus laevis. J Cell Biol. 151**,** 1369-80.

Tanaka, H., Iguchi, N., Toyama, Y., Kitamura, K., Takahashi, T., Kaseda, K., Maekawa, M., Nishimune, Y., 2004. Mice deficient in the axonemal protein Tektin-t exhibit male infertility and immotile-cilium syndrome due to impaired inner arm dynein function. Mol Cell Biol. 24**,** 7958-64.

Tanaka, T., Huang, X., Halicka, H. D., Zhao, H., Traganos, F., Albino, A. P., Dai, W., Darzynkiewicz, Z., 2007. Cytometry of ATM activation and histone H2AX phosphorylation to estimate extent of DNA damage induced by exogenous agents. Cytometry A. 71**,** 648-61.

Tanaka, Y., Okada, Y., Hirokawa, N., 2005. FGF-induced vesicular release of Sonic hedgehog and retinoic acid in leftward nodal flow is critical for left-right determination. Nature. 435**,** 172-7.

Tang, C. J., Fu, R. H., Wu, K. S., Hsu, W. B., Tang, T. K., 2009. CPAP is a cell-cycle regulated protein that controls centriole length. Nat Cell Biol. 11**,** 825-31.

Tao, B., Bu, S., Yang, Z., Siroky, B., Kappes, J. C., Kispert, A., Guay-Woodford, L. M., 2009. Cystin localizes to primary cilia via membrane microdomains and a targeting motif. J Am Soc Nephrol. 20**,** 2570-80.

Tarnasky, H., Cheng, M., Ou, Y., Thundathil, J. C., Oko, R., van der Hoorn, F. A., 2010. Gene trap mutation of murine outer dense fiber protein-2 gene can result in sperm tail abnormalities in mice with high percentage chimaerism. BMC Dev Biol. 10**,** 67.

Tay, S. Y., Ingham, P. W., Roy, S., 2005. A homologue of the Drosophila kinesin-like protein Costal2 regulates Hedgehog signal transduction in the vertebrate embryo. Development. 132**,** 625-34.

Thomas, J., Morle, L., Soulavie, F., Laurencon, A., Sagnol, S., Durand, B., 2010. Transcriptional control of genes involved in ciliogenesis: a first step in making cilia. Biol Cell. 102**,** 499-513.

Tran, P. V., Haycraft, C. J., Besschetnova, T. Y., Turbe-Doan, A., Stottmann, R. W., Herron, B. J., Chesebro, A. L., Qiu, H., Scherz, P. J., Shah, J. V., Yoder, B. K., Beier, D. R., 2008. THM1 negatively modulates mouse sonic hedgehog signal transduction and affects retrograde intraflagellar transport in cilia. Nat Genet. 40**,** 403-10.

Tsang, W. Y., Bossard, C., Khanna, H., Peranen, J., Swaroop, A., Malhotra, V., Dynlacht, B. D., 2008. CP110 suppresses primary cilia formation through its interaction with CEP290, a protein deficient in human ciliary disease. Dev Cell. 15**,** 187-97.

Tsou, M. F., Stearns, T., 2006. Mechanism limiting centrosome duplication to once per cell cycle. Nature. 442**,** 947-51.

Tucker, R. W., Pardee, A. B., Fujiwara, K., 1979. Centriole ciliation is related to quiescence and DNA synthesis in 3T3 cells. Cell. 17**,** 527-35.

Tyler, K. M., Fridberg, A., Toriello, K. M., Olson, C. L., Cieslak, J. A., Hazlett, T. L., Engman, D. M., 2009. Flagellar membrane localization via association with lipid rafts. J Cell Sci. 122**,** 859-66.

Valente, E. M., Silhavy, J. L., Brancati, F., Barrano, G., Krishnaswami, S. R., Castori, M., Lancaster, M. A., Boltshauser, E., Boccone, L., Al-Gazali, L., Fazzi, E., Signorini, S., Louie, C. M., Bellacchio, E., International Joubert Syndrome Related Disorders Study, G., Bertini, E., Dallapiccola, B., Gleeson, J. G., 2006. Mutations in CEP290, which encodes a centrosomal protein, cause pleiotropic forms of Joubert syndrome. Nat Genet. 38**,** 623-5.

Vandenberg, L. N., Levin, M., 2010. Far from solved: a perspective on what we know about early mechanisms of left-right asymmetry. Dev Dyn. 239**,** 3131-46.

Varjosalo, M., Li, S. P., Taipale, J., 2006. Divergence of hedgehog signal transduction mechanism between Drosophila and mammals. Dev Cell. 10**,** 177-86.

Verhey, K. J., Gaertig, J., 2007. The tubulin code. Cell Cycle. 6**,** 2152-60.

Vieira, O. V., Gaus, K., Verkade, P., Fullekrug, J., Vaz, W. L., Simons, K., 2006. FAPP2, cilium formation, and compartmentalization of the apical membrane in polarized Madin-Darby canine kidney (MDCK) cells. Proc Natl Acad Sci U S A. 103**,** 18556-61.

Vogel, P., Read, R., Hansen, G., Freay, L., Zambrowicz, B., Sands, A., 2009. Situs inversus and related ciliopathies in Dpcd-/-, Pkd1l1-/- and Nme7-/- mice. Vet Pathol.

Voronina, V. A., Takemaru, K., Treuting, P., Love, D., Grubb, B. R., Hajjar, A. M., Adams, A., Li, F. Q., Moon, R. T., 2009. Inactivation of Chibby affects function of motile airway cilia. J Cell Biol. 185**,** 225-33.

Wallingford, J. B., Mitchell, B., 2011. Strange as it may seem: the many links between Wnt signaling, planar cell polarity, and cilia. Genes Dev. 25**,** 201-13.

Walther, Z., Vashishtha, M., Hall, J. L., 1994. The Chlamydomonas FLA10 gene encodes a novel kinesin-homologous protein. J Cell Biol. 126**,** 175-88.

Wang, B., Fallon, J. F., Beachy, P. A., 2000a. Hedgehog-regulated processing of Gli3 produces an anterior/posterior repressor gradient in the developing vertebrate limb. Cell. 100**,** 423-34.

Wang, G., Amanai, K., Wang, B., Jiang, J., 2000b. Interactions with Costal2 and suppressor of fused regulate nuclear translocation and activity of cubitus interruptus. Genes Dev. 14**,** 2893-905.

Wang, S. W., Kim, B. S., Ding, K., Wang, H., Sun, D., Johnson, R. L., Klein, W. H., Gan, L., 2001. Requirement for math5 in the development of retinal ganglion cells. Genes Dev. 15**,** 24-9.

Ward, H. H., Brown-Glaberman, U., Wang, J., Morita, Y., Alper, S. L., Bedrick, E. J., Gattone, V. H., 2nd, Deretic, D., Wandinger-Ness, A., 2011. A conserved signal and GTPase complex are required for the ciliary transport of polycystin-1. Mol Biol Cell. 22**,** 3289-305.

Ward, I. M., Chen, J., 2001. Histone H2AX is phosphorylated in an ATR-dependent manner in response to replicational stress. J Biol Chem. 276**,** 47759-62.

Watanabe, D., Saijoh, Y., Nonaka, S., Sasaki, G., Ikawa, Y., Yokoyama, T., Hamada, H., 2003. The left-right determinant Inversin is a component of node monocilia and other 9+0 cilia. Development. 130**,** 1725-34.

Weatherbee, S. D., Niswander, L. A., Anderson, K. V., 2009. A mouse model for Meckel syndrome reveals Mks1 is required for ciliogenesis and Hedgehog signaling. Hum Mol Genet. 18**,** 4565-75.

Webster, D. R., Wehland, J., Weber, K., Borisy, G. G., 1990. Detyrosination of alpha tubulin does not stabilize microtubules in vivo. J Cell Biol. 111**,** 113-22.

Wen, X., Lai, C. K., Evangelista, M., Hongo, J. A., de Sauvage, F. J., Scales, S. J., 2010. Kinetics of hedgehog-dependent full-length Gli3 accumulation in primary cilia and subsequent degradation. Mol Cell Biol. 30**,** 1910-22.

Westlake, C. J., Baye, L. M., Nachury, M. V., Wright, K. J., Ervin, K. E., Phu, L., Chalouni, C., Beck, J. S., Kirkpatrick, D. S., Slusarski, D. C., Sheffield, V. C., Scheller, R. H., Jackson, P. K., 2011. Primary cilia membrane assembly is initiated by Rab11 and transport protein particle II (TRAPPII) complex-dependent trafficking of Rabin8 to the centrosome. Proc Natl Acad Sci U S A. 108**,** 2759-64.

Wicks, S. R., de Vries, C. J., van Luenen, H. G., Plasterk, R. H., 2000. CHE-3, a cytosolic dynein heavy chain, is required for sensory cilia structure and function in Caenorhabditis elegans. Dev Biol. 221**,** 295-307.

Wilkinson, C. J., Carl, M., Harris, W. A., 2009. Cep70 and Cep131 contribute to ciliogenesis in zebrafish embryos. BMC Cell Biol. 10**,** 17.

Williams, C. L., Li, C., Kida, K., Inglis, P. N., Mohan, S., Semenec, L., Bialas, N. J., Stupay, R. M., Chen, N., Blacque, O. E., Yoder, B. K., Leroux, M. R., 2011. MKS and NPHP modules cooperate to establish basal body/transition zone membrane associations and ciliary gate function during ciliogenesis. J Cell Biol. 192**,** 1023-41.

Williams, C. L., Winkelbauer, M. E., Schafer, J. C., Michaud, E. J., Yoder, B. K., 2008. Functional redundancy of the B9 proteins and nephrocystins in Caenorhabditis elegans ciliogenesis. Mol Biol Cell. 19**,** 2154-68.

Wilson, C. W., Chen, M. H., Chuang, P. T., 2009. Smoothened adopts multiple active and inactive conformations capable of trafficking to the primary cilium. PLoS One. 4**,** e5182.

Wloga, D., Rogowski, K., Sharma, N., Van Dijk, J., Janke, C., Edde, B., Bre, M. H., Levilliers, N., Redeker, V., Duan, J., Gorovsky, M. A., Jerka-Dziadosz, M., Gaertig, J., 2008. Glutamylation on alpha-tubulin is not essential but affects the assembly and functions of a subset of microtubules in Tetrahymena thermophila. Eukaryot Cell. 7**,** 1362-72.

Wloga, D., Webster, D. M., Rogowski, K., Bre, M. H., Levilliers, N., Jerka-Dziadosz, M., Janke, C., Dougan, S. T., Gaertig, J., 2009. TTLL3 Is a tubulin glycine ligase that regulates the assembly of cilia. Dev Cell. 16**,** 867-76.

Won, J., Marin de Evsikova, C., Smith, R. S., Hicks, W. L., Edwards, M. M., Longo-Guess, C., Li, T., Naggert, J. K., Nishina, P. M., 2011. NPHP4 is necessary for normal photoreceptor ribbon synapse maintenance and outer segment formation, and for sperm development. Hum Mol Genet. 20**,** 482-96.

Wu, L. N., Lu, M., Genge, B. R., Guo, G. Y., Nie, D., Wuthier, R. E., 2002. Discovery of sonic hedgehog expression in postnatal growth plate chondrocytes: differential regulation of sonic and Indian hedgehog by retinoic acid. J Cell Biochem. 87**,** 173-87.

Wu, S., Mehta, S. Q., Pichaud, F., Bellen, H. J., Quiocho, F. A., 2005. Sec15 interacts with Rab11 via a novel domain and affects Rab11 localization in vivo. Nat Struct Mol Biol. 12**,** 879-85.

Yan, W., 2009. Male infertility caused by spermiogenic defects: lessons from gene knockouts. Mol Cell Endocrinol. 306**,** 24-32.

Yang, J., Liu, X., Yue, G., Adamian, M., Bulgakov, O., Li, T., 2002. Rootletin, a novel coiled-coil protein, is a structural component of the ciliary rootlet. J Cell Biol. 159**,** 431-40.

Yin, X., Takei, Y., Kido, M. A., Hirokawa, N., 2011. Molecular motor KIF17 is fundamental for memory and learning via differential support of synaptic NR2A/2B levels. Neuron. 70**,** 310-25.

Yin, Y., Bangs, F., Paton, I. R., Prescott, A., James, J., Davey, M. G., Whitley, P., Genikhovich, G., Technau, U., Burt, D. W., Tickle, C., 2009. The Talpid3 gene (KIAA0586) encodes a centrosomal protein that is essential for primary cilia formation. Development. 136**,** 655-64.

Yoder, B. K., Hou, X., Guay-Woodford, L. M., 2002. The polycystic kidney disease proteins, polycystin-1, polycystin-2, polaris, and cystin, are co-localized in renal cilia. J Am Soc Nephrol. 13**,** 2508-16.

Yoshimura, S., Egerer, J., Fuchs, E., Haas, A. K., Barr, F. A., 2007. Functional dissection of Rab GTPases involved in primary cilium formation. J Cell Biol. 178**,** 363-9.

Yu, X., Ng, C. P., Habacher, H., Roy, S., 2008. Foxj1 transcription factors are master regulators of the motile ciliogenic program. Nat Genet. 40**,** 1445-53.

Zamore, P. D., Tuschl, T., Sharp, P. A., Bartel, D. P., 2000. RNAi: double-stranded RNA directs the ATP-dependent cleavage of mRNA at 21 to 23 nucleotide intervals. Cell. 101**,** 25-33.

Zeng, H., Hoover, A. N., Liu, A., 2010. PCP effector gene Inturned is an important regulator of cilia formation and embryonic development in mammals. Dev Biol. 339**,** 418-28.

Zhang, S., Hemmerich, P., Grosse, F., 2007a. Centrosomal localization of DNA damage checkpoint proteins. J Cell Biochem. 101**,** 451-65.

Zhang, X., Yuan, Z., Zhang, Y., Yong, S., Salas-Burgos, A., Koomen, J., Olashaw, N., Parsons, J. T., Yang, X. J., Dent, S. R., Yao, T. P., Lane, W. S., Seto, E., 2007b. HDAC6 modulates cell motility by altering the acetylation level of cortactin. Mol Cell. 27**,** 197-213.

Zhang, X. M., Ellis, S., Sriratana, A., Mitchell, C. A., Rowe, T., 2004. Sec15 is an effector for the Rab11 GTPase in mammalian cells. J Biol Chem. 279**,** 43027-34.

Zhao, C., Omori, Y., Brodowska, K., Kovach, P., Malicki, J., 2012. Kinesin-2 family in vertebrate ciliogenesis. Proc Natl Acad Sci U S A. 109**,** 2388-93.

Zhu, D., Shi, S., Wang, H., Liao, K., 2009. Growth arrest induces primary-cilium formation and sensitizes IGF-1-receptor signaling during differentiation induction of 3T3-L1 preadipocytes. J Cell Sci. 122**,** 2760-8.

Zuo, X., Guo, W., Lipschutz, J. H., 2009. The exocyst protein Sec10 is necessary for primary ciliogenesis and cystogenesis in vitro. Mol Biol Cell. 20**,** 2522-9.

Appendix 1 siRNA sequences

Appendix 1 siRNA sequences

Gene Symbol	siRNA	Sequence	Source
Non targeting		UGGUUUACAUGUCGACUAA	Dharmacon OnTarget Plus
Gfp		GGCUACGUCCAGGAGCGCACC	Dharmacon OnTarget Plus
Ift88	1	GUAGCUAGCUGCUUUAGAA	Dharmacon OnTarget Plus
	2	CGUCAGCUCUCACUAAUAA	Dharmacon OnTarget Plus
	3	CGGAGAAUGUUGAAUGUUU	Dharmacon OnTarget Plus
	4	GCUUGGAGCUUAUUACAUU	Dharmacon OnTarget Plus
Cda	1	UAUAAAUGCCACAGCACGU	Dharmacon OnTarget Plus
	2	GCCGACAAGUCAUGAGAGA	Dharmacon OnTarget Plus
	3	GCACAUUCGUAGUCAGGAC	Dharmacon OnTarget Plus
	4	CCGAAGGGUACAAGGAUUU	Dharmacon OnTarget Plus
Ttc30b	1	CAAAAGCACUAUUCGAUAU	Dharmacon OnTarget Plus
	2	UGAGAUAAUUGGAUGGAAU	Dharmacon OnTarget Plus
	3	GUCAAGUGAGAUUGUGUAA	Dharmacon OnTarget Plus
	4	ACAAUUAUGCUAAGGGACA	Dharmacon OnTarget Plus
Ttc30a1	1	AGAUGUAGGUAUUAGACGA	Dharmacon OnTarget Plus
	2	GGAAGUACCAUCCGAUAAA	Dharmacon OnTarget Plus
	3	CUAAAGUUCCCGACGGUGA	Dharmacon OnTarget Plus
	4	UGUCAAAGCACAUGAUAGU	Dharmacon OnTarget Plus
Ttc30a2	1	UAGCCGAGUCCUUCGUUUA	Dharmacon OnTarget Plus
	2	GGGCAUUGAUGUUCGCAGU	Dharmacon OnTarget Plus
	3	GAGAUCAUAGGGUGGAAUA	Dharmacon OnTarget Plus
	4	ACCCAGAUGGUUUGGUCAA	Dharmacon OnTarget Plus
Spag1	1	UCAGAUAGACGGCGAGAAU	Dharmacon OnTarget Plus
	2	GCAGAGAGGUUUAAGACGA	Dharmacon OnTarget Plus
	3	GGGAAGUGCAGAUGAGCGU	Dharmacon OnTarget Plus
	4	GCAGAUAGAUUGUGGGAUC	Dharmacon OnTarget Plus
Wdr60	1	UGAAAGGGUUGGCGAGUUA	Dharmacon OnTarget Plus
	2	GCUACCUGCUCAAGCGUUA	Dharmacon OnTarget Plus
	3	AAGCAAGGUUGGACGGAGU	Dharmacon OnTarget Plus
	4	GCAUAUAAUUAUCAGAGCA	Dharmacon OnTarget Plus
Wdr78	1	GCAAUGACUUAUACGUAGA	Dharmacon OnTarget Plus
	2	AAACGUUCCUAGCGCUAAA	Dharmacon OnTarget Plus
	3	CCAUGUGGCCAGAGCGUAU	Dharmacon OnTarget Plus
	4	AGUCAACAAUACCGGCUAA	Dharmacon OnTarget Plus
Wdr16	1	UCGCACAUCUACCGCGUUA	Dharmacon OnTarget Plus
	2	GGAUCGGAGUGACGGCCAU	Dharmacon OnTarget Plus
	3	GGGCCUCAAUGUCGGCAAU	Dharmacon OnTarget Plus
	4	CGUCAGUGUGAGCGCAGAU	Dharmacon OnTarget Plus
Ppp3r1	1	GCAGAACCCUUUAGUACAG	Dharmacon OnTarget Plus
	2	UAGGCUGAUUCAUCUAUUA	Dharmacon OnTarget Plus
	3	UCAAAGGCGAUAAGGAACA	Dharmacon OnTarget Plus
	4	GGAAUUCUGUGCUGUAAGU	Dharmacon OnTarget Plus
Wdr92	1	AAGAGGAUCCUGUCGCUAA	Dharmacon OnTarget Plus
	2	CGACAUGAGAACACAGCAU	Dharmacon OnTarget Plus
	3	CAUUGAAGACGGUUGGAUU	Dharmacon OnTarget Plus
	4	CGUUGAAGAUUGAAUUUGU	Dharmacon OnTarget Plus
Ttc26	1	GUGAGUAGCUUGUUACGUU	Dharmacon OnTarget Plus

Gene Symbol	siRNA	Sequence	Source
	2	GGCUCAACCUAGUGAUUUA	Dharmacon OnTarget Plus
	3	CGACACUAACUUAUGGAUU	Dharmacon OnTarget Plus
	4	UCGUAGGGAUUUAUUGAUA	Dharmacon OnTarget Plus
Ttc28	1	CAGCUGAGCGGGAACGAAU	Dharmacon OnTarget Plus
	2	CCGGGAACCCUGACGUCAA	Dharmacon OnTarget Plus
	3	GUUAGGGAACUACGAGCAA	Dharmacon OnTarget Plus
	4	UGCAAUAACUCGCGUUGAA	Dharmacon OnTarget Plus
Epb4.1l4b	1	GCGUGGACCUGCCGAAACA	Dharmacon OnTarget Plus
	2	CUGGCUGGAUCACGCGAAA	Dharmacon OnTarget Plus
	3	CUAUGAAACGGCCGUGGAA	Dharmacon OnTarget Plus
	4	CUGUGGAGAAGCCGGAAAU	Dharmacon OnTarget Plus
Ccdc151	1	ACUCAGAGGACUACGCUUA	Dharmacon OnTarget Plus
	2	GCCUCGGAAUCGCGCAAUA	Dharmacon OnTarget Plus
	3	UGUUAGAGGGUGACCGGAA	Dharmacon OnTarget Plus
	4	UGGAGUAGCUGAAUCGCAU	Dharmacon OnTarget Plus
RP23-464C2.9	1	CAAGAUGCCAUGAUGAUUA	Dharmacon OnTarget Plus
	2	GGAGAGGCGGACACAGUUA	Dharmacon OnTarget Plus
	3	GCCGGAGGGACUUGGAUUU	Dharmacon OnTarget Plus
	4	CGGAUGUGGACCAUAGUUA	Dharmacon OnTarget Plus
Tscot	1	CGUUGGGCACUCUGCGCAA	Dharmacon OnTarget Plus
	2	GGUUUAAUCUUCCGCACCA	Dharmacon OnTarget Plus
	3	CAAUUGGUGUUGUGGCCUA	Dharmacon OnTarget Plus
	4	CGUGCUAGUUCUAUGGAAG	Dharmacon OnTarget Plus
Sdccag8	1	UCGCAAAUAGUUCGACUUA	Dharmacon OnTarget Plus
	2	UCACAGAGCUGCUGGGCGA	Dharmacon OnTarget Plus
	3	GAUUAUGACACGAGAAGAU	Dharmacon OnTarget Plus
	4	CCAUCGAGAGGCUGACUAA	Dharmacon OnTarget Plus
Lrrc48	1	GAUUAGGUGUCAGCCAUUG	Dharmacon OnTarget Plus
	2	UGGCUGGAUUUGUCCUUUA	Dharmacon OnTarget Plus
	3	GCACUGAGAGCAUCGGUGA	Dharmacon OnTarget Plus
	4	GGAGAUCAAUCAAUUCGUC	Dharmacon OnTarget Plus
Fam92a	1	GCGAAACCCAUCUGAUCGA	Dharmacon OnTarget Plus
	2	GCAAGAUGUUGAGGCGCAA	Dharmacon OnTarget Plus
	3	UUGUAAAGAUGAAGCGAGA	Dharmacon OnTarget Plus
	4	CUGUAUGCCUCUACCGAGA	Dharmacon OnTarget Plus
Fam92b	1	GCGUGGAAUUUACGGGCAU	Dharmacon OnTarget Plus
	2	GAGGUGUAUUCCAGCGCUU	Dharmacon OnTarget Plus
	3	CCGGGCAGAUAUCAAGAAA	Dharmacon OnTarget Plus
	4	GCUCUACGGUGCCCAAAUA	Dharmacon OnTarget Plus
Bbs5	1	CUGAAGUGUACCUCGUUUA	Dharmacon OnTarget Plus
	2	GAAUAAGCAACAAGAUCGU	Dharmacon OnTarget Plus
	3	CUUCUAAAAUGUACCGUGA	Dharmacon OnTarget Plus
	4	GGUUACAACUGCAUAUUGA	Dharmacon OnTarget Plus
Tctex1d2	1	CAACUACACUCACGAUGUU	Dharmacon OnTarget Plus
	2	AUGACUAGAUACUUGGGUA	Dharmacon OnTarget Plus
	3	ACUAUUGAAUCGUUGGGAA	Dharmacon OnTarget Plus
	4	GUAUAAAAUGGUGGUGCAA	Dharmacon OnTarget Plus
Tcte3	1	AAGCCUAGCAUGUUCGAGA	Dharmacon OnTarget Plus
	2	CCGGUGUCUAAGAGAGAAA	Dharmacon OnTarget Plus
	3	CACAUUUGGUAGAAACUAA	Dharmacon OnTarget Plus
	4	UGACUCAAUUGCUGAUGUA	Dharmacon OnTarget Plus

Gene Symbol	siRNA	Sequence	Source
Tctex1d1	1	AAUUAGUGAUUCCGAGAUA	Dharmacon OnTarget Plus
	2	GAUGAAUCCUCUCGCCUCA	Dharmacon OnTarget Plus
	3	AGUCAGUGCCAUUCACAUA	Dharmacon OnTarget Plus
	4	AAGUGGUCCUUGUGUGUUA	Dharmacon OnTarget Plus
Tctex1d4	1	CCUCUAGGUUCACGAGUUA	Dharmacon OnTarget Plus
	2	GGUGUGUGCUACUGCGGUU	Dharmacon OnTarget Plus
	3	GGCACUAUGUGAACAGAUA	Dharmacon OnTarget Plus
	4	UGAUGAGACCCGACCUAUA	Dharmacon OnTarget Plus
Zmynd10	1	ACUGGGAGAAGCACGGAAA	Dharmacon OnTarget Plus
	2	GAAUAAACUGGAUGGGCAA	Dharmacon OnTarget Plus
	3	GCUAAUCAACCAUGGGAAG	Dharmacon OnTarget Plus
	4	CCGCAAGCUGAUACUGCUA	Dharmacon OnTarget Plus
Ccdc63	1	UUAAGAAGAUCAACUGCGA	Dharmacon OnTarget Plus
	2	CCGGGAAGGUCACGGACAU	Dharmacon OnTarget Plus
	3	UCGUGAAGUCUCCGAAGAA	Dharmacon OnTarget Plus
	4	CCGCCUACGACCACGUCUA	Dharmacon OnTarget Plus
Ccdc114	1	CGAUGAACGACAACCGGAU	Dharmacon OnTarget Plus
	2	AGAAGCUAGUGCUGCGUUA	Dharmacon OnTarget Plus
	3	GCAAAAGGCAGAACAGCGA	Dharmacon OnTarget Plus
	4	ACCUGAAUAUGGACCGCAA	Dharmacon OnTarget Plus
Prdm1	1	GUACAUACAUAGUGAACGA	Dharmacon OnTarget Plus
	2	GAGAGAGUACAGCGUGAAA	Dharmacon OnTarget Plus
	3	CUGCCAAGUUUACGCAAUU	Dharmacon OnTarget Plus
	4	GCAAAGAGGUUAUUGGCGU	Dharmacon OnTarget Plus
Prdm2	1	AGGAUAAGCACUACGGCAA	Dharmacon OnTarget Plus
	2	CGAGAUAGCAGCUGCGAUU	Dharmacon OnTarget Plus
	3	AAGCAGACAUGCCGAAUGA	Dharmacon OnTarget Plus
	4	CCAAAGGUGUCCGGCGAAA	Dharmacon OnTarget Plus
Gtl3	1	GACCAAUAUUUCUUCGUAU	Dharmacon OnTarget Plus
	2	GUGAGAGACGCACGCAACA	Dharmacon OnTarget Plus
	3	GGGCAUAUGGCACGAACUA	Dharmacon OnTarget Plus
	4	GCAAACUGCCGUAUCCGAA	Dharmacon OnTarget Plus
Mllt4	1	GGAAUAUCGACGACGAGAA	Dharmacon OnTarget Plus
	2	GGAAAUAAUUCUUGACGAU	Dharmacon OnTarget Plus
	3	AGUGAAAGCUUCUCGUAAA	Dharmacon OnTarget Plus
	4	CAGGAGGAGGAGCGAGUAA	Dharmacon OnTarget Plus
Catnb	1	GUGAAAUUCUUGGCUAUUA	Dharmacon OnTarget Plus
	2	GCGCUUGGCUGAACCAUCA	Dharmacon OnTarget Plus
	3	CAGCAAAUCAUGCGCCUUU	Dharmacon OnTarget Plus
	4	AAGCUGACCUGAUGGAGUU	Dharmacon OnTarget Plus
Cdhr2	1	AGAGUGAGGCCAUCGACUA	Dharmacon OnTarget Plus
	2	GCAAUAAUCUCUUCCGCAU	Dharmacon OnTarget Plus
	3	GUCCAGGUCUUCCGGAUUA	Dharmacon OnTarget Plus
	4	CAGGGAAUCUGACGGUGAA	Dharmacon OnTarget Plus
Abcd2	1	GAGAAUUACCCAUACGGAA	Dharmacon OnTarget Plus
	2	GCUACUAGAACUUCGGAAA	Dharmacon OnTarget Plus
	3	GGACACUGCUAUCCGUUUA	Dharmacon OnTarget Plus
	4	CGACGUUGAAGGAAAGAUA	Dharmacon OnTarget Plus
Azi1	1	GUGAAGCGUGUGCGUGAUA	Dharmacon OnTarget Plus
	2	CAUGAGUGCCACCGAGAAA	Dharmacon OnTarget Plus
	3	GCACCCAGCUUCACCGCUA	Dharmacon OnTarget Plus

Gene Symbol	siRNA	Sequence	Source
	4	CCGAGGAGAAGGAGCGACU	Dharmacon OnTarget Plus
Wdr35	1	GCGUGAAUCUGGCGUCAUU	Dharmacon OnTarget Plus
	2	GAGCAAGCUGUGAGCGCAU	Dharmacon OnTarget Plus
	3	UUGCAGAUGAAGAGGCGAA	Dharmacon OnTarget Plus
	4	UAUCAGAAGUUGACUACCA	Dharmacon OnTarget Plus
CycB	1	CAAGUUCCAUCGUGUCAUC	Dharmacon OnTarget Plus
	2	GGAGAAACCCUUCGCCAUU	Dharmacon OnTarget Plus
	3	CGGCAAAGUUCUAGAGGGC	Dharmacon OnTarget Plus
	4	GAAAGAGCAUCUAUGGUGA	Dharmacon OnTarget Plus
Gapdh	1	GUGUGAACCACGAGAAAUA	Dharmacon OnTarget Plus
	2	GGAGAAACCUGCCAAGUAU	Dharmacon OnTarget Plus
	3	UCAAGAAGGUGGUGAAGCA	Dharmacon OnTarget Plus
	4	UGGUGAAGCAGGCAUCUGA	Dharmacon OnTarget Plus
Smo	1	GCUACAAGAACUAUCGGUA	Dharmacon OnTarget Plus
	2	GGAGUAGUCUGGUUCGUGG	Dharmacon OnTarget Plus
	3	GAGCGUAGCUUCCGGGACU	Dharmacon OnTarget Plus
	4	CAAUUGGCCUGGUGCUUAU	Dharmacon OnTarget Plus
Wdr35	1	GGAUGUAUCAAGAUAUGGATT	Ambion Silencer Select
	2	GCAGCCCAAUCAUCGAGUATT	Ambion Silencer Select
	3	GGCUUAUCAUUGUCUGGAUTT	Ambion Silencer Select
Dync2h1	1	CCUUAAACAGCUUUUCAGATT	Ambion Silencer
	2	GCCAAGUGGGACAAAUUCGTT	Ambion Silencer
	3	CGUAGACUUAACCUACAAATT	Ambion Silencer
Azi1 3'UTR	Pool	AGACACAGGGCUAAGGGUA	Dharmacon OnTarget Plus
		CAGCUGUUCUAUAGUAAAA	Dharmacon OnTarget Plus
		CCCUUGGGAUGACGAGCCA	Dharmacon OnTarget Plus
		GUGUCCAGGUCACGCUCCA	Dharmacon OnTarget Plus

Appendix 2 Movie legends

Movie 5.1 Live imaging of ciliogenesis suggests *Ccdc63* has a role in cilia formation and possibly cilia stability A representative field of cells imaged every 30 min for 18h. The cells were treated with Non-targeting siRNA (Neg) (A), *Ift88* #3 siRNA (B), *Ccdc63* #1 siRNA (C) and *Ccdc63* #4 siRNA. As documented in Figure 5.6, *Ccdc63* siRNA leads to fewer cilia and decreased cilia stability.

Movie 6.1 *Azi1*$^{Gt/Gt}$ mutant sperm is immotile (A) Wild type sperm diluted 1:5 swimming through methyl cellulose. (B) *Azi1*$^{Gt/Gt}$ sperm swimming in M2 media undiluted. *Azi1*$^{Gt/Gt}$ sperm is immotile

All movies are .avi files.

Appendix 3 Mill et al. 2011

Mill, P., Lockhart, P. J., Fitzpatrick, E., Mountford, H. S., **Hall, E. A.**, Reijns, M. A., Keighren, M., Bahlo, M., Bromhead, C. J., Budd, P., Aftimos, S., Delatycki, M. B., Savarirayan, R., Jackson, I. J., Amor, D. J., 2011. Human and mouse mutations in WDR35 cause short-rib polydactyly syndromes due to abnormal ciliogenesis. Am J Hum Genet. 88**,** 508-15.

Human and Mouse Mutations in *WDR35* Cause Short-Rib Polydactyly Syndromes Due to Abnormal Ciliogenesis

Pleasantine Mill,[1,8,*] Paul J. Lockhart,[2,3,8,*] Elizabeth Fitzpatrick,[2] Hayley S. Mountford,[2] Emma A. Hall,[1] Martin A.M. Reijns,[1] Margaret Keighren,[1] Melanie Bahlo,[4] Catherine J. Bromhead,[4] Peter Budd,[1] Salim Aftimos,[5] Martin B. Delatycki,[2,3,6] Ravi Savarirayan,[3,7] Ian J. Jackson,[1,9] and David J. Amor[3,7,9]

Defects in cilia formation and function result in a range of human skeletal and visceral abnormalities. Mutations in several genes have been identified to cause a proportion of these disorders, some of which display genetic (locus) heterogeneity. Mouse models are valuable for dissecting the function of these genes, as well as for more detailed analysis of the underlying developmental defects. The short-rib polydactyly (SRP) group of disorders are among the most severe human phenotypes caused by cilia dysfunction. We mapped the disease locus from two siblings affected by a severe form of SRP to 2p24, where we identified an in-frame homozygous deletion of exon 5 in *WDR35*. We subsequently found compound heterozygous missense and nonsense mutations in *WDR35* in an independent second case with a similar, severe SRP phenotype. In a mouse mutation screen for developmental phenotypes, we identified a mutation in *Wdr35* as the cause of midgestation lethality, with abnormalities characteristic of defects in the Hedgehog signaling pathway. We show that endogenous WDR35 localizes to cilia and centrosomes throughout the developing embryo and that human and mouse fibroblasts lacking the protein fail to produce cilia. Through structural modeling, we show that WDR35 has strong homology to the COPI coatamers involved in vesicular trafficking and that human SRP mutations affect key structural elements in WDR35. Our report expands, and sheds new light on, the pathogenesis of the SRP spectrum of ciliopathies.

There are a number of recessive disorders characterized by skeletal dysplasia and multiorgan anomalies,[1] some of which have been shown to be caused by mutations in the development, structure, or function of primary cilia (ciliopathies).[2] Short-rib polydactylies (SRPs) are a prime example, being a heterogeneous group of disorders characterized by skeletal defects, short ribs and limbs, and polydactyly. Visceral features can include polycystic kidneys, laterality defects, and cardiovasular and brain abnormalities. SRPs have been classified into four types, (Saldino-Noonan syndrome, type I [MIM 263530]; Majewski syndrome, type II [MIM 263520]; Verma-Naumoff syndrome, type III [MIM 263510]; Beemer-Langer syndrome, type IV [MIM 269860]), which display clinical and molecular overlap. Although locus heterogeneity has been demonstrated in SRP (see below), the relative contribution of both allelic heterogeneity and genetic background modification remains unclear. This question extends to other disorders that share similar overlapping clinical features. Asphyxiating thoracic dystrophy (ATD, Jeune syndrome [MIM 208500]) has skeletal features similar to those of SRP, and patients usually die in infancy, although some survive and later may develop liver and kidney disease and retinal degeneration.[3] Ellis van Creveld syndrome (EVC, chondroectodermal dysplasia [MIM 22550]) is most similar histologically to SRP III but often presents postnatally, with distinct radiological and clinical features such as congenital heart disease, supernumerary digits, and ectodermal dysplasia.[1] In addition, patients with cranioectodermal dysplasia (CED, Sensenbrenner syndrome [MIM 218330]) display craniofacial and skeletal abnormalities, hair and tooth defects, and variable liver, kidney, brain, and retinal anomalies.[4]

Primary cilia are complex organelles protruding from the surface of nondividing cells. Their formation is organized by the basal body; a modified centriole structure from which the microtubule-based axoneme extends. The assembly and maintenance of cilia requires the dynamic bidirectional movement of the multiprotein complexes along the axoneme from cell body to cilia tip.[5] This process, termed intraflagellar transport (IFT), involves a conserved core machinery organized into trains composed of either IFT-B (anterograde) or IFT-A (retrograde) components and is driven by kinesin or dynein molecular motors, respectively.[6–8] In addition to the transport of structural units, IFT is also essential for the localization and function of key developmental signaling components, such as the Gli transcription factors, which transduce Hedgehog (Hh) signaling.[9] The loss of Hh regulation may be a hallmark of some clinical features observed in ciliopathies.

In cases in which mutated genes have been identified in skeletal dysplasias, it is not known whether a correlation exists between severity of disease and the particular

[1]Medical Research Council Human Genetics Unit, Institute of Genetics and Molecular Medicine, Western General Hospital, Edinburgh EH4 2XU, UK; [2]Bruce Lefroy Center for Genetic Health Research, Murdoch Childrens Research Institute, Parkville, Victoria 3052, Australia; [3]Department of Paediatrics, The University of Melbourne, Parkville, Victoria 3052, Australia; [4]Bioinformatics Division, The Walter and Eliza Hall Institute, Parkville, Victoria 3052, Australia; [5]Northern Regional Genetic Services, Auckland Hospital, Auckland 1148, New Zealand; [6]Clinical Genetics, Austin Health, Heidelberg, Victoria 3081, Australia; [7]Victoria Clinical Genetics Service, Murdoch Childrens Research Institute, Parkville, Victoria 3052, Australia
[8]These authors contributed equally to this work
[9]These authors contributed equally to this work
*Correspondence: pleasantine.mill@hgu.mrc.ac.uk (P.M.), paul.lockhart@mcri.edu.au (P.J.L.)
DOI 10.1016/j.ajhg.2011.03.015.

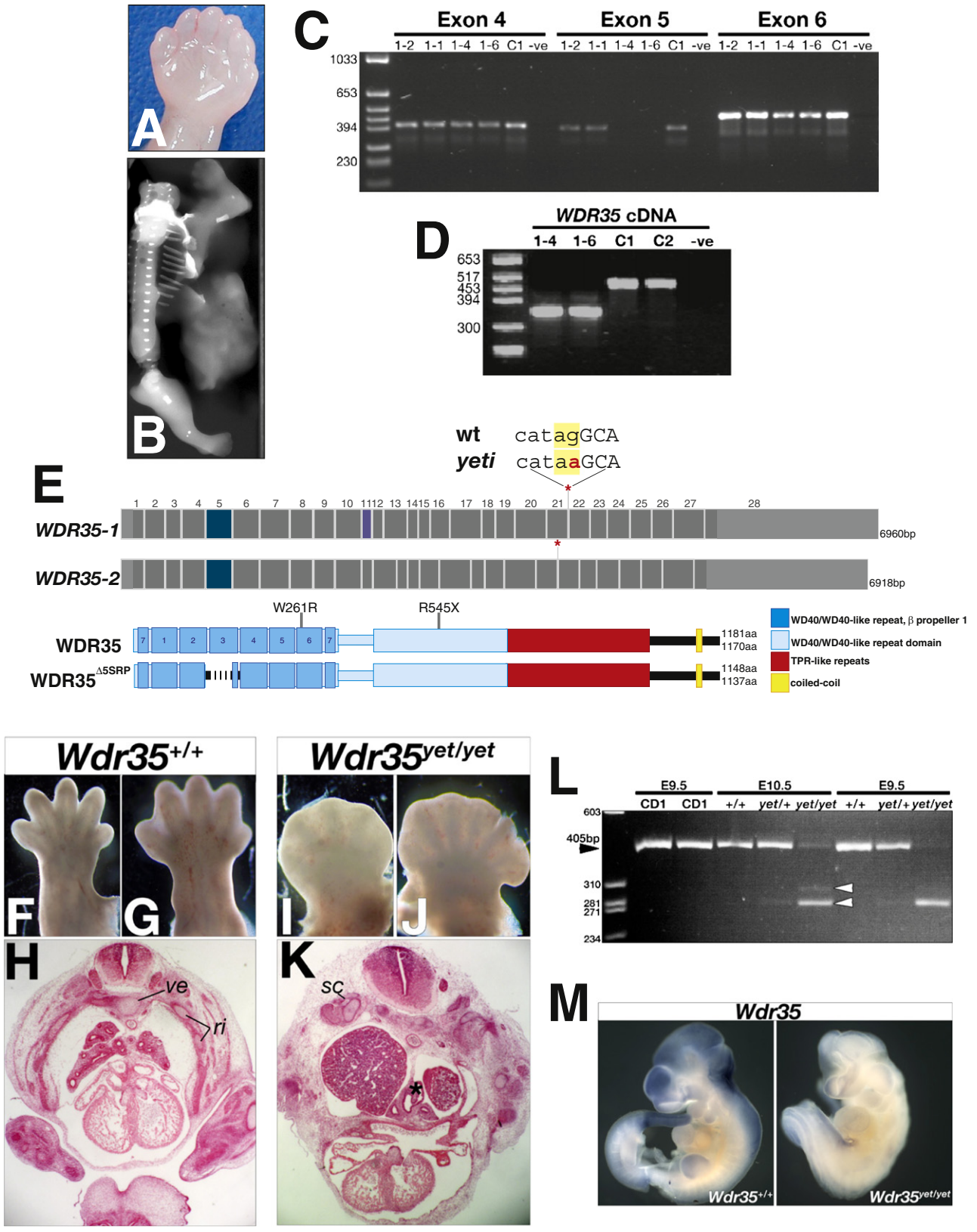

Figure 1. ***WDR35*** **Is Mutated in Atypical Short-Rib Polydactyly Syndrome in Humans and in the** ***yeti*** **Mutant Mouse**
(A and B) Characteristic postaxial polydactyly, extreme micromelia, and short ribs (A) as presented in postmortem survey of 13 week conceptus (SRP-3-1) (B).
(C) Genomic PCR spanning exons 4, 5, or 6 of *WDR35* from DNA of parents (SRP-1-1, SRP-1-2) or affected concepti (SRP-1-4, SRP-1-6). Deletion of a 2847 bp genomic fragment (2:20177392-20180238, assembly GRCh37) results in the loss of exon 5 in homozygous individuals. Reaction products for the control (C1) and no template (-ve) are shown.

protein or ciliary process affected. Homozygous and compound-heterozygous mutations in the retrograde dynein motor *DYNC2H1* (MIM 603297) have recently been identified in cases of both SRP type III and ATD/Jeune syndrome,[10,11] and *IFT80* (MIM 611177), which encodes a component of the anterograde IFT-B complex, is mutated in some other cases of ATD.[12] In contrast, mutations recently identified in the less severe CED/Sensenbrenner syndrome affect components of the IFT-A retrograde complex *IFT122* (MIM 606045)[13] or *WDR35* (MIM 613602).[14] Most recently, mutations in Never-in-mitosis Kinase 1 (*NEK1* [MIM 604588]), a gene involved in initiating ciliogenesis,[15–17] were identified in several SRP type II cases, including a potential example of digenic diallelic inheritance with *DYNC2H1*.[18] Mouse mutations have been found in many of these genes[17,19–22] and will be valuable models for understanding ciliopathic phenotype-genotype correlations.

We previously identified a New Zealand family of Maori descent with two consecutive pregnancies complicated by an unclassifiable SRP syndrome that was most similar to SRP type III but was novel in that it was associated with acromesomelic hypomineralisation and campomelia.[23] These affected siblings exhibited several additional hallmarks of ciliopathic disease, including polysyndactyly, laterality defects, and cystic kidneys. After institutional ethics approval and informed consent, human samples were collected for molecular analysis. Using genome-wide SNP genotyping and CNV analysis, we mapped the disease locus to a 5.5 Mb region of chromosome 2p24 (Figure S1A available online) and identified a homozygous deletion of three SNPs within *WDR35* (NM_001006657.1) (Figure S1B). This deletion was heterozygous in both parents and the unaffected sibling but was homozygous in the two affected siblings. Direct sequencing of the parents and affected siblings over this region identified a 2847 bp deletion spanning exon 5 of *WDR35* (Figure 1C). PCR analysis of cDNA from patient cell lines confirmed the loss of the 129 bp exon 5 from the *WDR35* mRNA (Figure 1D). *WDR35* encodes two isoforms that share seven closely spaced WD40 repeats at the amino terminus and a tetratricopeptide repeat-like motif at the carboxyl terminus (Figure 1E). WD40 repeats are involved in intracellular trafficking, cargo recognition, and binding,[24,25] and the $WDR35^{\Delta 5}$ mutation results in the in-frame deletion of one of these repeats (Figure 1E). WDR35 is orthologous with Ift121, which fractionates with complex A IFT particles in *C. reinhardtii*[25] and mammals.[26] Mutations in the *C. elegans* ortholog (*ifta-1*) display classic truncated retrograde cilia phenotypes with accumulations of IFT machinery and transport profiles consistent with phenotypes observed when other complex A subunits are mutated.[27] We also performed candidate-gene sequencing of *WDR35* in two cases with a clinical diagnosis of Jeune syndrome and four additional cases with severe SRP phenotypes (two unclassifiable SRPs, one Beemer-Langer [type IV] SRP, and one Majewski [type II] SRP). Heteroallelic mutations in *WDR35* were identified in one fetus (Figure S1C) with an SRP phenotype associated with extreme micromelia, postaxial polydactyly, and facial abnormalities (Figures 1A and 1B). A de novo nonsense mutation (c.1633C>T [p.Arg545X]) was identified on the paternal allele, and a missense mutation affecting a highly conserved tryptophan residue (c.781T>C [p.Trp261Arg]; Figure 4A) was shown to be maternally inherited.

Independently, we isolated the mutant mouse line *yeti* in a recessive ENU mutagenesis screen for genes affecting embryonic development. Mutant embryos die before late day 12.5 postcoitum (12.5 dpc) and exhibit a range of severe defects. They display cardiovascular defects including generalized edema, hemorrhages, and a randomized and mislooped heart tube. Delayed and randomized embryo turning is also observed, and polysyndactlyly is seen in rare, surviving, later-stage embryos (Figures 1I and 1J). Additionally, *yeti* mutants display failure of the somite derivatives, including the putative ribs, to migrate and properly differentiate (Figure 1K), hypoplastic lungs with tracheal-esophageal fistula, and diaphragmatic hernia. We mapped the *yeti* locus to a 3.5 Mb interval between rs6278243 and rs29154438 on chromosome 12 and undertook genomic sequencing of candidate genes. A single G>A mutation was identified in the splice acceptor site of exon 22 of *Wdr35* (Figure 1E; chr12:9026683, ENSMUST00000085745, NCBIM37). RT-PCR analysis of cDNA from *yeti* mutant litters using primers in the adjacent exons confirmed aberrant splicing of the *Wdr35* mRNA in heterozygous and homozygous *yeti* embryos (Figure 1L). Sequencing of these mutant splice variants revealed frameshifts in all *yeti* transcripts. In situ hybridization with 5′ and 3′ UTR *Wdr35* riboprobes

(D) RT-PCR amplification of *WDR35* spanning exons 4–6 from affected concepti (SRP-1-4, SRP-1-6) and control fibroblasts (C1, C2).
(E) Schematic of the predicted domain organization of two coding human *WDR35* transcripts, with or without exon 11 (violet). The location of the WDR35 mutations in SRP-1 (blue; homozygous SRPΔ5) and SRP-3 (p.Trp261Arg and p.Arg545X) -affected concepti are shown. The splice acceptor mutation at the intron 21-exon 22 junction in *yeti* mice is indicated (*).
(F–K) Gross embryonic phenotypes of wild-type (F–H) compared to *yeti* mutant littermates (I–K). Embryonic day 12.5 (E12.5) forelimb (F, I) and hindlimb (G, J) defects in *yeti* mouse mutants include impaired outgrowth along the proximal-distal axis and polysyndactyly. (H, K) E11.5 transverse hematoxylin- and eosin-stained sections of the $Wdr35^{yet/yet}$ thoracic cavity show failure of the somite derivatives, such as the sclerotome (sc) derivatives (ri, ribs; ve, vertebra), to migrate out from the midline in mutants and tracheoesophageal fistula with hypoplastic lungs (asterisk).
(L) RT-PCR amplification of a *Wdr35* fragment covering exons 21–24 shows the presence of aberrantly spliced of transcripts in the *yeti* mutant (white arrowheads) compared to wild-type (black arrowhead).
(M) Whole-mount in situ hybridization of *Wdr35* in E10.5 wild-type and *yeti* littermates shows nonsense-mediated decay of mRNA in mutant embryos.

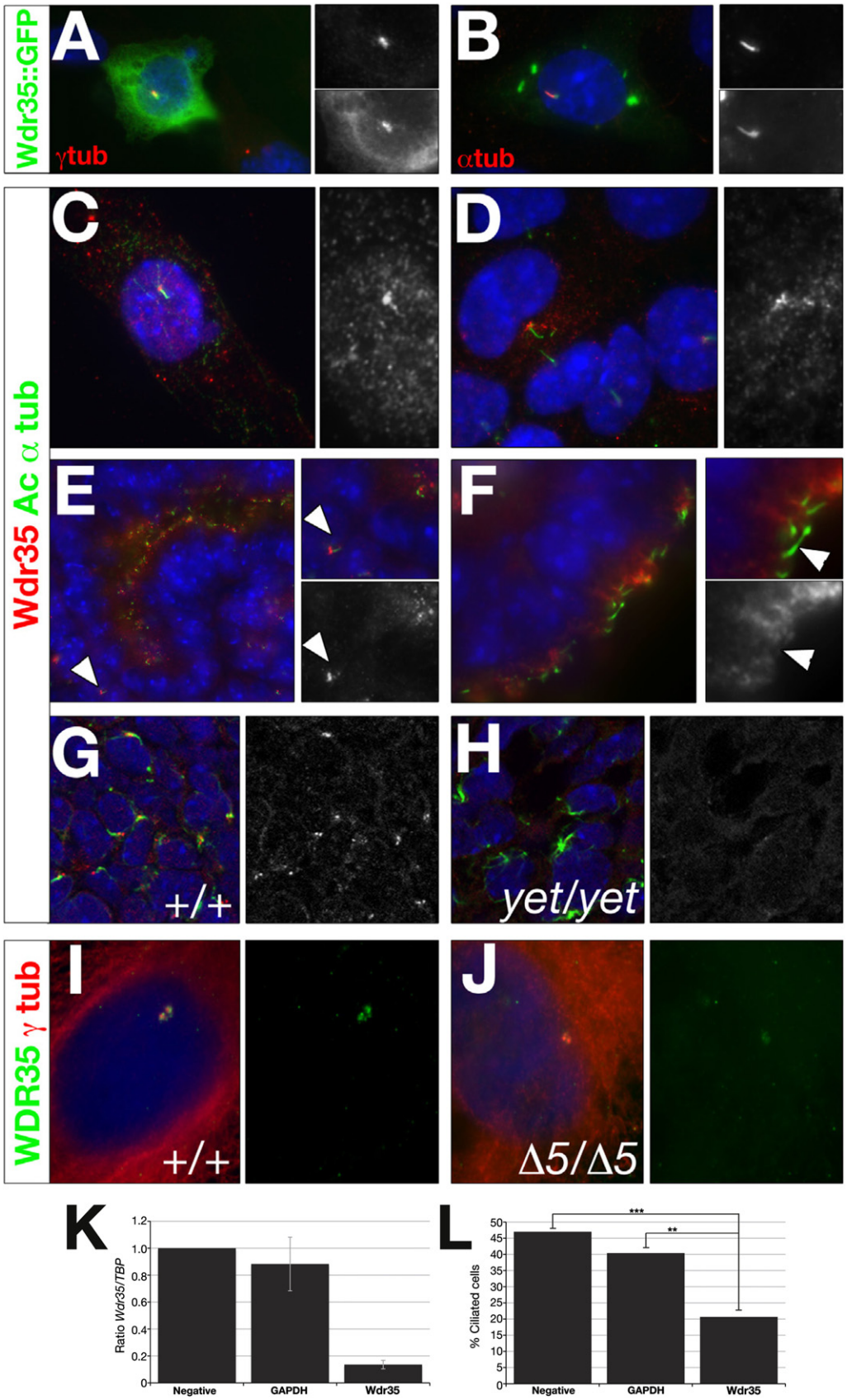

Figure 2. *Wdr35* Localizes to Cilia and Is Required for Ciliogenesis
(A and B) NIH-3T3 (A) or IMCD3 (B) cells were microporated with full-length mouse *Wdr35::GFP* and serum starved for 36 hr before costaining with antibodies directed against γ-tubulin (A) or acetylated α-tubulin (red; B). Nuclei are stained with DAPI (blue). Magnification of regions of interest are shown in singl-channel images indicating colocalization.

in mutant embryos revealed that mutant transcripts are subject to nonsense-mediated decay (Figure 1M). Noncomplementation of the *yeti* allele with an embryonic-stem-cell-derived "targeted trap" null *tm2a* allele of *Wdr35* proves that the *yeti* mutant phenotype is due to this point mutation in *Wdr35* (Figure S2). The phenotypic parallels, in particular polydactyly and failure of migration and differentiation of somite derivatives leading to absent or shortened ribs, strongly suggest that the human mutations in *WDR35*, like the mouse mutations, result in a complete loss of function.

Little is functionally known about mammalian WDR35 aside from its biochemical association with other IFT-A components,[26] so we characterized the cellular and in vivo localization of WDR35. Initially, we generated a full-length mouse Wdr35 protein tagged with GFP and expressed it in cultured cells. Significant staining was observed in the periciliary region in mouse NIH 3T3 cells, shown by partial colocalization with γ-tubulin (Figure 2A). In IMCD3 cells, which have more prominent cilia, Wdr35::GFP was also detected along the cilia axonemes, where it colocalized with acetylated α-tubulin (Figure 2B). To examine endogenous Wdr35 localization, we generated two independent antibodies directed against different, unique epitopes. Immunofluorescence studies in IMCD3 cells confirmed that Wdr35 accumulated at and around centrosomes and basal bodies of serum-starved cells, with fainter punctate staining along the cilia axoneme (Figures 2C and 2D). Immunofluorescence analysis of wild-type mouse sections labeled both primary and specialized cilia, as well as centrosomes, throughout the embryo. The intensity of staining was enriched in highly ciliated tissues, including the developing lung and nervous system (Figures 2E and 2F, Figure S4). Importantly, this WDR35 localization was lost in *yeti* mutant sections, as shown in the limb bud mesenchyme at 11.5 dpc (Figures 2G and 2H). Likewise, $WDR35^{\Delta 5}$ SRP fibroblasts had only remnant expression of endogenous $WDR35^{\Delta 5}$ (Figures 2I and 2J). Collectively, these data suggest that both $WDR35^{\Delta 5}$ and *yeti* are loss-of-function alleles of *WDR35*. Given WDR35's subcellular localization and the gross ciliopathic phenotype of these mammalian mutants, our data suggest that WDR35 is an essential component of the cilia. To independently verify that WDR35 is required for ciliogenesis, we used a siRNA strategy to knock down expression of *Wdr35* in NIH 3T3 cells and quantified the number of cells with cilia. Reduction of *Wdr35* mRNA levels by 85% resulted in a 50% reduction in the number of ciliated cells compared to the scrambled siRNA control (Figures 2K and 2L).

To better characterize the cellular function of WDR35 in primary cilia, we analyzed primary fibroblasts from human (Figures 3A–3D) and mouse (Figures 3E–3K) controls and *WDR35* mutants. Cilia axonemes were clearly detectable by acetylated α-tubulin staining, a marker of stabilized microtubules, in human (Figures 3A and 3B) and mouse (Figures 3E and 3F) control cells. However, these structures were completely absent in both human (Figures 3C and 3D) and mouse (Figures 3G and 3H) mutant cells. Instead, extended perinuclear microtubule arrays were prominent via acetylated α-tubulin staining in both human and mouse mutant cells (Figure 3C compared to Figure 3A and Figure 3G compared to Figure 3E). Because loss of retrograde IFT transport results in accumulation of anterograde IFT components in mutant cilia, we examined the localization of complex B protein IFT88 (MIM 600595) in *WDR35* mutant fibroblasts. Consistent with a functional role in retrograde IFT trains, some cilia-like structures remained in these mutant cells, as shown by restricted IFT88 accumulations around the γ-tubulin-positive basal bodies (Figures 3D and 3H).

Clinical distinction between syndromes in the skeletal dysplasia spectrum could result from underlying differences in the degrees of disruption to cilia structure and/or function, as a result of different mutations in the same gene. Mutations in *WDR35* were recently identified in a subset of patients with Sensenbrenner syndrome/CED.[14] Therefore, we undertook homology modeling of *WDR35* mutations on the predicted protein structure to gain additional insight into the molecular genetics underlying the clinical phenotypes (Figure 4). All of the *WDR35* missense mutations identified to date in both Sensenbrenner[14] and SRP (Figure 4A) affect highly conserved WDR35 residues, suggesting that they are all

(C and D) IMCD3 cells were serum starved for 36 hr before costaining with antibodies directed against acetylated α-tubulin (green) and Wdr35 (red; C, 085 antibody; D, 02 antibody). Nuclei are stained with DAPI (blue).
(E and F) Wild-type 13.5 dpc mouse kidney (E) and choroid plexus (F) sections were costained with antibodies directed against acetylated α-tubulin (green) and Wdr35 (red, 085 antibody). Nuclei are stained with TOTO-3 (blue). Primary cilia in the mesenchyme (E) and ciliated epithelia lining lumen (F) are indicated.
(G and H) Shown are 0.4 μm confocal images of section immunohistochemistry of 11.5 dpc limb-bud mesenchyme from wild-type (G) and $Wdr35^{yet/yet}$ (H) embryos stained with antibodies directed against acetylated α-tubulin (green), Wdr35 (085 antibody: red), and TOTO-3 (blue). See also Figure S3E for additional support, by immunoblot analysis, that *yeti* is a null allele of Wdr35. See also Figure 4 for preadsorbtion with peptide for demonstration of the specificity of antibody studies.
(I and J) Primary fibroblast cells from a control (I) or $WDR35^{\Delta 5/\Delta 5}$ SRP patient (J) were serum starved for 36–48 hr before costaining with antibodies directed against WDR35 (green, 02 antibody) and γ-tubulin (red). Fainter, nonspecific staining of cytoplasmic microtubules by γ-tubulin is observed in human control and mutant fibroblasts. Nuclei are stained with DAPI (blue).
(K and L) *Wdr35* siRNA knockdown leads to reduced cilia formation. ShhLIGHT II cells were transfected with siRNAs against *Wdr35*. qRT-PCR shows significantly reduced levels of *Wdr35* mRNA after siRNA treatment (K). A 50% reduction in the number of ciliated cells was observed when *Wdr35* mRNA was knocked down to 15% of wild-type levels (L). Negative: scramble siRNA; ***$p < 0.001$; **$p < 0.01$ (Chi-squared). Bars represent standard deviations. Statistical significance was determined via a Student's t test.

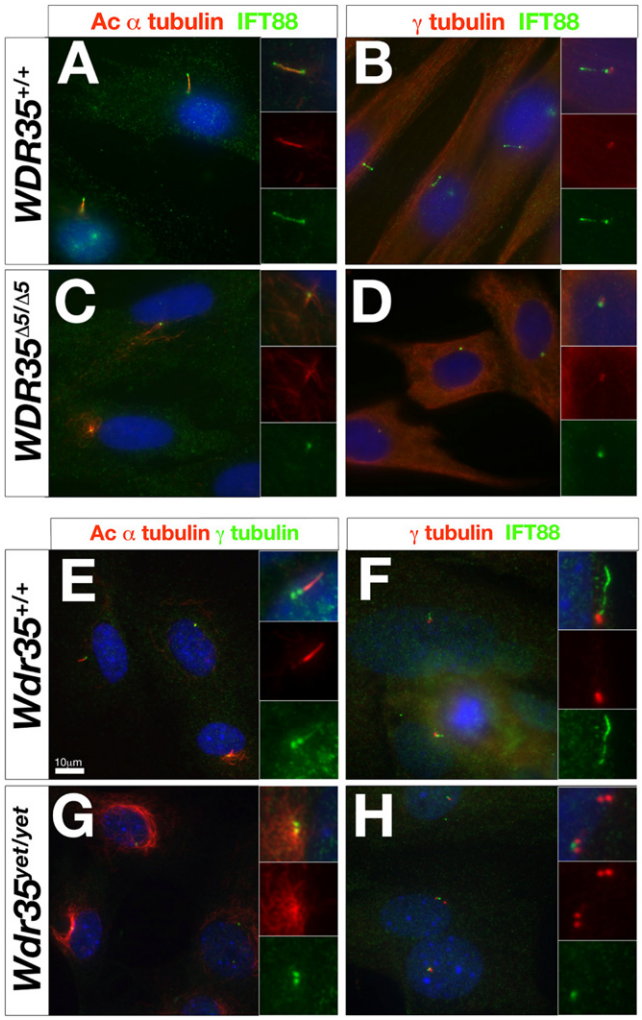

Figure 3. *Wdr35* Is Required for Mammalian Ciliogenesis
(A–D) Primary fibroblast cells from a control (A and B) or *WDR35*$^{\Delta5/\Delta5}$ SRP patient (C and D) were serum starved for 36–48 hr before costaining with antibodies directed against IFT88 (green) and acetylated α-tubulin (red) (A and C) or IFT88 (green) and γ-tubulin (red) (B and D). Nuclei are stained with DAPI (blue). Inserts show higher magnification of individual cilia in merged or single channels.
(E–H) Primary mouse embryonic fibroblasts derived from 11.5 dpc control *Wdr35*$^{+/+}$ (E and F) or *Wdr35*$^{yet/yet}$ mutants (G and H) were cultured and serum starved and then costained with antibodies directed against γ-tubulin (green) and acetylated α-tubulin (red) (E and G) or IFT88 (green) and γ-tubulin (red) (F and H). Nuclei are stained with DAPI (blue). Inserts show high magnification of individual cilia in merged or single channels. Scale bar represents 10 μm.

likely to be pathogenic. However, homology modeling reveals striking differences in the functional consequences of the *WDR35* mutations in SRP versus Sensenbrenner syndrome cases. A similar configuration of N-terminal WD40 repeats and C-terminal tetratricopeptide repeat (TPR)-like motifs observed in WDR35 (Figure 1E) is found in other IFT complex A and B proteins.[24] The WD40/WD40-like repeats are involved in intracellular trafficking, cargo recognition, and binding.[24,25] A similar protein structure is also shared with the coat complexes COPI, COPII, and clathrin, which are involved in vesicle trafficking,[24,28] and it was recently shown that in coat proteins, the N-terminal WD40-like β-propeller is essential for vesicular cage formation.[29] Taking advantage of the high secondary-structure homology of WDR35 to the structure of yeast β′-COP[29], we used structure-prediction algorithms and homology to model the structure of WDR35 (Figure S6). WDR35 is predicted to fold into two seven-bladed β-propellers, each with an offset WD40-like repeat, followed by an extended TPR-containing α-solenoid domain (Figures 4B and 4C). This model highlights the consequences of the human SRP mutations: the *WDR35*$^{\Delta5}$ mutation results in an in-frame deletion of the third blade in the N-terminal seven-bladed propeller, whereas the SRP-3-1 missense mutation (p.Trp261Arg) changes one of seven highly conserved tryptophan residues at the inner face of the same propeller (Figures 4C and 4D). That both SRP deletion and missense mutations impact the N-terminal β-propeller, which has been implicated in higher-order organization of COPI complexes, suggests that these mutations interrupt key interaction motifs required for IFT-A train assembly or stability, resulting in abrogated retrograde transport. This hypothesis is consistent with the severe ciliogenesis phenotype observed in our SRP human and mouse *WDR35* mutants. In contrast, missense mutations identified in the milder Sensenbrenner/CED cases[14] are found in more C-terminal domains of WDR35, suggesting that interactions with specific cargo or other IFT components may be affected, resulting in impairment, but not complete inhibition, of retrograde transport.

WDR35 has been recently implicated in Sensenbrenner syndrome/CED and now, through our work, in a clinically distinct syndrome of severe SRP. Our results show that SRP and CED are allelic, demonstrating not only that the SRPs show locus heterogeneity but that clinically distinct ciliopathies with severe and moderate presentation can result from allelic heterogeneity in the same gene. Given the parallels with the null mouse mutants, our current study suggests that the more severe human disease, SRP, is the result of complete loss of function of WDR35, resulting in profound ciliogenesis defects. Furthermore, molecular modeling has shown that SRP mutations affect key structural elements in the N-terminal β-propeller domain, which by homology with the COPI, COPII, and clathrin proteins is involved in higher complex organization of transport modules. Given the broad developmental expression of *WDR35* and the multisystem defects observed in both human and mouse mutants, future tissue-specific mutation studies of *Wdr35* in mice will be needed to determine which are the primary defects underlying the pleiotropic loss of WDR35. Mutant studies in lower-order model organisms, such as *Chlamydomonas* and *C. elegans*, have been very powerful for identifying cilia phenotypes. However, the complexities of mammalian cilia's structure and function, in particular with respect to its role in developmental signaling, emphasize the

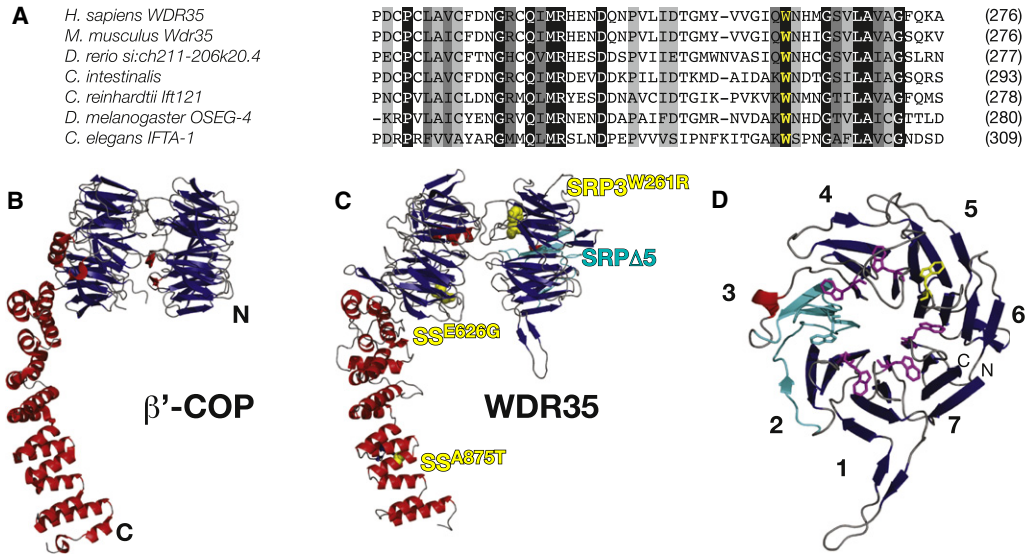

Figure 4. Structural Similarities between WDR35 and the Canonical COPI Coat Complex Suggest Conserved Functional Importance of the N-Terminal WD40-like β-Propeller

(A) Amino acid sequence alignment of WDR35 sequence at W261 (yellow) demonstrates complete conservation of the tryptophan residue. WDR35 sequences are from *Homo sapiens* (ENST00000345530), *Mus musculus* (ENSMUST00000085745), *Danio rerio* (XP_693887.2), *Ciona intestinalis* (ENSCINT0000018168), *Chlamydomonas reinhardtii* (XP_001702021), *Drosophila melanogaster* (FBtr0072797), and *Caenorhabditis elegans* (C54G7.4).

(B and C) (B) Ribbon diagram of *S. cerevisiae* β′−COP (PDB ID: 3mkqA) from the crystal structure[29] and the predicted architecture of human WDR35 (residues 6–933) based on homology modeling with the use of the yeast β′-COP structure as a template (C). For details of the protein structure modeling, see Figure S6. Starting from its N terminus (N), WDR35 is predicted to have two seven-bladed β-propeller domains (viewed side-on in the presented orientation) followed by an α-solenoid domain composed of the TPR-like repeat α helices. SRPΔ5 mutants are predicted to lose one full blade (cyan) of the N-terminal β-propeller domain. The p.Trp261Arg mutation affects a key tryptophan residue (yellow sphere) on the axial face of this same β-propeller in conceptus SRP-3-1. β strands are shown as blue arrows and α helices as red ribbons. Sensenbrenner missense mutations p.Glu626Gly and p.Ala875Thr,[14] highlighted in yellow, affect residues outside this domain.

(D) Ribbon diagram of the proposed structural model for the N-terminal seven-bladed WD40-like β-propeller (residues 6–330) of human WDR35, with β strands shown in blue and the α-helix in red. Seven key tryptophan residues that are central to the WD-like repeats are shown as purple sticks; p.Trp261Arg is located in blade 6 and is shown as yellow sticks. Deletion of *WDR35Δ5* leads to an in-frame deletion of four offset β strands (2d–3c: cyan) resulting in the loss of a full blade of the β-propeller. Amino and carboxy-termini are labeled with N and C, respectively. Blades of the propeller are numbered according to the secondary structure alignment in Figure S6.

importance of mouse molecular genetics. The use of mouse models for investigating the role of the IFT machinery and specific cargo will provide further insight into the pathogenesis of ciliopathies and the reasons underlying the variability in clinical presentation.

Supplemental Data

Supplemental data include six figures and two tables and can be found with this article online at http://www.cell.com/AJHG.

Acknowledgments

We thank K. Pope (Clinical Research Coordinator, MCRI) and the families involved in this research. We thank I. Algianis, E. Maher , and C. Patel for sharing clinical samples for *WDR35* screening. We are grateful to P. Perry and M. Pearson for imaging assistance. We thank D. FitzPatrick, A. Jackson, and T. Kunath for critical comments on the manuscript. This work was funded by the Medical Research Council (UK) and the National Health and Medical Research Council Australia (program grant 490037). Support to P.M. was provided by fellowships from the National Sciences and Engineering Research Council of Canada and the Caledonian Research Foundation. P.J.L. was supported by a National Health and Medical Research Council Australia RD Wright Fellowship (334346).

Received: January 26, 2011
Revised: March 13, 2011
Accepted: March 18, 2011
Published online: April 7, 2011

Web Resources

The URLs for data presented herein are as follows:

Mouse Genome Informatics, http://www.informatics.jax.org/
Online Mendelian Inheritance in Man (OMIM), http://www.ncbi.nlm.nih.gov/Omim

References

1. Superti-Furga, A., and Unger, S. (2007). Nosology and classification of genetic skeletal disorders: 2006 revision. Am. J. Med. Genet. A. *143*, 1–18.
2. Baker, K., and Beales, P.L. (2009). Making sense of cilia in disease: the human ciliopathies. Am. J. Med. Genet. C. Semin. Med. Genet. *151C*, 281–295.

3. Ho, N.C., Francomano, C.A., and van Allen, M. (2000). Jeune asphyxiating thoracic dystrophy and short-rib polydactyly type III (Verma-Naumoff) are variants of the same disorder. Am. J. Med. Genet. *90*, 310–314.
4. Amar, M.J., Sutphen, R., and Kousseff, B.G. (1997). Expanded phenotype of cranioectodermal dysplasia (Sensenbrenner syndrome). Am. J. Med. Genet. *70*, 349–352.
5. Pedersen, L.B., and Rosenbaum, J.L. (2008). Intraflagellar transport (IFT) role in ciliary assembly, resorption and signalling. Curr. Top. Dev. Biol. *85*, 23–61.
6. Kozminski, K.G., Beech, P.L., and Rosenbaum, J.L. (1995). The Chlamydomonas kinesin-like protein FLA10 is involved in motility associated with the flagellar membrane. J. Cell Biol. *131*, 1517–1527.
7. Pazour, G.J., Dickert, B.L., and Witman, G.B. (1999). The DHC1b (DHC2) isoform of cytoplasmic dynein is required for flagellar assembly. J. Cell Biol. *144*, 473–481.
8. Porter, M.E., Bower, R., Knott, J.A., Byrd, P., and Dentler, W. (1999). Cytoplasmic dynein heavy chain 1b is required for flagellar assembly in Chlamydomonas. Mol. Biol. Cell *10*, 693–712.
9. Liu, A., Wang, B., and Niswander, L.A. (2005). Mouse intraflagellar transport proteins regulate both the activator and repressor functions of Gli transcription factors. Development *132*, 3103–3111.
10. Merrill, A.E., Merriman, B., Farrington-Rock, C., Camacho, N., Sebald, E.T., Funari, V.A., Schibler, M.J., Firestein, M.H., Cohn, Z.A., Priore, M.A., et al. (2009). Ciliary abnormalities due to defects in the retrograde transport protein DYNC2H1 in short-rib polydactyly syndrome. Am. J. Hum. Genet. *84*, 542–549.
11. Dagoneau, N., Goulet, M., Geneviève, D., Sznajer, Y., Martinovic, J., Smithson, S., Huber, C., Baujat, G., Flori, E., Tecco, L., et al. (2009). DYNC2H1 mutations cause asphyxiating thoracic dystrophy and short rib-polydactyly syndrome, type III. Am. J. Hum. Genet. *84*, 706–711.
12. Beales, P.L., Bland, E., Tobin, J.L., Bacchelli, C., Tuysuz, B., Hill, J., Rix, S., Pearson, C.G., Kai, M., Hartley, J., et al. (2007). IFT80, which encodes a conserved intraflagellar transport protein, is mutated in Jeune asphyxiating thoracic dystrophy. Nat. Genet. *39*, 727–729.
13. Walczak-Sztulpa, J., Eggenschwiler, J., Osborn, D., Brown, D.A., Emma, F., Klingenberg, C., Hennekam, R.C., Torre, G., Garshasbi, M., Tzschach, A., et al. (2010). Cranioectodermal Dysplasia, Sensenbrenner syndrome, is a ciliopathy caused by mutations in the IFT122 gene. Am. J. Hum. Genet. *86*, 949–956.
14. Gilissen, C., Arts, H.H., Hoischen, A., Spruijt, L., Mans, D.A., Arts, P., van Lier, B., Steehouwer, M., van Reeuwijk, J., Kant, S.G., et al. (2010). Exome sequencing identifies WDR35 variants involved in Sensenbrenner syndrome. Am. J. Hum. Genet. *87*, 418–423.
15. Shalom, O., Shalva, N., Altschuler, Y., and Motro, B. (2008). The mammalian Nek1 kinase is involved in primary cilium formation. FEBS Lett. *582*, 1465–1470.
16. White, M.C., and Quarmby, L.M. (2008). The NIMA-family kinase, Nek1 affects the stability of centrosomes and ciliogenesis. BMC Cell Biol. *9*, 29.
17. Upadhya, P., Birkenmeier, E.H., Birkenmeier, C.S., and Barker, J.E. (2000). Mutations in a NIMA-related kinase gene, Nek1, cause pleiotropic effects including a progressive polycystic kidney disease in mice. Proc. Natl. Acad. Sci. USA *97*, 217–221.
18. Thiel, C., Kessler, K., Giessl, A., Dimmler, A., Shalev, S.A., von der Haar, S., Zenker, M., Zahnleiter, D., Stöss, H., Beinder, E., et al. (2011). NEK1 mutations cause short-rib polydactyly syndrome type majewski. Am. J. Hum. Genet. *88*, 106–114.
19. Cortellino, S., Wang, C., Wang, B., Bassi, M.R., Caretti, E., Champeval, D., Calmont, A., Jarnik, M., Burch, J., Zaret, K.S., et al. (2009). Defective ciliogenesis, embryonic lethality and severe impairment of the Sonic Hedgehog pathway caused by inactivation of the mouse complex A intraflagellar transport gene Ift122/Wdr10, partially overlapping with the DNA repair gene Med1/Mbd4. Dev. Biol. *325*, 225–237.
20. Huangfu, D., and Anderson, K.V. (2005). Cilia and Hedgehog responsiveness in the mouse. Proc. Natl. Acad. Sci. USA *102*, 11325–11330.
21. May, S.R., Ashique, A.M., Karlen, M., Wang, B., Shen, Y., Zarbalis, K., Reiter, J., Ericson, J., and Peterson, A.S. (2005). Loss of the retrograde motor for IFT disrupts localization of Smo to cilia and prevents the expression of both activator and repressor functions of Gli. Dev. Biol. *287*, 378–389.
22. Qin, J., Lin, Y., Norman, R.X., Ko, H.W., and Eggenschwiler, J.T. (2011). Intraflagellar transport protein 122 antagonizes Sonic Hedgehog signaling and controls ciliary localization of pathway components. Proc. Natl. Acad. Sci. USA *108*, 1456–1461.
23. Kannu, P., McFarlane, J.H., Savarirayan, R., and Aftimos, S. (2007). An unclassifiable short rib-polydactyly syndrome with acromesomelic hypomineralization and campomelia in siblings. Am. J. Med. Genet. A. *143A*, 2607–2611.
24. Avidor-Reiss, T., Maer, A.M., Koundakjian, E., Polyanovsky, A., Keil, T., Subramaniam, S., and Zuker, C.S. (2004). Decoding cilia function: defining specialized genes required for compartmentalized cilia biogenesis. Cell *117*, 527–539.
25. Cole, D.G. (2003). The intraflagellar transport machinery of Chlamydomonas reinhardtii. Traffic *4*, 435–442.
26. Mukhopadhyay, S., Wen, X., Chih, B., Nelson, C.D., Lane, W.S., Scales, S.J., and Jackson, P.K. (2010). TULP3 bridges the IFT-A complex and membrane phosphoinositides to promote trafficking of G protein-coupled receptors into primary cilia. Genes Dev. *24*, 2180–2193.
27. Blacque, O.E., Li, C., Inglis, P.N., Esmail, M.A., Ou, G., Mah, A.K., Baillie, D.L., Scholey, J.M., and Leroux, M.R. (2006). The WD repeat-containing protein IFTA-1 is required for retrograde intraflagellar transport. Mol. Biol. Cell *17*, 5053–5062.
28. Jékely, G., and Arendt, D. (2006). Evolution of intraflagellar transport from coated vesicles and autogenous origin of the eukaryotic cilium. Bioessays *28*, 191–198.
29. Lee, C., and Goldberg, J. (2010). Structure of coatomer cage proteins and the relationship among COPI, COPII, and clathrin vesicle coats. Cell *142*, 123–132.